UNIVERSIDAD DE GRANADA

PROGRAMA DE DOCTORADO EN QUÍMICA

FACULTAD DE CIENCIAS

Departamento de Química Inorgánica

TESIS DOCTORAL

Hidrogenación selectiva de aldehídos α,β-insaturados y foto-degradación de contaminantes empleando catalizadores basados en xerogeles de carbón

Selective hydrogenation of α,β-unsaturated aldehydes and photo-degradation of pollutants using catalysts based on carbon xerogels

Esther Bailón García

Granada, Abril 2015

Editor: Universidad de Granada. Tesis Doctorales
Autor: Esther María José Bailón García
ISBN: 978-84-9163-589-5
URI: http://hdl.handle.net/10481/42973

Hidrogenación selectiva de aldehídos α,β-insaturados y foto-degradación de contaminantes empleando catalizadores basados en xerogeles de carbón

Por

ESTHER BAILÓN GARCÍA

Memoria presentada para aspirar al grado de Doctor
por la Universidad de Granada

Fdo.: Esther Bailón García
Licenciada en Ingeniería Química

Los Directores de la Tesis

Prof. Dr. Francisco J. Maldonado Hódar
Catedrático del Departamento de Química Inorgánica, Universidad de Granada

Prof. Dr. Agustín F. Pérez Cadenas
Prof. Titular del Departamento de Química Inorgánica, Universidad de Granada

HIDROGENACIÓN SELECTIVA DE ALDEHÍDOS α,β-INSATURADOS Y FOTO-DEGRADACIÓN DE CONTAMINANTES EMPLEANDO CATALIZADORES BASADOS EN XEROGELES DE CARBÓN

Tesis presentada para aspirar al grado de Doctor en Química por

ESTHER BAILÓN GARCÍA

Realizada bajo la dirección del Catedrático de Química Inorgánica Prof. Dr. Francisco José Maldonado Hódar y del Prof. Titular Dr. Agustín Francisco Pérez Cadenas, en la Facultad de Ciencias de la Universidad de Granada, y juzgada el día 29 de abril de 2015, en dicha Facultad, por el siguiente Tribunal:

PRESIDENTE:

Prof. Dr. Carlos Moreno Castilla, Catedrático de Química Inorgánica, Universidad de Granada.

VOCALES:

Prof. Em. Dr. Jacob A. Moulijn, Full Professor, Catalysis Engineering, Delft University of Technology, Países Bajos.
Prof. Dr. José Manuel López Nieto, Profesor de Investigación del Instituto de Tecnología Química, CSIC, Valencia.
Prof. Dra. Rosa M. Martín Aranda, Catedrática de Química Inorgánica de la Universidad Nacional de Educación a Distancia.

SECRETARIO:

Prof. Dr. José Rivera Utrilla, Catedrático de Química Inorgánica, Universidad de Granada.

Francisco José Maldonado Hódar y Agustín Francisco Pérez Cadenas como directores de la presente Tesis Doctoral y la doctoranda Esther Bailón García

GARANTIZAN QUE

el trabajo ha sido realizado por la doctoranda respetando los derechos de otros autores a ser citados cuando se han utilizado sus resultados o publicaciones.

Y para que conste a los efectos oportunos, en el cumplimiento de la legislación vigente, firmamos el presente certificado en Granada a 7 de Abril del 2015.

Fdo.: Francisco J. Maldonado Hódar
Catedrático de Química Inorgánica de la Universidad de Granada

Fdo.: Agustín F. Pérez Cadenas
Profesor Titular de Química Inorgánica de la Universidad de Granada

Fdo.: Doctoranda Esther Bailón García
Licenciada en Ingeniería Química

“Me enseñaron que el camino del progreso no es ni rápido ni fácil”

“La vida no es fácil, para ninguno de nosotros.
Pero... ¡Qué importa! Hay que perseverar
y, sobre todo, tener confianza en uno mismo.
Hay que sentirse dotado para realizar alguna cosa
y que esa cosa hay que alcanzarla,
cueste lo que cueste”

Marie Curie

Agradecimientos:

Quiero expresar mi más profundo agradecimiento a mis Directores de Tesis, Prof. Dr. Francisco José Maldonado Hódar y Prof. Dr. Agustín Francisco Pérez Cadenas, por vuestra dirección, preocupación y dedicación durante esta etapa, así como, por ser un gran apoyo no solo a nivel científico sino también a nivel personal, creyendo siempre en mis capacidades y dándome la fuerza para seguir cuando aparecían dificultades a lo largo de estos años predoctorales.

Agradecer también al Prof. Dr. Francisco Carrasco Marín por ser la brújula que siempre me ha indicado el Norte durante esta travesía, gran parte del trabajo aquí reflejado se debe a sus sabios consejos. Agradecerle por su trato paternal y por considerarme como "una hija más".

Al Prof. Dr. Carlos Moreno Castilla por darme la oportunidad de realizar esta Tesis en el Grupo de Investigación en Materiales de Carbón de la Universidad de Granada, sin olvidarme del resto de miembros de dicho grupo: Pepe, Isa, Mª Úngeles, los cuales me han confirmado la gran suerte que he tenido de poder realizar la presente Tesis Doctoral en este excelente grupo humano y científico.

También quiero dar las gracias a toda la gente que he conocido durante estos cuatro años de trabajo en el laboratorio de adsorción y catálisis y que se han convertido en más que amigos. Mis compañeros de laboratorio Zula, Jose, David, Hakim, Mari, Carmen y Abdallah los cuales nos hemos convertido en la familia del carbón, apoyándonos siempre ante las dificultades y compartiendo grandes momentos. Por otro lado, están los compañeros del Departamento de Química General: Mahmoud, Raúl, Valente, Jacob, Iván, Ricardo, Alegría, Antonio e Inma, grandes personas y científicos. No quiero olvidarme de la gente que ha estado de estancia en el laboratorio y que sin duda han dejado huella: Filipa, Adrián, Norberto, Nelsón y Amra. A todos gracias por cada uno de los momentos especiales que me habéis regalado.

Agradecer al Prof. Dr. Maurizio Prato por permitirme realizar mis estancias predoctorales en Trieste, una ciudad con un encanto especial que me enamoró y me

permitió conocer a gente especial como Susanna, Tatiana, Zois, Caroline, Michela, Michel, Arturo, Dani y Cristina.

Quiero agradecer también al Grupo de Carbones de la Universidad de Jaén: Vicky, Miguel Ángel, María, y Paco, por sus consejos y amistad.

A los miembros del Centro de Investigación Científica de la Universidad de Granada, especialmente a María del Mar y Alicia (Técnicos especialistas de TEM y SEM), las que me han dado luz a mis ojos haciéndome "ver" las cosas que no alcanzaba a ver.

A mi familia y amigos, en especial a mis padres, por su apoyo incondicional tanto en los buenos como malos momentos. Mencionar a mi hermana Toñi, la cual ha aguantado mis sesiones orales de cada congreso, gracias por aguantar a tu "pesailla". Destacar a Juan, una gran persona y casi un hermano el cual me ha aportado sonrisas dentro de la tristeza. Finalmente a Noelia, por ser una gran amiga y ayudarme a levantarme cuando más lo necesitaba.

Este Trabajo de Investigación ha sido financiado por el Ministerio de Ciencia e Innovación, proyecto CTM2010-18889 al cual está asociada la concesión de una beca del Programa de Formación de Personal Investigador, la Junta de Andalucía, proyecto P12-RNM-2892 y el Ministerio de Economía y Competitividad, proyecto CTQ2013-44789-R.

a Antonia y José, mis padres

a Toñi, mi hermana

a Juan, un hermano

Contenidos y estructura de la Tesis

CONTENIDOS Y ESTRUCTURA DE LA TESIS

En la presente Tesis Doctoral se recoge la síntesis de diferentes materiales basados en carbón, fundamentalmente xerogeles de carbón y materiales compuestos óxidos metálicos-xerogel de carbón, y se analiza su comportamiento como soportes de catalizadores metálicos en reacciones de hidrogenación selectiva de aldehídos α,β insaturados, en concreto citral y cinamaldehído, por el interés industrial de sus alcoholes insaturados derivados, así como, su comportamiento como foto-catalizadores en procesos de descontaminación. Los resultados experimentales obtenidos y la discusión de los mismos se presentan en esta Memoria divididos en nueve Capítulos.

El **primer Capítulo** está dedicado al estudio del estado del arte de la hidrogenación selectiva de aldehídos α,β insaturados, fundamentalmente citral, así como las posibles estrategias existentes para mejorar la actividad fotocatalítica de los materiales empleados en fotocatálisis. Se comienza planteando la importancia y necesidad de obtener los alcoholes insaturados, las dificultades que esta reacción implica y las posibles estrategias para conseguir obtener los productos objetivo. Finalmente, se analizan los resultados previamente obtenidos sobre diferentes materiales de carbón.

En el **segundo Capítulo** se describen los materiales y métodos utilizados. Se exponen en profundidad los métodos de preparación de los diferentes materiales desarrollados en la presente Tesis, así como las técnicas para la caracterización de los mismos.

En el **tercer Capítulo** se recoge la optimización de las condiciones de operación en la reacción de hidrogenación de citral (velocidad de agitación, masa de catalizador, presión y temperatura) realizándose además un estudio difusional para analizar la existencia de problemas difusionales internos y externos de materia. Se selecciona aquellas condiciones óptimas en las cuales se eliminan dichos problemas difusionales y se obtiene el mejor comportamiento catalítico. Finalmente, se optimiza el tamaño de partícula de la fase activa dado que este tipo de reacciones son sensibles a la estructura.

En el **cuarto Capítulo** se analiza el comportamiento como soporte de platino de un xerogel de carbono estructurado en microesferas sintetizado en nuestro laboratorio en comparación con otros soportes inorgánicos clásicos (SiO_2, TiO_2 y Al_2O_3) en la reacción de hidrogenación de citral, en base a sus características ácidas, morfológicas y texturales. También se analiza la influencia del pretratamiento en diferentes atmósferas (He ó H_2) para todos los catalizadores empleados. En este Capítulo se concluye que el platino soportado sobre el xerogel de carbón presenta un mejor comportamiento catalítico en términos de selectividad, independientemente del pretramiento empleado, comparable únicamente con los resultados obtenidos para Pt/TiO_2 tras el pretratamiento en H_2.

El **quinto Capítulo** se centra en explicar las diferencias tan significativas, tanto en términos de selectividad como de actividad, observadas en el Capítulo anterior cuando se realizan diferentes pretratamientos del catalizador Pt/TiO_2. Se analizan los cambios producidos en las propiedades texturales y químicas del catalizador tras pre-tratamientos en He, H_2 o un tratamiento consecutivo He-H_2 por diferentes técnicas y los resultados se relacionan con el comportamiento catalítico en la hidrogenación selectiva de citral.

En el **sexto Capítulo** se compara la eficiencia de diferentes materiales carbonosos como soportes de platino en los catalizadores de hidrogenación selectiva de citral. Los soportes carbonosos empleados son dos carbones activados (un carbón activado comercial y un carbón activado sintetizado en nuestro laboratorio) y dos xerogeles de carbón (uno microporoso y otro micro-mesoporoso). La influencia de la porosidad y las impurezas en los carbones activados determina el comportamiento de sus respectivos catalizadores. En este capítulo se muestra, como en capítulos anteriores, que el xerogel de carbón microporoso estructurado en microesferas es el soporte óptimo debido a sus características texturales, morfológicas y su alta pureza.

En el **séptimo Capítulo**, una vez seleccionado el xerogel de carbón como soporte, se aborda la selección de la fase activa a emplear. Como metales catalíticamente activos se estudian rutenio, platino e iridio, que de acuerdo con la bibliografía son los que muestran un mejor comportamiento en este tipo de reacciones. Se analiza la influencia del pretratamiento y la reutilización de los catalizadores,

encontrando diferente comportamiento entre los metales. Los catalizadores usados son analizados desde un punto de vista textural y químico para tratar de explicar estas diferencias observadas.

En estos primeros Capítulos se ha concluido que el mejor soporte estudiado es un xerogel de carbón estructurado en microesferas. Respecto a la fase activa se escoge el platino debido a su mayor actividad y selectividad y a su menor coste frente al iridio pese a que muestra mayor desactivación.

Se han sintetizado también materiales compuestos óxidos metálicos-xerogel de carbón, seleccionándose los óxidos: TiO_2, SiO_2, ZrO_2, CeO_2 y V_2O_5. Estos materiales son usados tanto como soportes de platino en reacciones de hidrogenación selectiva como foto-catalizadores en aplicaciones medioambientales. La aplicación de estos materiales en hidrogenación y foto-catálisis han dado lugar a un elevado volumen de resultados, parte de los cuales se recogen en el **octavo Capítulo**. Así, los posteriores Apartados 8.1, 8.2 y 8.3 recogen los resultados incluidos en la solicitud de tres patentes que se están actualmente tramitando.

El **Apartado 8.1** se dedica al estudio del comportamiento catalítico de catalizadores metálicos soportados sobre materiales compuestos TiO_2-xerogel de carbón y SiO_2-xerogel de carbón en reacciones de hidrogenación selectiva (citral y cinamaldehído). Se analiza el efecto sinérgico entre ambas fases en comparación con los óxidos y xerogeles de carbón puros, en base a sus características texturales y químicas. Se pone de manifiesto que estos materiales son excelentes soportes para el desarrollo de catalizadores altamente activos y selectivos, que mantienen selectividades muy elevadas a conversión total (presentan rendimientos muy elevados) en tiempos muy cortos (menos de 60 min de reacción).

En el **Apartado 8.2** se demuestra el potencial de materiales compuestos ZrO_2-xerogel de carbón como foto-catalizadores en la degradación de contaminantes industriales, usando como referencia el foto-catalizador P25. Además, estos materiales son activos con radiación visible, lo cual facilita el proceso de descontaminación avanzada (reemplazando la luz ultravioleta) y lo hace económicamente más viable. También se analiza el grado de mineralización logrado y se realizan análisis de

toxicidad de las aguas descontaminadas. Estas propiedades foto-catalíticas se relacionan con las características texturales y químicas del material compuesto empleado.

En el **Apartado 8.3** se estudia la actividad foto-catalítica de microesferas de xerogel de carbón recubiertas con oxido de titanio. Al igual que en el Apartado anterior se usa radiación visible en lugar de ultravioleta y se realizan mediciones de la toxicidad así como del grado de mineralización alcanzado.

Finalmente, en el **noveno Capítulo** se estudia la aplicación de xerogeles de carbón para aplicaciones biomédicas. A pesar del progresivo avance de la aplicación de los materiales de carbón en dichas aplicaciones y de las excelentes propiedades que presentan los aerogeles y xerogeles de carbón, no se encontró ninguna referencia sobre la utilización de estos materiales en tales aplicaciones. En este Capítulo se recoge un estudio preliminar de la funcionalización de materiales basados en xerogel de carbón y el estudio de su toxicidad en el crecimiento de osteocitos.

Parte de los resultados del trabajo de investigación realizado durante el desarrollo de esta Tesis se recogen en los siguientes artículos de difusión internacional:

- Bailón-García, E., Maldonado-Hódar, F.J., Pérez-Cadenas, A.F., Carrasco-Marín, F. *Catalysts supported on carbon materials for the selective hydrogenation of citral*. Catalysts, 3 (2013) 853-877.

- Bailón-García, E., Carrasco-Marín, F., Pérez-Cadenas, A.F., Maldonado-Hódar, F.J. *Microspheres of carbon xerogel: An alternative Pt-support for the selective hydrogenation of citral*. Applied Catalysis A: General, 482 (2014) 315-326.

- Bailón-García, E., Carrasco-Marín, F., Pérez-Cadenas, A.F., Maldonado-Hódar, F.J. *Development of carbon xerogels as alternative Pt-supports for the selective hydrogenation of citral*. Catalysis Communications, 58 (2015) 64-69.

- Bailón-García, E., Carrasco-Marín, F., Pérez-Cadenas, A.F., Maldonado-Hódar, F.J. *Influence of the pretreatment conditions on the development and performance*

of active sites of Pt/TiO_2 catalysts used for the selective citral hydrogenation. Submitted to Journal of Catalysis.

- Bailón-García, E., Carrasco-Marín, F., Pérez-Cadenas, A.F., Maldonado-Hódar, F.J. *Fitting the experimental conditions and characteristics of Pt/C catalysts for the selective hydrogenation of citral*. Submitted to Catalysis Science & Technology.

- Bailón-García, E., Carrasco-Marín, F., Pérez-Cadenas, A.F., Maldonado-Hódar, F.J. *About the active phase selection in designing selective hydrogenation catalysts supported on nanostructured carbon xerogels.* Submitted to RSC Advances.

- Bailón-García, E., Carrasco-Marín, F., Pérez-Cadenas, A.F., Maldonado-Hódar, Cok, M., Bosi, S., Prato, M. *A preliminary study about the use of functionalized carbon xerogel in osteocytes growth.* In progress.

- Bailón-García, E., Carrasco-Marín, F., Pérez-Cadenas, A.F., Maldonado-Hódar, F.J. *Development of new mesoporous carbon-zirconia composites.* In progress.

- Bailón-García, E., Carrasco-Marín, F., Pérez-Cadenas, A.F., Maldonado-Hódar, F.J. C*arbon – TiO_2 composites as selective Pt-catalyst supports for hydrogenation of citral: effect of the percentage of titanium dioxide*. In progress.

- Bailón-García, E., Maldonado-Hódar, F.J., Pérez-Cadenas, A.F., Carrasco-Marín, F. *TiO_2 coated carbon xerogel microspheres for the photocatalytic degradation of Orange G under visible light.* In progress.

- Bailón-García, E., Maldonado-Hódar, F.J, Pérez-Cadenas, A.F., Carrasco-Marín, F. *Selective hydrogenation of citral to unsaturated alcohols over Pt/SiO_2 – carbon xerogel catalysts.* In progress.

Además, algunos de los resultados recogidos en la presente Tesis han dado lugar a la solicitud de las siguientes patentes:

- Bailón-García, E., Carrasco-Marín, F., Pérez-Cadenas, A.F., Maldonado-Hódar, F.J. *Método de preparación de materiales compuestos óxido inorgánico-carbón y sus aplicaciones en el desarrollo de catalizadores específicos para la hidrogenación selectiva de α,β-insaturados.* IPR-523.

- Bailón-García, E., Carrasco-Marín, F., Pérez-Cadenas, A.F., Maldonado-Hódar, F.J. *Foto-catalizadores estructurados con alto rendimiento bajo radiación visible basados en recubrimientos de microesferas de xerogel de carbón con óxido de titanio.* IPR 571.

- Bailón-García, E., Carrasco-Marín, F., Pérez-Cadenas, A.F., Maldonado-Hódar, F.J. *Método de preparación de materiales compuestos óxido de Zirconio-Carbón y sus aplicaciones como foto-catalizadores activos en la degradación de compuestos orgánicos.* IPR 572.

Los resultados más relevantes de esta Tesis se han presentado, además, en los siguientes congresos tanto nacionales como internacionales:

- The Annual World Conference on Carbon (CARBON). Cracovia, Krakow, Poland, June 2012.

- Reunión de la Sociedad Española de Catálisis (SECAT). Sevilla, España, Junio 2013.

- XXXIV Reunión Bienal de la Real Sociedad Española de Química (RSEQ). Santander, España, Septiembre 2013.

- XXII Reunión del Grupo Español del Carbón (GEC). Madrid, España, Octubre 2014.

- 10th International Symposium on the Characterization of Porous Solids (COPS). Granada, Spain, May 2014.

- XXXIX Reunión Ibérica de Adsorción (RIA). Baeza, España, Septiembre 2014.

Índice

CAPÍTULO I: INTRODUCCIÓN 35

1.1. AEROGELES Y XEROGELES DE CARBÓN 37

1.1.1. Geles de carbón: preparación y propiedades superficiales 38

1.1.1.1. Preparación de la mezcla, gelificación y curado 39

1.1.1.2. Secado del hidrogel 41

1.1.1.3. Carbonización 41

1.1.2. Dopado de los geles de carbón 42

1.2. CATALYSTS SUPPORTED ON CARBON MATERIALS FOR THE SELECTIVE HYDROGENATION OF CITRAL 47

1.2.1. Introduction 49

1.2.2. Hydrogenation selectivity 53

1.2.3. The type of transition metal as catalytic phase 56

1.2.4. Carbon materials as supports 58

1.2.4.1. Activated carbons 59

1.2.4.2. Graphite 61

1.2.4.3. Carbon nanotubes 65

1.2.4.4. Composite materials 68

1.2.5. Conclusions 71

1.3. MATERIALES CARBONOSOS COMO MODIFICADORES DE LA ACTIVIDAD FOTO-CATALÍTICA EN LA ELIMINACIÓN DE CONTAMINANTES DEL AGUA 71

1.3.1. Mecanismo de las reacciones foto-catalíticas 72

1.3.2. Estrategias para mejorar el foto-catalizador 74

1.3.2.1. Desarrollo de catalizadores activos bajo luz visible 75

1.3.2.2. Minimización de la recombinación electrón-hueco 80

1.3.2.3. Incremento del área superficial 82

1.3.3. Materiales carbonosos para la mejora de la foto-actividad de TiO_2 84

1.3.3.1. Carbón-activado/TiO_2 84

1.3.3.2. Nanotubos de carbón/TiO_2 86
1.3.3.3. Fullerenos C_{60}/TiO_2 89
1.3.3.4. Grafeno/TiO_2 89

1.4. OBJETIVOS DE LA TESIS 90
1.5. BIBLIOGRAFÍA 91

CAPÍTULO II: MATERIALES Y MÉTODOS 117

2.1. PREPARACIÓN DE LOS MATERIALES UTILIZADOS COMO SOPORTES DE CATALIZADORES DE HIDROGENACIÓN Y/O FOTO-CATALIZADORES 119

2.1.1. Carbones activados 119
2.1.2. Xerogeles de carbón 120
2.1.3. Materiales compuestos xerogeles de carbón-óxidos metálicos 122

2.1.3.1. Materiales compuestos xerogel de carbón-TiO_2 122
2.1.3.2. Esferas de xerogel de carbón recubiertas con TiO_2 123
2.1.3.3. Materiales compuestos xerogel de carbón-ZrO_2 ó SiO_2 124

2.1.4. Óxidos metálicos comerciales 124

2.2. PREPARACIÓN DE CATALIZADORES SOPORTADOS DE IRIDIO, RUTENIO Y PLATINO 125
2.3. TÉCNICAS DE CARACTERIZACIÓN 126

2.3.1. Caracterización textural y morfológica de las muestras 127

2.3.1.1. Microscopía electrónica de barrido (SEM) 127
2.3.1.2. Adsorción física de gases 127
2.3.1.3. Porosimetría de mercurio 131

2.3.2. Caracterización química de los soportes 132

2.3.2.1. Análisis elemental 132
2.3.2.2. Espectroscopía de infrarrojo 132
2.3.2.3. Análisis termogravimétrico 132
2.3.2.4. Medida del pH punto cero de carga 133
2.3.2.5. Desorción térmica programada 133

2.3.2.6. Difracción de rayos-X 133

2.3.3. Caracterización de los catalizadores 134

2.3.3.1. Espectroscopía de fotoemisión de rayos-X 134

2.3.3.2. Microscopía electrónica de transmisión de alta resolución 135

2.3.3.3. Quimisorción de H_2 135

2.3.3.4. Adsorción/desorción de n-butilamina 136

2.4. HIDROGENACIÓN DE CITRAL 137

2.5. FOTO-DEGRADACIÓN DE ORANGE G 139

2.6. BIBIOGRAFÍA 141

CAPÍTULO III: FITTING THE EXPERIMENTAL CONDITIONS AND CHARACTERISTICS OF Pt/C CATALYSTS FOR THE SELECTIVE HYDROGENATION OF CITRAL 145

3.1. INTRODUCTION 147

3.2. EXPERIMENTAL 150

3.2.1. Preparation of the catalysts 150

3.2.2. Characterization of the catalysts 151

3.2.3. Catalytic performance 152

3.3. RESULTS AND DISCUSSION 153

3.3.1. Textural and chemical properties 153

3.3.2. Evaluation of the external mass transfer limitations 157

3.3.3. Internal mass transfer limitations 161

3.3.4. Effect of hydrogen pressure 163

3.3.5. Effect of temperature 164

3.3.6. Influence of the platinum particle size 167

3.3.7. Influence of Pt- support 169

3.4. CONCLUSIONS 171

3.5. REFERENCES 171

CAPÍTULO IV: MICROSPHERES OF CARBON XEROGEL: AN ALTERNATIVE Pt-SUPPORT FOR THE SELECTIVE HYDROGENATION OF CITRAL (INORGANIC SUPPORTS) 179

4.1. INTRODUCTION 181
4.2. EXPERIMENTAL 182
4.2.1. Preparation of the catalysts 182
4.2.2. Textural and chemical characterization 183
4.2.3. Catalytic performance 185
4.3. RESULTS AND DISCUSSION 185
4.3.1. Characterization of the supports and catalysts 185
4.3.2. Catalytic performance 192
4.4. CONCLUSIONS 198
4.5. SUPPORTING INFORMATION 199
4.6. REFERENCES 200

CAPÍTULO V: INFLUENCE OF THE PRETREATMENT CONDITIONS ON THE DEVELOPMENT AND PERFORMANCE OF ACTIVE SITES OF Pt/TiO_2 CATALYSTS USED FOR THE SELECTIVE HYDROGENATION OF CITRAL 207

5.1. INTRODUCTION 209
5.2. EXPERIMENTAL 210
5.2.1. Preparation of the catalysts 210
5.2.2. Textural and chemical characterization 210
5.2.3. Catalytic performance 212
5.3. RESULTS AND DISCUSSION 213
5.4. CONCLUSIONS 225
5.5. REFERENCES 226

CAPÍTULO VI: DEVELOPMENT OF CARBON XEROGELS AS ALTERNATIVE Pt-SUPPORTS FOR THE SELECTIVE HYDROGENATION OF CITRAL (CARBON SUPPORTS) 233

6.1. INTRODUCTION 235
6.2. EXPERIMENTAL 235
6.3. RESULTS AND DISCUSSION 237
6.4. CONCLUSIONS 245
6.5. REFERENCES 246

CAPÍTULO VII: ABOUT THE ACTIVE PHASE SELECTION IN DESIGNING SELECTIVE HYDROGENATION CATALYSTS SUPPORTED ON CARBON XEROGELS MICROSPHERES 251

7.1. INTRODUCTION 253
7.2. EXPERIMENTAL 255
7.3. RESULTS AND DISCUSSION 257

7.3.1. Morphology and textural characterization 257
7.3.2. Metal-characterization: nature and dispersion 258
7.3.3. Catalytic performance 262

7.4. CONCLUSIONS 269
7.5. REFERENCES 270

CAPÍTULO VIII: DESARROLLO DE NUEVOS MATERIALES COMPUESTOS DE XEROGEL DE CARBÓN Y ÓXIDO INORGÁNICO. PATENTES EN TRÁMITE 275

8.1. MÉTODO DE PREPARACIÓN DE MATERIALES COMPUESTOS ÓXIDO INORGÁNICO – CARBÓN Y SUS APLICACIONES EN EL DESARROLLO DE CATALIZADORES ESPECÍFICOS PARA LA HIDROGENACIÓN SELECTIVA DE α,β-INSATURADOS 281

8.1.1. Origen de la invención 285
8.1.2. Grado de difusión de la invención 286

8.1.3. Estado de la técnica 286
8.1.4. Objeto de la invención 290
8.1.5. Aplicaciones de la invención 293
8.1.6. Descripción general de la invención 294
8.1.7. Grado de desarrollo de la invención 297
8.1.8. Proyecto de desarrollo tecnológico de la invención 297
8.1.9. Explotación y comercialización de la patente 297
8.1.10. Bibliografía 298

8.2. MÉTODO DE PREPARACIÓN DE MATERIALES COMPUESTOS ÓXIDO DE ZIRCONIO-CARBÓN Y SUS APLICACIONES COMO FOTO-CATALIZADORES ACTIVOS EN LA DEGRADACIÓN DE COMPUESTOS ORGÁNICOS 307

8.2.1. Origen de la invención 311
8.2.2. Grado de difusión de la invención 312
8.2.3. Estado de la técnica 312
8.2.4. Objeto de la invención 314
8.2.5. Aplicaciones de la invención 317
8.2.6. Descripción general de la invención 318
8.2.7. Grado de desarrollo de la invención 319
8.2.8. Proyecto de desarrollo tecnológico de la invención 320
8.2.9. Explotación y comercialización de la patente 320
8.2.10. Bibliografía 321

8.3. FOTO-CATALIZADORES ESTRUCTURADOS CON ALTO RENDIMIENTO BAJO RADIACIÓN VISIBLE BASADOS EN RECUBRIMIENTOS DE MICROESFERAS DE XEROGEL DE CARBÓN CON ÓXIDO DE TITANIO 325

8.3.1. Origen de la invención 329
8.3.2. Grado de difusión de la invención 330
8.3.3. Estado de la técnica 330
8.3.4. Objeto de la invención 334
8.3.5. Aplicaciones de la invención 336

8.3.6. Descripción general de la invención....338
8.3.7. Grado de desarrollo de la invención....340
8.3.8. Proyecto de desarrollo tecnológico de la invención....340
8.3.9. Explotación y comercialización de la patente....341
8.3.10. Bibliografía....341

CAPÍTULO IX: A PRELIMINARY STUDY ABOUT THE FUNCTIONALIZED CARBON XEROGEL IN OSTEOCYTES GROWTH....349

9.1. INTRODUCTION....351
9.2. EXPERIMENTAL....353
9.2.1. Preparation of carbon xerogel spheres....353
9.2.2. Preparation of composites carbon xerogel spheres - carbon nanofibers....353
9.2.3. Functionalization of carbon samples....354
9.2.3.1. Tour reaction....354
9.2.3.2. Prato reaction....355
9.2.4. Characterization of the samples....357
9.2.4.1. Morphology of A8NF samples....357
9.2.4.2. Textural characterization....357
9.2.4.3. Chemical characterization....358
9.2.4.4. Functionalization degree....358
9.2.4.5. Thermogravimetric analysis....359
9.2.4.6. Toxicity tests on osteocytes....360
9.3. RESULTS AND DISCUSSION....361
9.3.1. Characterization of A8NF samples....361
9.3.2. Functionalization degree of A8NF samples....364
9.3.3. Cells viability test....365
9.4. CONCLUSIONS....367
9.5. REFERENCES....369

Capítulo I

INTRODUCCIÓN

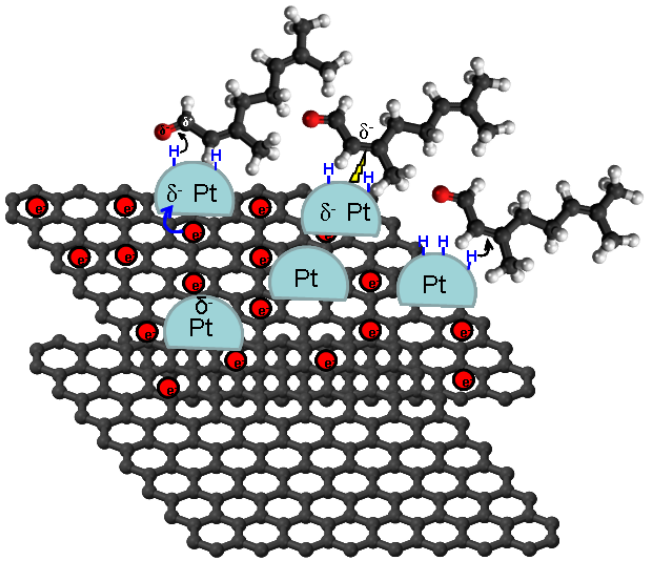

1.1. AEROGELES Y XEROGELES DE CARBÓN

Los geles de carbón son carbones nanoestructurados obtenidos por carbonización de geles orgánicos tradicionalmente preparados mediante policondensación sol-gel de monómeros orgánicos como el resorcinol (R) y formaldehido (F)[1]. Estos materiales tienen una gran versatilidad dado su control estructural tanto a nivel nanoscópico como microscópico, así como por sus características químicas superficiales, teniendo además una composición química completamente conocida. Tanto su área superficial, volumen de poros y distribución de tamaño de poros pueden ser controladas dependiendo de las condiciones de síntesis dando lugar a un amplio abanico de materiales con propiedades únicas. Los geles de carbón pueden prepararse en varios formatos, como monolitos, polvo, formando parte de recubrimientos o como películas delgadas, lo que facilita su aplicabilidad. Por todo lo anteriormente expuesto, los geles de carbón son unos materiales muy versátiles e interesantes para su aplicación en procesos de adsorción y catálisis.

En aplicaciones catalíticas, el inconveniente de otros materiales de carbono como el carbón activado, es la presencia de impurezas inorgánicas que pueden interferir dando lugar a reacciones secundarias y consecuentemente, afectando a la selectividad de los productos deseados. Este aspecto se evita con el uso de geles de carbón, dada la elevada pureza química de los reactivos usados en la síntesis. Por otro lado, la estructura porosa juega un papel determinante en los modos de adsorción de la moléculas de reactivos y productos, de ahí que un control de ésta pueda mejorar la selectividad hacia el/los productos deseados.

Los geles de carbón están formados por partículas primarias interconectadas. Su microporosidad se debe a su estructura intra-particular, mientras que la meso y macroporosidad se debe a los espacios entre partículas (estructura inter-particular), por lo tanto, la estructura microporosa y mesoporosa puede ser controlada independientemente en función de las condiciones de síntesis.

A continuación se analizan los aspectos fundamentales que influyen en el diseño de los geles de carbón, y se recogen los principales resultados disponibles en la literatura acerca de la preparación de geles de carbón dopados con metales y de

materiales compuestos sintetizados a partir de dichos geles. Finalmente se recogen también los resultados principales de la revisión bibliográfica llevada a cabo sobre las dos aplicaciones en catálisis estudiadas en la presente Tesis: hidrogenación selectiva de aldehídos αβ-insaturados y degradación foto-catalítica de contaminantes.

1.1.1. Geles de carbón: preparación y propiedades superficiales

Los geles de carbón son materiales obtenidos a partir de la carbonización de geles orgánicos. Estos geles orgánicos se sintetizan mediante policondensación de ciertos monómeros orgánicos, siguiendo multiples variaciones del proceso sol-gel originalmente desarrollado por Pekala y col.[1], que empleaba resorcinol y formaldehído en medio acuoso en presencia de un catalizador de polimerización básico (Na_2CO_3). En estas condiciones la policondensación de resorcinol y formaldehído transcurre en dos etapas: una reacción de adición de moléculas F a las posiciones libres del anillo aromático de R (posiciones 2, 4 y 6) formando derivados hidroximetil–R, seguido por una reacción de condensación a través de los grupos hidroxílicos, por lo que el subproducto de condensación es agua. Se forman así estructuras poli-aromáticas, en las cuales los anillos están enlazados entre sí mediante puentes metilen ($–CH_2–$) y metilén-éter ($–CH_2–O–CH_2–$). La reacción de adición está catalizada por bases mientras que la de condensación está catalizada por ácidos. Así pues, la policondensación de R-F produce *clusters* de macromoléculas que crecen reaccionando unos con otros hasta formar partículas coloidales. Inicialmente estas partículas coloidales son independientes y están formando un sol (Figura 1.1), que por movimiento Browniano comienzan a agregarse debido a la reacción de sus grupos superficiales[2], formando un gel con una estructura entrelazada.

El proceso de síntesis de los geles de carbón consta pues de tres etapas fundamentales las cuales se esquematizan en la Figura 1.1:

i) Preparación de la mezcla, polimerización, gelificación y curado

ii) Secado del hidrogel formado en la etapa anterior

iii) Carbonización del gel orgánico seco, el cual a veces es sometido posteriormente a un proceso de activación.

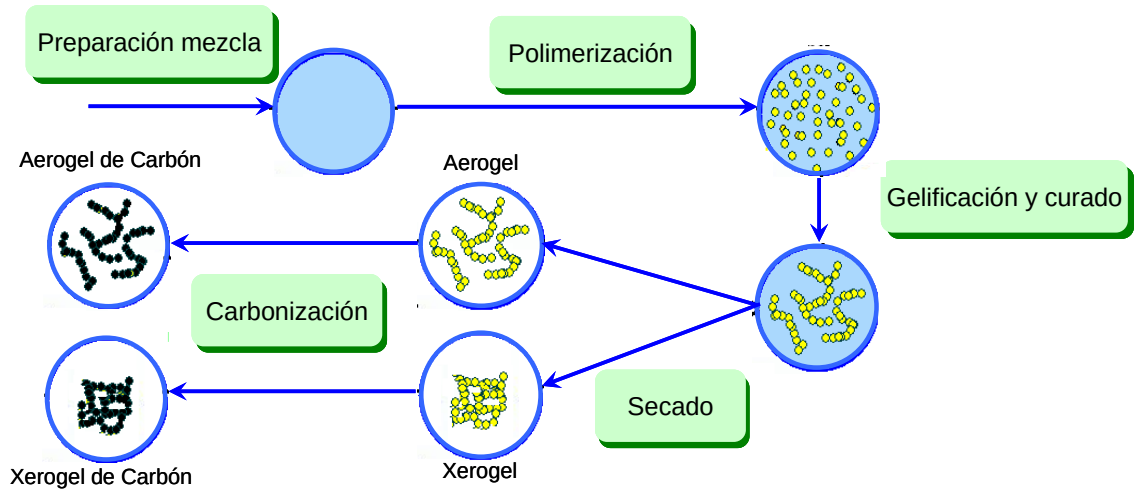

Figura 1.1. Esquema de síntesis de los geles de carbón.

La textura porosa de estos materiales, y consecuentemente sus aplicaciones, va a depender de las condiciones experimentales de cada una de estas etapas, como se resume a continuación.

1.1.1.1. Preparación de la mezcla, gelificación y curado

En esta primera etapa se mezclan los monómeros orgánicos, que como ya se ha comentado anteriormente son fundamentalmente resorcinol (R) y formaldehído (F), en una relación molar dada y utilizando un disolvente que puede ser agua (W), o un disolvente orgánico (alcohol). Además, se adiciona un catalizador de polimerización (C), normalmente carbonatos de metales alcalinos. La variación de las proporciones molares de los diferentes reactivos afecta fuertemente a las propiedades del gel formado. Los principales parámetros que afectan a la polimerización R-F son las relaciones molares R/F, R/W y R/C, el pH y la temperatura. La influencia de estos parámetros se comenta brevemente a continuación.

El parámetro más importante sería la relación molar R/F pues afecta directamente a la polimerización. La relación R/F = 1:2 es la más empleada[1], ya que es con la que se obtienen mejores características texturales. La relación R/F = 1:1 produce poca densidad de entrecruzamientos y la 1:3 induce a un efecto de dilución, ya que no todo el formaldehído se incorpora a la estructura física del polímero que se va formando por razones estéricas.

El cambio de la relación molar R/C, así como del tipo de catalizador empleado afecta también enormemente a las propiedades texturales del gel obtenido, de modo que con un simple cambio de este parámetro se puede pasar de un gel exclusivamente microporoso a un gel mesoporoso o macroporoso. El uso de una baja relación molar R/C (alta concentración de catalizador) genera un gran número de partículas primarias de pequeño tamaño ampliamente interconectadas entre sí, generando poros pequeños entre las partículas. Por el contrario, a relaciones R/C altas (baja concentración de catalizador) se generan partículas primarias más grandes interconectadas entre sí generando así porosidad más ancha. Además, el tipo de catalizador empleado afecta a dichas propiedades texturales. Morales-Torres y col.[3] muestran que la naturaleza del catión empleado, cuando se usa carbonatos alcalinos como catalizador, afecta significativamente a la estructura porosa de los geles. Los autores observan que, a pesar de que la concentración de carbonato es constante en todos los casos, el grado de solapamiento entre las partículas primarias aumenta paulatinamente con el tamaño del catión alcalino presente, es decir, en el sentido Li-Cs, favoreciendo así la formación de *clusters* de partículas que a su vez dejan espacios mayores entre ellos[3].

La elección de un disolvente orgánico frente al agua tiene la ventaja de eliminar la etapa de intercambio de disolvente previo al secado supercrítico, necesaria cuando utilizamos agua como disolvente. Además la elección del disolvente afecta también a la cinética de polimerización[4], y consecuentemente al tamaño de partícula, morfología y porosidad de las muestras.

Otro parámetro de síntesis que afecta a las características de los geles es el valor del pH de la mezcla[1,5]. A valores de pH muy bajos se produce la precipitación de los reactantes, mientras que a valores de pH muy altos se dificulta la reacción de condensación. Los valores de pH utilizados para la síntesis de estos materiales están en el rango de 5,4–7,6. En dicho intervalo, la superficie y la porosidad de los aerogeles aumentan a medida que lo hace al valor de pH.

Así, una vez preparada la mezcla, el proceso de polimerización y curado se lleva a cabo, comúnmente, en un molde cerrado sometiendo dichos moldes a una secuencia consistente en diferentes periodos a distintas temperaturas, en los cuales, se

produce la formación inicial de clústeres seguido del posterior entrecruzamiento de mismos generándose así la estructura del gel.

1.1.1.2. Secado del hidrogel

Esta etapa es crucial para mantener las propiedades texturales del gel orgánico obtenido en la primera etapa. La eliminación del disolvente se puede realizar por evaporación térmica (dando lugar a xerogeles), por congelación y posterior sublimación (criogeles), o reemplazando los disolventes por fluidos supercríticos (aerogeles). El secado térmico causa un colapso importante de la estructura macro y meso-porosa debido a las tensiones generadas en el interior de los poros por el menisco formado en la interfase líquido-vapor. Recientemente se ha puesto de manifiesto que un secado térmico precedido de un adecuado intercambio previo del agua de los hidrogeles por acetona, minimiza notablemente el colapso de la meso-macro porosidad[6]. Este colapso puede reducirse mediante el método de congelación-sublimación del disolvente que evitaría la formación de la interfase vapor-líquido, aunque no es recomendable (en materiales monolíticos) cuando el disolvente es agua debido a que la expansión del volumen que ésta presenta en fase sólida genera grietas en el material.

La mejor estrategia para preservar la estructura porosa del hidrogel durante la etapa de secado es el empleo de fluidos supercríticos[6], como el CO_2. Sin embargo estos procesos tienen la desventaja de necesitar de altas presiones para trabajar a temperaturas moderadas, y por tanto implica un mayor coste del proceso de síntesis que encarece notablemente el precio final de los aerogeles de carbón, lo que dificulta la implantación de estos materiales en procesos a nivel industrial.

1.1.1.3. Carbonización

Tras el secado del gel orgánico se lleva a cabo una carbonización o pirólisis para obtener el correspondiente gel de carbón. Durante este proceso el gel es calentado en atmósfera inerte entre 500 y 1500 ºC. Este proceso afecta a las propiedades texturales del material debido a un proceso de encogimiento y a la liberación de gases desde el interior del material.

Finalmente, los geles de carbón, como cualquier otro material carbonoso, pueden ser sometidos a procesos de activación para incrementar el volumen poros, la anchura de poro y el área superficial.

1.1.2. Dopado de los geles de carbón

Los geles de carbón dopados con metales pueden obtenerse siguiendo dos métodos: i) adicionando un precursor metálico a la mezcla inicial resorcinol-formaldehido[7,8], o bien ii) mediante intercambio iónico, es decir, con el uso de un derivado de resorcinol funcionalizado que actúe como sitio de anclaje de metales dopantes después de haber obtenido el gel[9,10]. En cualquier caso, cuando el precursor metálico se adiciona a la mezcla inicial R-F, la estructura porosa de la matriz carbonosa se ve afectada por la presencia de éste, ya que el precursor metálico no solo afecta al pH inicial sino también a la química del proceso sol-gel, a la pirólisis del gel orgánico y a la activación del aerogel de carbón.

Los geles de carbón dopados con metales son materiales muy interesantes que presentan diversas aplicaciones. Pueden utilizarse como catalizadores tanto en fase gas como en fase líquida, presentando en este último caso menores pérdidas de fase activa por lixiviación que los catalizadores tradicionalmente obtenidos mediante técnicas de impregnación[11,12]. También presentan una mayor conductividad eléctrica que los geles no dopados lo que aumenta su uso potencial como electrodos, o como electro-catalizadores[13]. Actualmente, se está investigando su aplicación como electrodos para supercondensadores[14-20]. Finalmente, cabe recordar que pueden emplearse también en procesos de adsorción; en este caso el dopante favorece la obtención del tamaño y distribución de porosidad deseada[21] o bien ayuda en el proceso de adsorción por interacción con el adsorbato[22].

En su aplicación como catalizadores, los geles de carbón dopados presentan una serie de ventajas, y alguna desventaja, frente al empleo de catalizadores soportados preparados por impregación. Si en la preparación de geles dopados el precursor metálico se adiciona a la mezcla inicial, las partículas metálicas se forman junto con la matriz orgánica, principalmente durante la carbonización, de modo que su movilidad queda reducida y consecuentemente, son altamente resistentes a la sinterización y/o

lixiviación. Además, la descomposición del promotor para obtener la fase activa ocurre también durante la carbonización, evitando el pretratamiento necesario al obtener dichos materiales por impregnación. Sin embargo, algunas de estas partículas pueden quedar completamente rodeadas por la matriz orgánica, y por tanto aisladas de los reactivos e inactivas en las reacciones de catálisis.

Moreno-Castilla y col.[23,24] obtienen aerogeles orgánicos dopados con Cr, Cu, Fe, Co y Ni con diferentes propiedades texturales y morfológicas. La morfología de estas muestras consiste en microesferas más o menos fusionadas, de diferente tamaño según el metal empleado como consecuencia del pH inicial de la mezcla inducido por el precursor metálico y su diferente actividad catalítica en el proceso de polimerización. Observan como las partículas de mayor tamaño se obtienen en los aerogeles dopados con Cr (10 micras) donde el pH inicial era fuertemente ácido (1,9), seguido de Cu (2,5 micras) y Fe (0,6 micras) con pH inicial 4.9 y 5.4, respectivamente. En los aerogeles de carbón dopados con Co y Ni donde el pH era cercano a la neutralidad (6,4) se observaron tamaños mucho más pequeños. De este modo, el tamaño de estas partículas determina las características texturales del gel de modo que el solapamiento de las partículas más pequeñas (muestras dopadas con Co y Ni) dan lugar a la presencia de mesoporos, mientras que con las de mayor tamaño solo se obtenien macroporos debido a partículas de mayor tamaño. Los XPS mostraron inequívocamente enlaces del metal con los grupos fenólicos de la superficie de la matriz polimérica.

Estos metales además afectan al proceso de pirólisis y al posterior proceso de activación. Moreno-Castilla y col.[21] analizan este efecto empleando aerogeles dopados con Fe, Co, Ni y Cu junto con una muestra de aerogeles sin dopar. La pirólisis fue seguida mediante la evolución de los perfiles de H_2O, CO_2, CO y CH_4 por espectroscopia infrarroja. Los resultados indicaron que los perfiles de desorción de CH_4 y CO_2, y por tanto la estructura química del aerogel, depende de la naturaleza del metal presente en la mezla original, indicando la participación del metal en la polimerización. Además, el uso de Fe, Co o Ni como metales dopantes produce durante la carbonización una grafitización parcial del aerogel de carbón. Adicionalmente, las muestras dopadas, así como la muestra sin dopar, se activaron con vapor de agua. Así, la activación de vapor de la muestra sin dopar produjo un aumento importante de su microporosidad, y por consiguiente de su área superficial, mientras que la meso y

macroporosidad no se vio afectada en la misma medida. En el caso de la muestra dopada con Fe, con aproximadamente el mismo porcentaje de activación que la muestra sin dopar, la activación de vapor afectó en gran medida al desarrollo de su volumen de meso y macroporos y tuvo un efecto mucho menor sobre su volumen de microporos. El mismo fenómeno se observó en las muestras dopadas con Co y Ni, aunque sus grados de activación fueron más altos que los de las muestras anteriores debido a que el Co y Ni actúan como catalizadores de gasificación durante el tratamiento con vapor. Este efecto fue también observado por los mismos autores en la activación con vapor de agua de aerogeles de carbón dopados con Pt, Pd y Ag[7], observando un gran incremento de los volúmenes de mesoporos y macroporos, así como un mayor porcentaje de activación en el aerogel dopado con Pt frente al material sin dopar, debido a que el Pt actúa como catalizador de gasificación.

Del mismo modo, Bekyarova y col.[25] ponen de manifiesto que el dopado no solo afecta al pH inicial de la mezcla y de ahí a las propiedades texturales del gel, sino que además la naturaleza del metal dopante afecta a la química del proceso sol-gel y por tanto a la estructura del gel. Estos autores preparan aerogeles dopados con Zr y Ce obteniendo, a pesar del mismo pH de la solución, propiedades texturales muy diferentes: el dopado con Zr da lugar a aerogeles microporosos con moderadas áreas superficiales, mientras que con el dopado con Ce obtuvieron materiales con baja área superficial y muy baja microporosidad.

Una estrategia para evitar o paliar en gran media el que parte de las partículas metálicas queden atrapadas en la red carbonosa del gel dopado, y no puedan ser accesibles a los reactivos, es adicionar el metal tras la polimerización, pero antes del curado, y así las partículas metálicas se forman exclusivamente en la superficie externa del gel.

A su vez, el uso de surfactantes en la síntesis del gel permite un mejor control estructural de éste. La molécula de surfactante (S) se incorpora a la estructura química del polímero RF, formando estructuras RFS que ofrecen sitios de anclaje del metal[26]. Recientemente Maldonado-Hódar y col.[27,28] han incorporado surfactantes a la disolución de R-F, favoreciendo así que las especies MoO_4^{2-} se anclen en los sitios generados por el surfactante en el posterior dopado con Molibdeno. De este modo, las

partículas metálicas se forman solo en la superficie del gel pero fuertemente ancladas al soporte. Además, muestran que la naturaleza del surfactante influye enormemente en las interacciones entre los aniones molibdato con los centros activos, y por tanto en la cantidad de metal anclado en la superficie. Se observa que el uso de surfactantes catiónicos, o no iónicos, favorecen interacciones atractivas entre los iones molibdato con el hidrogel mediante interacciones electrostáticas, o la presencia de grupos oxigenados superficiales activos, respectivamente. En el caso del surfactante aniónico, se generan interacciones repulsivas con los aniones molibdato por lo que se consiguen menores cargas metálicas. Además, la adición del surfactante afecta a las propiedades texturales y morfología del gel. De modo que el uso de surfactantes en la síntesis de xerogeles de carbono es ciertamente una estrategia novedosa en la adaptación de las características de este tipo de material.

Por otro lado, se han obtenido materiales compuestos carbón - óxido inorgánico, de gran interés en aplicaciones foto-catalíticas o electro-catalíticas, donde el óxido se encuentre íntimamente ligado a la estructura carbonosa, mejorando las propiedades electrónicas de éstos debido a diversos factores que se analizarán en detalle en la Sección 1.3 de esta Introducción. Moreno-Castilla y col.[29-31] sintetizaron materiales compuestos SiO_2, Al_2O_3 y TiO_2 - gel de carbón induciendo la hidrólisis de un alcóxido metálico en la mezcla R-F, bajo agitación y a una temperatura controlada. La matriz carbonosa influyó en la fase cristalina obtenida. En el caso del material compuesto C - TiO_2, una carbonización a 900 ºC, temperatura a la cual es estable la fase rutilo, detectaron una mezcla de anatasa y rutilo. Por tanto, la matriz carbonosa no solo minimizó la sinterización de las nanopartículas de óxido de titanio sino que de alguna manera estabilizó la fase anatasa.

Para aplicaciones en fase líquida, como es el caso de la hidrogenación selectiva de compuestos α,β-insaturados, o la foto-degradación de contaminantes en fase líquida, se precisa de materiales mesoporosos para maximizar el contacto con los reactivos. En este sentido, se están realizando grandes esfuerzos en la síntesis de materiales compuestos mesoporosos óxido de titanio-carbón. La principal estrategia utilizada en este caso consiste en el empleo de materiales plantilla (por ejemplo SiO_2 o surfactantes), que durante la síntesis del gel posibiliten la generación de la mesoporosidad. El inconveniente de este método es que durante la posterior

eliminación de la plantilla se produce un bloqueo o colapso de la mesoporosidad generada[32,33], por lo que la puesta a punto de nuevas estrategias de síntesis, para este tipo de materiales compuestos, se considera no solo necesario sino especialmente relevante.

A continuación, se recogen los resultados más relevantes encontrados en la bibliografía consultada sobre la hidrogenación selectiva de citral, catalizada por metales soportados sobre materiales de cabón. El citral es el aldehído α,β-insaturado cuya hidrogenación selectiva ha sido más extensamente estudiada en la presente Tesis, de ahí que se le haya prestado una atención especial en este Capítulo introductorio. Esta revisión bibliográfica ha dado lugar a la publicación de un artículo en la revista Catalysts, 3 (2013) 853-877, el cual se expone tal cual como Sección 1.2 del presente Capítulo.

CATALYSTS SUPPORTED ON CARBON MATERIALS FOR THE SELECTIVE HYDROGENATION OF CITRAL

Article published in Catalysts, 3 (2013) 853-877, doi:10.3390/catal3040853

catalysts

ISSN 2073-4344

www.mdpi.com/journal/catalysts

Review

Catalysts Supported on Carbon Materials for the Selective Hydrogenation of Citral

Abstract: The heterogeneously catalyzed selective-hydrogenation of citral is one of the more feasible ways for obtaining its appreciated unsaturated-alcohols, nerol and geraniol, which are present in over 250 essential oils. Thus, citral has very recently come to be produced petro-chemically in very large quantities, and so partial hydrogenation of citral has become a very economical route for the production of these compounds. However, the selective hydrogenation of citral is not easy, because citral is an α,β-unsaturated aldehyde which possesses three double bonds that can be hydrogenated: an isolated C=C bond and the conjugated C=O and C=C bonds. For this reason, in catalyst selection there are several important issues which affect the product selectivity, for example, the active metal and metal particle size which are factors related to the catalyst preparation method, catalyst precursor, or support surface area, as well as other factors such as porosity, the addition of a second catalytic metal, and, of course, the type of catalyst support. About this last one, carbon materials are very interesting supports for this type of hydrogenation reaction due to their unique chemical and textural properties. This review collects and analyzes the results obtained in the selective hydrogenation of citral catalyzed by carbon material supported metals.

Keywords: citral; hydrogenation; activated carbon; graphite; carbon nanotubes

Abstract

The heterogeneously catalyzed selective-hydrogenation of citral is one of the more feasible ways for obtaining its appreciated unsaturated-alcohols, nerol and geraniol, which are present in over 250 essential oils. Thus, citral has very recently come to be produced petro-chemically in very large quantities, and so partial hydrogenation of citral has become a very economical route for the production of these compounds. However, the selective hydrogenation of citral is not easy, because citral is an α,β-unsaturated aldehyde which possesses three double bonds that can be hydrogenated: an isolated C=C bond and the conjugated C=O and C=C bonds. For this reason, in catalyst selection there are several important issues which affect the product selectivity, for example, the active metal and metal particle size which are factors related to the catalyst preparation method, catalyst precursor, or support surface area, as well as other factors such as porosity, the addition of a second catalytic metal, and, of course, the type of catalyst support. About this last one, carbon materials are very interesting supports for this type of hydrogenation reaction due to their unique chemical and textural properties. This review collects and analyzes the results obtained in the selective hydrogenation of citral catalyzed by carbon material supported metals.

1.2. CATALYSTS SUPPORTED ON CARBON MATERIALS FOR THE SELECTIVE HYDROGENATION OF CITRAL

1.2.1. Introduction

Since ancient times, essential oils and extracts have been used for many different applications such as perfumes, air fresheners, cosmetics and medicinal substances. These compounds were mainly extracted by steam distillation or solvent extraction of different vegetable raw materials. These essential oils consist primarily in terpenes, where their unsaturated alcohols play a very important role. In particular, nerol and geraniol are present in over 250 essential oils as ninde oil (66.3%)[34], rose oil (59.0%)[35], palmarosa oil (80.9% geraniol in leaf)[36], monarda fistulosa oil (>95%)[37], citronella oil (24.8%)[38], among other essential oils.

Geraniol was isolated from palmarosa oil while nerol was obtained from the oil of neroli[39,40]. These monoterpenes are widely used in fragrance and flavour industries. A survey of consumer products between 1996–2001 revealed that they are present in 76% of 73 investigated deodorants on the European market—95% in vapo-spray deodorants, 91% in aerosol sprays deodorants and 46% in roll-on deodorants[41]—in the 41% of 59 investigated domestic and occupational products[42], and in the 33% of cosmetic formulations[43], their production in that year being more than 1000 metric tons[44]. In addition, recent studies revealed that geraniol exhibits various biochemical and pharmacological properties as a potential antimicrobial agent[45], an effective plant based insect repellent (currently being marketed by Fulltec® and BugBand®, for example)[46-48], an anti-inflammatory[49], anthelmintic[50,51], anti-oxidant[52,53] and anti-herpetic agent[54], and furthermore, geraniol exerts *in vitro* and *in vivo* antitumor activity against murine leukemia, hepatoma and melanoma cells[55-59]. Furthermore, this molecule is an important intermediate in the synthesis of other organic molecules with high added value[60] such as phellandrene, myrcene, ocimene, linalool and vitamins A and E[61].

This increase in the use of geraniol and nerol makes necessary a chemical synthesis of this compound. Actually, the industrial production of these compounds is mainly done from β-pinene by companies such as International Flavors and Fragrances

(IFF), Pinova, DRT and TECNAL Corporation[62,63]. This process[64], shown in Figure 1.2, involves the pyrolysis of β-pinene, which yields 90% myrcene by passing it through a tube at 550–600 °C with a very short contact time. Then, in a second step (myrcene hydrochlorination), hydrogen chloride is added to myrcene in the presence of a small amount of cuprous chloride catalyst and an organic quaternary ammonium salt to effect a preferential addition at the allylic double bond resulting in the formation of a higher proportion of geranyl or neryl chloride, linalyl chloride and a little myrcenyl chloride. After removal of the catalyst, the crude mixture of chlorides is converted to a mixture of acetates (or formates) by addition of sodium acetate or sodium formate with a phase-transfer catalyst (PTC) or in the presence of a nitrogen base to give predominantly geranyl acetate (50%–55%), neryl acetate (40%–50%) and small amount of linalyl acetate. Saponification of the acetates or formates gives the corresponding alcohols and the sodium acetate or formate which is recycled. Fractionation of the crude alcohol mixture gives both geraniol and nerol products, usually as mixtures. Further fractional distillation yields about 98% geraniol[63,64].

The drawback of the industrial manufacturing process is the multitude of needed stages, including a pyrolysis, with the difficulties that it entails, the need of large amount of reagents, and the corresponding loss of performance of each stage. For these reasons, the selective hydrogenation of citral is one of the more feasible ways for obtaining these unsaturated alcohols being a single step synthesis. Furthermore, citral has very recently come to be produced petrochemically in very large quantities, and so partial hydrogenation of citral has become a very economical route for the production of geraniol and nerol[64]. Therefore, the hydrogenation of citral is attracting the attention of a large number of scientists worldwide. Citral (3,7-dimethyl-2,6-octadienal) is a monoterpene found in plants and citrus fruits. It is an isomeric mixture of the acyclic aldehydes geranial (citral E) and neral (citral Z).

On the other hand, carbon materials show several advantages when they are used as supports in heterogeneous catalysis and especially in hydrogenation reactions[65]:

i) Carbon surface is relatively inert, preventing the occurrence of unwanted reactions catalyzed by the support surface or reaction of the support with the active phase.

ii) The cost of conventional carbon materials is lower than other conventional supports.

iii) Carbon materials may be obtained in different forms (granules, pellets, fibers, foams, monoliths, fabrics, coatings, *etc.*)

iv) The active phase, usually expensive, can be easily recovered by simple calcination of the support.

v) They have a high surface area and its porous framework can be modified to obtain the pore size distribution (PSD) optimum for each particular reaction.

vi) They are stable at high temperatures in non-oxidizing atmospheres (even above 700 °C).

vii) Although carbon is usually a material with a hydrophobic nature, the chemical nature of their surface can be modified chemically to give them some hydrophilicity.

Despite all these advantages, carbon materials are not the main supports studied in the hydrogenation of citral as derived from the reviewed literature, being these mentioned only in 17% of the reviewed literature, and mainly they are used as reference materials. Within the carbon materials, the classical materials have been the most studied in the selective hydrogenation of citral (activated carbons and graphite were studied in the 57% and 19% of the citations, respectively). However, nowadays non-traditional carbon materials such as carbon nanotubes are widely being studied for this application (21% of the reviewed literature), and finally some works using advanced composite materials like Carbon-TiO_2 can also be found. Although carbon xerogels and aerogels are very interesting carbon materials especially as catalyst supports[66-70], we have not found works in the reviewed literature where they have been used in the selective hydrogenation of citral. Moreover, only a few works mention these materials for the hydrogenation of α,β unsaturated aldehydes[71-73].

Finally, it should be mentioned that in the catalyst selection for the citral hydrogenation, there are several important issues which affect the product selectivity, such as the active metal[74-77], the metal-particle size[76,78-80], the support material or the use of bimetallic catalysts[78,81-83], as well as other factors relating to the operating conditions as the used solvent, which is important in the formation of acetals, the stirring, the operation temperature and pressure as well as the initial concentrations.

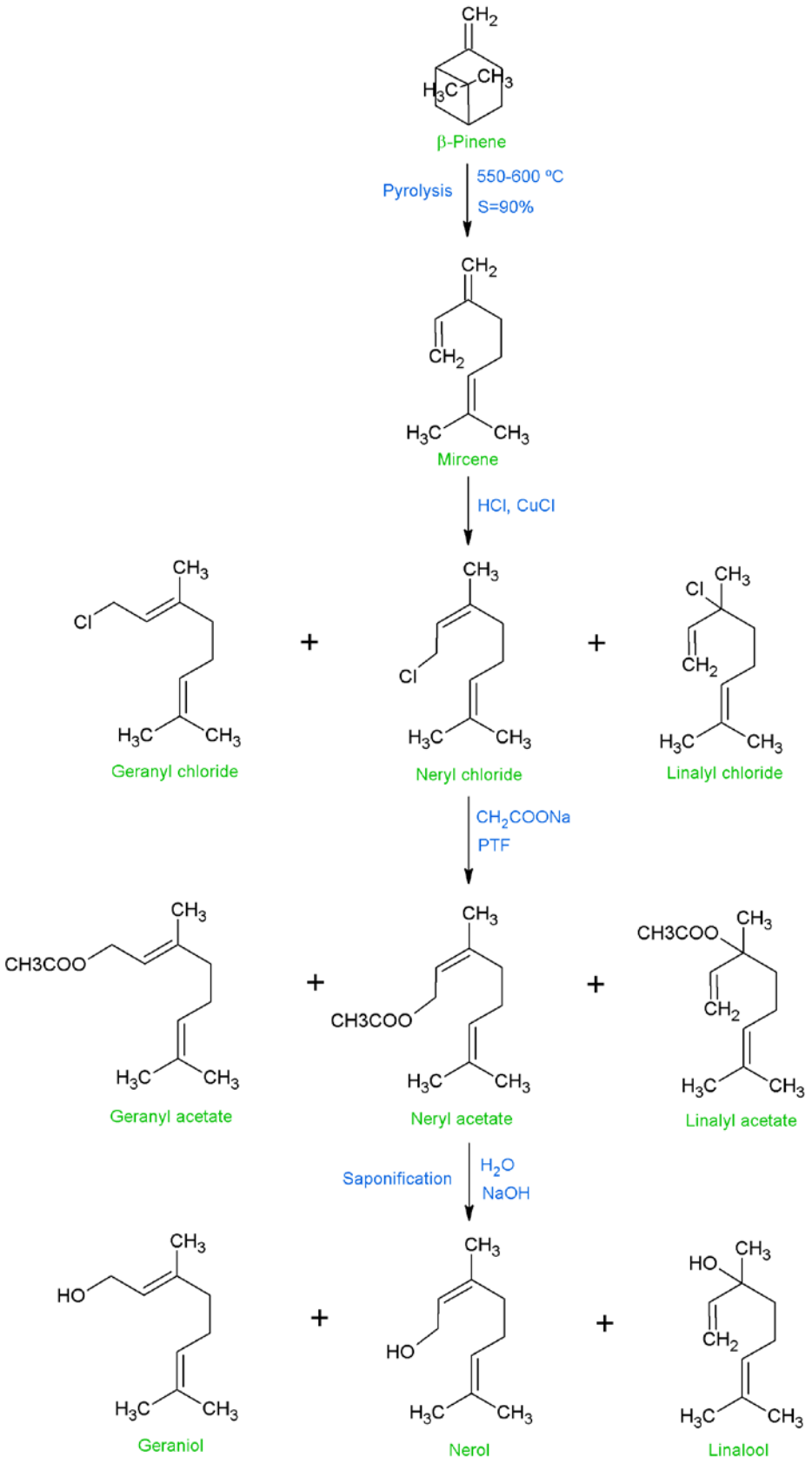

Figure 1.2. Industrial-scale production process of nerol and geraniol. Powered by International Flavors and Fragrances (IFF), Pinova, and Dérivés Tecnal Résiniques et Terpéniques (DRT). Adapted from H. Surburg, *et al.*[64]

In this review, a widely used explanation about the different and possible reaction routes during the hydrogenation of citral, as well as a deep review of the role in the activity and selectivity of the main transition metal as catalyst in this reaction are shown. The more significant results using carbon materials, as catalyst supports in the selective hydrogenation of citral, have been collected. These results are shown and discussed by type of material, and finally, some challenges for the future are proposed.

1.2.2. Hydrogenation selectivity

The selective hydrogenation of citral to nerol and geraniol is not easy, because citral is an α,β-unsaturated aldehyde which possesses three double bonds that can be hydrogenated: an isolated C=C bond in addition of the conjugated bonds C=O and C=C. A completed reaction scheme is shown in Figure 1.3. Thermodynamics favors hydrogenation of the C=C over the C=O bond[84], and for kinetic reasons, the C=C bond is more reactive than the C=O group[84]. Therefore, in the presence of most of the monometallic catalysts based on VIII group elements, the saturated aldehyde or alcohol is obtained[85,86]. Consequently, the challenge is to selectively enhance the hydrogenation of the C=O bond to produce nerol and geraniol, decreasing in parallel the hydrogenation of the corresponding conjugated C=C bond reducing the formation of citronellal, and what is even more difficult, to avoid consecutives hydrogenations to single unsaturated or saturated alcohol (citronellol and 3,7 dimethyloctanol, respectively), as well as to avoid cyclization routes which produces isopulegol and its saturated alcohol menthol. Finally, other undesired reactions can take place with the use of some reaction media, such as alcohols, which can create citronellal acetals. Therefore, a highly selective hydrogenation process to nerol and geraniol can only be achieved with an optimal design of the catalyst. Nowadays, the more extended proposal for this goal turn around to activate the adsorption modes of C=O group and/or prevent the adsorption modes of C=C group[87]. In this way, Figure 1.4 shows the different adsorption modes of the molecule of citral[88].

The knowledge of the adsorption modes is very important for understanding the selectivity of the hydrogenation of the α,β-unsaturated aldehydes. Basically, there are three basic ways to obtain the hydrogenation of the C=O bond and, hence, the desired unsaturated alcohol: (i) the first is to hinder the C=C molecular adsorption. This

hindrance can be achieved by an increase of the repulsive electron interactions with the surface using metals with more extended d-orbitals like osmium or iridium, or increasing the (111) face presence in the metal surface, and finally, also using an electronically dense surface by means of an active support (i.e. graphite). (ii) The second way is to favor the interaction of the C=O bond with the surface using Lewis acid promoters as for example the partially reducible oxides TiO_2 or CeO_2 in which new acid Lewis sites can be created by oxygen vacancies. (iii) The third way is a combination of both mentioned strategies, favoring the C=O adsorption and hindering the C=C adsorption at the same time. This would be achieved combining satisfactory electropositive and electronegative metals which produces a charge transfer between them that favors the electronic repulsion against the C=C adsorption, being equally created polarized sites δ^+-δ^- that favor the interaction with the C=O bond[88].

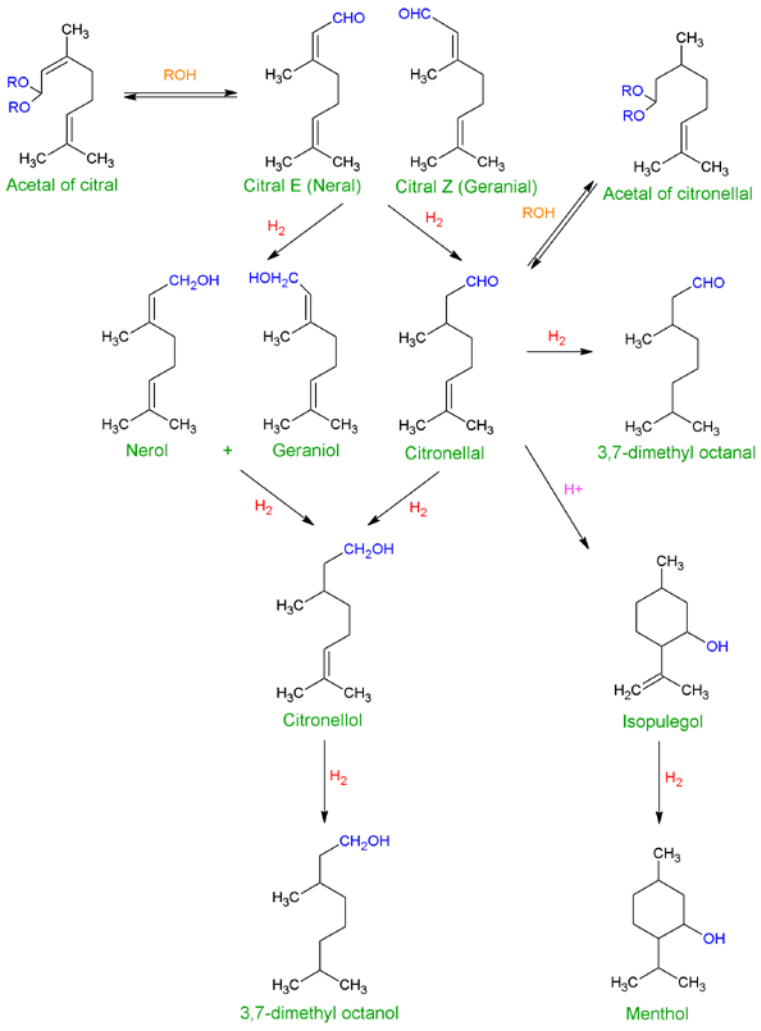

Figure 1.3. Reaction scheme of the citral hydrogenation. Adapted from T. Ekou, *et al.*[89]

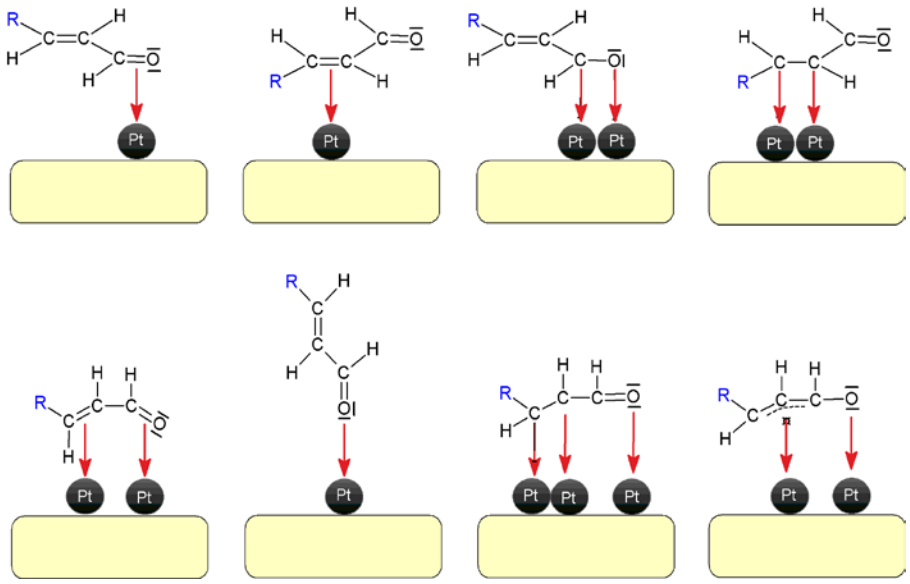

Figure 1.4. Adsorption modes of the α,β-unsaturated aldehyde molecule. Adapted from P. Claus.[88]

Also, other factors relating to the catalytic system should be considered such as the solvent. The solvent is important not only for preventing the formation of acetals, but also because it could affect the selectivity and the hydrogenation rates. Generally, the higher is the polarity of the solvent, the higher is the hydrogenation rates, due to an increase of the H_2 solubility in the solvent[90-92]. Related to the product distribution, some authors have obtained a trend modifying the polarity of the solvent. Polar solvents activated the C=O hydrogenation whereas non-polar solvents favored the C=C bond hydrogenation over non acidic catalysts to avoid the acetals formation over alcohol solvents[93-95]. Additionally, supercritical CO_2 has been used as non-conventional solvent due to its important benefits such as: (i) the higher solubility of hydrogen than conventional solvents; (ii) much easier separation after reaction; (iii) and the improvement of selectivity in the C=O hydrogenation. The higher selectivity towards the unsaturated alcohols using supercritical CO_2 has been ascribed to specific interactions between CO_2 and the citral molecules[96-98].

Another way to favor the C=O interaction with the catalyst may be achieved by adding a water film to the surface of the catalysts. In this sense, Jiang *et al.*[99] used a combination of Ru/AlO(OH) and water improving the catalyst activity and its selectivity to geraniol and nerol. The interactions between water molecules and the surface hydroxyl groups of the support made possible a water film adhesion around the

catalyst particles. This water favoured the citral adsorption throughout the C=O bond due to its more polarized bond character. In a similar way, with SLPC (supported liquid-phase catalyst) the selectivity towards the unsaturated alcohols can be modified adding water (or another polar solvent) to an organic media[100,101]. The drawback of this type of methodology is that the entire surface should be covered by water in order to maintain the desired selectivity[102].

1.2.3. The type of transition metal as catalytic phase

In the hydrogenation of α,β-unsaturated aldehydes, usually transition metals supported on oxides or carbon materials are used as catalysts. The selection of the catalytic phase is very important due to its influence on the product's selectivity. In general, Ir and Os catalysts show moderately high selectivities to C=O hydrogenation, while Pt, Ru and Co possess moderate selectivities and Pd, Rh and Ni are unselective or poorly selective to the unsaturated alcohol. These trends were confirmed by Sokolskii *et al.*[103,104] in the crotonaldehyde hydrogenation with catalysts supported on carbon finding the following selectivity trend to the unsaturated alcohol: Os > Ir > Ru> Rh ≈ Pt ≈ Pd, and also by Giroir-Fendler *et al.*[74] in the hydrogenation of cinnamaldehyde using coal and graphite as supports finding the trend Ir> Pt> Ru> Rh> Pd with both supports. This increase of selectivity is attributed to an electronic effects according to theoretical calculations of Delbecq and Soutet and semi-empirical calculations of Hückel[87,105]. According to these authors, the selectivity to the unsaturated alcohol can be correlated with the metal d-band width. With increasing electron density and, hence, d-orbital population, the repulsive four electron interaction of the C=C double bond with the metal surface increases, however, the interaction of the metal surface with the C=O π-system is favored[88,106]. Thus, the binding of unsaturated molecules on metal surfaces is based on the distinction between stabilizing two-electron (of the C=O) and destabilizing four-electron interactions (of the C=C)[107]. The C=C coordination is very sensitive to Pauli repulsion with the surface. A metal with more diffuse orbitals will increase the Pauli repulsion and therefore weaken the C=C adsorption. This is the case of Ru and Os which have a large radial expansion of the d orbitals and therefore give a good selectivity to unsaturated alcohol. In contrast, Pd has more contracted d orbitals, and in this case the molecule can easily approach the surface and a flat η4 mode is preferred[108]. As a result, Pd gives a poor selectivity in unsaturated alcohol. The calculated metal d-

band width is Ni< Pd< Ru< Pt< Ir, Os, which is in agreement with the experimentally obtained selectivities toward the unsaturated alcohol[105,109].

In the selective hydrogenation of citral, the above mentioned tendency was also shown by Vannice and Singh[86] who examined the influence of the active metal on the activity and selectivity in the liquid phase hydrogenation of citral at 300 K and 1 atm using silica as support. These researchers found the following trend in activity Pd> Pt> Ir> Os> Ru> Rh> Ni> Co >> Fe and in selectivity was found that Os showed high selectivity to unsaturated alcohols (88%), the Ru and Co showed moderate selectivity (55%) and Rh, Ni and Pd were more selective to citronellal and isopulegol (0% unsaturated alcohols). In turn, Manikandan *et al.*[110] analyzed Pt and Ru catalysts intercalated in a silicate (Montmorillonite) obtaining a selectivity of 60% for Pt and 45% for Ru. Taking into account the literature review collected in Table 1.1 and the results obtained by Vannice and Singh, a reasonable activity trend for the most α, β-unsaturated aldehydes independently of the support and the conditions employed would be the following: Ni< Pd<<< Rh< Ru, Pt, Co< Ir, Os.

With regard to the selectivity, the susceptibility of the Ir to the formation of unsaturated alcohols in the hydrogenation of citral as well as with other aldehydes[111] is not clear. Comparing the results (Table 1.1) for Ir/TiO_2 in the same operating conditions, some authors achieved selectivities as high as 91%–100 % while others get a moderate selectivity of 60%, whereas using other supports like SiO_2, very different selectivities among 100%, 40% or 15% were obtained. However, it seems clear that with Ir catalyst, low conversions are achieved (5%–10 %). Thus, despite that Os and Ir seem to be the most selective to unsaturated alcohols in the hydrogenation of citral, they are the least active. On the other hand, Pt and Ru are the most employed in the literature (they are present in 68% of the reviewed papers): Pt because it shows moderate activity and selectivity, and Ru because it combines an acceptable catalytic performance with the cheapest price among the best metals. Obviously, the ideal would be to achieve a high selectivity with a great conversion without losing sight of the economic factor. For this reason, the challenge is to improve the selectivity of Pt and Ru by adding a second metal or enhancing electronic effects of the support.

Table 1.1. Effect of the type of metal on the selectivity toward the unsaturated alcohol in the selective hydrogenation of citral.

Metal	Support	Tª (°C)	P (Bar)	S (%)	C (%)	Ref.
Rh	TiO_2	70	70	10	100	[112]
Rh	TiO_2	70	70	11	94	[113]
Rh	SiO_2	35	1	5.2	100	[114]
Pt	TiO_2	70	70	58	98	[112]
Pt	TiO_2	90	100	68	95	[115]
Pt	SiO_2	100	20	56	30	[116]
Ir	TiO_2	90	6.2	100	11.2	[117]
Ir	SiO_2	90	6.2	47	5	[118]
Ir	Nb_2O_5	90	6.2	82	15	[119]
Ir	SiO_2	90	6.2	44	3	[119]
Ir	TiO_2	90	6.2	91	10	[118]
Ir	SiO_2	70	4	100	10	[120]
Ir	TiO_2	70	4	100	10	[120]
Ir	SiO_2	27	1	15	5	[77]
Os	SiO_2	27	1	88	5	[77]
Co	TiO_2	90	70	50	80	[75]
Co	C	120	10	60	17	[121]
Au	TiO_2	80	40	16	6	[122]
Ru	TiO_2	80	40	22	15	[122]
Ru	TiO_2	126	50	42	76.8	[123]
Ru	Al_2O_3	126	50	48	12.2	[123]
Pd	TiO_2	80	40	8	27	[122]
Pd	SiO_2	130	70	0	100	[124]
Ni	Al_2O_3	70	1	0	n.d.	[125]
Ni	Cr_2O_3	120	40	0	n.d.	[126]
Ni	Graphite	50	50	0	100	[127]

1.2.4. Carbon materials as supports

In heterogeneous catalysis, the active phase is deposited on a support material which normally is catalytically inert. These supports are usually metal oxides or carbon with the aim of maximizing the specific surface area to achieve a greater dispersion of the active phase. However, the use of micro-mesoporous supports may not be suitable for hydrogenation reactions in liquid phase where hydrogen solubility in the solvent is

small, because when very active metals are used, isomerization reactions may occur to a greater extent than the desired ones due to an immediate decrease of the hydrogen concentration on the active site[128,129]. Sometimes, we find in the literature that selectivity results in these types of reactions—including citral hydrogenation—can be affected by the above mentioned process, but the explanation is attributed to other factors.

1.2.4.1. Activated carbons

The activated carbons are the supports most studied in hydrogenation of citral. These materials do not present electronic effect like the partially reducible oxides, or graphite which could enhance the selectivity towards unsaturated alcohols, but due to their high surface areas they are very interesting for the preparation of bimetallic catalysts. For these reasons, most authors who used activated carbon as support, used them for preparing bimetallic catalysts, or as reference materials.

Galvagno *et al.*[76,130,131] studied the influence of Ru particle size, type or metal precursor and the reaction media, using a commercial activated carbon with a surface area between 900 and 1100 m^2/g by impregnation with $RuCl_3$ and different metal loading. Due to the high surface area of the carbon support, Ru could be dispersed better than using other supports such as Al_2O_3 or SiO_2. Metal particle sizes among 3.7 and 10.3 nm, with Ru loading among 0.5 and 10 wt.% were obtained treating the impregnated catalysts at 300 °C in H_2. They found that the specific catalytic activity per Ru surface atom as well as the product distribution did not depend of Ru particle size supported on the activated carbon. On the other hand, making a catalytic comparison among the supports activated' carbons, Al_2O_3 and SiO_2[76,131], the authors explained that due to the hydrophobic nature of the carbon support, which leads to a weaker interaction between the catalyst and the solvent (ethanol), the poisoning effect on the Ru active sites decreased, and higher amounts of unsaturated alcohols were also obtained.

On the other hand, in other works activated carbons were used to prepare bimetallic catalysts[81,121,132-137] employing their high surface areas to improve the dispersion of the bimetallic clusters. Vilella *et al.*[136] studied the influence of the addition of different Ge and Sn loading to Pt/activated carbon catalysts. These catalysts were

prepared by successive impregnation of the precursor salts (H_2PtCl_6 and $SnCl_2$ or $GeCl_4$). They used a commercial carbon with an apparent surface area of 987 m^2/g and high ash content. The activated carbon was demineralised and a fraction of this was oxidized with a HNO_3 treatment. Pt-Sn catalysts worked better than Pt alone increasing both activity and selectivity towards reaching 78% of selectivity at 70% of conversion. By contrast, the addition of Ge forming the Pt-Ge clusters decreased the activity and the selectivity towards unsaturated alcohols, which was ascribed to very few oxidized Ge species being placed near Pt in order to polarize the carbonyl group of the citral molecule. This can explain the catalysts' low selectivity to unsaturated alcohols. Moreover, the formation of unsaturated alcohols did not improve with the addition of Ge because this would be mainly located over the support without modifying either electronically or geometrically the Pt sites. In order to enhance the numbers of Pt-Ge clusters, these catalysts were again prepared by controlled surface reactions which could ensure a contact between Pt and Ge[134] and using the oxidised activated carbon, in this case, a clear improvement of the selectivity to unsaturated alcohols was detected.

Vilella *et al.*[137] also studied the catalytic performance of two different activated carbon-based supports using Pt and Pt-Sn clusters: an activated carbon in powder shape against a commercial activated carbon felt. Differences in selectivity to unsaturated alcohols were found, which were ascribed to the different surface acid characteristics of the supports as well as to the presence of Sn^0 species, being the catalysts supported on carbon powders (equilibrium pH 10) more selective than that supported on carbon felts (equilibrium pH 7) and obtaining a larger amount of isopulegol than the latter. Sn^0 species produced blocking or dilution of de Pt particles. This effect was produced mainly on the felts based catalyst which provoked that this catalyst were less active and selective (80 % and 68 % of selectivity, for activated carbon and carbon felt, respectively, at 95 % of conversion).

Neri *et al.*[132] have also studied bimetallic Pt-Sn catalysts supported on activated carbon, prepared by co-impregnation (2 wt.% of Pt), obtaining an increase in selectivity towards unsaturated alcohols (from 40%–90%) by increasing the Sn loading from 0–0.82 wt.%.

Another bimetallic catalyst supported on carbon is Pt-Co. Bertero *et al.*[121] prepared Pt/C, Co/C and Pt-Co/C catalysts using a sub-bituminous carbon of high surface area (1300 m^2/g) by impregnation of acetylacetonete precursor salts. The catalysts were reduced at 150 °C and 500 °C in H_2 flow. The activity and selectivity of the bimetallic catalysts were higher than the monometallic ones, suggesting the creation of new polarizated sites which would activate the C=O bond hydrogenation. Moreover, secondary reactions such as decarbonylation and hydrogenolysis observed with the monometallic catalysts would be inhibited using the bimetallic ones.

Active carbon cloths (Figure 1.5) also have been employed in the selective hydrogenation of citral. Aumo *et al.*[138,139] studied Pt catalysts supported on carbon cloth and on woven active carbon fiber. Unsaturated alcohols selectivities of 80% – 100% for carbon fiber catalysts were reached against a selectivity of 49% – 62 % for the activated carbon catalysts used for comparison. However, the authors mentioned that the price of these types of cloths is still a limiting factor for extended use.

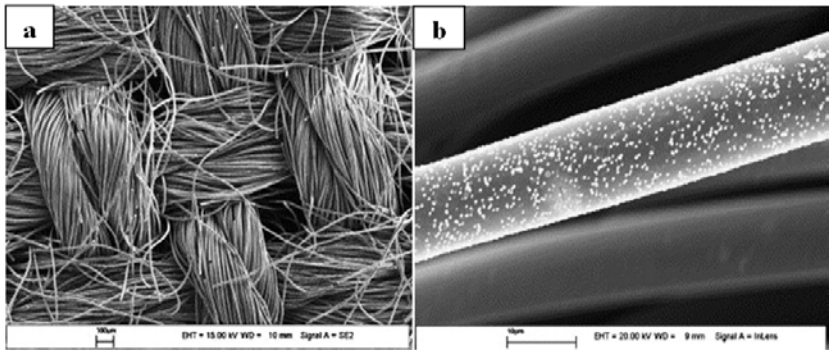

Figure 1.5. SEM images of the (**a**) woven activated carbon and (**b**) Pt-woven activated carbon catalyst[139].

1.2.4.2. Graphite

In general, the literature shows that graphite-supported catalysts are more selective towards the unsaturated alcohol than other conventional supports (alumina, activated carbon, or silica). This higher selectivity would be explained on the basis of electron transfer from the graphitic support to the metal particles located at the edges of the basal planes (Figure 1.6). The increased charge density on the metal particles would

decrease the probability of adsorption via the C=C bond, and therefore hindering its hydrogenation[140].

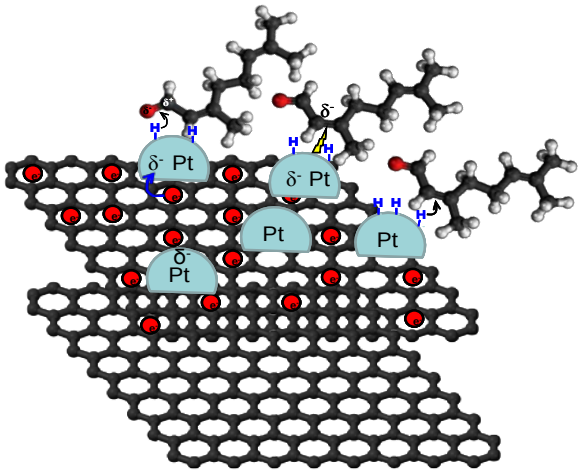

Figure 1.6. Electron transfer from the graphitic support to the metal particles.

Steffan *et al.*[141] studied the catalytic behaviour of Pt catalysts supported on SiO_2, Al_2O_3, activated carbon and graphite. The reaction was carried out at 140 °C, 70 bar H_2, 1.5 g of catalyst and an initial citral concentration of 0.56 M in n-hexane, as reaction media. They found the following trend in selectivity to unsaturated alcohols Pt/AC < Pt/Al_2O_3 < Pt/SiO_2 < Pt/G. For the carbon based catalysts Pt/G and Pt/AC, the use of graphite as support yielded a higher selectivity towards geraniol and nerol compared to activated carbon, in agreement with previous results for the hydrogenation of cinnamaldehyde [142]. However, this work also showed than Pt catalysts supported on graphite were much more selective to nerol and geraniol than those supported on other conventional supports such as silica or alumina.

Bachiller-Baeza *et al.*[143] studied Ru and Ru-Fe catalysts supported on a high-surface-area graphite (S_{BET} 295 m^2/g) and activated carbon (S_{BET} 964 m^2/g). The activated carbon was demineralised by acid treatments, and the graphite was treated in He at 900 °C in order to remove the surface oxygen groups. Monometallic catalysts were prepared by incipient wetness of the supports with an aqueous solution of $RuNO(NO_3)_3$, and bimetallic catalysts were prepared by a co-impregnation method with aqueous solution of $RuNO(NO_3)_3$ and $Fe(NO_3)_3 \cdot 9H_2O$. The catalysts were reduced in H_2 flow at 400 °C for 2 h. The liquid-phase hydrogenation of citral was carried out in

isopropanol at atmospheric pressure under H_2 at 60 °C, 850 rpm of agitation. A citral/Ru molar ratio of 30 was used. Contrary to what was expected the initial activities and the selectivity to unsaturated alcohols (≈38%) for both monometallic Ru catalysts were similar. Authors ascribed this behaviour to the absence of oxygen groups at the surface of the graphite during the impregnation which would restrain the metal-support interaction. Oxygen groups were not present on the support before impregnation, but they were introduced into the carbon materials during the catalyst preparation procedure due to the very high oxidizing character of the ruthenium precursor ($RuNO(NO_3)_3$). The presence of these oxygen functional groups at the surface of the graphite also impeded the electron donor effect of the macro-ligand graphite. On the other hand, using Fe as promoter, the selectivity was enhanced due to the bimetallic effect. However, bimetallic catalysts supported on graphite achieved higher selectivity to unsaturated alcohols than those on activated carbon probably due to the lower oxygen content and the maximum electronic transfer from support to the metals. This work clearly shows the importance of the surface chemistry of carbon materials in the selective hydrogenation of citral.

Asedegbega-Nieto *et al.*[127] studied the catalytic behaviour of Ru-Cu and Ni-Cu bimetallic catalysts supported on a high surface area graphite. Bimetallic catalysts with different Cu loadings were prepared by a co-impregnation method employing ethanolic solutions of ruthenium acetyl acetonate and copper acetate for the Ru–Cu system, and nickel nitrate and copper nitrate for the Ni–Cu system. The graphite was treated under inert atmosphere at 900 °C in order to remove oxygen groups before its impregnation, and the catalysts were treated in hydrogen flow at 350 °C, for the Ru–Cu system, and 350 °C for the Ni–Cu system, both for 2 h. The reaction were carried out at 50 bar of pressure, 50 °C, initial citral concentration of 0.03 M in isopropanol under 500 rpm of stirring. Regarding the Ru-Cu system, the monometallic catalyst (only Ru) produced citronellal and unsaturated alcohols. The addition of Cu did not modify the activity, but the selectivity to unsaturated alcohols decreased probably due to a poor Ru-Cu interaction where the Cu phase would be mainly covering the Ru particles. Regarding the Ni-Cu system, the saturated aldehydes were the main product obtained, and when Cu was added, changes in the selectivity were not observed. Therefore, Cu did not enhance selectivity to unsaturated alcohols in any case.

Court *et al.*[144] prepared Ni-M (M=Al, Cr, Cu, Co, Mo) bimetallic catalyst supported on graphite by incipient wetness using an aqueous solution of the appropriated composition of the two metal salts, and later reduction with naphthalene sodium. Hydrogenations were carried out at 80 °C under constant hydrogen pressure (1.01 MPa) using a citral concentration in 2-propanol of 0.195 M. It was expected that Ni-Cr catalysts were more selective to citronellal whereas Ni-Mo catalysts were more selective to citronellol. However, in none of the cases, the bimetallic catalysts modified the selectivity of Ni to unsaturated alcohols.

Cerro-Alarcón *et al.*[145] studied the behaviour of Ni catalysts supported on a high surface area graphite (200 m^2/g) and 3 wt.% oxygen surface content. Two different metal salts were used, namely, $Ni(NO_3)_2 \cdot 6H_2O$ and $Ni(CH_3COO)_2 \cdot 4H_2O$, and with different pre-treatment: reduction in H_2 at 400 °C for 2 h, and hydrazine based treatments; reduction of the impregnated support directly with hydrazine, or reduction-deposition *in situ* of Ni precursor with hydrazine. The hydrogenation of citral was performed operating at 50 °C, a H_2 pressure of 5 MPa, under 500 rpm of stirring, and using around 0.4–0.5 g catalyst and 0.4–0.5 mL of citral in 100 mL of 2-propanol. The catalytic results indicated that the determining factor in the activity data was the reduction method employed independently of the Ni precursor. While the treatment of reduction in hydrogen flow Ni^0 was obtained, the reduction with hydrazine provided low proportions of Ni^0 sites and mainly oxidised Ni^{2+} and/or Ni^{3+} species. These oxidised Ni species can activate the unsaturated aldehyde hydrogenation via the C=O bond. In fact, when only Ni^0 was present the hydrogenation activity was the highest; several orders of magnitude higher than those observed for catalysts prepared by reduction with hydrazine, however, these catalysts were not selective to the unsaturated alcohol formation. On the contrary, catalysts pre-treated with hydrazine were much more selective to unsaturated alcohols than the hydrogen pre-treated ones, but with very poor activities.

Zhao *et al.*[146] prepared catalysts for the selective hydrogenation of citral towards citronellal, instead to the unsaturated alcohols, using Pd catalysts supported on a graphite oxide (GO) pre-treated with 1,1,3,3-tetramethylguanidine (TMG). It is known that the use of palladium-supported catalysts in citral hydrogenations together with basic promoters, such as NaOH or $NaCO_3$, leads to higher selectivity toward

citronellal[147,148]. In this case, the above mentioned procedure was the basis to modify the GO surface for immobilizing Pd nanoparticles and using $Pd(CH_3COO)_2$ in ethanol solution. In a last step, the catalyst was reduced in a $NaBH_4$ aqueous solution, obtaining the GO supported Pd nanocatalysts. This type of catalyst had small Pd particle sizes, in a narrow size distribution, which produced a selectivity to citronellal of 89.6% with a high activity.

1.2.4.3. Carbon nanotubes

Recently[149], carbon nanotube (CNT) structures have been found to produce remarkable catalytic effects when they are used as a support for selective hydrogenation reactions due to their unique properties such as excellent electrical and thermal conductivity, uniform pore size distribution, development of meso and macropore bodies[150], and high length-to-diameter aspect ratio, the latter providing them a high external surface area[151]. These special properties could influence the metallic particle size distribution, dispersion, metal oxidation state, but also can reduce problems as mass transfer rates obtaining high catalytic performances in comparison with other conventional supports[152]. Besides, due to their three-dimensional nanoscale structure of rolled up graphene layers, a transfer of electronic density from the support to the deposited metallic particles[153,154] could take place affecting the properties of the metallic phase and their catalytic behaviour[155]. For these reasons, they have been recently used as supports in the selective hydrogenation of citral, because they can improve the selectivity to the unsaturated alcohol due to a transfer of the p-electrons from the graphene layer to the metal particles. Moreover, the curvature of the CNT channel could also induce an extra modification on the molecular adsorption on the metallic phase, which also would modify the catalytic activity and/or selectivity of the hydrogenation reaction. However, during the CNT synthesis other carbon forms and amorphous carbon are formed as well. Therefore, it is necessary to have a good knowledge of the purity of CNT when using them for catalytic applications.

Asedegbega-Nieto *et al.*[156], studied the catalytic behaviour of four different carbon materials, including two types of carbon nanotubes with very similar sizes, as supports of Pt catalysts: commercial carbon nanotubes obtained by arc discharge (CNT1) with a 30–40 wt.% of nanotube content, carbon nanotubes obtained by CVD

(CNT2), carbon black and a high surface area graphite, pretreated at 900 °C in He flow in order to remove surface groups. The Pt catalysts were prepared by impregnation of the supports with hexachloroplatinic acid obtaining the smallest particle sizes on graphite and carbon black probably due to their highest surface area in comparison with CNTs. Figure 1.7 shows some pictures of Pt supported on carbon nanotubes. Citral hydrogenation reactions were carried out at 50 °C and H_2 pressure of 50 bar, with 500 rpm of stirring, employing isopropanol as solvent. Regarding the catalytic results, Pt supported on carbon, graphite and CNT1 showed similar selectivity to unsaturated alcohols, around 30%, but using CNT2 which had much fewer carbon impurities, a selectivity of 62% was achieved. The presence of graphitized carbon in CNT1 conferred to this catalyst a behaviour similar to the graphite-supported one, probably because the Pt particles were localized mainly on the carbon impurities, which have a flat-like morphology and not the round-shaped structure of CNTs; consequently, the carbon impurities did not produce the effect of electronic transfer of the CNTs. In this line, Qin *et al.*[157] also obtained higher selectivity using carbon nanotubes produced by CVD than using activated carbon as supports of Pt catalysts: 59% *vs.* 26%, respectively.

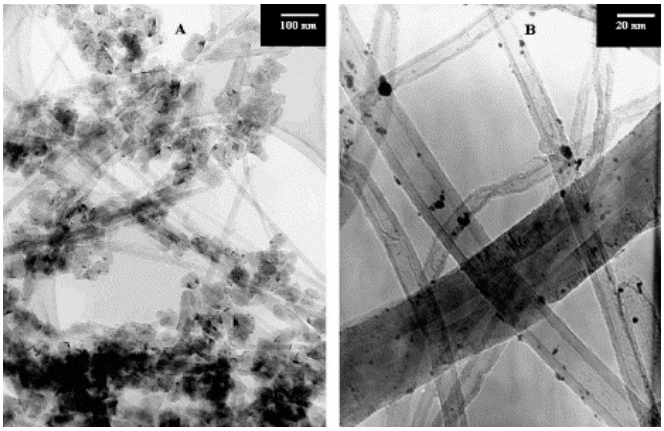

Figure 1.7. Pt catalysts supported on carbon nanotubes[156].

Functionalized carbon nanotubes have also been studied as catalyst supports similar to graphite. So, Qin *et al.*[157,158] modified carbon nanotubes by functionalization with polyacrylic acid (PAA). In this work Pt was introduced into pure and PAA grafting multi-walled carbon nanotubes (MWNTs) by electroless metal deposition method as used as catalysts for hydrogenation of citral. These catalysts exhibited higher activity when compared with Pt impregnated activated carbon catalyst, similar to previous

discussed results[156]. However, a decrease in the selectivity to unsaturated alcohols from 59% for MWNTs without functionalization, to 7% for PAA grafted MWNTs, was observed. This result is related to the large amount of carboxylic groups that PAA treatment fixed on the outside of the MWNTs, which decreased the electronic effect of the support. Moreover, PAA prevented the formation of Pt (111) affecting the various product distributions obtained. The PAA treatment in the nanotube leads to better dispersion of Pt nanoparticles and, therefore, better activities, but worse selectivity towards unsaturated alcohols.

Zgolicz *et al.*[159] also functionalized carbon nanotubes by thermal and oxidative treatments. Pt and Pt-Fe catalysts supported by multi-wall carbon nanotubes were developed to study the influence of the support surface composition on the catalytic performance for the unsaturated alcohols. The citral hydrogenation was performed at 70 °C and atmospheric pressure in a discontinuous reactor using 0.3 mL of citral, 0.300 g of catalyst in 30 mL of 2-propanol. Low numbers of oxygen groups on the support surface produced an optimized Pt size. The Pt loading of the catalysts was 5 wt.% which together with the presence of Fe, yields a very high selectivity (96 %) to unsaturated alcohols.

Bimetallic catalysts have also been prepared using CNT as supports. Ananthan *et al.*[160] prepared Pt, Ru and Pt-Ru catalysts over carbon nanotubes to study the effect of these bimetallic particles. They also studied the effect on the catalysts of the carbon nanotube surface chemistry by a previous functionalization of the support with nitric acid followed by two different heat treatments (375 °C and 675 °C in N_2 flow), in order to partially remove the oxygen-containing groups from the CNT surface. The catalytic results showed that as expected the removal of oxygen-containing groups increased both activity and selectivity. In fact, the selectivity to the unsaturated alcohols reached 95% by using bimetallic catalysts, due to a close contact between Pt and Ru nanoparticles where a charge transfer could be developed from Ru to Pt atoms. Recently[161], these authors have developed Pt-Au bimetallic catalysts supported on CNT confirming the above mentioned effect of the oxygen groups on CNT, however the Pt-Ru system was more selective to unsaturated alcohols than the Pt-Au; 95% *vs.* 70%, respectively.

1.2.4.4. Composite materials

By attempting to combine the carbon materials and partially reducible oxide properties, new composite materials have been developed as supports for the selective hydrogenation of citral. In this line, the influence of the supports carbon-TiO_2 and carbon-CeO_2 on the deposited metal phase have been mainly studied[133,162-165].

Partilly Pt catalyst supported by reducible oxides have shown very good selectivity to C=O bond hydrogenation as it was described[115,166]. Figure 1.8 shows a scheme for the preferred orientation of citral when it is hydrogenated on TiO_2[112], pretreated at high temperatures.

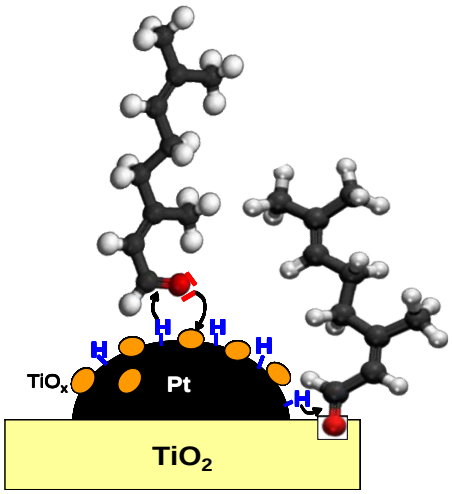

Figure 1.8. Citral being hydrogenated on Pt supported on TiO_x. ⬭ Ti^{3+} or Ti^{4+} species and □ oxygen vacancies and ⚫— C=O bond[112,167].

Zhu *et al.*[163-165] prepared carbon nanofibers (CNFs)–TiO_2 composites as supports for Pd catalysts. In this way, TiO_2 was impregnated with aqueous solutions of $Ni(NO_3)_2 \cdot 6H_2O$ or mixture of $Ni(NO_3)_2 \cdot 6H_2O$ and $Cu(NO_3)_2 \cdot 3H_2O$, and then a reduction treatment at 600 °C in N_2/H_2 (80:20) was carried out. CNFs were grown by methane decomposition at 873K for 5h, and finally, Ni and Cu particles were removed by means of a treatment with HNO_3 at 120 °C. A TiO_2 coated cordierite monolith was also prepared by a sol-gel method [164] which also was used for CNFs growing. The CNF-TiO_2 support contained 38% of carbon phase, which was composed by CNFs, 95%, and amorphous carbon, 5%. Pd catalyst was prepared by impregnation with an aqueous

solution of $PdCl_2$ and then it was tested in the citral hydrogenation with the aim of obtaining citronellal as the main product. A commercial Pd/activated carbon catalyst (Pd/AC) was also tested for comparison. Pd/CNF-TiO_2 catalyst had a very low surface area—58.1 m^2/g *versus* 810 m^2/g—of Pd/activated carbon. Moreover, the porosity was also very different being that Pd/CNF-TiO_2 is mainly mesoporous with an average pore diameter of 9.7 nm while Pd/AC was microporous with an average pore diameter of 2.1 nm. Regarding the activity and selectivity of these supports, Pd/AC was more active than Pd/CNF-TiO_2 (90% conversion after 4 h and 32 h, respectively) which could be explained by the higher Pd dispersion and narrow Pd particle size distribution in Pd/AC due to its larger surface area; conversely, a poorly dispersed catalyst with larger Pd particles was obtained over Pd/CNF-TiO_2 due to its smaller surface area which would lead to lower catalytic activity than for Pd/AC. In regards to selectivity to citronellal, considering that palladium catalysts are very active in the hydrogenation of the C=C bonds, the selectivity towards citronellal was expected to be very high in both cases, however the selectivity towards citronellal achieved with Pd/CNF-TiO_2 was significantly higher than Pd/AC, and particularly at high conversion (88% *versus* 35% selectivity, respectively, at 90% conversion). This result suggested that the porosity of the supports could play an important role, as explained by the following: on the catalyst external surface citral would be firstly hydrogenated to citronellal and then citronellal can be easily desorbed from Pd crystals to the solution. Inside the porosity, the product distribution should be different. If the reaction took place in the macro- and meso-pore network of the catalyst, the main products would be citronellal as they occur on the external surface because these pore sizes are wide enough to not influence product diffusions, while if the reaction took place inside the micropores, citral would also be hydrogenated to citronellal but it would be confined inside the micropores and, therefore, it would be completely hydrogenated to 3,7-dimethyloctanol. According to this explanation, at low conversions the selectivity to citronellal was similar in both catalysts due to only the external surface being involved in the reaction, however, at higher conversions, the selectivity to citonellal using Pd/AC decreased, increasing the formation of 3,7-dimethyloctanol in the microporosity of the active carbon.

Regarding the TiO_2 coated cordierite monolith[164], it was used to grow CNFs in order to be employed as structured supports of Pd catalyst as well. The obtained results

showed a very good selectivity to citronellal which was also explained in terms of decreasing internal diffusion limitation.

On the other hand, Serrano-Ruiz *et al.*[133] dispersed ceria on a carbon Norit in order to enhance the amount and surface area of partially reducible CeO_2 sites which acts to improve the selectivity towards unsaturated alcohols. The composite material was prepared by impregnation of carbon (previously outgassed) with an acetonic solution of $Ce(NO_3)_3 \cdot 6H_2O$ obtaining a CeO_2 loading of 20 wt.%. On this support, Pt and Pt-Sn catalysts were deposited, and then, they were pre-treated at both 200 °C, and 500 °C, in order to evaluate the strong metal–support interactions effect. Bimetallic catalyst achieved higher selectivity to unsaturated alcohols than monometallic ones, increasing the selectivity parallel to the amount of Sn; however, regarding the conversion, the trends were the opposite: conversion decreased when the Sn loading increased which was ascribed to some Pt particles being able to be covered by Sn species. On the other hand, reduction treatment at 500 °C increased the selectivity to geraniol and nerol by 50% in both monometallic and bimetallic catalysts, explained by the presence of new $Pt–SnO_x$ and/or $Pt–CeO_x$ active sites. It is noteworthy that although bimetallic cluster and partially reducible oxide were used, and being well known that both favour the C=O bond hydrogenation, a selectivity to unsaturated alcohol was achieved that was not too high (35%).

Bachiller-Baeza *et al.*[162] also prepared composite materials, as supports of Ru catalysts, using Ce or Mg as promoter phases in combination with activated carbon (AC) or Al_2O_3. Composites were prepared by different impregnations procedures, where $RuNO(NO_3)_3$ pre-impregnated supports, Ru/AC or Ru/Al_2O_3, were again impregnated with aqueous solutions of $Ce(NO_3)_3$ or $Mg(NO_3)_2$. All the composite catalysts and Ru free supports were tested in the selective hydrogenation of citral and crotonaldehyde. Addition of MgO or CeO_2 decreased the hydrogenation activity. However, while MgO did not influence the selectivity, CeO_2 increased the selectivity to unsaturated alcohols, especially on carbon supported catalysts. Finally, the authors suggested that defects on the surface of the promoter were highly selective sites for unsaturated aldehydes hydrogenation due to their influence on the C=O bond activation.

1.2.5. Conclusions

Three types of carbon materials have been mainly used as catalyst supports in the selective hydrogenation of citral: activated carbons, graphite, and carbon nanotubes. In most cases, Pt was the metal supported, followed by Ru, and only a few works have been found focusing on the use of carbon composite materials in this reaction. It is noteworthy that no work has been found where carbon aerogels or xerogels were used as support, in spite of the extensive uses these materials have for very different catalyzed heterogeneous reactions. Carbon materials have shown very good performance as catalyst support for citral hydrogenation; both characteristic porosity and chemical surface can be used to modify selectivity in different ways. Moreover, very high selectivity to the unsaturated alcohols, nerol and geraniol, has also been reported in some cases. It should be mentioned that the amount of work discovered for citral hydrogenation is smaller than that of other α,β-unsaturated aldehydes. Thus, we consider that it is still possible to improve the catalyst development for this reaction, which is a challenge that can be addressed with new carbon materials, such as carbon gels, carbon nanotubes or carbon fibers, or new carbon material-oxide composites, though optimizing in all cases the metal particle sizes and their distribution throughout the porosity of the supports.

1.3. MATERIALES CARBONOSOS COMO MODIFICADORES DE LA ACTIVIDAD FOTO-CATALÍTICA EN LA ELIMINACIÓN DE CONTAMINANTES DEL AGUA

La foto-catálisis es un proceso químico donde intervienen los electrones de la banda de conducción y/o los huecos de la banda de valencia de un semiconductor, generados cuando éste se irradia con una luz de longitud de onda adecuada, dando lugar bien a procesos de oxidación de compuestos catalizada por dichos huecos, y/o a procesos de reducción catalizados por los electrones foto-generados. En general podemos distinguir tres etapas clave durante los procesos de foto-catálisis:

1. Absorción de los fotones incidentes para la generación del par electrón - hueco donde la energía de la luz incidente debe ser mayor que la diferencia de energía

entre la banda de valencia y la banda de conducción del material, para que un electrón promocione desde la primera a la segunda.

2. La separación y migración de los electrones y huecos foto-generados (ambos son centros activos) para evitar la recombinación electrón - hueco que desactive al foto-catalizador.

3. Reacción química superficial, para lo cual es importante una gran superficie activa para maximizar el número de centros activos.

1.3.1. Mecanismo de las reacciones foto-catalíticas

El mecanismo del proceso foto-catalítico es complejo y además muy dependiente de una serie de parámetros experimentales, tales como pH, características y concentración del catalizador, intensidad y frecuencia de la radiación, naturaleza y concentración de los reactivos, o presencia de aditivos, entre otros. Este mecanismo ha sido estudiado por multitud de autores[168-170], y se resume a continuación.

Cuando un foto-catalizador es irradiado con fotones de energía mayor que su banda prohibida (diferencia de energía entre la banda de valencia y la banda de conducción) se promueve el salto de un electrón desde la banda de valencia a la banda de conducción, a la vez que se genera un hueco en la banda de valencia, obteniéndose un par electrón - hueco que será responsable de la reacción foto-catalítica (Ecuación 1), produciéndose simultáneamente las correspondientes reacciones de oxidación y de reducción en la superficie del semiconductor; los huecos foto-generados dan lugar a las reacciones de foto-oxidación, mientras que los electrones de la banda de conducción dan lugar a las reacciones de foto-reducción, como se representa en la Figura 1.9.

En soluciones acuosas, los huecos después de migrar a la superficie reaccionan con las sustancias adsorbidas, principalmente con el agua (Ecuación 2) o con iones OH^- (Ecuación 3), generando radicales $OH^\bullet$. Además, cuando los procesos foto-catalíticos se llevan a cabo en ambientes aeróbicos el oxígeno adsorbido es la principal especie aceptora de electrones (Ecuación 5). No obstante, para procesos de eliminación de contaminantes de aguas en muchas ocasiones se adiciona al reactor peróxido de hidrogeno, aumentado así considerablemente la velocidad de la foto-degradación debido a la generación de radicales $OH^\bullet$ adicionales (Ecuación 6). De este modo, los

contaminantes orgánicos adsorbidos en la superficie de las partículas del foto-catalizador se oxidan con estos radicales transformándose en otros productos intermedios, o en CO_2, dependiendo de que la oxidación sea parcial, o completa, respectivamente.

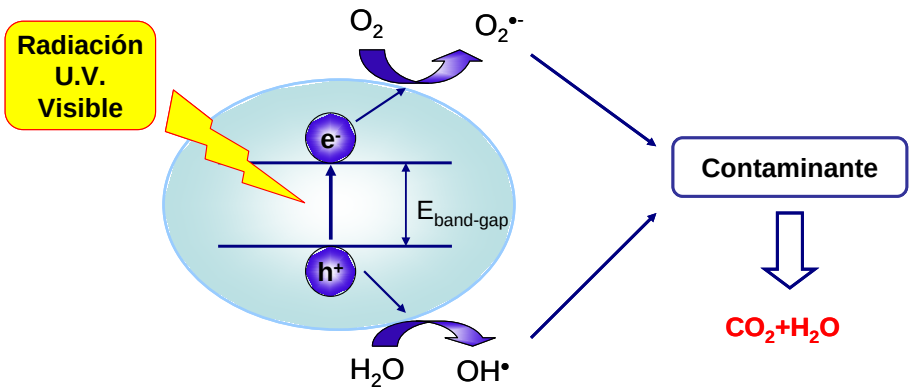

Figura 1.9. Activación del foto-catalizador mediante radiación electromagnética y proceso de degradación de contaminantes. ● TiO_2

Finalmente, si los electrones y los huecos no se capturan, transfieren o se separan, pueden recombinarse en tiempos del orden de los nanosegundos[168] (Ecuación 7); esta es la principal causa del bajo rendimiento de las reacciones foto-catalíticas[171].

$$C + h\nu \rightarrow h^+ + e^- \quad (1)$$

$$h^+ + H_2O_{ads} \rightarrow H_2O^{\bullet+}{}_{ads} \leftrightarrow OH^{\bullet}_{ads} + H^+ \quad (2)$$

$$h^+ + OH^-_{ads} \rightarrow OH^{\bullet}_{ads} \quad (3)$$

$$h^+ + RH_{ads} \rightarrow RH^{\bullet+}_{ads} \leftrightarrow R^{\bullet}_{ads} + H^+ \quad (4)$$

$$e^- + O_{2\,ads} \rightarrow O_2{}^{\bullet-}{}_{ads} \quad (5)$$

$$O_2{}^{\bullet-}{}_{ads} + H^+ \leftrightarrow HO_2{}^{\bullet}{}_{ads}$$

$$2HO_2{}^{\bullet}{}_{ads} \leftrightarrow H_2O_{2ads} + O_{2ads}$$

$$e^- + H_2O_{2\,ads} \rightarrow OH^{\bullet}_{ads} + OH^-_{ads} \quad (6)$$

$$h^+ + e^- \rightarrow \text{calor} / \text{luminiscencia} \quad (7)$$

Debido a que los principales radicales que intervienen en estos procesos de descontaminación son los hidroxilo, por su elevado poder oxidante, durante los últimos

años se han venido desarrollando nuevos métodos, conocidos como procesos avanzados de oxidación, con el fin de aumentar el rendimiento foto-catalítico mediante el aumento de la generación de estos radicales altamente oxidantes. Estos procesos se resumen en la Tabla 1.2.

Tabla 1.2. Tecnologías basadas en procesos avanzados de oxidación usadas para el tratamiento de aguas.

Procesos no Fotoquímicos	Procesos Fotoquímicos
• Oxidación en agua sub/supercrítica	• UV de vacío (UVV)
• Reactivo Fenton (Fe^{2+}/H_2O_2)	• UV/reactivo químico
• Oxidación electroquímica	• Foto-Fenton ($UV/Fe^{2+}/H_2O_2$)
• Radiólisis	• UV/O_3
• Plasma no térmico	• UV/H_2O_2
• Ultrasonidos	• $UV/K_2O_8S_2$
• Ozonización:	
- en medio alcalino (O_3/OH^-)	
- en presencia de H_2O_2 (O_3/H_2O_2)	
- catalítica	

1.3.2. Estrategias para mejorar el foto-catalizador

Los materiales con propiedades foto-catalíticas deben reunir las siguientes características: i) ser foto-activos especialmente bajo luz visible o UV cercano, ii) ser biológica y químicamente inertes, iii) económicamente viables y v) estables. El óxido de titanio satisface la mayor parte de estos criterios, de ahí que sea el foto-catalizador más empleado[172]. Sin embargo, el TiO_2 solo puede adsorber el 3-5% de la energía presente en el espectro solar debido a su elevada banda prohibida (3,2 eV para la fase anatasa y 3,0 eV para la fase rutilo), lo cual restringe el uso del dióxido de titanio puro en aplicaciones con luz visible[173,174]. Además, el dióxido de titanio tiene un área superficial baja, y por tanto presenta bajo número de sitios activos accesibles a los reactivos. Consecuentemente, los esfuerzos para mejorar las prestaciones foto-catalíticas deben enfocarse sobre: i) la disminución de la banda prohibida para emplear luz visible, ii) la minimización la recombinación electrón - hueco y iii) el aumento del

área superficial para así aumentar el número y calidad de sitios activos, así como la adsorción de los contaminantes.

1.3.2.1. Desarrollo de catalizadores activos bajo luz visible

Para mejorar la eficiencia de estos semiconductores bajo luz solar (o visible) es necesario modificar el material de modo que se facilite la absorción de luz visible. En este sentido, la mayoría de los estudios están enfocados en la introducción de agentes dopantes o en el empleo de otros materiales como sensibilizadores[175,176].

La introducción de agentes dopantes en el óxido de titanio puede producir nuevos estados híbridos entre la banda de conducción y valencia, y por tanto disminuir la energía de la banda prohibida facilitando la absorbción de luz visible. Por otro lado, la mejora que se produciría por el uso de sensibilizadores se debe a la absorción directa de la luz visible por el sensibilizador, y la liberación de electrones desde éste al dióxido de titanio en una reacción de oxidación.

El dopado puede realizarse con elementos metálicos o no metálicos:

a) Dopado con metales.

El óxido de titanio se ha dopado con metales de transición como cromo, cobalto, vanadio y hierro, extendiendo la respuesta de éste a una mayor amplitud del espectro electromagnético, entre ellas la región visible, mejorando así su actividad foto-catalítica[177-179]. Sin embargo esta estrategia tiene como desventaja que los metales usados como dopantes actúan como sitios de recombinación de los electrones y huecos. Además estos metales dopantes aumentan la inestabilidad térmica de la fase anatasa[180]. De modo que, en muchas ocasiones pese a la disminución de la energía de la banda prohibida ocasionada al dopar con metales, la actividad foto-catalítica no mejora debido a que el metal actúa atrapando los electrones foto-generados y facilita la recombinación electrón hueco, o bien en otras ocasiones el metal no se incorpora en la red del óxido de titanio. Además, los metales al incorporarse suelen permanecer en la superficie del óxido de titanio bloqueando los sitios fotoactivos[181]. Otras limitaciones del dopado con

metales son la foto-corrosión del catalizador y obviamente el coste relativo del dopado[182].

b) Dopado con no metales

En este caso el dopado con nitrógeno y azufre son los más extendidos[183,184] para mejorar la actividad foto-catalítica con radiación solar. No obstante, estas estrategias todavía tienen algunos problemas: i) dificultad de obtener una alta concentración de nitrógeno en el óxido de titanio dopado; ii) el dopaje con nitrógeno normalmente genera gran número de defectos cristalinos, los cuales actúan como centros de recombinación de los electrones y huecos generados, disminuyendo la actividad foto-catalítica[185], iii) la necesidad de recuperación y reutilización del catalizador debido al coste del dopado, lo cual a su vez plantea otros inconvenientes como es la separación del sólido del efluente, o la inestabilidad del dióxido de titanio dopado con nitrógeno que lleva consigo una pérdida paulatina del nitrógeno superficial durante su uso en reacción.

Sato[186,187] realizó, por primera vez, el dopaje con N del dióxido de titanio adicionando NH_4OH a la mezcla sol-gel. Hoy día, el dopado con nitrógeno se está estudiando, optimizando diferentes aspectos electrónicos de estos materiales[183,188,189]. Esto es posible porque el nitrógeno debido a su tamaño atómico (similar al del oxígeno) y a su pequeña energía de ionización, le permite introducirse fácilmente en la red del óxido de titanio.

Entre las técnicas empleadas para el dopado con nitrógeno cabe destacar: sputtering[190,191] o implantación iónica[192,193], que se basan en el tratamiento directo de TiO_2 con iones energéticos de nitrógeno, o bien procedimientos en fase gas[194], deposición atómica[195] o deposición por láser pulsado[196]. Sin embargo, la técnica más versátil para la síntesis de nanopartículas de TiO_2 dopadas con nitrógeno es el método sol-gel, ya que permite un control de la estructura, morfología y porosidad del material. Este método se basa en la hidrólisis de un alcóxido de titanio en presencia de un precursor de nitrógeno (aminas, nitratos, sales de amonio, amoniaco o urea)[197-199].

Una modificación reciente de la técnica sol-gel para preparar este tipo de materiales consiste en utilizar precursores de titanio en combinación de surfactantes nitrogenados, como cloruro de dodecilamonio (DDAC), de modo que éste actúe como plantilla estructural del dióxido de titanio (Figura 1.10) y a la vez como agente dopante de nitrógeno que resistiría tras la eliminación de la plantilla[200-202].

Otros elementos no metálicos como fluor, carbono, fósforo y azufre también se han estudiado, aunque en menor medida debido a la dificultad que presentan este tipo de dopados. El flúor no reduce la banda prohibida del TiO_2, sin embargo mejora la acidez de la superficie y provoca la formación de iones reducidos Ti^{3+} debido a la compensación de carga entre F^- y Ti^{4+}. Estos estados intermedios se localizan en la banda prohibida mejorando la eficiencia de los procesos foto-inducidos [179].

Cuando el C, P o S dopan el TiO_2 también se obtienen resultados positivos bajo luz visible[203-205]. Estos dopantes no metálicos estrechan de manera efectiva la banda prohibida del TiO_2[206,207] debido al cambio de parámetros de red, y a la presencia de estados intermedios entre la banda de conducción y de valencia[205]. Esto no sólo permite la absorción de la luz visible, sino que la presencia de estos niveles intermedios aumenta el tiempo de vida de los portadores de carga foto-generados.

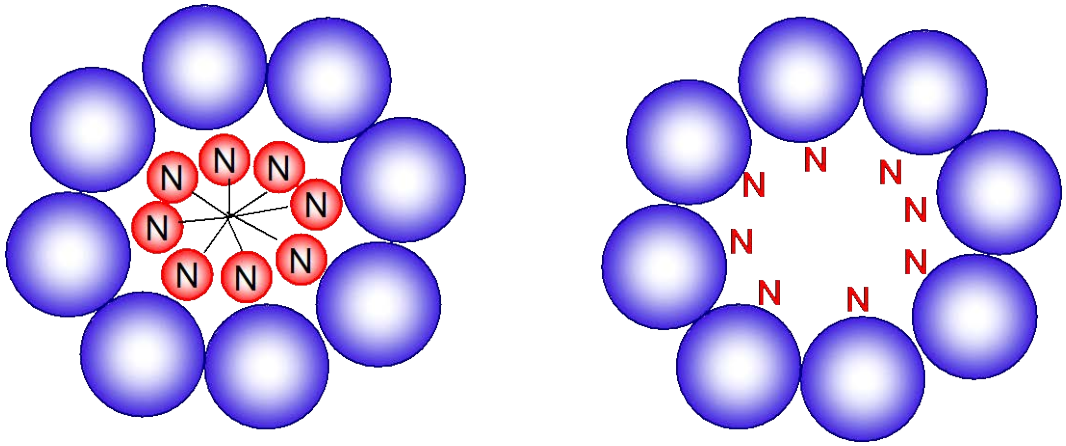

Figura 1.10. Preparación de dioxido de titanio dopado con nitrogeno mediante un metodo sol-gel con el empleo de surfactantes nitrogenados. Adaptado de H. Choi y col.[202]. ● TiO_2

c) Empleo de sensibilizadores.

Como ya se ha comentado, este proceso consiste en la adicción de sustancias con propiedades redox[208-211] (colorantes, metales, materiales carbonosos…) capaces de excitarse bajo luz visible y transferir un electrón a la banda de conducción del semiconductor, el cual puede reaccionar con el oxígeno adsorbido dando lugar a iones superóxido que participen en el proceso de foto-oxidación. Además, al ceder un electrón a la banda de conducción del semiconductor el sensibilizador quedará cargado positivamente, de modo que será capaz de capturar un electrón de la banda de valencia del semiconductor, generando así un hueco. Es decir, el uso de sensibilizadores permite la generación del par electrón-hueco en el semiconductor bajo radiaciones menos energéticas, como es la luz visible.

El mecanismo de sensibilización mediante el uso de colorantes se ilustra en la Figura 1.11. Bajo radiación visible, el colorante se excita, y en presencia de oxido de titanio puede transferir electrones a la banda de conducción de éste para iniciar el proceso foto-catalítico. El inconveniente de esta técnica radica en la necesidad de regenerar el colorante, lo que obliga a adicionar al medio otras sustancias con propiedades redox, o mediadores, como el par I^{3-}/I^{-} [212] o EDTA[209]. Un esquema del proceso de sensibilización por colorantes se muestra a continuación[213]:

$$S \xrightarrow{h\upsilon} S^*$$
$$S^* \xrightarrow{TiO_2} S^+ + e^-$$
$$S^+ + e^- \rightarrow S$$

En resumen, el colorante (S) se excita bajo luz de menor energía que la necesaria para excitar al óxido de titanio, pasando a un extado excitado (S^*) el cual en presencia del óxido de titanio cede un electrón a la banda de conducción de éste pasando a un estado de menor energía (S^+). Para aumentar la eficacia del sensibilizador se precisa de la adición de mediadores que aporten los electrones necesarios para regenerar al colorante para completar el ciclo.

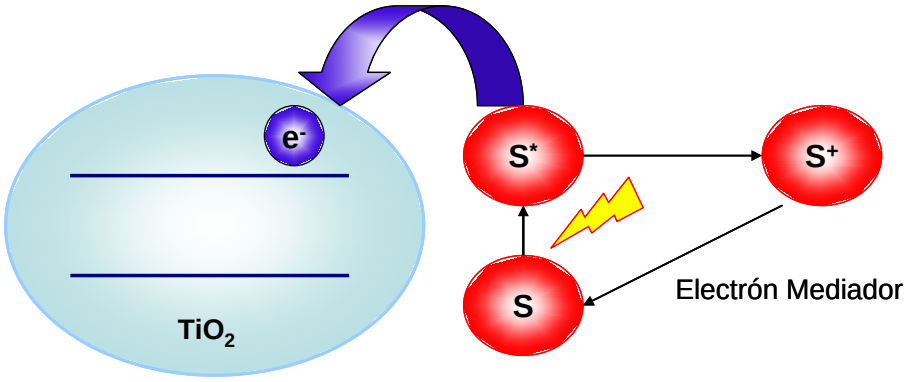

Figura 1.11. Mecanismo de sensibilización del dióxido de titanio bajo luz visible con el uso de colorantes. Adaptado de M. Ni y col.[214]

En la Tabla 1.3, se recogen algunos de los colorantes más empleados como sensibilizadores, y las longitudes de onda donde correspondientes a su máxima adsorción[215,216].

Tabla 1.3. Colorantes más empleados como sensibilizadores y longitud de onda a la cual se produce la máxima absorción.

Colorante	λ_{max} (nm)
Azul de metileno	665
Azur A	635
Azur B	647
Azur C	620
fenosafranina	520
Safranina-O	520
Safranina-T	520
Fluoresceina	490
Eritrosina	530
Rodamina B	551
Rosa de bengala	550
Naranja de acridina	492
Crastal violeta	578
Verde malaquita	625
Violeta de metilo	580

Otro modo de sensibilización consiste en el uso simultáneo de semiconductores mixtos, como por ejemplo ZnO/TiO_2[217], CdS/TiO_2[218,219] y Bi_2S_3/TiO_2[220]. Estos sistemas producen una disminución de la velocidad de recombinación electrón - hueco, y además son altamente eficientes bajo radiación visible. Si un semiconductor con mayor energía de banda prohibida (semiconductor 1) se acopla con un semiconductor de menor energía de banda prohibida pero con una banda de conducción más negativa (semiconductor 2), y éstos se irradian con luz visible, los electrones de la banda de conducción del semiconductor 2 (excitados por la luz visible) son transferidos a la banda de conducción del semiconductor 1 obteniéndose una mayor separación de los electrones y los huecos foto-generados en semiconductor 1 y por tanto, una mejor actividad foto-catalítica y sensibilización bajo luz visible. Además, se lograría compensar las desventajas de cada semiconductor por separado, induciendo un efecto sinérgico[217,221]. Así ocurre, por ejemplo, en el sistema acoplado CdS/TiO_2 donde el CdS tiene una energía de banda prohibida de 2,4 eV apropiada para absorber luz visible, pero es propenso a foto-corrosión anódica en medio acuoso. El acoplamiento con TiO_2 evita la foto-corrosión a la vez que produce una mejor separación de las cargas, y por tanto una mejor actividad en el visible[219,222].

Otros sensibilizadores eficientes son los materiales carbonosos los cuales se describirán en profundidad en la Sección 1.3.3.

1.3.2.2. Minimización de la recombinación electrón-hueco

El mayor inconveniente en foto-catálisis es la recombinación de los transportadores de carga pues reduce la eficiencia quántica (porcentaje de fotones que chocan con la superficie foto-reactiva que producirá un par electrón-hueco, medida de la sensibillidad del foto-catalizador)[180]. Cuando ocurre la recombinación, el electrón excitado vuelve a la banda de valencia sin reaccionar con las especies adsorbidas disipando energía en forma de luz o calor[223,224]. La recombinación puede ocurrir tanto en la superficie como en el interior de la estructura y en general, impurezas, bordes de grano, defectos o cualquier factor que introduzca imperfecciones en el cristal favorecen este proceso[225]. El dopado con iones[226], y la reducción del tamaño de cristal[227,228] pueden favorecer la separación del par electrón-hueco disminuyendo su recombinación. Otra estrategia que ha mostrado buenos resultados en este sentido con el dióxido de

titanio es inducir la mezcla de fases, como ocurre en el dióxido de titanio comercial P25®, el cual contiene un 80 % de fase anatasa y un 20% de la rutilo. Esto se explica en base a que el potencial de la banda de conducción del rutilo es más positivo que el de la anatasa lo cual significa que la fase rutilo puede actuar como un aceptor de los electrones foto-generados desde la banda de conducción de la fase anatasa (Figura 1.12). De modo que un íntimo contacto entre ambas fases aumenta la separación de los huecos y electrones fotogenerados y por tanto reduce su recombinación[229,230].

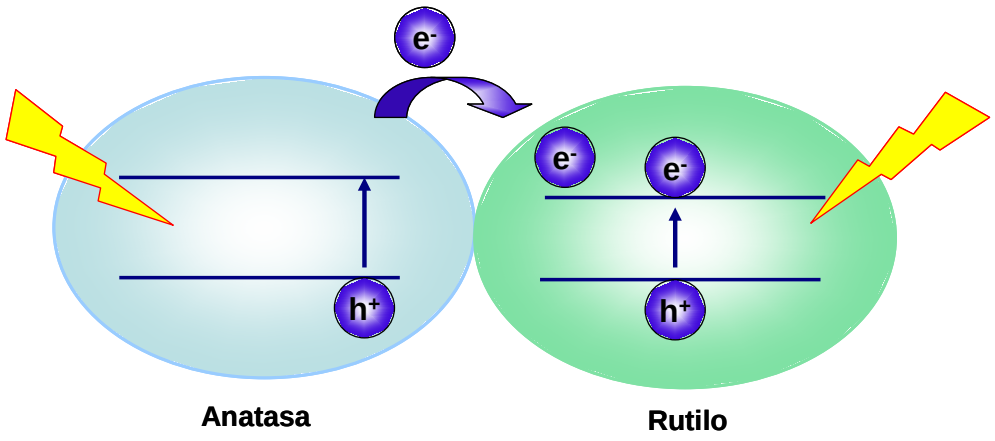

Figura 1.12. Mejora de la recombinación electrón-hueco entre las fases anatasa y rutilo del TiO_2. Adaptado de V. Etacheri y col.[230]

Otra estrategia que se utiliza frecuentemente para aumentar la vida media de los electrones y huecos foto-generados es añadir metales u otros agentes que actúen como captores de huecos o electrones. Los metales del grupo VIII[231-233] incrementa la velocidad de la reacción foto-catalìtica en el TiO_2 debido a la captura de los electrones de la banda de conducción elevando así el tiempo de vida medio del par electrón-hueco. En muchos trabajos se concluye que el platino es el metal del grupo VIII más activo para incrementar la actividad del TiO_2[234,235].

El tamaño de partícula también afecta enormemente a la recombinación electrón-hueco, ya que ésta ocurre en los bordes de grano y en los defectos; si se reduce el tamaño de partícula la distancia que deben recorrer los electrones y huecos hasta la superficie externa donde tienen lugar las reacciones con las especies a descontaminar es menor, y por lo tanto se reduce la probabilidad de recombinación[228] (Figura 1.13). Sin embargo, también hay trabajos que muestran una mayor recombinación al disminuir el

tamaño de partícula, debido a un incremento del número de defectos superficiales[236]. Por tanto, todavía es necesario e importante profundizar en el estudio de nuevas rutas de síntesis que produzcan partículas de tamaño y calidad adecuada, ya que por efectos cuánticos se produce un aumento considerable de la banda prohibida cuando el tamaño de partícula de óxido de titanio se reduce por debajo de 2 nm. Así, Satoh y col.[237] detectaron que la reducción del tamaño de partícula del dióxido de titanio no modifica la banda prohibida hasta los 2 nm, pero a tamaños inferiores ésta se incrementa hasta 3,9 eV para 1 nm, tamaño por debajo del cual el incremento de la banda prohibida es exponencial.

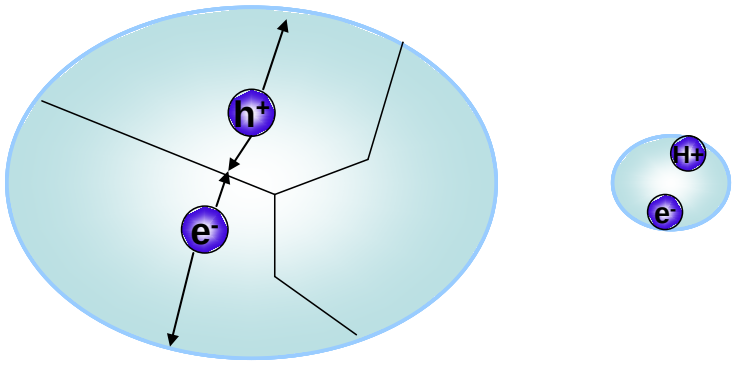

Figura 1.13. Efecto del tamaño de partícula y bordes de grano en la recombinación electrón-hueco. Adaptado de A. Kudo y col.[225]. ● TiO_2

Así, la nanotecnología adaptada a la síntesis de este tipo de materiales se está enfocando en minimizar la recombinación electrón-hueco.

1.3.2.3. Incremento del área superficial

Como ya se ha mencionado anteriormente, dado que la foto-catálisis es un proceso superficial donde los reactivos son oxidados y/o reducidos en la superficie del catalizador, es importante disponer de una elevada superficie específica tanto para maximizar el número de sitios activos como para facilitar la transferencia de los reactivos hacia dichos sitios activos. Este incremento del área superficial puede realizarse mediante el uso de materiales altamente porosos y/o reduciendo el tamaño de partícula del foto-catalizador[214,238]. La obtención de una alta relación área superficial-volumen de partículas manométricas, fibras, tubos, etc. es otra razón importante para tratar de diseñar materiales foto-catalíticos a nanoescala. Otra posibilidad es el empleo

de soportes con áreas superficiales altas que faciliten la transferencia de los reactivos a los sitios activos.

Hoy día se está investigando la preparación de oxido de titanio con diferentes morfologías, fundamentalmente nano-partículas con suficiente cristalinidad y tamaño controlado, con el objetivo de obtener áreas superficiales altas y reducir la recombinación electrón-hueco[239]. También se han sintetizado nanotubos, nanofibras, nanoagujas, nanocintas, etc mediante síntesis hidrotermales. Estas morfologías tienen características porosas muy interesantes y adecuadas, presentan mejores propiedades de transferencia de carga[240], y además la recombinación en los límites de grano es menor, lo que se traduce en un mejor rendimiento foto-catalítico[228,236].

El empleo de partículas de tamaño nanométrico de TiO_2 con fines catalíticos también conlleva problemas o desventajas frente a otros formatos: (i) dificultad de separar el foto-catalizador de la solución tras la reacción; (ii) agregación de partículas en suspensión; (iii) dificultad para su aplicación en sistemas de flujo continuo[241]. Por estos motivos, el óxido de titanio ha sido soportado sobre diferentes materiales como alúmina, zeolita, gel de sílice, perlas de vidrio, cuarzo, acero, arcillas y carbón activado. En este sentido el empleo de materiales carbonosos como soportes de materiales foto-catalíticos tiene varias ventajas: i) el carbón adsorbe en un amplio rango la luz visible y por tanto puede actuar como sensibilizador produciendo una modificación de la banda prohibida (foto-sensibilización); ii) minimización de la recombinación electrón-hueco debido a la adsorción de electrones por parte del componente carbonoso, o mediante una mejor dispersión de las partículas de óxido de titanio disminuyendo el tamaño de éstas, y/o iii) puede mejorar el rendimiento catalítico ya que también adsorbe los reactivos. La mayoría de los materiales de carbón son muy porosos y tienen una elevada capacidad de adsorción de las sustancias reaccionantes, facilitando la transferencia de los reactivos a los sitios activos (calidad) y/o aumentando el número de sitios activos (cantidad) cuando se consigue una buena dispersión de partículas pequeñas de dióxido de titanio[242]. De este modo, la combinación de materiales de carbón con óxidos metálicos foto-activos puede dar lugar a materiales con altas prestaciones en foto-catálisis, mejorando la actividad bajo radiación UV e incluso dando lugar a materiales activos bajo luz visible.

1.3.3. Materiales carbonosos para la mejora de la foto-actividad de TiO_2

Las cualidades que debe tener un buen material para utilizarse como soporte del dióxido de titanio para aplicaciones foto-catalíticas son: (i) transparencia total o parcial a la radiación UV; (ii) ser químicamente inerte respecto a las moléculas contaminantes, sus productos intermedios y el sistema acuoso circundante; (iii) no afectar de forma negativa a la capacidad foto-catalítica del óxido de titanio; (iv) área superficial alta y buena capacidad de adsorción de los contaminantes; (v) poder recuperar el foto-catalizador de manera rápida y fácil, así como su reutilización con o sin regeneración. Por todas estas cualidades el carbón activado (entre otros materiales carbonosos) es uno de los materiales carbonosos que se ha utilizado y estudiado ampliamente como soporte para TiO_2[243].

1.3.3.1. Carbón-activado/TiO_2

Las técnicas de preparación de materiales compuestos carbón-activado/TiO_2 descritas en la bibliografía consultada son tan variadas como: mezcla mecánica[244], suspensiones acuosas[245,246], sol-gel[247], técnicas hidrotermales[248], deposición química de vapor[249-251], hidrólisis a baja temperatura[252], calcinación de resinas[253] y métodos sonoquímicos[254].

El carbón activo no solo actúa como soporte, sino que juega un papel activo en el mecanismo de foto-catálisis dando lugar a un efecto sinérgico entre el soporte y las partículas de dióxido de titanio aumentando su actividad foto-catalítica[255]. Este efecto se puso de manifiesto mediante el análisis de los productos intermedios obtenidos, los cuales eran diferentes a los obtenidos empleando el dióxido de titanio puro[255].

En el carbón activado los reactivos se adsorben sobre su superficie quedando retenidos cerca de los sitios foto-catalíticos donde reaccionan transformándose probablemente en diferentes compuestos intermedios antes de su desorción. En ausencia de carbón activado la probabilidad de que los reactivos se transformen en el producto final de degradación es menor, por lo que las soluciones tratadas suelen contener una mayor concentración de productos intermedios de degradación (Figura 1.14)[251].

Minero y col.[256] han establecido que el radical hidroxilo generado mediante foto-catálisis no se desplaza muy lejos del centro foto-áctivo por lo que la foto-degradación debe tener lugar virtualmente sobre la superficie del catalizador. Además, las investigaciones de Hernann y col.[257], y Matos y col.[258] sobre el mencionado efecto indican que se produce la adsorción de los contaminantes en la superficie del carbón activado seguido de la transferencia de éstos al TiO_2 a través de la interfase, dando lugar a la degradación completa como consecuencia del mayor tiempo de residencia del contaminante sobre el centro activo (Figura 1.14). Además, los compuestos orgánicos son hidrófobos mientras que las partículas de TiO_2, cuando se expone a la radiación UV, son hidrófilas. Por esta razón también el empleo de carbones activados como soporte mejora el rendimiento del proceso foto-catalítico.

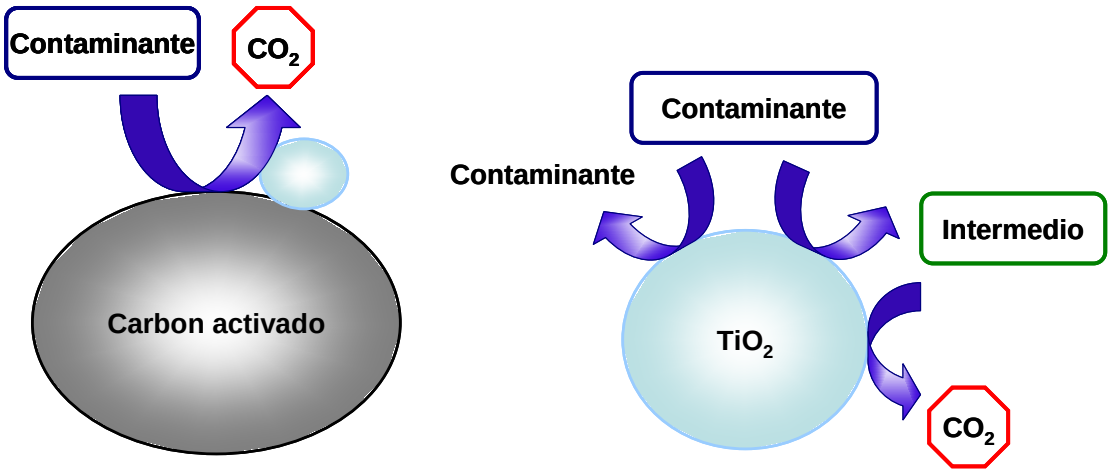

Figura 1.14. Efecto sinérgico en materiales carbón activado/TiO_2. Adaptado de X. Zhang y col.[251]

Como ejemplo de la importancia que tiene el tipo de porosidad de los materiales de carbón en foto-catálisis cabe mencionar el trabajo de Yuan y col.[253], que estudian la adsorción y la degradación fotocatalítica de β-ciclodestrina usando tres materiales compuestos de TiO_2 y fibras de carbón activado con diferentes tamaños de poro. Los tres materiales mejoraron la actividad catalítica del P25 debido a la presencia de la fase carbón, encontrándose además una clara relación entre el tamaño de poro y la actividad foto-catalítica. En el material con menor tamaño de poro, la ciclodestrina no accede a los ultramicroporos, dando lugar a una menor adsorción, y consecuentemente menor degradación. Al aumentar el tamaño de poros en el segundo (1,3-2 nm) y tercer (2-8 nm) material compuesto, la actividad foto-catalitica mejoró significativamente,

obteniéndose valores muy similares a persar de ser texturalmente diferentes, microporoso y mesoporoso, respectivamente; sin embargo sí se observaron comportamientos diferentes entre el material microporos y mesoporos durante la reutilización de los mismos. Mientras que el material microporoso sufrió una pérdida de actividad como consecuencia de tener una estructura porosa menos favorable a los procesos difusionales, el mesoporoso no se vio afectado.

Pese a las ventajas encontradas del carbón activado en la mejora de la actividad foto-catalítica del TiO_2, no se logra una reducción de la banda prohibida del óxido de titanio, de modo que no puede usarse luz visible para el proceso foto-catalítico.

1.3.3.2. Nanotubos de carbón/TiO_2

Los nanotubos de carbón son materiales carbonosos muy interesantes en el ámbito de la foto-catálisis debido a sus propiedades estructurales, químicas, térmicas y eléctricas. Estos materiales mejoran la actividad foto-catalítica mediante las tres rutas mencionadas en el apartado 1.3.2: alta área superficial para la adsorción de los reactivos, retardo de la recombinación electrón-hueco, y absorción de luz visible por modificación de la banda prohibida y/o sensibilización[259,260].

El área superficial específica de los nanotubos de carbón se sitúa en el rango de los 200-900 m^2g^{-1}, inferior a la de los carbones activados, pero suficientemente elevada para la dispersión del óxido de titanio. Además, son capaces de producir un retardo en la recombinación electrón-hueco, explicable en base a la conductividad eléctrica que presentan algunos nanotubos. El TiO_2 es un semiconductor tipo n pero en presencia de nanotubos de carbón, los electrones foto-generados pueden moverse libremente hacia la superficie del nanotubo, de modo que el nanotubo de carbón actúa como un aceptor de electrones (Figura 1.15a). Esto da lugar a un exceso de huecos en la banda de valencia del TiO_2 los cuales pueden emigrar a la superficie, sin recombinación con los electrones. Por tanto, en estos materiales compuestos el TiO_2 se comportaría realmente como un semiconductor tipo p[261]. Además, debido a la alta conductividad[262] y alta capacidad de almacenamiento eléctrico (un electrón por cada 32 átamos de carbono)[263], algunos nanotubos de carbón actúan como sumideros de electrones fotogenerados. En este sentido, Xu y col.[264] sugieren que dado la geometría de los nanotubos los

electrones pueden acumularse en los extremos de éstos proporcionando sitios de reducción altamente efectivos.

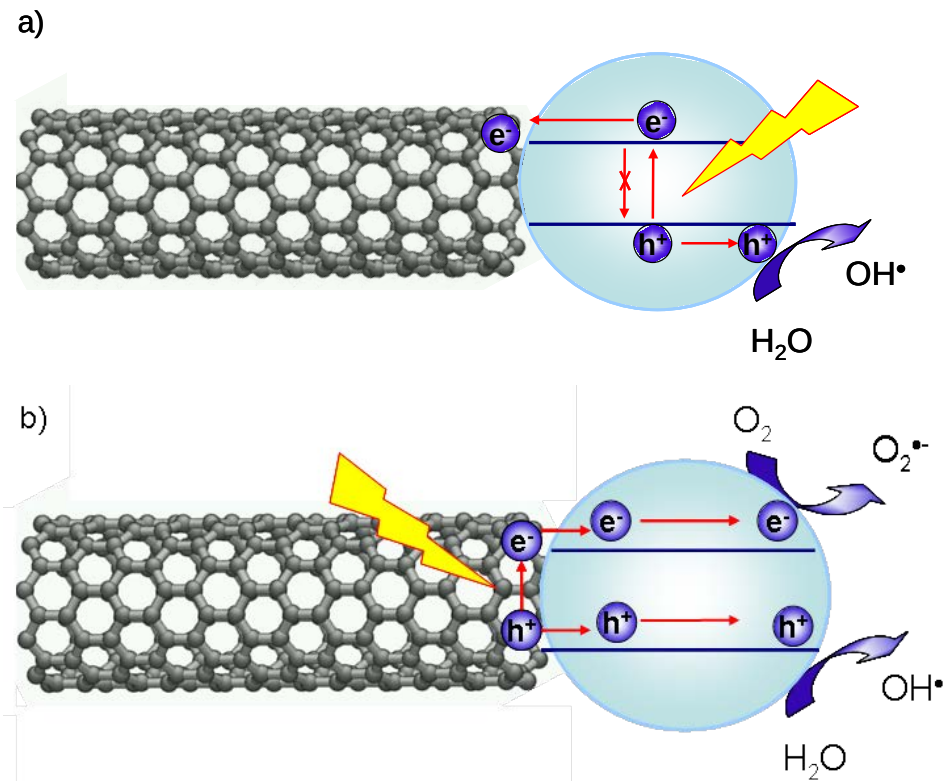

Figura 1.15. Mecanismos propuestos para el sinergismo encontrado en materiales compuestos CNT-TiO_2. a) Inhibición de la recombinación electrón hueco actuando como aceptor de los electrones foto-generados en el dióxido de titanio. b) Sensibilización del dióxido de titanio por el nanotubo de carbón generándose un par electrón-hueco que se transfiere al dióxido de titanio[265]. Adaptado de K. Woan y col.[259]. ● TiO_2

Los nanotubos también pueden actuar como sensibilizadores, transfiriendo electrones al óxido de titanio y permitiendo la absorción de luz visible (Figura 1.15b). De este modo, los electrones foto-generados en los nanotubos de carbón se transfieren a la banda de conducción del TiO_2 reduciendo así a las moléculas de oxígeno adsorbidas en su superficie y generando radicales superóxido. Simultáneamente, el nanotubo de carbono también transfiere el hueco positivo al TiO_2 que puede participar en una reacción de oxidación del agua formando radicales hidroxilo. Existe un acuerdo bastante amplio, sobre los mecanismos electrón-hueco anteriormente mencionados a través del material compuesto CNT/TiO_2, sin embargo no hay tanto acuerdo sobre qué

tipo de contacto es necesario entre ambas fases para que dichos mecanismos puedan producirse. Así, mientras hay autores que opinan que la simple mezcla física[266,267], o una adecuada interfase consecuencia de una elevada dispersión[254,265,266,268] sería suficiente para permitir tales efectos, otros creen que deben de producirse enlaces químicos[259,269].

Por otro lado, Lue y col.[270] han analizado el efecto de los defectos estructurales en los nanotubos. Para ello generan defectos en los nanotubos deliberadamente mediante tratamientos térmicos antes de usarlos como foto-catalizadores. Estos autores proponen que dichas vacantes provocan estados intermedios en la banda prohibida debido a un reordenamiento local dentro del tubo de carbono, lo cual le confiere de por sí foto-actividad bajo luz visible.

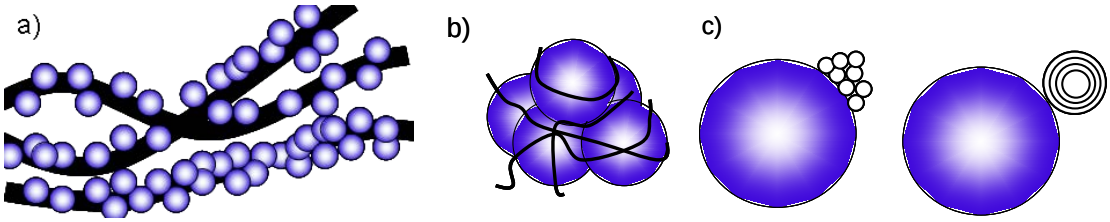

Figura 1.16. Morfologías de los materiales compuestos CNT-TiO_2 a) nanopartículas TiO_2 sobre nanotutos de carbón, b) nanotubos de carbón sobre partículas de TiO_2 y c) Nanotubos de pared simple y multiple sobre una partícula de TiO_2. Adaptado de Y. Yao y col.[266]. ● TiO_2

La deposición de las nanopartículas de dióxido de titanio sobre la superficie de los nanotubos afecta considerablemente al efecto sinérgico entre ambas fases, siendo necesario en cualquier caso, la obtención de una fina dispersión nanopartículas de TiO_2[271]. Yao y col.[266] han comparado diferentes métodos de preparación: deposición de pequeñas nanopartículas de titanio (5 nm) sobre nanotubos de carbón (Figura 1.16a), frente a nanotubos depositados sobre partículas grandes de dióxido de titanio (100 nm) (Figura 1.16b), usando tanto nanotubos de pared simple como de pared múltiple. Estos autores encuentran una actividad mayor cuando se emplean nanotubos de pared simple sobre partículas de 100 nm de TiO_2, lo que sugiere que tanto por la morfología como por el tipo de contacto que proporcionan, los nanotubos de pared simple presentan un mejor comportamiento. (Figura 1.16c).

1.3.3.3. Fullerenos C_{60}/TiO_2

Los fullerenos C_{60} poseen también unas propiedades electrónicas únicas, por tanto, pueden actuar mejorando la actividad foto-catalítica del TiO_2 en un modo similar al de los nanotubos de carbón. Los fulerenos C_{60} absorben moderadamente en el visible y fuertemente en la región UV del espectro[272-274]. Bajo luz UV/visible, los fullerenos C_{60} se excitan desde su estado fundamental a uno transitorio (≈1,2 ns[275]), un estado monoexcitado ($^1C_{60}^*$), que luego pasa rápidamente (a una velocidad de $5{,}0\cdot10^{-8}$ s^{-1}) a un estado triplemente excitado ($^3C_{60}^*$) de mayor duración (> 40 μs)[276,277]. Cabe destacar que los fullerenos en sus estados excitados son donantes y receptores de electrones mucho mejores que en su estado fundamental (capaz de aceptar hasta seis electrones)[276].

En fullerenos C_{60}, los estados excitados $^1C_{60}^*$ y $^3C_{60}^*$ se encuentran, en torno a 1,7[278] y 1,5 eV[279] por encima del estado fundamental, respectivamente. Dado que el potencial de reducción de un electrón de los fullerenos C_{60} o de sus estados excitados es de -0.2 eV (Vs NHE)[280], los electrones pueden transferirse de la banda de conducción del TiO_2 (-0,5 eV vs NHE) al fullereno C_{60}, dando lugar a la formación de un anión C_{60}^-. Este anión puede reaccionar con las especies adsorbidas en la interfase C_{60}-TiO_2. Sin embargo, los estados excitados de los fullerenos C_{60} también pueden actuar como donantes de electrones al TiO_2, dependiendo del entorno y las condiciones experimentales.

Así, existen trabajos recientes sobre materiales compuestos C_{60}-TiO_2, donde se describe el papel del fullereno tanto como electrón aceptor minimizando la recombinación electrón-hueco[281-284] (Figura 1.15a), o como electrón donor mediante el efecto sensibilizador que ejercería el fullereno sobre el dióxido de titanio[285] (Figura 1.15b).

1.3.3.4. Grafeno/TiO_2

El grafeno es un material carbonoso novedoso y muy interesante cuyas aplicaciones están siendo estudiadas en multitud de campos[286]. El interés de su empleo en foto-catálisis radica en aprovechar sus propiedades redox, y sobre todo, su

conductividad[287,288]. Las láminas de grafeno tienen un área superficial teórica de 2600 m^2 g^{-1}[289] permitiendo un transporte balístico, lo que significa que los electrones pueden viajar sin dispersarse con movilidades que exceden los 15.000 m^2 V^{-1} s^{-1} a temperatura ambiente[289-292], convirtiéndolos en sumideros de electrones potencialmente ideales, o puentes de transferencia de electrones. Su estructura, de un átomo de grosor, proporciona una elevada transparencia a la radiación[293], y acepta algunas modificaciones químicas que permite su uso como parte de un material compuesto[294-298]. Por tanto, la síntesis de materiales compuestos de grafeno y TiO_2 puede dar lugar a foto-catalizadores con elevadas prestaciones.

Zhang y col.[296] prepararon un material compuesto de óxido de grafeno-TiO_2 mediante un método hidrotermal, y analizaron su actividad foto-catalítica en la degradación de azul de metileno comparándolo con un P25 y con un material compuesto CNT-TiO_2. Los resultados de degradación fueron mejores en presencia de grafeno, debido a la mayor capacidad de adsorción del contaminante, a la minimización de la recombinación del par electrón-hueco a causa de su buena conductividad eléctrica, así como a una extensión de la absorción de la luz hacia mayores longitudes de onda en el rango del visible, favorecida por la transparencia del grafeno y a la disminución de la banda prohibida del dióxido de titanio por la presencia de enlaces Ti-O-C (similar al dopado con C).

1.4. OBJETIVOS DE LA TESIS

El objetivo principal de la presente Tesis Doctoral es el desarrollo de métodos experimentales de síntesis de materiales avanzados basados en xerogeles de carbón, incluyendo tanto materiales puros de carbón como materiales compuestos carbón – óxido inorgánico. Para la aplicación de estos materiales en catálisis se presta especial atención a parámetros tales como su microestructura, porosidad, acidez, dispersión e interacciones metal-soporte, tipo de centros activos, etc. Así pues, los métodos de síntesis anteriormente desarrollados en nuestros laboratorios se han ido adaptando para optimizar las propiedades de dichos materiales en diversas aplicaciones.

La hidrogenación selectiva de aldehídos alfa-beta insaturados requiere de catalizadores específicos que favorezcan la hidrogenación del grupo C=O en lugar del

C=C, termodinámicamente más favorable. En el desarrollo de catalizadores específicos para tal reacción se estudia la influencia del soporte, de la fase activa y de las condiciones de pre-tratamiento. Se efectúa una intensiva caracterización de los soportes y catalizadores aplicando una amplia variedad de técnicas experimentales. También se optimizan las condiciones de reacción para asegurar la ausencia de limitaciones difusionales y obtener el máximo rendimiento. De este modo se han podido establecer correlaciones entre las propiedades fisicoquímicas de los soportes, incluyendo diversos soportes inorgánicos, materiales de carbón y materiales compuestos, con su comportamiento catalítico, más específicamente, con el rendimiento a alcoholes insaturados. Debido a que los mejores resultados se obtuvieron con catalizadores soportados sobre xerogeles de carbón estructurados en microesferas y TiO_2 puros, en este último caso, específicamente tras un pre-tratamiento en hidrógeno, también se consideró la preparación de materiales compuestos (C/TiO_2), y recubrimientos cuyo desarrollo y prestaciones están siendo patentados.

Teniendo en cuenta la naturaleza de todos estos materiales, se planteó adicionalmente el estudio de sus aplicaciones en foto-catálisis, en este caso mediante procesos de degradación de azo-colorantes, contaminantes típicos del agua. El objetivo en este caso fue optimizar el material para aumentar sus prestaciones bajo radiación visible, aunque también se llevan a cabo experimentos usando radiación ultravioleta.

Finalmente, teniendo en cuenta el progresivo avance del uso de los materiales de carbón en aplicaciones biomédicas, y dado, que a pesar de las excelentes propiedades que presentan los aerogeles y xerogeles de carbón no se encontró ninguna referencia sobre la utilización de estos materiales en tales aplicaciones, se apostó también por esta línea, razón por la cual se incluye un capítulo referente a los trabajos realizados durante una estancia en la Universidad de Trieste, bajo la supervisión del Prof. Maurizio Prato, uno de los grandes especialistas en estos temas.

1.5. BIBLIOGRAFÍA

[1] R.W. Pekala. Organic aerogels from the polycondensation of resorcinol with formaldehyde, *Journal of Materials Science* **24**(9), 3221-3227, 1-9-1989.

[2] T. Yamamoto, T. Yoshida, T. Suzuki, S.R. Mukai, and H. Tamon. Dynamic and Static Light Scattering Study on the Sol-Gel Transition of Resorcinol-Formaldehyde Aqueous Solution, *Journal of Colloid and Interface Science* **245**(2), 391, 2002.

[3] S. Morales-Torres, F.J. Maldonado-Hódar, A.F. Pérez-Cadenas, and F. Carrasco-Marín. Textural and mechanical characteristics of carbon aerogels synthesized by polymerization of resorcinol and formaldehyde using alkali carbonates as basification agents, *Physical Chemistry Chemical Physics* **12**(35), 10365-10372, 2010.

[4] D. Fairén-Jiménez, F. Carrasco-Marín, and C. Moreno-Castilla. Inter- and Intra-Primary-Particle Structure of Monolithic Carbon Aerogels Obtained with Varying Solvents, *Langmuir* **24**(6), 2820, 2008.

[5] C. Lin and J.A. Ritter. Effect of synthesis pH on the structure of carbon xerogels, *Carbon* **35**(9), 1271, 1997.

[6] E. Gallegos-Suárez, A.F. Pérez-Cadenas, F.J. Maldonado-Hódar, and F. Carrasco-Marín. On the micro- and mesoporosity of carbon aerogels and xerogels. The role of the drying conditions during the synthesis processes, *Chemical Engineering Journal* **181-182**, 851, 2012.

[7] F.J. Maldonado-Hódar, M.A. Ferro-García, J. Rivera-Utrilla, and C. Moreno-Castilla. Synthesis and textural characteristics of organic aerogels, transition-metal-containing organic aerogels and their carbonized derivatives, *Carbon* **37**(8), 1199, 1999.

[8] F.J. Maldonado-Hódar, C. Moreno-Castilla, J. Rivera-Utrilla, and M.A. Ferro-García. Metal-carbon aerogels as catalysts and catalyst supports, *Studies in Surface Science and Catalysis* **130**, 1007, 2000.

[9] T.F. Baumann, G.A. Fox, J.H. Satcher, N. Yoshizawa, R. Fu, and M.S. Dresselhaus. Synthesis and Characterization of Copper-Doped Carbon Aerogels, *Langmuir* **18**(18), 7073, 2002.

[10] L.C. Cotet, M. Baia, L. Baia, I.C. Popescu, V. Cosoveanu, E. Indrea, J. Popp, and V. Danciu. Structural properties of some transition metal highly doped carbon aerogels, *Journal of Alloys and Compounds* **434–435**(0), 854, 2007.

[11] J.H. Ramirez, F.J. Maldonado-Hódar, A.F. Pérez-Cadenas, C. Moreno-Castilla, C.A. Costa, and L.M. Madeira. Azo-dye Orange II degradation by heterogeneous Fenton-like reaction using carbon-Fe catalysts, *Applied Catalysis B: Environmental* **75**(3–4), 312, 2007.

[12] F. Duarte, F.J. Maldonado-Hódar, A.F. Pérez-Cadenas, and L.M. Madeira. Fenton-like degradation of azo-dye Orange II catalyzed by transition metals on carbon aerogels, *Applied Catalysis B: Environmental* **85**(3–4), 139, 2009.

[13] A.F. Pérez-Cadenas, C.H. Ros, S. Morales-Torres, M. Pérez-Cadenas, P.J. Kooyman, C. Moreno-Castilla, and F. Kapteijn. Metal-doped carbon xerogels for the electro-catalytic conversion of CO_2 to hydrocarbons, *Carbon* **56**, 324, 2013.

[14] C. Moreno-Castilla, M.B. Dawidziuk, F. Carrasco-Marín, and Z. Zapata-Benabithe. Surface characteristics and electrochemical capacitances of carbon aerogels obtained from resorcinol and pyrocatechol using boric and oxalic acids as polymerization catalysts, *Carbon* **49**(12), 3808, 2011.

[15] C. Moreno-Castilla, M.B. Dawidziuk, F. Carrasco-Marín, and E. Morallón. Electrochemical performance of carbon gels with variable surface chemistry and physics, *Carbon* **50**(9), 3324, 2012.

[16] Z. Zapata-Benabithe, F. Carrasco-Marín, and C. Moreno-Castilla. Preparation, surface characteristics, and electrochemical double-layer capacitance of KOH-activated carbon aerogels and their O- and N-doped derivatives, *Journal of Power Sources* **219**(0), 80, 2012.

[17] Z. Zapata-Benabithe, F. Carrasco-Marín, and C. Moreno-Castilla. Electrochemical performance of Cu- and Ag-doped carbon aerogels, *Materials Chemistry and Physics* **138**(2–3), 870, 2013.

[18] Z. Zapata-Benabithe, J. de Vicente, F. Carrasco-Marín, and C. Moreno-Castilla. Synthesis, surface characteristics, and electrochemical capacitance of Cu-doped carbon xerogel microspheres, *Carbon* **55**(0), 260, 2013.

[19] Z. Zapata-Benabithe, F. Carrasco-Marín, J. de Vicente, and C. Moreno-Castilla. Carbon Xerogel Microspheres and Monoliths from Resorcinol–Formaldehyde Mixtures with Varying Dilution Ratios: Preparation, Surface Characteristics, and Electrochemical Double-Layer Capacitances, *Langmuir* **29**(20), 6166, 2013.

[20] Z. Zapata-Benabihe, C. Moreno-Castilla, and F. Carrasco-Marín. Influence of the boron precursor and drying method on surface properties and electrochemical behavior of boron-doped carbon gels, *Langmuir* **30**(6), 1716, 2014.

[21] F.J. Maldonado-Hódar, C. Moreno-Castilla, and A.F. Pérez-Cadenas. Surface morphology, metal dispersion, and pore texture of transition metal-doped monolithic carbon aerogels and steam-activated derivatives, *Microporous and Mesoporous Materials* **69**(1–2), 119, 2004.

[22] M. Sánchez-Polo, J. Rivera-Utrilla, and U. von Gunten. Bromide and iodide removal from waters under dynamic conditions by Ag-doped aerogels, *Journal of Colloid and Interface Science* **306**(1), 183, 2007.

[23] C. Moreno-Castilla, F.J. Maldonado-Hódar, and A.F. Pérez-Cadenas. Physicochemical Surface Properties of Fe, Co, Ni, and Cu-Doped Monolithic Organic Aerogels, *Langmuir* **19**(14), 5650, 2003.

[24] C. Moreno-Castilla and F.J. Maldonado-Hódar. Carbon aerogels for catalysis applications: An overview, *Carbon* **43**(3), 455, 2005.

[25] E. Bekyarova and K. Kaneko. Structure and Physical Properties of Tailor-Made Ce,Zr-Doped Carbon Aerogels, *Advanced Materials* **12**(21), 1625-1628, 1-11-2000.

[26] H. Jirglová and F.J. Maldonado-Hódar. Chemical Interactions of Surface-Active Agents with Growing Resorcinol-Formaldehyde Gels, *Langmuir* **26**(20), 16103, 2010.

[27] F.J. Maldonado-Hódar, H. Jirglová, A.F. Pérez-Cadenas, and S. Morales-Torres. Chemical control of the characteristics of Mo-doped carbon xerogels by surfactant-mediated synthesis, *Carbon* **51**(0), 213, 2013.

[28] F. J. Maldonado-Hódar, A. F. Pérez-Cadenas, and H. Jirglová, Patent No. ES2366848B8 (6 December 2012).

[29] C. Moreno-Castilla, F.J. Maldonado-Hódar, F. Carrasco-Marín, and E. Rodríguez-Castellón. Surface Characteristics of Titania/Carbon Composite Aerogels, *Langmuir* **18**(6), 2295, 2002.

[30] C. Moreno-Castilla and F.J. Maldonado-Hodar. Synthesis and surface characteristics of silica- and alumina-carbon composite xerogels, *Physical Chemistry Chemical Physics* **2**(20), 4818-4822, 2000.

[31] F.J. Maldonado-Hódar, C. Moreno-Castilla, and J. Rivera-Utrilla. Synthesis, pore texture and surface acid-base character of TiO_2/carbon composite xerogels and aerogels and their carbonized derivatives, *Applied Catalysis A: General* **203**(1), 151, 2000.

[32] H.M. Luo, Y.F. Yang, Y.X. Sun, X. Zhao, and J.Q. Zhang. Preparation of fructose-based attapulgite template carbon materials and their electrochemical performance as supercapacitor electrodes, *Journal of Solid State Electrochemistry* , 1-10, 2015.

[33] W. Schmidt, "Titanium-Based Nanoporous Materials",in *Ordered Porous Solids: Recent Advances and Prospects,* edited by V. Valtchec, S. Mintova, and M. Tsapatsis (Elsevier, Amsterdam, 2009), p.63.

[34] K.H.C. Baser, M. Kürkçüoglu, and B. Demirci. Ninde Oil (Aeollanthus myrianthus Taylor) Revisited: Analysis of a Historical Oil, *Journal of Essential Oil Research* **17**(2), 137, 2005.

[35] H. Baydar and N.G. Baydar. The effects of harvest date, fermentation duration and Tween 20 treatment on essential oil content and composition of industrial oil rose (Rosa damascena Mill.), *Industrial Crops and Products* **21**(2), 251, 2005.

[36] V.S. Dubey and R. Luthra. Biotransformation of geranyl acetate to geraniol during palmarosa (Cymbopogon martinii, Roxb. wats. var. motia) inflorescence development, *Phytochemistry* **57**(5), 675, 2001.

[37] D.Z. Simon, J. Beliveau, and C. Aube. Extraction by hydrodiffusion of the essential oil of Monarda fistulosa grown in the province of Quebec: Assay of

geraniol in the hydrodiffused oil, *International Journal of Crude Drug Research* **24**(3), 120, 1986.

[38] B.R. Rajeswara Rao, A.K. Bhattacharya, G.R. Mallavarapu, and S. Ramesh. Yellowing and crinkling disease and its impact on the yield and composition of the essential oil of citronella (Cymbopogon winterianus Jowitt.), *Flavour and Fragrance Journal* **19**(4), 344-350, 2004.

[39] P.Z. Bedoukian, *geraniol and nerol. perfumery and flavoring synthetics*, third, revised edition ed. (Allured Publishing Corporation, Wheaton (USA), 1986).

[40] G.S. Clark. Geraniol, *Perfumer & Flavorist* **23**, 19, 1998.

[41] S.C. Rastogi, J.D. Johansen, P. Frosch, T. Menne, M. Bruze, J.P. Lepoittevin, B. Dreier, K.E. Andersen, and I.R. White. Deodorants on the European market: quantitative chemical analysis of 21 fragrances, *Contact Dermatitis* **38**(1), 29, 1998.

[42] S.C. Rastogi, S. Heydorn, J.D. Johansen, and D.A. Basketter. Fragrance chemicals in domestic and occupational products, *Contact Dermatitis* **45**(4), 221, 2001.

[43] S.C. Rastogi, J.D. Johansen, and T. Menné. Natural ingredients based cosmetics. Content of selected fragrance sensitizers, *Contact Dermatitis* **34**(6), 423, 1996.

[44] W. Chen and A.M. Viljoen. Geraniol: A review of a commercially important fragrance material, *South African Journal of Botany* **76**(4), 643, 2010.

[45] K. Sato, S. Krist, and G. Buchbauer. Antimicrobial effect of vapours of geraniol, (R)-(–)-linalool, terpineol, γ–terpinene and 1,8-cineole on airborne microbes using an airwasher, *Flavour and Fragrance Journal* **22**(5), 435-437, 2007.

[46] *http://www.bugband.net*2013).

[47] *http://www.fulltec.org*2013).

[48] D.P. Papachristos, K.I. Karamanoli, D.C. Stamopoulos, and U. Menkissoglu-Spiroudi. The relationship between the chemical composition of three essential oils and their insecticidal activity against Acanthoscelides obtectus (Say), *Pest Management Science* **60**(5), 514-520, 2004.

[49] P. Ji, M.S. Si, Y. Podnos, and D.K. Imagawa. Monoterpene geraniol prevents acute allograft rejection, *Transplantation Proceedings* **34**(5), 1418, 2002.

[50] I. Hierro, A. Valero, P. Pérez, P. González, M.M. Cabo, M.P. Montilla, and M.C. Navarro. Action of different monoterpenic compounds against Anisakis simplex s.l. L3 larvae, *Phytomedicine* **11**(1), 77, 2004.

[51] M.C. Navarro, M.A. Noguera, M.C. Romero, M.P. Montilla, J.M. González de Selgas, and A. Valero. Anisakis simplex s.l.: Larvicidal activity of various monoterpenic derivatives of natural origin against L3 larvae in vitro and in vivo, *Experimental Parasitology* **120**(4), 295, 2008.

[52] A.E. Edris. Pharmaceutical and therapeutic potentials of essential oils and their individual volatile constituents: A review, *Phytotherapy Research* **21**(4), 308, 2007.

[53] M. Tiwari and P. Kakkar. Plant derived antioxidants-Geraniol and camphene protect rat alveolar macrophages against t-BHP induced oxidative stress, *Toxicology in Vitro* **23**(2), 295, 2009.

[54] Y. Shoji, H. Ishige, N. Tamura, W. Iwatani, M. Norimatsu, J. Shimada, and Y. Mizushima. Enhancement of anti-herpetic activity of antisense phosphorothioate oligonucleotides 5' end modified with geraniol, *Journal of Drug Targeting* **5**(4), 261, 1998.

[55] S.T. Ahmad, W. Arjumand, A. Seth, S. Nafees, S. Rashid, N. Ali, and S. Sultana. Preclinical renal cancer chemopreventive efficacy of geraniol by modulation of multiple molecular pathways, *Toxicology* **290**(1), 69, 2011.

[56] S.H. Kim, H.C. Bae, E.J. Park, C.R. Lee, B.J. Kim, S. Lee, H.H. Park, S.J. Kim, I. So, T.W. Kim, and J.H. Jeon. Geraniol inhibits prostate cancer growth by targeting cell cycle and apoptosis pathways, *Biochemical and Biophysical Research Communications* **407**(1), 129, 2011.

[57] A. Madankumar, S. Jayakumar, S. Asokkumar, S. Raghunandhakumar, C. Naveenkumar, and T. Devaki. Chemopreventive potential of geraniol on 4-Nitroquinoline-1 oxide induced oral carcinogenesis in rats, *International Journal of Research in Pharmaceutical Sciences* **2**(4), 531, 2011.

[58] M.P. Polo and M.G. de Bravo. Effect of geraniol on fatty-acid and mevalonate metabolism in the human hepatoma cell line Hep G2, *Biochemistry and Cell Biology* **84**(1), 102-111, 1-2-2006.

[59] D.A. Wiseman, S.R. Werner, and P.L. Crowell. Cell cycle arrest by the isoprenoids perillyl alcohol, geraniol, and farnesol is mediated by p21 Cip1 and p27 Kip1 in human pancreatic adenocarcinoma cells, *Journal of Pharmacology and Experimental Therapeutics* **320**(3), 1163, 2007.

[60] J. Groling, *ullmann's encyclopedia of industrial chemistry*, Seven ed. (Electronic Release, Weinheim, 2003).

[61] M. Eisenacher, S. Beschnitt, and W. Hölderich. Novel route to a fruitful mixture of terpene fragrances in particular phellandrene starting from natural feedstock geraniol using weak acidic boron based catalyst, *Catalysis Communications* **26**(0), 214, 2012.

[62] L.P. Somogyi and A. Kishi, "Aroma Chemicals and the Flavour and Fragance Industry; Chemical Economics Handbook (CEH) Product Review",in *Tecchnical Report for SRI International*,(CA (USA), Menlo Park, 2001).

[63] R Weiss, New York Patent No. US28823223 (14 April 1959).

[64] H. Surburg and J. Panten, *common fragrance and flavor materials: preparation, properties and uses*, 5th ed. (WILEY-VCH, Weinheim, Germany, 2006).

[65] P. Serp and J.L. Figueiredo, *carbon materials for catalysis* (John Wiley & Sons, Hoboken, N.J., 2009).

[66] A.F. Pérez-Cadenas, C.H. Ros, S. Morales-Torres, M. Pérez-Cadenas, P.J. Kooyman, C. Moreno-Castilla, and F. Kapteijn. Metal-doped carbon xerogels for the electro-catalytic conversion of CO_2 to hydrocarbons, *Carbon* **56**, 324, 2013.

[67] C. Moreno-Castilla and F.J. Maldonado-Hódar. Carbon aerogels for catalysis applications: An overview, *Carbon* **43**(3), 455, 2005.

[68] S. Morales-Torres, F.J. Maldonado-Hódar, A.F. Pérez-Cadenas, and F. Carrasco-Marín. Design of low-temperature Pt-carbon combustion catalysts for VOC's treatments, *Journal of Hazardous Materials* **183**(1-3), 814, 2010.

[69] F.J. Maldonado-Hódar, C. Moreno-Castilla, and A.F. Pérez-Cadenas. Catalytic combustion of toluene on platinum-containing monolithic carbon aerogels, *Applied Catalysis B: Environmental* **54**(4), 217, 2004.

[70] F. Duarte, F.J. Maldonado-Hódar, A.F. Pérez-Cadenas, and L.M. Madeira. Fenton-like degradation of azo-dye Orange II catalyzed by transition metals on carbon aerogels, *Applied Catalysis B: Environmental* **85**(3–4), 139, 2009.

[71] P.V. Samant, M.F.R. Pereira, and J.L. Figueiredo. Mesoporous carbon supported Pt and Pt–Sn catalysts for hydrogenation of cinnamaldehyde, *Catalysis Today* **102–103**(0), 183, 2005.

[72] N. Mahata, F. Gonçalves, M.F. Pereira, and J.L. Figueiredo. Selective hydrogenation of cinnamaldehyde to cinnamyl alcohol over mesoporous carbon supported Fe and Zn promoted Pt catalyst, *Applied Catalysis A: General* **339**(2), 159, 2008.

[73] B.F. Machado, S. Morales-Torres, A.F. Pérez-Cadenas, F.J. Maldonado-Hódar, F. Carrasco-Marín, A.M.T. Silva, J.L. Figueiredo, and J.L. Faria. Preparation of carbon aerogel supported platinum catalysts for the selective hydrogenation of cinnamaldehyde, *Applied Catalysis A: General* **425–426**(0), 161, 2012.

[74] A. Giroir-Fendler, D. Richard, and P. Gallezot, *heterogeneus catalysis and fine chemicals. studies in surface science and catalysis.* (Elsevier, Amsterdam, 1988).

[75] K. Kouachi, G. Lafaye, C. Especel, O. Cherifi, and P. Marecot. Effects of support and metal loading on the characteristics of Co based catalysts for selective hydrogenation of citral, *Journal of Molecular Catalysis A-Chemical* **280**(1-2), 52, 2008.

[76] G. Neri, L. Mercadante, A. Donato, A.M. Visco, and S. Galvagno. Influence of Ru precursor, support and solvent in the hydrogenation of citral over ruthenium catalysts, *Catalysis Letters* **29**(3), 379, 1994.

[77] U.K. Singh and M.A. Vannice. Liquid-phase citral hydrogenation over SiO_2-supported group VIII metals, *Journal of Catalysis* **199**(1), 73, 2001.

[78] B. Coq, P.S. Kumbhar, C. Moreau, P. Moreau, and M.G. Warawdekar. Liquid phase hydrogenation of cinnamaldehyde over supported ruthenium catalysts: Influence of particle size, bimetallics and nature of support, *Journal of Molecular Catalysis* **85**(2), 215, 1993.

[79] A. Giroir-Fendler, D. Richard, and P. Gallezot. Chemioselectivity in the catalytic hydrogenation of cinnamaldehyde. Effect of metal particle morphology, *Catalysis Letters* **5**(2), 175, 1990.

[80] A.J. Plomp, H. Vuori, A.O. Krause, K.P. de Jong, and J.H. Bitter. Particle size effects for carbon nanofiber supported platinum and ruthenium catalysts for the selective hydrogenation of cinnamaldehyde, *Applied Catalysis A: General* **351**(1), 9, 2008.

[81] G. Neri, C. Milone, A. Donato, L. Mercadante, and A.M. Visco. Selective Hydrogenation of Citral Over Pt-Sn Supported on Activated Carbon, *Journal of Chemical Technology and Biotechnology* **60**(1), 83, 1994.

[82] G. Neri, L. Mercadante, C. Milone, R. Pietropaolo, and S. Galvagno. Hydrogenation of citral and cinnamaldehyde over bimetallic Ru-Me/Al_2O_3 catalysts, *Journal of Molecular Catalysis A: Chemical* **108**(1), 41, 1996.

[83] V. Ponec. On the role of promoters in hydrogenations on metals; α,β−unsaturated aldehydes and ketones, *Applied Catalysis A: General* **149**(1), 27, 1997.

[84] P. Barbaro and F. Liguori, *heterogenized homogeneous catalysts for fine chemicals production: materials and processes* (Springer, 2010).

[85] P. Claus and Y. Önal, "Regioselective Hydrogenations. Handbook of Heterogeneous Catalysis",in *Handbook of Heterogeneous Catalysis*, Second ed. edited by G. Ertl, H. Knözinger, F. Schüth, and J. Weitkamp (WILEY-VCH, 2008), pp.3311-3312.

[86] A. Vannice and U.K. Singh. Citral hydrogenation over Pt and other group VIII metals, *Abstracts of Papers of the American Chemical Society* **223**, U437, 2002.

[87] F. Delbecq and P. Sautet. A Density Functional Study of Adsorption Structures of Unsaturated Aldehydes on Pt(111): A Key Factor for Hydrogenation Selectivity, *Journal of Catalysis* **211**(2), 398, 2002.

[88] P. Claus. Selective hydrogenation of α,β−unsaturated aldehydes and other C=O and C=C bonds containing compounds, *Topics in Catalysis* **5**(1), 51, 1998.

[89] T. Ekou, A. Vicente, G. Lafaye, C. Especel, and P. Marecot. Bimetallic Rh-Ge and Pt-Ge catalysts supported on TiO_2 for citral hydrogenation II. Catalytic properties, *Applied Catalysis A-General* **314**(1), 73, 2006.

[90] P. Maki-Arvela, L.P. Tiainen, A.K. Neyestanaki, R. Sjoholm, T.K. Rantakyla, E. Laine, T. Salmi, and D.Y. Murzin. Liquid phase hydrogenation of citral: suppression of side reactions, *Applied Catalysis A-General* **237**(1-2), 181, 2002.

[91] J. Hájek, N. Kumar, P. Mäki-Arvela, T. Salmi, D.Y. Murzin, I. Paseka, T. Heikkilä, E. Laine, P. Laukkanen, and J. Väyrynen. Ruthenium-modified MCM-41 mesoporous molecular sieve and Y zeolite catalysts for selective hydrogenation of cinnamaldehyde, *Applied Catalysis A: General* **251**(2), 385, 2003.

[92] T.E. Berty, H.H. Reamer, and B.H. Sage. Phase Behavior in the Hydrogen-Cyclohexane System, *Journal of Chemical & Engineering Data* **11**(1), 25, 1966.

[93] J. Hájek, N. Kumar, P. Mäki-Arvela, T. Salmi, D.Y. Murzin, I. Paseka, T. Heikkilä, E. Laine, P. Laukkanen, and J. Väyrynen. Ruthenium-modified MCM-41 mesoporous molecular sieve and Y zeolite catalysts for selective hydrogenation of cinnamaldehyde, *Applied Catalysis A: General* **251**(2), 385, 2003.

[94] I. Kun, G. Szöllösi, and M. Bartók. Crotonaldehyde hydrogenation over clay-supported platinum catalysts, *Journal of Molecular Catalysis A: Chemical* **169**(1–2), 235, 2001.

[95] H. Yamada and S. Goto. The Effect of Solvents Polarity on Selective Hydrogenation of Unsaturated Aldehyde in Gas-Liquid-Solid Three Phase Reactor, *Journal of Chemical Engineering of Japan* **36**(5), 586, 2003.

[96] M. Burgener, R. Furrer, T. Mallat, and A. Baiker. Hydrogenation of citral over Pd/alumina: comparison of "supercritical" CO_2 and conventional solvents in continuous and batch reactors, *Applied Catalysis A-General* **268**(1-2), 1, 2004.

[97] F. Zhao, S.i. Fujita, S. Akihara, and M. Arai. Hydrogenation of Benzaldehyde and Cinnamaldehyde in Compressed CO_2 Medium with a Pt/C Catalyst: A Study on Molecular Interactions and Pressure Effects, *The Journal of Physical Chemistry A* **109**(19), 4419, 2005.

[98] R. Liu, F. Zhao, S.i. Fujita, and M. Arai. Selective hydrogenation of citral with transition metal complexes in supercritical carbon dioxide, *Applied Catalysis A: General* **316**(2), 127, 2007.

[99] H.J. Jiang, H.B. Jiang, D.M. Zhu, X.L. Zheng, H.Y. Fu, H. Chen, and R.X. Li. Cooperation between the surface hydroxyl groups of the support and organic additives in the highly selective hydrogenation of citral, *Applied Catalysis A: General* **445-446**, 351, 2012.

[100] S.i. Fujita, Y. Sano, B.M. Bhanage, and M. Arai. Supported liquid-phase catalysts containing ruthenium complexes for selective hydrogenation of α,β-unsaturated aldehyde: importance of interfaces between liquid film, solvent, and support for the control of product selectivity, *Journal of Catalysis* **225**(1), 95, 2004.

[101] W. Strohmeier, B. Graser, R. Mar-çec, and K. Holke. Comparison of the activity of homogeneous catalysts in liquid phase without solvent and as supported liquid phase catalysts (SLPC), *Journal of Molecular Catalysis* **11**(2–3), 257, 1981.

[102] S.i. Fujita, Y. Sano, B.M. Bhanage, and M. Arai. Supported liquid-phase catalysts containing ruthenium complexes for selective hydrogenation of α,β-unsaturated aldehyde: importance of interfaces between liquid film, solvent, and support for the control of product selectivity, *Journal of Catalysis* **225**(1), 95, 2004.

[103] D. Sokolskii, N. Anisimova, A. Zharmagambetova, S. Mukhamedzhanova, and L. Edygenova. Pt-Fe_2O_3 catalytic system for hydrogenation reactions, *Reaction Kinetics and Catalysis Letters* **33**(2), 399, 1987.

[104] D.V. Sokolskii, A.M. Pak, M.A. Ginzburg, and V.F. Vozdvizhenskii. Hydrogenation of Citral on Group-VIII Metals, *Doklady Akademii Nauk Sssr* **239**(4), 897, 1978.

[105] F. Delbecq and P. Sautet. Competitive C=C and C=O Adsorption of α,β–Unsaturated Aldehydes on Pt and Pd Surfaces in Relation with the Selectivity of Hydrogenation Reactions: A Theoretical Approach, *Journal of Catalysis* **152**(2), 217, 1995.

[106] P. Claus and Y. Önal, "Regioselective Hydrogenations. Handbook of Heterogeneous Catalysis",in *Handbook of Heterogeneous Catalysis*, Second ed. edited by G. Ertl, H. Knözinger, F. Schüth, and J. Weitkamp (WILEY-VCH, 2008), pp.3311-3312.

[107] P. Sautet. Theoretical chemistry as a tool for interpreting catalysts selectivities, *Topics in Catalysis* **13**(3), 213, 2000.

[108] J.L. Davis and M.A. Barteau. Vinyl substituent effects on the reactions of higher oxygenates on Pd(111), *Journal of Molecular Catalysis* **77**(1), 109, 1992.

[109] C.S. Fadley and D.A. Shirley. 3rd Materials Research Symposium- Electronic Density of States, *Gaithersburg,MD.* 1969.

[110] D. Manikandan, D. Divakar, and T. Sivakumar. Selective hydrogenation of citral over noble metals intercalated montmorillonite catalysts, *Catalysis Letters* **123**(1-2), 107, 2008.

[111] P. Claus and Y. Önal, "Regioselective Hydrogenations. Handbook of Heterogeneous Catalysis",in *Handbook of Heterogeneous Catalysis*, Second ed. edited by G. Ertl, H. Knözinger, F. Schüth, and J. Weitkamp (WILEY-VCH, 2008), pp.3311-3312.

[112] T. Ekou, L. Ekou, A. Vicente, G. Lafaye, S. Pronier, C. Especel, and P. Marecot. Citral hydrogenation over Rh and Pt catalysts supported on TiO_2: Influence of the preparation and activation protocols of the catalysts, *Journal of Molecular Catalysis A-Chemical* **337**(1-2), 82, 2011.

[113] A. Vicente, T. Ekou, G. Lafaye, C. Especel, P. Marecot, and C.T. Williams. Influence of the nature of the precursor salts on the properties of Rh-Ge/TiO_2 catalysts for citral hydrogenation, *Journal of Catalysis* **275**(2), 202, 2010.

[114] L. Sordelli, R. Psaro, G. Vlaic, A. Cepparo, S. Recchia, C. Dossi, A. Fusi, and R. Zanoni. EXAFS studies of supported Rh-Sn catalysts for citral hydrogenation, *Journal of Catalysis* **182**(1), 186, 1999.

[115] S.A. Ananthan and V. Narayanan. Liquid phase selective hydrogenation of citral over Ru/TiO_2 and Pt/TiO_2 nano catalysts, *Proceedings of the International Conference on Nanoscience, Engineering and Technology, ICONSET 2011* , 23-29, 2011.

[116] S. Mukherjee and M.A. Vannice. Solvent effects in liquid-phase reactions - I. Activity and selectivity during citral hydrogenation on Pt/SiO_2 and evaluation of mass transfer effects, *Journal of Catalysis* **243**(1), 108, 2006.

[117] G. Diaz, A. Gomez-Cortes, O. Hernandez-Cristobal, J.J. Murcia, G. Borda, and H. Rojas. Hydrogenation of Citral Over $IrAu/TiO_2$ Catalysts. Effect of the Preparation Method, *Topics in Catalysis* **54**(8-9), 467, 2011.

[118] H. Rojas, G. Borda, P. Reyes, J.J. Martinez, J. Valencia, and J.L.G. Fierro. Citral hydrogenation over Ir/TiO_2 and $Ir/TiO_2/SiO_2$ catalysts, *Catalysis Today* **133**, 699, 2008.

[119] G. Borda, H. Rojas, J. Murcia, J.L.G. Fierro, P. Reyes, and M. Oportus. Hydrogenation of citral on Ir/SiO_2 catalysts. Effect of the addition of Nb_2O_5 on surface and catalytic properties, *Reaction Kinetics and Catalysis Letters* **92**(2), 369, 2007.

[120] P. Reyes, H. Rojas, G. Pecchi, and J.L.G. Fierro. Liquid-phase hydrogenation of citral over Ir-supported catalysts, *Journal of Molecular Catalysis A-Chemical* **179**(1-2), 293, 2002.

[121] N.M. Bertero, A.F. Trasarti, B. Moraweck, A. Borgna, and A.J. Marchi. Selective liquid-phase hydrogenation of citral over supported bimetallic Pt-Co catalysts, *Applied Catalysis A-General* **358**(1), 32, 2009.

[122] R.X. Liu and F.Y. Zhao. Selective hydrogenation of citral over Au-based bimetallic catalysts in supercritical carbon dioxide, *Science China-Chemistry* **53**(7), 1571, 2010.

[123] A.M. Silva, O.A.A. Santos, M.J. Mendes, E. Jordao, and M.A. Fraga. Hydrogenation of citral over ruthenium-tin catalysts, *Applied Catalysis A-General* **241**(1-2), 155, 2003.

[124] A. Vicente, G. Lafaye, C. Especel, P. Marecot, and C.T. Williams. The relationship between the structural properties of bimetallic $Pd-Sn/SiO_2$ catalysts and their performance for selective citral hydrogenation, *Journal of Catalysis* **283**(2), 133, 2011.

[125] L.P. Tiainen, P. Maki-Arvela, and T. Salmi. Modelling of citral hydrogenation kinetics on an Ni/Al_2O_3 catalyst, *Catalysis Today* **48**(1-4), 57, 1999.

[126] A.M. Pak, S.R. Konuspaev, G.D. Zakumbaeva, and D.V. Sokolskii. Hydrogenation of Citral to Citronellol Over Ni-Cr_2O_3, *Reaction Kinetics and Catalysis Letters* **16**(4), 339, 1981.

[127] E. Asedegbega-Nieto, B. Bachiller-Baeza, A. Guerrero-Ruiz, and I. Rodriguez-Ramos. Modification of catalytic properties over carbon supported Ru-Cu and Ni-Cu bimetallics - I. Functional selectivities in citral and cinnamaldehyde hydrogenation, *Applied Catalysis A-General* **300**(2), 120, 2006.

[128] A.F. Pérez-Cadenas, M.M.P. Zieverink, F. Kapteijn, and J.A. Moulijn. High performance monolithic catalysts for hydrogenation reactions, *Catalysis Today* **105**(3-4), 623, 2005.

[129] A.F. Pérez-Cadenas, F. Kapteijn, M.M.P. Zieverink, and J.A. Moulijn. Selective hydrogenation of fatty acid methyl esters over palladium on carbon-based monoliths: Structural control of activity and selectivity, *Catalysis Today* **128**(1–2), 13, 2007.

[130] S. Galvagno, C. Milone, A. Donate, G. Neri, and R. Pietropaolo. Influence of metal particle size in the hydrogenation of citral over Ru/C, *Catalysis Letters* **18**(4), 349, 1993.

[131] S. Galvagno, C. Milone, G. Neri, A. Donato, and R. Pietropaolo. Hydrogenation of Cinnamaldehyde and Citral Over Ru Supported Catalysts, *Heterogeneous Catalysis and Fine Chemicals III* **78**, 163, 1993.

[132] G. Neri, C. Milone, S. Galvagno, A.P.J. Pijpers, and J. Schwank. Characterization of Pt-Sn/carbon hydrogenation catalysts, *Applied Catalysis A: General* **227**(1–2), 105, 2002.

[133] J.C. Serrano-Ruiz, A. Sepulveda-Escribano, F. Rodríguez-Reinoso, and D. Duprez. Pt-Sn catalysts supported on highly-dispersed ceria on carbon - Application to citral hydrogenation, *Journal of Molecular Catalysis A-Chemical* **268**(1-2), 227, 2007.

[134] I.M. Vilella, I. Borbath, F. Somodi, J.L. Margitfalvi, S.R. de Miguel, and O.A. Scelza. The influence of the preparation method on the behaviour of PtGe catalysts supported on activated carbon in citral hydrogenation, *Catalysis Letters* **125**(3-4), 254, 2008.

[135] I.M.J. Vilella, S.R. de Miguel, and O.A. Scelza. Hydrogenation of citral on Pt and PtSn supported on activated carbon felts (ACF), *Latin American Applied Research* **35**(1), 51, 2005.

[136] I.M.J. Vilella, S.R. de Miguel, and O.A. Scelza. Pt, PtSn and PtGe catalysts supported on granular carbon for fine chemistry hydrogenation reactions, *Journal of Molecular Catalysis A: Chemical* **284**(1-2), 161, 2008.

[137] I.M.J. Vilella, S.R. Miguel, C.S.-M.d.L. Lecea, A. Linares-Solano, and O.A. Scelza. Catalytic performance in citral hydrogenation and characterization of PtSn

catalysts supported on activated carbon felt and powder, *Applied Catalysis A: General* **281**(1–2), 247, 2005.

[138] J. Aumo, S. Oksanen, J.P. Mikkola, T. Salmi, and D.Y. Murzin. Hydrogenation of citral over activated carbon cloth catalyst, *Industrial & Engineering Chemistry Research* **44**(14), 5285-5290, 6-7-2005.

[139] J. Aumo, S. Oksanen, J.P. Mikkola, T. Salmi, and D.Y. Murzin. Novel woven active carbon fiber catalyst in the hydrogenation of citral, *Catalysis Today* **102**, 128, 2005.

[140] A. Giroir-Fendler, D. Richard, and P. Gallezot, "Selectivity in Cinnamaldehyde Hydrogenation of Group-VIII Metals Supported on Graphite and Carbon",in *Studies in Surface Science and Catalysis. Heterogeneous Catalysis and Fine Chemicals Proceedings of an International Symposium*, Volume 41 ed. edited by M. Guisnet (Elsevier, 1988), pp.171-178.

[141] M. Steffan, F. Klasovsky, J. Arras, C. Roth, J. Radnik, H. Hofmeister, and P. Claus. Carbon-carbon double bond versus carbonyl group hydrogenation: Controlling the intramolecular selectivity with polyaniline-supported platinum catalysts, *Advanced Synthesis and Catalysis* **350**(9), 1337, 2008.

[142] P. Gallezot and D. Richard. Selective Hydrogenation of α, β-Unsaturated Aldehydes, *Catalysis Reviews* **40**(1-2), 81, 1998.

[143] B. Bachiller-Baeza, A. Guerrero-Ruiz, P. Wang, and I. Rodríguez-Ramos. Hydrogenation of citral on activated carbon and high-surface-area graphite-supported ruthenium catalysts modified with iron, *Journal of Catalysis* **204**(2), 450, 2001.

[144] J. Court, J. Jablonski, and S. Hamarthibault. Hydrogenation of Citral in the Liquid-Phase Over New Bimetallic Ni-M Catalysts Supported on Graphite, *Heterogeneous Catalysis and Fine Chemicals III* **78**, 155, 1993.

[145] M. Cerro-Alarcón, B. Bachiller-Baeza, A. Guerrero-Ruiz, and I. Rodríguez-Ramos. Effect of the reduction-preparation method on the surface states and catalytic properties of supported-nickel particles, *Journal of Molecular Catalysis A: Chemical* **258**(1-2), 221, 2006.

[146] Y. Zhao, H. Zhang, C. Huang, S. Chen, B. Yu, J. Xu, and Z. Liu. Pd nanoparticles immobilized on graphite oxide modified with a base: Highly efficient catalysts for selective hydrogenation of citral, *Science China Chemistry* **56**(2), 203, 2013.

[147] V. Satagopan and S.B. Chandalia. Selectivity Aspects in the Multiphase Hydrogenation of Alpha,Beta-Unsaturated Aldehydes Over Supported Noble-Metal Catalysts .1, *Journal of Chemical Technology and Biotechnology* **59**(3), 257, 1994.

[148] K.C. Tin, N.B. Wong, R.X. Li, Y.Z. Li, and X.J. Li. Studies on catalytic hydrogenation of citral by water-soluble palladium complex, *Journal of Molecular Catalysis A-Chemical* **137**(1-3), 113, 1999.

[149] P. Serp and J.L. Figueiredo, *carbon materials for catalysis* (John Wiley & Sons, Hoboken, N.J., 2009).

[150] Q.H. Yang, P.X. Hou, S. Bai, M.Z. Wang, and H.M. Cheng. Adsorption and capillarity of nitrogen in aggregated multi-walled carbon nanotubes, *Chemical Physics Letters* **345**(1–2), 18, 2001.

[151] J.M. Nhut, L. Pesant, J.P. Tessonnier, G. Winé, J. Guille, C. Pham-Huu, and M.J. Ledoux. Mesoporous carbon nanotubes for use as support in catalysis and as nanosized reactors for one-dimensional inorganic material synthesis, *Applied Catalysis A: General* **254**(2), 345, 2003.

[152] Y. Li, G.H. Lai, and R.X. Zhou. Carbon nanotubes supported Pt–Ni catalysts and their properties for the liquid phase hydrogenation of cinnamaldehyde to hydrocinnamaldehyde, *Applied Surface Science* **253**(11), 4978, 2007.

[153] H. Ma, L. Wang, L. Chen, C. Dong, W. Yu, T. Huang, and Y. Qian. Pt nanoparticles deposited over carbon nanotubes for selective hydrogenation of cinnamaldehyde, *Catalysis Communications* **8**(3), 452, 2007.

[154] R.M.M. Abbaslou, A. Tavassoli, J. Soltan, and A.K. Dalai. Iron catalysts supported on carbon nanotubes for Fischer–Tropsch synthesis: Effect of catalytic site position, *Applied Catalysis A: General* **367**(1–2), 47, 2009.

[155] T. Bligaard. Linear Energy Relations and the Computational Design of Selective Hydrogenation/Dehydrogenation Catalysts, *Angewandte Chemie International Edition* **48**(52), 9782, 2009.

[156] E. Asedegbega-Nieto, A. Guerrero-Ruiz, and I. Rodríguez-Ramos. Modification of the stereo selectivity in the citral hydrogenation by application of carbon nanotubes as support of the Pt particles, *Carbon* **44**(4), 804, 2006.

[157] F. Qin, W. Shen, C.C. Wang, and H.L. Xu. Selective hydrogenation of citral over a novel platinum/MWNTs nanocomposites, *Catalysis Communications* **9**(11-12), 2095, 2008.

[158] G.Q. Guo, F. Qin, D. Yang, C.C. Wang, H.L. Xu, and S. Yang. Synthesis of platinum nanoparticles supported on poly(acrylic acid) grafted MWNTs and their hydrogenation of citral, *Chemistry of Materials* **20**(6), 2291-2297, 25-3-2008.

[159] P.D. Zgolicz, J.P. Stassi, M.J. Yañez, O.A. Scelza, and S.R. de Miguel. Influence of the support and the preparation methods on the performance in citral hydrogenation of Pt-based catalysts supported on carbon nanotubes, *Journal of Catalysis* **290**(0), 37, 2012.

[160] S.A. Ananthan, N. Vengidusamy, K. Giribabu, and R. Suresh. Carbon nanotunes supported Pt and Pt-Ru catalysts for selective hydrogenation of citral: Effect of promoters and thermal activation of catalysts, *Advanced Materials Research* **584**, 229, 2012.

[161] S.A. Ananthan and V. Narayanan. MWCNT Supported Pt-Au Nanocatalysts for Liquid Phase Selective Hydrogenation of Citral, *International Journal of Mardern Chemistry* **1**(2), 45, 2012.

[162] B. Bachiller-Baeza, I. Rodríguez-Ramos, and A. Guerrero-Ruiz. Influence of Mg and Ce addition to ruthenium based catalysts used in the selective hydrogenation of alpha,beta-unsaturated aldehydes, *Applied Catalysis A-General* **205**(1-2), 227, 2001.

[163] J. Zhu, M.H. Lu, M.S. Li, J.J. Zhu, and Y.H. Shan. Selective Hydrogenation of Citral over a Carbon-titania Composite Supported Palladium Catalyst, *Chinese Journal of Chemistry* **29**(4), 655, 2011.

[164] J. Zhu, M. Li, and M. Lu, "Synthesis of Carbon Nanofiber-Titania-Cordierite Monolith Composite and Its Application As Catalyst Support on Citral Hydrogenation, *Advanced Materials Research* **535-537**, pp.178-185.

[165] J. Zhu, M. Lu, M. Li, J. Zhu, and Y. Shan. Synthesis of carbon-titania composite and its application as catalyst support, *Materials Chemistry and Physics* **132**(2-3), 316, 2012.

[166] S.A. Ananthan and V. Narayanan. Liquid-Phase Hydrogenation of Citral Over Pt/TiO_2 and $Pt-Fe/TiO_2$ Catalysts, *Asian Journal of Chemistry* **23**(1), 183, 2011.

[167] D. Li, N. Ichikuni, S. Shimazu, and T. Uematsu. Hydrogenation of CO_2 over sprayed Ru/TiO_2 fine particles and strong metal–support interaction, *Applied Catalysis A: General* **180**(1–2), 227, 1999.

[168] M.R. Hoffmann, S.T. Martin, W. Choi, and D.W. Bahnemann. Environmental Applications of Semiconductor Photocatalysis, *Chemical Reviews* **95**(1), 69-96, 1-1-1995.

[169] A.L. Linsebigler, G. Lu, and J.T. Yates. Photocatalysis on TiO_2 Surfaces: Principles, Mechanisms, and Selected Results, *Chemical Reviews* **95**(3), 735-758, 1-5-1995.

[170] M.A. Fox and M.T. Dulay. Heterogeneous photocatalysis, *Chemical Reviews* **93**(1), 341-357, 1-1-1993.

[171] L. Cao, A. Huang, F.J. Spiess, and S.L. Suib. Gas-Phase Oxidation of 1-Butene Using Nanoscale TiO_2 Photocatalysts, *Journal of Catalysis* **188**(1), 48, 1999.

[172] A. Mills and S. Le Hunte. An overview of semiconductor photocatalysis, *Journal of Photochemistry and Photobiology A: Chemistry* **108**(1), 1, 1997.

[173] M. Pelaez, N.T. Nolan, S.C. Pillai, M.K. Seery, P. Falaras, A.G. Kontos, P.S.M. Dunlop, J.W.J. Hamilton, J.A. Byrne, K. O'Shea, M.H. Entezari, and D.D. Dionysiou. A review on the visible light active titanium dioxide photocatalysts for environmental applications, *Applied Catalysis B: Environmental* **125**(0), 331, 2012.

[174] W. Ren, Z. Ai, F. Jia, L. Zhang, X. Fan, and Z. Zou. Low temperature preparation and visible light photocatalytic activity of mesoporous carbon-doped crystalline TiO_2, *Applied Catalysis B: Environmental* **69**(3–4), 138, 2007.

[175] J. Zhang, Y. Wu, M. Xing, S.A.K. Leghari, and S. Sajjad. Development of modified N doped TiO_2 photocatalyst with metals, nonmetals and metal oxides, *Energy & Environmental Science* **3**(6), 715-726, 2010.

[176] S. Lee, Y. Lee, D.H. Kim, and J.H. Moon. Carbon-Deposited TiO_2 3D Inverse Opal Photocatalysts: Visible-Light Photocatalytic Activity and Enhanced Activity in a Viscous Solution, *ACS Applied Materials & Interfaces* **5**(23), 12526-12532, 22-11-2013.

[177] M. Iwasaki, M. Hara, H. Kawada, H. Tada, and S. Ito. Cobalt Ion-Doped TiO_2 Photocatalyst Response to Visible Light, *Journal of Colloid and Interface Science* **224**(1), 202, 2000.

[178] E. Borgarello, J. Kiwi, M. Graetzel, E. Pelizzetti, and M. Visca. Visible light induced water cleavage in colloidal solutions of chromium-doped titanium dioxide particles, *Journal of the American Chemical Society* **104**(11), 2996-3002, 1-6-1982.

[179] A.M. Czoska, S. Livraghi, M. Chiesa, E. Giamello, S. Agnoli, G. Granozzi, E. Finazzi, C.D. Valentin, and G. Pacchioni. The Nature of Defects in Fluorine-Doped TiO_2, *The Journal of Physical Chemistry C* **112**(24), 8951-8956, 27-5-2008.

[180] W. Choi, A. Termin, and M.R. Hoffmann. The Role of Metal Ion Dopants in Quantum-Sized TiO_2: Correlation between Photoreactivity and Charge Carrier Recombination Dynamics, *The Journal of Physical Chemistry* **98**(51), 13669, 1994.

[181] M. Kang. The superhydrophilicity of Al–TiO_2 nanometer sized material synthesized using a solvothermal method, *Materials Letters* **59**(24–25), 3122, 2005.

[182] K. Demeestere, J. Dewulf, T. Ohno, P.H. Salgado, and H. Van Langenhove. Visible light mediated photocatalytic degradation of gaseous trichloroethylene and dimethyl sulfide on modified titanium dioxide, *Applied Catalysis B: Environmental* **61**(1–2), 140, 2005.

[183] C. Di Valentin, E. Finazzi, G. Pacchioni, A. Selloni, S. Livraghi, M.C. Paganini, and E. Giamello. N-doped TiO_2: Theory and experiment, *Chemical Physics* **339**(1-3), 44, 2007.

[184] Y. Izumi, T. Itoi, S. Peng, K. Oka, and Y. Shibata. Site Structure and Photocatalytic Role of Sulfur or Nitrogen-Doped Titanium Oxide with Uniform Mesopores under Visible Light, *The Journal of Physical Chemistry C* **113**(16), 6706-6718, 26-3-2009.

[185] H. Irie, Y. Watanabe, and K. Hashimoto. Nitrogen-Concentration Dependence on Photocatalytic Activity of $TiO_{2-x}N_x$ Powders, *The Journal of Physical Chemistry B* **107**(23), 5483-5486, 17-5-2003.

[186] S. Sato, R. Nakamura, and S. Abe. Visible-light sensitization of TiO_2 photocatalysts by wet-method N doping, *Applied Catalysis A: General* **284**(1-2), 131, 200.

[187] S. Sato. Photocatalytic activity of NO_x-doped TiO_2 in the visible light region, *Chemical Physics Letters* **123**(1-2), 126, 1986.

[188] S.U.M. Khan, M. Al-Shahry, and W.B. Ingler. Efficient Photochemical Water Splitting by a Chemically Modified n-TiO_2, *Science* **297**(5590), 2243, 2002.

[189] N. Serpone. Is the Band Gap of Pristine TiO_2 Narrowed by Anion- and Cation-Doping of Titanium Dioxide in Second-Generation Photocatalysts?, *The Journal of Physical Chemistry B* **110**(48), 24287-24293, 7-11-2006.

[190] J.M. Mwabora, T. Lindgren, E. Avendaño, T.F. Jaramillo, J. Lu, S.E. Lindquist, and C.G. Granqvist. Structure, Composition, and Morphology of Photoelectrochemically Active $TiO_{2-x}N_x$ Thin Films Deposited by Reactive DC Magnetron Sputtering, *The Journal of Physical Chemistry B* **108**(52), 20193-20198, 1-12-2004.

[191] Y. Nakano, T. Morikawa, T. Ohwaki, and Y. Taga. Deep-level optical spectroscopy investigation of N-doped TiO_2 films, *Applied Physics Letters* **86**(13), 1-3, 2005.

[192] L. Jinlong, M. Xinxin, S. Mingren, X. Li, and S. Zhenlun. Fabrication of nitrogen-doped mesoporous TiO_2 layer with higher visible photocatalytic activity by plasma-based ion implantation, *Thin Solid Films* **519**(1), 101, 2010.

[193] J. Premkumar. Development of Super-Hydrophilicity on Nitrogen-Doped TiO_2 Thin Film Surface by Photoelectrochemical Method under Visible Light, *Chemistry of Materials* **16**(21), 3980-3981, 22-9-2004.

[194] C.W.H. Dunnill, Z.A. Aiken, J. Pratten, M. Wilson, D.J. Morgan, and I.P. Parkin. Enhanced photocatalytic activity under visible light in N-doped TiO_2 thin films produced by APCVD preparations using t-butylamine as a nitrogen source and their potential for antibacterial films, *Journal of Photochemistry and Photobiology A: Chemistry* **207**(2-3), 244, 2009.

[195] V. Pore, M. Heikkilä, M. Ritala, M. Leskelä, and S. Areva. Atomic layer deposition of TiO2-xNx thin films for photocatalytic applications, *Journal of Photochemistry and Photobiology A: Chemistry* **177**(1), 68, 2006.

[196] L. Zhao, Q. Jiang, and J. Lian. Visible-light photocatalytic activity of nitrogen-doped TiO_2 thin film prepared by pulsed laser deposition, *Applied Surface Science* **254**(15), 4620, 2008.

[197] X. Qiu, Y. Zhao, and C. Burda. Synthesis and Characterization of Nitrogen-Doped Group VB Visible-Light-Photoactive Metal Oxide Nanoparticles, *Advanced Materials* **19**(22), 3995-3999, 19-11-2007.

[198] T.C. Jagadale, S.P. Takale, R.S. Sonawane, H.M. Joshi, S.I. Patil, B.B. Kale, and S.B. Ogale. N-Doped TiO_2 Nanoparticle Based Visible Light Photocatalyst by Modified Peroxide Sol–Gel Method, *The Journal of Physical Chemistry C* **112**(37), 14595-14602, 26-8-2008.

[199] D. Mitoraj and H. Kisch. On the Mechanism of Urea-Induced Titania Modification, *Chemistry- A European Journal* **16**(1), 261, 2010.

[200] H. Choi, E. Stathatos, and D.D. Dionysiou. Sol-gel preparation of mesoporous photocatalytic TiO_2 films and TiO_2/Al_2O_3 composite membranes for environmental applications, *Applied Catalysis B: Environmental* **63**(1-2), 60, 2006.

[201] H. Choi, A.C. Sofranko, and D.D. Dionysiou. Nanocrystalline TiO_2 Photocatalytic Membranes with a Hierarchical Mesoporous Multilayer Structure: Synthesis, Characterization, and Multifunction, *Advanced Functional Materials* **16**(8), 1067-1074, 19-5-2006.

[202] H. Choi, M.G. Antoniou, M. Pelaez, A.A. de la Cruz, J.A. Shoemaker, and D.D. Dionysiou. Mesoporous Nitrogen-Doped TiO_2 for the Photocatalytic Destruction of the Cyanobacterial Toxin Microcystin-LR under Visible Light Irradiation, *Environmental Science & Technology* **41**(21), 7530-7535, 5-10-2007.

[203] S. Sakthivel and H. Kisch. Daylight Photocatalysis by Carbon-Modified Titanium Dioxide, *Angewandte Chemie - International Edition* **42**(40), 4908, 2003.

[204] H. Irie, Y. Watanabe, and K. Hashimoto. Carbon-doped Anatase TiO_2 Powders as a Visible-light Sensitive Photocatalyst, *Chemistry Letters* **32**(8), 772, 2003.

[205] D.B. Hamal and K.J. Klabunde. Synthesis, characterization, and visible light activity of new nanoparticle photocatalysts based on silver, carbon, and sulfur-doped TiO_2, *Journal of Colloid and Interface Science* **311**(2), 514, 2007.

[206] K. Nagaveni, M.S. Hegde, N. Ravishankar, G.N. Subbanna, and G. Madras. Synthesis and Structure of Nanocrystalline TiO_2 with Lower Band Gap Showing High Photocatalytic Activity, *Langmuir* **20**(7), 2900, 2004.

[207] T. Morikawa, R. Asahi, T. Ohwaki, K. Aoki, and Y. Taga. Band-gap narrowing of titanium dioxide by nitrogen doping, *Japanese Journal of Applied Physics* **40**(6 A), L561-L563, 2001.

[208] R. Argazzi, N.Y. Murakami Iha, H. Zabri, F. Odobel, and C.A. Bignozzi. Design of molecular dyes for application in photoelectrochemical and electrochromic devices based on nanocrystalline metal oxide semiconductors, *Coordination Chemistry Reviews* **248**(13-14), 1299, 2004.

[209] K. Gurunathan. Photobiocatalytic production of hydrogen using sensitized TiO_2-MV^{2+} system coupled Rhodopseudomonas capsulata, *Journal of Molecular Catalysis A: Chemical* **156**(1-2), 59, 2000.

[210] K.B. Dhanalakshmi, S. Latha, S. Anandan, and P. Maruthamuthu. Dye sensitized hydrogen evolution from water, *International Journal of Hydrogen Energy* **26**(7), 669, 2001.

[211] K. Gurunathan, P. Maruthamuthu, and M.V.C. Sastri. Photocatalytic hydrogen production by dye-sensitized Pt/SnO_2 and $Pt/SnO_2/RuO_2$ in aqueous methyl viologen solution, *International Journal of Hydrogen Energy* **22**(1), 57, 1997.

[212] R. Abe, K. Sayama, and H. Arakawa. Efficient hydrogen evolution from aqueous mixture of I^- and acetonitrile using a merocyanine dye-sensitized Pt/TiO_2 photocatalyst under visible light irradiation, *Chemical Physics Letters* **362**(5-6), 441, 2002.

[213] H. Meng, W. Hou, X. Xu, J. Xu, and X. Zhang. TiO_2-loaded activated carbon fiber: Hydrothermal synthesis, adsorption properties and photo catalytic activity under visible light irradiation, *Particuology* **14**, 38, 2014.

[214] M. Ni, M.K.H. Leung, D.Y.C. Leung, and K. Sumathy. A review and recent developments in photocatalytic water-splitting using TiO_2 for hydrogen production, *Renewable and Sustainable Energy Reviews* **11**(3), 401, 2007.

[215] M. Mrowetz, W. Balcerski, A.J. Colussi, and M.R. Hoffmann. Oxidative Power of Nitrogen-Doped TiO_2 Photocatalysts under Visible Illumination, *The Journal of Physical Chemistry B* **108**(45), 17269-17273, 19-10-2004.

[216] A.K. Jana. Solar cells based on dyes, *Journal of Photochemistry and Photobiology A: Chemistry* **132**(1-2), 1, 2000.

[217] G. Marcì, V. Augugliaro, M.J. López-Muñoz, C. Martín, L. Palmisano, V. Rives, M. Schiavello, R.J.D. Tilley, and A.M. Venezia. Preparation Characterization and Photocatalytic Activity of Polycrystalline ZnO/TiO_2 Systems. 1. Surface and Bulk Characterization, *The Journal of Physical Chemistry B* **105**(5), 1026, 2001.

[218] N. Ghows and M.H. Entezari. Fast and easy synthesis of core-shell nanocrystal (CdS/TiO_2) at low temperature by micro-emulsion under ultrasound, *Ultrasonics Sonochemistry* **18**(2), 629, 2011.

[219] J.S. Jang, H.G. Kim, U.A. Joshi, J.W. Jang, and J.S. Lee. Fabrication of CdS nanowires decorated with TiO_2 nanoparticles for photocatalytic hydrogen production under visible light irradiation, *International Journal of Hydrogen Energy* **33**(21), 5975, 2008.

[220] R. Brahimi, Y. Bessekhouad, A. Bouguelia, and M. Trari. Visible light induced hydrogen evolution over the heterosystem Bi_2S_3/TiO_2, *Catalysis Today* **122**(1-2), 62, 2007.

[221] A. Hagfeldt and M. Graetzel. Light-Induced Redox Reactions in Nanocrystalline Systems, *Chemical Reviews* **95**(1), 49-68, 1-1-1995.

[222] L. Spanhel, H. Weller, and A. Henglein. Photochemistry of semiconductor colloids. 22. Electron ejection from illuminated cadmium sulfide into attached titanium and zinc oxide particles, *Journal of the American Chemical Society* **109**(22), 6632-6635, 1-10-1987.

[223] X. Chen and S.S. Mao. Titanium Dioxide Nanomaterials: Synthesis, Properties, Modifications, and Applications, *Chemical Reviews* **107**(7), 2891-2959, 23-6-2007.

[224] A. Sclafani and J.M. Herrmann. Comparison of the Photoelectronic and Photocatalytic Activities of Various Anatase and Rutile Forms of Titania in Pure Liquid Organic Phases and in Aqueous Solutions, *The Journal of Physical Chemistry* **100**(32), 13655-13661, 1-1-1996.

[225] A. Kudo and Y. Miseki. Heterogeneous photocatalyst materials for water splitting, *Chemical Society Reviews* **38**(1), 253-278, 2009.

[226] J.C. Yu, J. Yu, W. Ho, Z. Jiang, and L. Zhang. Effects of F^- doping on the photocatalytic activity and microstructures of nanocrystalline TiO_2 powders, *Chemistry of Materials* **14**(9), 3808, 2002.

[227] Z. Xu, J. Shang, C. Liu, C. Kang, H. Guo, and Y. Du. The preparation and characterization of TiO_2 ultrafine particles, *Materials Science and Engineering B: Solid-State Materials for Advanced Technology* **63**(3), 211, 1999.

[228] J.C. Yu, J. Yu, W. Ho, and L. Zhang. Preparation of highly photocatalytic active nano-sized TiO_2 particles via ultrasonic irradiation, *Chemical Communications* (19), 1942-1943, 2001.

[229] J. Yu, H. Yu, B. Cheng, M. Zhou, and X. Zhao. Enhanced photocatalytic activity of TiO_2 powder (P25) by hydrothermal treatment, *Journal of Molecular Catalysis A: Chemical* **253**(1-2), 112, 2006.

[230] V. Etacheri, M.K. Seery, S.J. Hinder, and S.C. Pillai. Highly Visible Light Active $TiO_{2-x}N_x$ Heterojunction Photocatalysts, *Chemistry of Materials* **22**(13), 3843-3853, 28-5-2010.

[231] S. Jin and F. Shiraishi. Photocatalytic activities enhanced for decompositions of organic compounds over metal-photodepositing titanium dioxide, *Chemical Engineering Journal* **97**(2-3), 203-211, 2004.

[232] F.B. Li and X.Z. Li. The enhancement of photodegradation efficiency using Pt-TiO_2 catalyst, *Chemosphere* **48**(10), 1103, 2002.

[233] S. Sakthivel, M.V. Shankar, M. Palanichamy, B. Arabindoo, D.W. Bahnemann, and V. Murugesan. Enhancement of photocatalytic activity by metal deposition: Characterisation and photonic efficiency of Pt, Au and Pd deposited on TiO_2 catalyst, *Water Research* **38**(13), 3001, 2004.

[234] A.V. Vorontsov, E.N. Savinov, and J. Zhensheng. Influence of the form of photodeposited platinum on titania upon its photocatalytic activity in CO and

acetone oxidation, *Journal of Photochemistry and Photobiology A: Chemistry* **125**(1–3), 113, 1999.

[235] A. Zielinska-Jurek and A. Zaleska. Ag/Pt-modified TiO_2 nanoparticles for toluene photooxidation in the gas phase, *Catalysis Today* **230**(0), 104, 2014.

[236] X. Hu, G. Li, and J.C. Yu. Design, Fabrication, and Modification of Nanostructured Semiconductor Materials for Environmental and Energy Applications, *Langmuir* **26**(5), 3031, 2009.

[237] N. Satoh, T. Nakashima, K. Kamikura, and K. Yamamoto. Quantum size effect in TiO_2 nanoparticles prepared by finely controlled metal assembly on dendrimer templates, *Nature Nanotechnology* **3**(2), 106-111, 2008.

[238] A.Z. Moshfegh. Nanoparticle catalysts, *Journal of Physics D: Applied Physics* **42**(23), 233001, 2009.

[239] P.V. Kamat. Meeting the Clean Energy Demand: Nanostructure Architectures for Solar Energy Conversion, *The Journal of Physical Chemistry C* **111**(7), 2834-2860, 1-2-2007.

[240] G.P. Lepore, C.H. Langford, J. Víchová, and Jr. Vlcek. Photochemistry and picosecond absorption spectra of aqueous suspensions of a polycrystalline titanium dioxide optically transparent in the visible spectrum, *Journal of Photochemistry and Photobiology, A: Chemistry* **75**(1), 67, 1993.

[241] I. Sopyan, M. Watanabe, S. Murasawa, K. Hashimoto, and A. Fujishima. An efficient TiO_2 thin-film photocatalyst: Photocatalytic properties in gas-phase acetaldehyde degradation, *Journal of Photochemistry and Photobiology A: Chemistry* **98**(1-2), 79, 1996.

[242] J. Zhao and X. Yang. Photocatalytic oxidation for indoor air purification: A literature review, *Building and Environment* **38**(5), 645, 2003.

[243] G. Li Puma, A. Bono, and J.G. Collin. Preparation of titanium dioxide photocatalyst loaded onto activated carbon support using chemical vapor deposition: A review paper, *Journal of Hazardous Materials* **157**(2-3), 209, 2008.

[244] J. Araña, J.M. Doña-Rodríguez, E. Tello Rendón, I.C. Garriga, O. González-Díaz, J.A. Herrera-Melián, J. Pérez-Peña, G. Colón, and J.A. Navío. TiO_2 activation by using activated carbon as a support: Part I. Surface characterisation and decantability study, *Applied Catalysis B: Environmental* **44**(2), 161, 2003.

[245] H.S. Hilal, L.Z. Majjad, N. Zaatar, and A. El-Hamouz. Dye-effect in TiO_2 catalyzed contaminant photo-degradation: Sensitization vs. charge-transfer formalism, *Solid State Sciences* **9**(1), 9, 2007.

[246] J. Araña, J.M. Doña Rodríguez, O. González Díaz, J.A. Herrera Melián, and J. Pérez Peña. The effect of modifying TiO_2 on catechol and resorcinol photocatalytic degradation, *Journal of Solar Energy Engineering, Transactions of the ASME* **129**(1), 80, 2007.

[247] Y. Li, S. Zhang, Q. Yu, and W. Yin. The effects of activated carbon supports on the structure and properties of TiO_2 nanoparticles prepared by a sol-gel method, *Applied Surface Science* **253**(23), 9254, 2007.

[248] S.X. Liu, X.Y. Chen, and X. Chen. A TiO_2/AC composite photocatalyst with high activity and easy separation prepared by a hydrothermal method, *Journal of Hazardous Materials* **143**(1-2), 257, 2007.

[249] C.S. Kuo, Y.H. Tseng, C.H. Huang, and Y.Y. Li. Carbon-containing nano-titania prepared by chemical vapor deposition and its visible-light-responsive photocatalytic activity, *Journal of Molecular Catalysis A: Chemical* **270**(1-2), 93, 2007.

[250] Z. Ding, X. Hu, P.L. Yue, G.Q. Lu, and P.F. Greenfield. Synthesis of anatase TiO_2 supported on porous solids by chemical vapor deposition, *Catalysis Today* **68**(1-3), 173, 2001.

[251] X. Zhang, M. Zhou, and L. Lei. Preparation of photocatalytic TiO_2 coatings of nanosized particles on activated carbon by AP-MOCVD, *Carbon* **43**(8), 1700, 2005.

[252] Y. Ao, J. Xu, D. Fu, X. Shen, and C. Yuan. Low temperature preparation of anatase TiO_2-coated activated carbon, *Colloids and Surfaces A: Physicochemical and Engineering Aspects* **312**(2-3), 125, 2008.

[253] R. Yuan, R. Guan, and J. Zheng. Effect of the pore size of TiO_2-loaded activated carbon fiber on its photocatalytic activity, *Scripta Materialia* **52**(12), 1329, 2005.

[254] Y. Yu, J.C. Yu, C.Y. Chan, Y.K. Che, J.C. Zhao, L. Ding, W.K. Ge, and P.K. Wong. Enhancement of adsorption and photocatalytic activity of TiO_2 by using carbon nanotubes for the treatment of azo dye, *Applied Catalysis B: Environmental* **61**(1-2), 1, 2005.

[255] L.F. Velasco, J.B. Parra, and C.O. Ania. Role of activated carbon features on the photocatalytic degradation of phenol, *Applied Surface Science* **256**(17), 5254, 2010.

[256] C. Minero, F. Catozzo, and E. Pelizzetti. Role of adsorption in photocatalyzed reactions of organic molecules in aqueous titania suspensions, *Langmuir* **8**(2), 481, 1992.

[257] J.M. Herrmann, J. Matos, J. Disdier, C. Guillard, J. Laine, S. Malato, and J. Blanco. Solar photocatalytic degradation of 4-chlorophenol using the synergistic effect between titania and activated carbon in aqueous suspension, *Catalysis Today* **54**(2-3), 255, 1999.

[258] J. Matos, J. Laine, J.M. Herrmann, D. Uzcategui, and J.L. Brito. Influence of activated carbon upon titania on aqueous photocatalytic consecutive runs of phenol photodegradation, *Applied Catalysis B: Environmental* **70**(1-4), 461-469, 2007.

[259] K. Woan, G. Pyrgiotakis, and W. Sigmund. Photocatalytic Carbon-Nanotube–TiO_2 Composites, *Advanced Materials* **21**(21), 2233-2239, 5-6-2009.

[260] J.L. Faria and W. Wang, "Carbon Materials in Photocatalysis.",in *Carbon materials for catalysis.*, edited by P. Serp and J. Figueiredo (John Wiley & Sons, Hoboken, NJ, 2009), pp.481-506.

[261] Y. Chen, J.C. Crittenden, S. Hackney, L. Sutter, and D.W. Hand. Preparation of a Novel TiO_2-Based p–n Junction Nanotube Photocatalyst, *Environmental Science & Technology* **39**(5), 1201-1208, 13-1-2005.

[262] R.H. Baughman, A.A. Zakhidov, and W.A. de Heer. Carbon Nanotubes--the Route Toward Applications, *Science* **297**(5582), 787, 2002.

[263] A. Kongkanand and P.V. Kamat. Electron Storage in Single Wall Carbon Nanotubes. Fermi Level Equilibration in Semiconductor–SWCNT Suspensions, *ACS Nano* **1**(1), 13, 2007.

[264] Z. Xu, Y. Long, S.Z. Kang, and J. Mu. Application of the Composite of TiO_2 Nanoparticles and Carbon Nanotubes to the Photo-Reduction of Cr(VI) in Water, *Journal of Dispersion Science and Technology* **29**(8), 1150, 2008.

[265] W. Wang, P. Serp, P. Kalck, and J.L. Faria. Visible light photodegradation of phenol on MWNT-TiO_2 composite catalysts prepared by a modified sol-gel method, *Journal of Molecular Catalysis A: Chemical* **235**(1-2), 194, 2005.

[266] Y. Yao, G. Li, S. Ciston, R.M. Lueptow, and K.A. Gray. Photoreactive TiO_2/carbon nanotube composites: Synthesis and reactivity, *Environmental Science and Technology* **42**(13), 4952, 2008.

[267] B. Ahmmad, Y. Kusumoto, S. Somekawa, and M. Ikeda. Carbon nanotubes synergistically enhance photocatalytic activity of TiO_2, *Catalysis Communications* **9**(6), 1410, 2008.

[268] G. An, W. Ma, Z. Sun, Z. Liu, B. Han, S. Miao, Z. Miao, and K. Ding. Preparation of titania/carbon nanotube composites using supercritical ethanol and their photocatalytic activity for phenol degradation under visible light irradiation, *Carbon* **45**(9), 1795, 2007.

[269] O. Akhavan, M. Abdolahad, Y. Abdi, and S. Mohajerzadeh. Synthesis of titania/carbon nanotube heterojunction arrays for photoinactivation of E. coli in visible light irradiation, *Carbon* **47**(14), 3280, 2009.

[270] Y. Luo, Y. Heng, X. Dai, W. Chen, and J. Li. Preparation and photocatalytic ability of highly defective carbon nanotubes, *Journal of Solid State Chemistry* **182**(9), 2521, 2009.

[271] C.Y. Yen, Y.F. Lin, C.H. Hung, Y.H. Tseng, C.C.M. Ma, M.C. Chang, and H. Shao. The effects of synthesis procedures on the morphology and photocatalytic activity of multi-walled carbon nanotubes/TiO_2 nanocomposites, *Nanotechnology* **19**(4), 2008.

[272] W. Krätschmer, K. Fostiropoulos, and D.R. Huffman. The infrared and ultraviolet absorption spectra of laboratory-produced carbon dust: evidence for the presence of the C60 molecule, *Chemical Physics Letters* **170**(2-3), 167, 1990.

[273] W. Krätschmer, L.D. Lamb, K. Fostiropoulos, and D.R. Huffman. Solid C60: A new form of carbon, *Nature* **347**(6291), 354, 1990.

[274] H. Ajie, M.M. Alvarez, S.J. Anz, R.D. Beck, F. Diederich, K. Fostiropoulos, D.R. Huffman, W. Krätschmer, Y. Rubin, K.E. Schriver, D. Sensharma, and R.L. Whetten. Characterization of the soluble all-carbon molecules C60 and C70, *Journal of Physical Chemistry* **94**(24), 8630, 1990.

[275] T.W. Ebbesen, K. Tanigaki, and S. Kuroshima. Excited-state properties of C60, *Chemical Physics Letters* **181**(6), 501, 1991.

[276] Q. Xie, E. Perez-Cordero, and L. Echegoyen. Electrochemical detection of C_{60}^{6-} and C_{70}^{6-}: Enhanced stability of fullerides in solution, *Journal of the American Chemical Society* **114**(10), 3978-3980, 1-5-1992.

[277] Y. Kajii, T. Nakagawa, S. Suzuki, Y. Achiba, K. Obi, and K. Shibuya. Transient absorption, lifetime and relaxation of C60 in the triplet state, *Chemical Physics Letters* **181**(2-3), 100, 1991.

[278] S.P. Sibley, S.M. Argentine, and A.H. Francis. A photoluminescence study of C60 and C70, *Chemical Physics Letters* **188**(3-4), 187, 1992.

[279] R.R. Hung and J.J. Grabowski. A precise determination of the triplet energy of C60 by photoacoustic calorimetry, *Journal of Physical Chemistry* **95**(16), 6073, 1991.

[280] P.V. Kamat, M. Haria, and S. Hotchandani. C60 Cluster as an Electron Shuttle in a Ru(II)-Polypyridyl Sensitizer-Based Photochemical Solar Cell, *The Journal of Physical Chemistry B* **108**(17), 5166-5170, 1-4-2004.

[281] V. Krishna, N. Noguchi, B. Koopman, and B. Moudgil. Enhancement of titanium dioxide photocatalysis by water-soluble fullerenes, *Journal of Colloid and Interface Science* **304**(1), 166, 2006.

[282] V. Apostolopoulou, J. Vakros, C. Kordulis, and A. Lycourghiotis. Preparation and characterization of [60] fullerene nanoparticles supported on titania used as a photocatalyst, *Colloids and Surfaces A: Physicochemical and Engineering Aspects* **349**(1-3), 189, 2009.

[283] J. Lin, R. Zong, M. Zhou, and Y. Zhu. Photoelectric catalytic degradation of methylene blue by C60-modified TiO_2 nanotube array, *Applied Catalysis B: Environmental* **89**(3-4), 425, 2009.

[284] Y. Long, Y. Lu, Y. Huang, Y. Peng, Y. Lu, S.Z. Kang, and J. Mu. Effect of C60 on the Photocatalytic Activity of TiO_2 Nanorods, *The Journal of Physical Chemistry C* **113**(31), 13899-13905, 8-7-2009.

[285] Y. Park, N.J. Singh, K.S. Kim, T. Tachikawa, T. Majima, and W. Choi. Fullerol-titania charge-transfer-mediated photocatalysis working under visible light, *Chemistry - A European Journal* **15**(41), 10843, 2009.

[286] A.K. Geim. Graphene: Status and prospects, *Science* **324**(5934), 1530, 2009.

[287] T.N. Lambert, C.A. Chavez, B. Hernandez-Sanchez, P. Lu, N.S. Bell, A. Ambrosini, T. Friedman, T.J. Boyle, D.R. Wheeler, and D.L. Huber. Synthesis and characterization of titania-graphene nanocomposites, *Journal of Physical Chemistry C* **113**(46), 19812, 2009.

[288] P.V. Kamat. Graphene-based nanoarchitectures. Anchoring semiconductor and metal nanoparticles on a two-dimensional carbon support, *Journal of Physical Chemistry Letters* **1**(2), 520, 2010.

[289] S. Stankovich, D.A. Dikin, G.H.B. Dommett, K.M. Kohlhaas, E.J. Zimney, E.A. Stach, R.D. Piner, S.T. Nguyen, and R.S. Ruoff. Graphene-based composite materials, *Nature* **442**(7100), 282, 2006.

[290] C. Berger, Z. Song, T. Li, X. Li, A.Y. Ogbazghi, R. Feng, Z. Dai, N. Alexei, M.E.H. Conrad, P.N. First, and W.A. De Heer. Ultrathin epitaxial graphite: 2D electron gas properties and a route toward graphene-based nanoelectronics, *Journal of Physical Chemistry B* **108**(52), 19912, 2004.

[291] K.S. Novoselov, A.K. Geim, S.V. Morozov, D. Jiang, M.I. Katsnelson, I.V. Grigorieva, S.V. Dubonos, and A.A. Firsov. Two-dimensional gas of massless Dirac fermions in graphene, *Nature* **438**(7065), 197, 2005.

[292] K.S. Novoselov, A.K. Geim, S.V. Morozov, D. Jiang, Y. Zhang, S.V. Dubonos, I.V. Grigorieva, and A.A. Firsov. Electric field in atomically thin carbon films, *Science* **306**(5696), 666, 2004.

[293] R.R. Nair, P. Blake, A.N. Grigorenko, K.S. Novoselov, T.J. Booth, T. Stauber, N.M.R. Peres, and A.K. Geim. Fine structure constant defines visual transparency of graphene, *Science* **320**(5881), 1308, 2008.

[294] E. Bekyarova, M.E. Itkis, P. Ramesh, C. Berger, M. Sprinkle, W.A. De Heer, and R.C. Haddon. Chemical modification of epitaxial graphene: Spontaneous grafting of aryl groups, *Journal of the American Chemical Society* **131**(4), 1336-1337, 2009.

[295] G. Williams, B. Seger, and P.V. Kamt. TiO_2-graphene nanocomposites. UV-assisted photocatalytic reduction of graphene oxide, *ACS Nano* **2**(7), 1487, 2008.

[296] H. Zhang, X. Lv, Y. Li, Y. Wang, and J. Li. P25-graphene composite as a high performance photocatalyst, *ACS Nano* **4**(1), 380, 2010.

Capítulo II

MATERIALES Y MÉTODOS

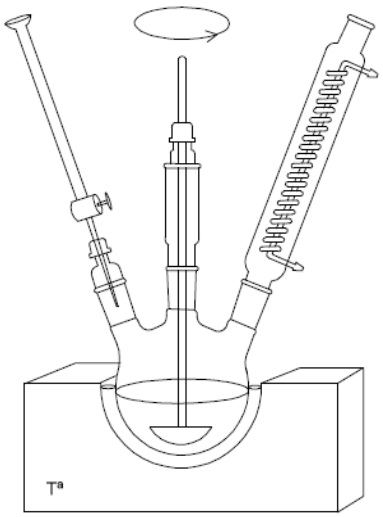

2. MATERIALES Y MÉTODOS

En este Capítulo se describe la preparación de todos los materiales que se han empleado en la Tesis, bien como soportes de catalizadores, catalizadores de hidrogenación o foto-catalizadores, así como la caracterización física y química de los mismos. También se describe la metodología y condiciones experimentales utilizadas en las reacciones de hidrogenación selectiva y la foto-degradación de moléculas orgánicas.

2.1. PREPARACIÓN DE LOS MATERIALES UTILIZADOS COMO SOPORTES DE CATALIZADORES DE HIDROGENACIÓN Y/O FOTO-CATALIZADORES

En esta Tesis se han preparado materiales de naturaleza muy diferente para su uso como soportes de catalizadores de hidrogenación o como foto-catalizadores. Estos materiales se clasifican en tres grupos: i) carbones activados; ii) xerogeles de carbón; iii) materiales compuestos xerogel de carbón - óxido metálico (TiO_2, SiO_2 y ZrO_2). También se describen los óxidos metálicos comerciales utilizados como referencia en los diferentes test catalíticos.

2.1.1. Carbones activados

Se ha preparado un carbón activado químicamente, denominado EG, a partir de hueso de aceituna para su empleo como soporte de catalizadores de hidrogenación. A efectos comparativos, también se ha utilizado un carbón activado comercial, el SorboNorit B3.

El carbón activado EG se preparó usando como materia prima hueso de aceituna procedente de la localidad granadina de Benalúa de las Villas, realizando una etapa de carbonización, seguida de una etapa de activación. Para ello, el hueso seco se carbonizó, en una primera etapa, en un horno tubular a 400 ºC con una velocidad de calentamiento de 10 ºC/min, manteniendo dicha temperatura durante 2 h, todo ello en flujo de nitrógeno de 300 cm^3/min. Posteriormente, este hueso carbonizado se somete a

una etapa de activación química con KOH en proporción másica hueso carbonizado: KOH de 1:7 siguiendo la secuencia térmica descrita a continuación:

1. Velocidad de calentamiento de 10 ºC/min hasta 350ºC, manteniendo esta temperatura durante 2 h.
2. Velocidad de calentamiento de 10 ºC/min hasta 850ºC, manteniendo esta temperatura durante 3 h.

El carbonizado activado EG, se lavó con HCl 1M y después con agua destilada hasta la ausencia de cloruros. Posteriormente, el carbón EG se desmineralizó utilizando el método de Bishop-Ward[1].

El rendimiento del carbón EG respecto a la cantidad inicial de hueso de aceituna fue del 14 %. En la Figura 2.1 se muestra el esquema correspondiente a esta preparación.

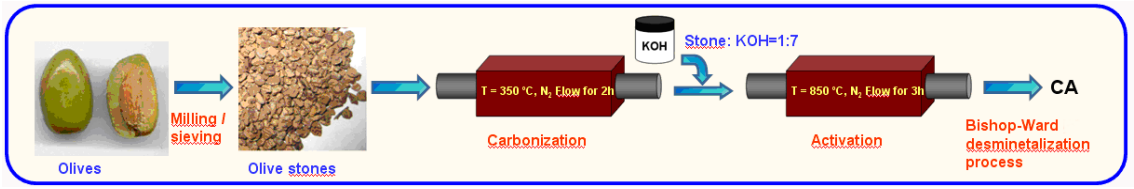

Figura 2.1. Esquema de preparación del carbón activado EG.

2.1.2. Xerogeles de carbón

Para la preparación de estos materiales, se sintetizaron xerogeles orgánicos a partir de la polimerización de una disolución acuosa de resorcinol (R) y Formaldehído (F), usando el ión carbonato (CO_3^{2-}) como catalizador (C) de polimerización, de acuerdo con el método originalmente desarrollado por Pekala[2-4].

Los reactivos utilizados, junto con la pureza y la empresa suministradora, han sido: resorcinol 99% y formaldehído 37% de Aldrich. Como catalizador se ha empleado carbonato de cesio 99.9% de Aldrich. Como disolvente se empleó agua bidestilada.

Los geles se prepararon a una temperatura de gelación de 85 ºC, con agitación de 250 rpm, manteniéndose durante 24 h a esas condiciones. El procedimiento de síntesis de los xerogeles orgánicos se describe a continuación. En un matraz de tres bocas se añadieron las cantidades adecuadas de R, agua y C. Esta disolución se calentó hasta la temperatura de polimerización (85 ºC) mediante un baño de aceite. Cuando se alcanzó dicha temperatura, se añadió la cantidad adecuada de F gota a gota. Una vez preparada la mezcla R, F y C se mantuvo a la temperatura de gelación durante 24 h.

Una vez trascurridas las 24 h, los geles se filtraron e introdujeron en acetona durante 72 h, renovando la acetona dos veces diariamente. Durante este proceso se produce un intercambio del agua del interior de los poros del gel por acetona, de modo que el posterior secado sea más rápido y se reduzca el colapso de la porosidad. Posteriormente, se secaron mediante el uso de microondas (Saivod MS-287 W) en atmósfera inerte de N_2 en periodos de tiempo de 1 min a una potencia de 384 W hasta pesada constante. En la Tabla 2.1 se recoge las relaciones molares de reactivos empleados en la síntesis de los diferentes geles orgánicos, los cuales fueron denominados: G1 y G8, respectivamente. En la Figura 2.2 se muestra el esquema de preparación de los xerogeles orgánicos.

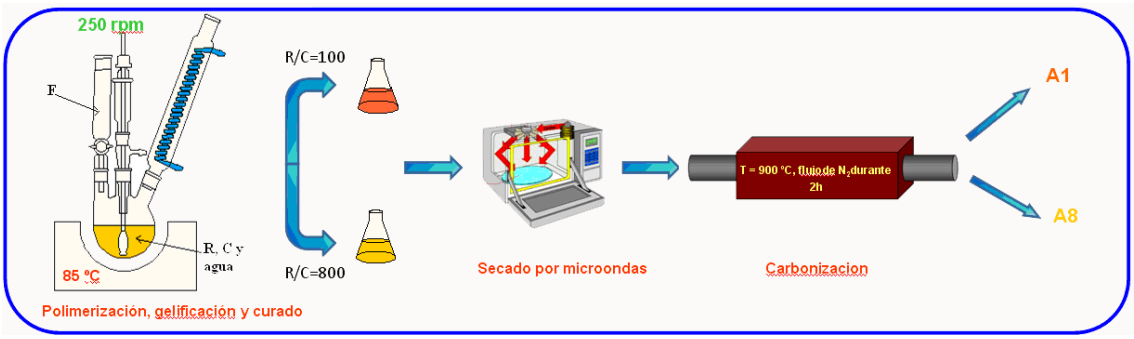

Figura 2.2. Esquema de preparación de los xerogeles de carbón.

Tabla 2.1. Composición de la mezcla inicial y relaciones molares.

Gel	R, (g)	F, (g)	C, (g)	Agua,(g)	R/F	R/C	R/W
G1	24,7	36,3	22,2	636	1/2	100	3/500
G8	24,7	36,3	2,8	636	1/2	800	3/500

Los xerogeles de carbón se obtuvieron sometiendo a los xerogeles orgánicos a un proceso de pirólisis a 900 ºC durante 2h, en flujo de N_2 de 150 $cm^3 \cdot min^{-1}$, usando una velocidad de calentamiento de 1 ºC· min^{-1}, para permitir una eliminación lenta de los gases de pirólisis. Transcurrido este tiempo, las muestras se enfriaron dentro del horno en atmósfera de nitrógeno. A los xerogeles de carbón obtenidos procedentes de los xerogeles G1 y G8, se les denomina A1 y A8, respectivamente.

Finalmente, estos xerogeles de carbón se molturaron y tamizaron hasta un diámetro inferior a 0,150 mm y se almacenaron en un desecador hasta su uso como soportes.

2.1.3. Materiales compuestos xerogeles de carbón-óxidos metálicos

La preparación de estos materiales se realizó mediante polimerización de una disolución acuosa de resorcinol (R) y Formaldehído (F), adicionando durante la síntesis un precursor del óxido metálico en cuestión. Los óxidos metálicos fueron: TiO_2, ZrO_2, SiO_2, CeO_2 y V_2O_5. La cantidad de precursor de la fase metálica a utilizar se calcula en función de los diferentes porcentajes de óxido metálico, en peso, que se desea alcanzar en el carbonizado final suponiendo que todo el R y F reaccionan y una pérdida de peso del 50% tras la carbonización.

Tras la síntesis, todos los materiales compuestos se molturaron y tamizaron hasta un diámetro inferior a 0,150 mm, almacenándose en un desecador hasta su uso como soportes. A continuación se recogen los diferentes materiales compuestos y se comentan algunos aspectos sobre la obtención de los mismos, habiéndose omitido deliberadamente determinados detalles, dado que las metodologías de síntesis se encuentran inmersas en varios procesos de solicitud de patente.

2.1.3.1. Materiales compuestos xerogel de Carbón - TiO_2

Los reactivos utilizados, junto con la pureza y la empresa suministradora, han sido: resorcinol 99% y formaldehído 37% suministrados por Aldrich. Como disolvente se empleo n-heptano 99% de Panreac y como precursor del óxido metálico se empleó un alcóxido metálico (isopropóxido de titanio IV 97% de Aldrich). La obtención de

estos materiales depende en gran parte de una secuencia metodológica muy concreta, de la que se pueden destacar algunos aspectos como: el empleo de surfactantes, un estricto control de la temperatura de polimerización, la adición de los diferentes componentes, la optimización de la velocidad de agitación y la etapa de secado asistida por microondas. Finalmente se carboniza siguiendo el mismo procedimiento descrito para los xerogeles de carbón en el apartado 2.1.2. De esta manera, se ha preparado una serie de materiales compuestos donde la fase óxido de titanio se encuentra altamente dispersa sobre la matriz de xerogel de carbón, y que se enumeran a continuación: CTiC10, CTi20, CTi30, CTi40, CTi50 y CTi80.

La nomenclatura empleada para denominar a estos materiales consiste en CTi (haciendo referencia a que son materiales compuestos xerogel de carbón-óxido de titanio), seguido del porcentaje teórico de óxido de titanio en el material. Por ejemplo, el material CTi10, es un material compuesto xerogel de carbón-TiO_2 que contiene, una vez carbonizado, un 10% en peso teórico de óxido de titanio en la matriz carbonosa.

2.1.3.2. Esferas de xerogel de carbón recubiertas con TiO_2

Para la síntesis de este tipo de materiales se sigue una variante del proceso descrito en el apartado anterior, caracterizada por una pre-gelación de la fase orgánica resorcinol-formaldehído, para finalizar con una etapa de secado y carbonización iguales a las ya descritas para los xerogeles de carbón en el apartado 2.1.2. Los reactivos empleados son los mismos que los empleados en apartado anterior.

De esta manera, se ha preparado una serie de materiales compuestos por microesferas de xerogel de carbón recubiertas de una fina capa, bien adherida, de óxido de titanio.

La nomenclatura empleada para denominar a estos materiales consiste en CTi, seguido del porcentaje teórico de óxido de titanio en el material, y por S2h; S hace referencia a que está compuesta por esferas, y 2h a una etapa de pre-gelación de 2h. Por ejemplo, el CTi40S2h, es un material compuesto xerogel de carbón-TiO_2 que contiene, una vez carbonizado, un 40% en peso teórico de óxido de titanio en forma de

recubrimiento de las esferas de xerogel de carbon (S), obtenidas mediante pre-gelación de la mezcla R-F durante 2h.

2.1.3.3. Materiales compuestos xerogel de carbón - ZrO_2 o SiO_2.

Los reactivos utilizados, junto con la pureza y la empresa suministradora, han sido: resorcinol 99% y formaldehído 37% de Aldrich. Como disolvente se empleó n-heptano 99% de Panreac y como precursor del óxido metálico se empleó propóxido de zirconio IV 70% o tetraetilortosilicato 98% suministrados por de Aldrich.

La obtención de estos materiales depende igualmente de una secuencia metodológica muy concreta que permite obtener xerogeles de carbón dopados con una elevada cantidad de óxidos inorgánicos de zirconio, silicio, cerio o vanadio muy bien dispersa sobre la matriz carbonosa.

De esta manera, se ha preparado una serie de materiales compuestos donde la fase óxido inorgánico se encuentra dispersa sobre la matriz de xerogel de carbón, y que se enumeran a continuación: CZr20, CZr30, CZr40, CSi30, CCe30 y CV30.

La nomenclatura empleada para denominar a estos materiales consiste en CM (haciendo referencia a que son materiales compuestos xerogel de carbón (C)-óxido metálico (M)), seguido del porcentaje teórico de óxido metálico en el material. Por ejemplo, el material CSi30, es un material compuesto xerogel de carbón-SiO_2 que contiene, una vez carbonizado, un 30% en peso teórico de óxido de silicio altamente en la matriz carbonosa.

2.1.4. Óxidos metálicos comerciales

Los óxidos metálicos comerciales que se han utilizado en este trabajo son: SiO_2 (Gel de sílice 100 de Merck); Al_2O_3 (oxido de aluminio ácido de Merck); TiO_2 (anatasa de Alfa Aesar); y ZrO_2 (óxido de zirconio IV 99% de Aldrich). Estos materiales se han utilizado como soportes de catalizadores metálicos en la hidrogenación selectiva de aldehídos α,β-insaturados, para lo cual, previo a la impregnación con la sal precursora del metal, se molturaron hasta un tamaño inferior a 0,150 mm.

Finalmente, como material de referencia en las reacciones de foto-degradación se utilizó un dióxido de titanio (TiO_2) anatasa-rutilo, P25 de Degussa. El P25 es el material comercial más empleado en este tipo de reacciones.

2.2. PREPARACIÓN DE CATALIZADORES SOPORTADOS DE IRIDIO, RUTENIO Y PLATINO

La técnica empleada para la preparación de los catalizadores soportados ha sido la impregnación por mojado incipiente con una disolución acuosa de una sal precursora del metal. La concentración en metales de la disolución empleada para la impregnación de los soportes, se estableció en función del volumen necesario para obtener finalmente catalizadores soportados con un 3% en peso del respectivo metal. Las sales precursoras utilizadas fueron cloruro de tetraaminplatino (II), $[Pt(NH_3)_4]Cl_2$, cloruro de iridio (IV), $[IrCl_4]$, y cloruro de rutenio (III), $[RuCl_3]$, todos ellos suministrados por Aldrich.

Los catalizadores se pre-trataron, para descomponer la sal precursora y obtener el metal en su forma reducida, antes de la caracterización y empleo en reacción. El pretratamiento se realizó, en la mayoría de los casos, a 400 ºC en un flujo de He usando una rampa de calentamiento de 5 $ºC \cdot min^{-1}$ durante 12 h. Con el fin de aumentar aún más el tamaño de partícula, y así obtener más variedad de tamaños de partícula, algunos catalizadores también se pre-trataron en flujo de H_2, esto es así, ya que en atmósfera de H_2 se forma un hidruro intermedio móvil, $[Pt(NH_3)_2H_2]$, que favorece movilidad y la aglomeración de las partículas de platino (Ecuaciones 1-2)[5], respecto a la descomposición de la sal en atmósfera inerte (Ecuaciones 3-4)[6]. Una vez finalizado el pre-tratamiento, las muestras se enfriaron a temperatura ambiente en la misma corriente gaseosa.

$$[Pt(NH_3)_4]Cl_2 + 2\,H_2 \longrightarrow [Pt(NH_3)_2H_2] + 2\,NH_3 + 2\,HCl \quad (1)$$

$$[Pt(NH_3)_2H_2] \longrightarrow Pt^0 + 2\,NH_3 + H_2 \quad (2)$$

La reacción (1) ocurre entre 275 y 315 ºC y la (2) entre 315 y 370 ºC, por lo que a la temperatura de activación empleada (400ºC) la sal precursora se ha descompuesto totalmente.

$$[Pt(NH_3)_4]Cl_2 \longrightarrow [Pt(NH_3)_2Cl_2] + 2\,NH_3 \quad (3)$$

$$3[Pt(NH_3)_2Cl_2] \longrightarrow 3\,Pt^0 + N_2 + 4\,NH_3 + 6\,HCl \quad (4)$$

La nomenclatura empleada para denominar a los catalizadores soportados consta del nombre del soporte, seguido del metal y de la carga metálica en % en peso, y finalmente del tamaño de partícula de metal obtenido por quimisorción. Por ejemplo, el A8Pt3-3, es un catalizador de Pt al 3% en peso, soportado sobre el xerogel A8, y con un tamaño promedio de Pt obtenido mediante quimisorción de H_2 de 3 nm. En los Capítulos posteriores se describen ampliamente los diferentes catalizadores soportados preparados.

2.3. TÉCNICAS DE CARACTERIZACIÓN

Los soportes y catalizadores se han caracterizado mediante diversas técnicas experimentales con objeto de estudiar su morfología, estructura porosa, área superficial y características químicas superficiales, así como la naturaleza y la dispersión de las correspondientes fases activas.

El análisis morfológico de las muestras se ha realizado mediante microscopía electrónica de barrido (SEM). El estudio del área superficial y de la porosidad se ha analizado mediante adsorción física de N_2 a -196ºC y CO_2 a 0ºC y, en algunos casos, porosimetría de mercurio. La naturaleza química se ha estudiado mediante las técnicas de análisis elemental, desorción térmica programada (DTP), espectroscopía de fotoemisión de rayos X (XPS), espectroscopía de infrarojo (FTIR), difracción de rayos X (DRX), análisis termogravimétrico (TG) y medida de pH del punto cero de carga.

Para la determinación de la dispersión y naturaleza química de la fase metálica de los catalizadores se han empleado las técnicas de quimisorción de H_2, difracción de rayos X (DRX), microscopía electrónica de transmisión (TEM) y espectroscopía de fotoemisión de rayos X (XPS).

2.3.1. Caracterización textural y morfológica de las muestras

2.3.1.1. Microscopía electrónica de barrido (SEM)

La morfología de las muestras se realizó mediante microscopía electrónica de barrido (SEM). El equipo usado es un microscopio de barrido de alta resolución del Centro de Instrumentación científica de la Universidad de Granada, modelo GEMINI-1430-VP de la casa LEO (Carl Zeiss), con el que se puede conseguir imágenes con aumentos de hasta 500.000 X.

2.3.1.2. Adsorción física de gases

Las muestras se han estudiado mediante adsorción física de nitrógeno y dióxido de carbono a -196 y 0 ºC respectivamente. Las isotermas se realizaron con un aparato volumétrico AUTOSORB-1C de la casa Quantachrome Instruments. Este aparato permite alcanzar un vacío de 10^{-7} mbar mediante la acción combinada de una bomba seca y una turbomolecular con trampa fría de N_2 líquido.

Para la realización de las isotermas, se coloca en un bulbo de vidrio alrededor de 0,1g de muestra seca y se desgasifica durante 12 horas a 110 ºC en vacío dinámico de aproximadamente 10^{-6} mbar. Los adsorbatos usados fueron nitrógeno (99,999%) y dióxido de carbono (99,999 %) suministrados por Air Liquide.

De los datos obtenidos de la adsorción de nitrógeno a -196 ºC se obtiene el área superficial aparente (S_{BET}), mediante el método de Brunauer, Emmet y Teller[7] (BET), y el volumen de microporos ($W_0(N_2)$), aplicando la ecuación de Dubinin-Radushkevich (DR)[8]. Por otro lado, también se han obtenido las isotermas de desorción de N_2, a cuyos datos se ha aplicado el método de Barrett, Joyner y Halenda (BJH)[9] para el cálculo del volumen de mesoporos.

De los datos obtenidos de la adsorción de CO_2 a 0 ºC se obtiene el volumen de microporos ($W_0(CO_2)$) y la energía de adsorción característica (E_0), mediante la aplicación de la ecuación de DR. Con estos dos datos y aplicando la ecuación de Stoeckli se ha obtenido la anchura media de los microporos (L_0).

A continuación se describen las ecuaciones y métodos anteriormente descritos.

Ecuación BET.

El fundamento se basa en que si se conoce la capacidad de la monocapa, es decir, la cantidad de adsorbato que se necesita para formar una monocapa estadística sobre la superficie del adsorbente y conocemos la superficie que ocupa una molécula de dicho adsorbato, entonces podremos saber la superficie del sólido en el que ha sido adsorbido.

La ecuación propuesta por BET sería:

$$\frac{P}{V_{ads}(P_0 - P)} = \frac{1}{V_m C} + \frac{C-1}{V_m C}\frac{P}{P_0} \qquad (5)$$

donde V_{ads}, es el volumen de gas adsorbido a la presión P; P_0 es la presión de saturación del adsorbato. Existen dos constantes: V_m (volumen de la monocapa) y C (constante estadística relacionada con el calor de adsorción), que se calculan al representar gráficamente $P/V(P_0-P)$ frente a P/P_0, una vez calculadas la pendiente y ordenada en el origen.

El parámetro C, calculado de la ecuación (5), está relacionado con el tiempo de vida media del adsorbato en la superficie del adsorbente. Si su valor fuese elevado, el tiempo de residencia del adsorbato sería grande, lo que indicaría un potencial de interacción superficial alto.

Una vez conocido el volumen de monocapa (V_m) y conociendo el área que ocupa una molécula de N_2 a -196 ºC (0,162 nm^2), se puede calcular el área superficial aparente aplicando la siguiente ecuación (6):

$$S_{BET}(m^2 g^{-1}) = V_m\left(cm^3 g^{-1}\right) x \frac{1(mol)}{22{,}4\left(cm^3\right)} x N_A\left(\frac{molec}{mol}\right) x 0{,}162\left(\frac{nm^2}{molec}\right) x 10^{-18}\left(\frac{m^2}{nm^2}\right) \qquad (6)$$

donde N_A es el número de Avogadro.

Ecuación de Dubinin-Radushkevich

Para el estudio de la porosidad de materiales microporosos, más que el concepto de superficie específica se utiliza el de volumen de microporos, ya que los microporos parecen llenarse como líquido. Por ello, hay que aplicar otro tipo de teoría a los datos de adsorción de nitrógeno y CO_2, a –196 ºC y 0 ºC, respectivamente, como es la ecuación de Dubinin-Radushkevich[8].

El modelo de Dubinin[8] caracteriza a los microporos por el llenado de su volumen con adsorbato en estado similar al líquido. La ecuación de Dubinin-Radushkevich es la siguiente:

$$W = W_0 \exp\left[-\left(\frac{A}{\beta E_0}\right)^2\right] \qquad (7) \qquad\qquad A = RT\ln\left(\frac{P}{P_0}\right) \qquad (8)$$

donde W es el volumen de gas adsorbido como líquido a una presión relativa de equilibrio P/P_0, W_0 es el volumen de microporos y A es el trabajo molar diferencial, definido por la ecuación (8). Los parámetros E_0 y β son específicos del sistema adsorbato-adsorbente. E_0 es la energía característica de adsorción y β es el cociente de afinidad para el N_2 a -196 ºC y para el CO_2 a 0 ºC, siendo 0,33 y 0,35 respectivamente. En el caso se toma β = 0,33 y β = 0,35. Los volúmenes molares empleados para N_2 y CO_2 a las temperaturas de trabajo fueron 34,65 $cm^3 \cdot mol^{-1}$ y 43,01 $cm^3 \cdot mol^{-1}$, respectivamente.

Al aplicar logaritmos a la ecuación (7) se obtiene una recta, de cuya intersección con el eje de ordenadas se obtiene el valor del volumen de microporos, W_0, y de la pendiente, la energía de adsorción característica, E_0, la cual está inversamente relacionada con la anchura media de los microporos, L_0. De este modo, se encuentran distintas ecuaciones empíricas que relacionan ambos valores. Stoeckli[10] propuso la siguiente ecuación:

$$L_0(nm) = \frac{10{,}8}{\left(E_0 - 11{,}4 kJ/mol\right)} \qquad (9)$$

Esta ecuación se cumple para valores de E_0 comprendidos entre 42 y 20 kJ·mol^{-1}. Cuando se obtienen valores inferiores de E_0, se aplica la ecuación de Dubinin[11] siguiente:

$$L_0(nm) = \frac{24}{E_0(kJ/mol)} \tag{10}$$

y la superficie específica viene dada por

$$S_{mic}\left(m^2/g\right) = \frac{W_0\left(cm^3/g\right)\cdot 2000}{L_0(nm)} \tag{11}$$

Una vez obtenidos los parámetros relativos al volumen de microporos, energía de adsorción característica y anchura media de poro, al aplicar las ecuaciones anteriores, podemos encontrarnos distintas situaciones:

- $W_0(N_2) < W_0(CO_2)$. Este caso se produce en carbonizados y carbones con un bajo grado de activación, por la presencia de constricciones a la entrada de los microporos que restringen el acceso del N_2 a su interior, debido a la baja temperatura a la que se lleva a cabo la adsorción. Sin embargo, al realizarse la adsorción de CO_2 a mayor temperatura esta puede acceder a estos microporos. En este caso se dice que la adsorción es activada.

- $W_0(N_2) = W_0(CO_2)$. Ocurre cuando la accesibilidad a la microporosidad de ambos adsorbatos es la misma en carbones con un grado de activación medio. En este caso no existen constricciones debido al mayor grado de activación de los carbones y se puede considerar que hay una distribución homogénea del tamaño de los microporos.

- $W_0(N_2) > W_0(CO_2)$. Se produce en carbones con un alto grado de activación, en los que existe una distribución muy ancha en el tamaño de los microporos. Esta diferencia en volumen de microporos se debe a la gran diferencia en la presión de saturación que existe entre ambos adsorbatos. Así, el N_2 llena todo el

volumen de microporos (ultramicroporos y supermicroporos), mientras que con CO_2 solo medimos a 0 ºC, los microporos más estrechos (menores de 0,7 nm en anchura) o ultramicroporos.

Método BJH

Con objeto de estudiar las características mesoporosas de los materiales se aplicó el método propuesto por Barrett, Joyner y Halenda (BJH) a los datos de la isoterma de N_2.

2.3.1.3. Porosimetría de mercurio

Esta técnica nos permite analizar la mayor parte del rango de mesoporosidad y la macroporosidad, obteniendo un volumen y una distribución de tamaños de poros. El mercurio es un líquido que no moja la superficie del sólido. Para que acceda a la porosidad hay que aplicar una presión externa mayor a la atmosférica. A medida que el poro sea más estrecho, mayor será la presión que tenemos que aplicar al mercurio para que se introduzca.

La presión externa aplicada (P) se relaciona con el radio de poro (r) mediante la ecuación de Washburn[12] (Ecuación 12). Ésta nos indica que el radio de poro, suponiendo poros con geometría cilíndrica, está inversamente relacionado con la presión aplicada.

$$r = \frac{-2\sigma\cos\theta}{P} \qquad (12)$$

En esta ecuación P es la presión total aplicada, σ la tensión superficial del mercurio, θ el ángulo de contacto del mercurio con las paredes del poro y r el radio del propio poro. El mercurio tiene un ángulo de contacto con la superficie comprendido entre 135º y 150º. Los valores empleados en los experimentos fueron: $\sigma = 480\ mN\cdot m^{-1}$, θ = 140º y un valor máximo de P = 275,6 MPa.

Con esta técnica se ha determinado el área superficial externa porosa (S_{ext}) de poros con diámetro superior a 4,4 nm; V_2, volumen de poros con un diámetro comprendidos entre 4,4 y 50 nm; V_3, volumen de poros con diámetro mayor a 50 nm (macroporos).

El equipo utilizado ha sido un porosímetro de mercurio de la casa MICROMERITICS, modelo Autopore IV.

2.3.2. Caracterización química de los soportes

2.3.2.1. Análisis elemental

El análisis elemental de las muestras se realizó en un analizador elemental Fisons Carlo Erba EA 1108 CHNS O del Centro de Instrumentación Científica de la Universidad de Granada, el cual determina el contenido de C, H, N y S; el contenido de O se calculó por diferencia.

2.3.2.2. Espectroscopía de infrarrojo

Los espectros de infrarrojo de las muestras se realizaron con un espectrómetro NICOLET 20SXB, con paquete de software OMNIC v.1.1 del Centro de Instrumentación Científica de la Universidad de Granada, con el cual hemos determinado espectros de transmitancia en la zona del Infrarrojo medio (4000-400 cm^{-1}) con una resolución de 0,5 cm^{-1}. Para realizar los espectros, se prepararon pastillas con KBr en las que la muestra estaba diluida al 0,1 % en peso.

2.3.2.3. Análisis termogravimétrico

Para conocer el contenido en cenizas de los carbones activados y así como el contenido de óxido metálico de las muestras se realizaron análisis termogravimétricos en flujo de aire. Los experimentos se realizaron con una termobalanza SHIMADZU mod. TGA-50H del Centro de Instrumentación Científica de la Universidad de Granada, a una velocidad de calentamiento de 10 $^{o}C \cdot min^{-1}$ y hasta pesada constante.

2.3.2.4. Medida del pH punto cero de carga

El pH_{PZC} de los soportes: aerogeles de carbón y carbones activados, se determinó utilizando una variante[13] del método propuesto por Schwarz y col.[14]. Para ello se añadieron 4 ml de agua destilada, y libre de CO_2, a 250 mg de carbón. La suspensión obtenida se mantuvo en agitación, y termostatizada a 25 ºC, midiendo periódicamente el pH hasta que éste alcanzó un valor constante. De esta forma, el pH final obtenido se ha considerado como el pH_{PZC}.

2.3.2.5. Desorción térmica programada

Para el análisis de las muestras mediante desorción térmica programada (DTP) se procedió de la siguiente forma: la muestra fue situada en un reactor tubular de cuarzo equipado en el centro con un termopar de corto tiempo de respuesta. La muestra se calentó en flujo de He (60 $cm^3 \cdot min^{-1}$) a 50 $ºC \cdot min^{-1}$ de velocidad de calentamiento hasta 1000 ºC. El análisis de los gases desorbidos en función del tiempo se llevó a cabo mediante un espectrómetro de masas Balzers, modelo MSC 200 Thermocube, el cual dispone de un sistema de inyección capilar termostatizado a 110 ºC. La calibración se realizó analizando los gases diluidos en Helio (10 % v/v), excepto para el agua, la cual fue realizada mediante un DTP de $CuSO_4 \cdot 5H_2O$.

El espectrómetro estaba controlado por un sistema informático de adquisición de datos, el cual analizaba las cantidades desorbidas de CO, CO_2 y H_2O mediante el registro de las siguientes señales m/z: 12, 14, 16, 17, 18, 22, 28 y 44.

2.3.2.6. Difracción de rayos-X

Los experimentos de difracción de rayos-X (DRX), en polvo, se llevaron a cabo con un equipo Philips PW 1710, usando la radiación CuKα, y eliminándose la radiación Kβ mediante un filtro de Ni. Este equipo pertenece al Centro de Instrumentación Científica de la Universidad de Granada.

2.3.3. Caracterización de los catalizadores

Para caracterizar los catalizadores se utiliza la técnica de adsorción física de gases y difracción de rayos X, comentada anteriormente, además de las técnicas de quimisorción de H_2, microscopía electrónica de transmisión (TEM) y espectroscopía de fotoemisión de rayos X (XPS) con el fin de determinar la dispersión, tamaño de partícula y naturaleza química de los catalizadores. Además, la ácidez de los catalizadores fue medida mediante pH_{PZC} y adsorción/desorción de n-butilamina.

2.3.3.1. Espectroscopía de fotoemisión de rayos-X

Los experimentos de espectroscopía de fotoemisión de rayos-X (XPS) se llevaron a cabo en los Servicios Centrales de Apoyo a la Investigación de la Universidad de Málaga. Para ello se utilizó un espectrómetro ESCA 5701 de Physical Electronics (PHI), usando como fuente la radiación MgKα (hν = 1253,6 eV) y un analizador hemiesférico de electrones. La fuente de rayos X operaba a 12 kV y 10 mA.

Las muestras molturadas se disponían en un portamuestras de acero y se introducía en la cámara de análisis desgasificándolas a una presión inferior a 10^{-8} Torr. Dependiendo de la composición de la muestra se registraron los espectros de las regiones C_{1s}, O_{1s}, Ti_{2p}, Si_{2p}, Al_{2p}, Zr_{3d}, V_{2p}, Ce_{3d}, Pt_{4f}, Pt_{4d}, Ir_{4f} y Ru_{3d} acumulando cada uno de ellos el suficiente número de barridos para obtener una buena relación señal/ruido.

Los espectros obtenidos, una vez restado el fondo, se deconvolucionaron por medio de un método iterativo de ajuste, usando funciones suma asimétricas Gaussianas-Lorentzianas para determinar el número de componentes, la energía de ligadura de los picos (EL) y las áreas de los mismos (análisis cuantitativo). La energía de ligadura del pico de la región C1s, correspondiente a C=C (aromático-alifático) se tomó como pico de referencia, asignándole el valor de 284,6 eV

2.3.3.2. Microscopía electrónica de transmisión de alta resolución

Los análisis mediante HRTEM se han realizado con un equipo Philips, modelo CM-20, con sistema EDAX de microanálisis mediante dispersión de energía de rayos X, perteneciente al Centro de Instrumentación Científica de la Universidad de Granada. La magnificación del equipo es de 660.000X, la máxima resolución es de 2,7 Å entre puntos y 1,4 Å entre líneas, y la tensión de aceleración es de pasos seleccionables de 20, 40, 80, 120, 160 y 200 KV.

2.3.3.3. Quimisorción de H_2

Las isotermas de quimisorción de H_2 se llevaron a acabo a 25 ºC. En un experimento normal se tomó en torno a 0,2 g de catalizador fresco y se introdujo en la cámara de adsorción para realizar en primer lugar el pretratamiento deseado. Una vez finalizado el pretratamiento el catalizador se desgasificó a alto vacío, del orden de 10^{-6} mbar durante 1 hora y a 350 ºC (50 ºC menos que la temperatura de pretratamiento). Posteriormente la muestra se enfrió a 25 ºC y se determinó la isoterma de adsorción de hidrógeno entre 50 y 310 mbar. Generalmente se obtuvo 5 puntos con un intervalo de 50 mbar. Una vez obtenida la isoterma de adsorción la muestra se desgasificó nuevamente hasta alto vacío durante 1 hora a 25 ºC y, a continuación, se determinó una segunda isoterma de adsorción. A partir de la primera isoterma se determina la cantidad total de H_2 quimisorbido (Q_T), mientras que la segunda representa el H_2 reversiblemente o más débilmente quimisorbido (Q_R). Para determinar la cantidad de hidrógeno quimisorbido en la superficie del metal se utilizó el método de Benson y Boudart[15] y de Wilson y Hall[16]. Este método lleva consigo la extrapolación de la porción lineal de la isoterma a presión cero.

Una vez determinada la cantidad de H_2 quimisorbida, la dispersión metálica (D) se calculó a partir de los valores de quimisorción total (Q_T) suponiendo que la quimisorción es disociativa y asumiendo una estequiometría H_2:M = 1:2. El tamaño medio de partícula ($\overline{d}$) está inversamente relacionado con la dispersión (D) calculada anteriormente. Así mediante la aplicación de la ecuación (13), se puede calcular el tamaño medio de partícula del metal empleado.

$$\bar{d}_M\ (nm) = \frac{k}{D} \qquad (13)$$

donde k es 1.08 para Pt, 0.91 para Ru y 1.11 para Ir[15-20].

2.3.3.4. Adsorción/desorción de n-butilamina

Para caracterizar la fortaleza ácida de los sitios activos de los catalizadores, y su número, se ha empleado la técnica de desorción térmica programada de la n-butilamina, una base relativamente fuerte (pK_b=3.23) que puede reaccionar con sitios ácidos incluso relativamente débiles[21-23]. Melo y col.[23] consideran como especies fisisorbidas a la cantidad de n-butilamina adsorbida debajo de 110 ºC, y como especies quimisorbidas en centros ácidos a aquellas adsorbidas a temperaturas superiores a 110ºC, considerando diferentes fortalezas ácidas dependiendo del rango de temperatura a la que desorban. Así, se considera sitios ácidos débiles si desorben entre 110 y 210 ºC; sitios ácidos de fortaleza media si lo hacen entre 210 y 330 ºC, y sitios ácidos fuertes si desorben a temperaturas superiores a 330ºC. Por tanto, la adsorción de n-butilamina se realiza a dos temperaturas diferentes: 90 ºC dónde la n-butilamina adsorbida dependerá del área superficial de la muestra; y 150 ºC en la que la n-butilamina solo depende de la acidez de la muestra.

Para cuantificar la cantidad de los diferentes tipos de sitios ácidos se realizó la adsorción y desorción de n-butilamina en un microreactor de cuarzo a presión atmosférica, utilizando 0,2 g de muestra (soporte o catalizador previamente pre-tratado in situ) y usando una corriente de He/Ar saturada con n-butilamina a 0 ºC. El caudal total fue 60 cm^3min^{-1} y la presión parcial de n-butilamina 28,92 Torr. El análisis de los gases de salida se realizó en continuo mediante un espectrómetro de masas modelo Prisma de Pfeiffer. Antes de la saturación con n-butilamina, las muestras se calentaron hasta la temperatura correspondiente (90 o 150 ºC) en flujo de He, cambiando posteriormente dicho flujo de He por otro de He/Ar saturado con n-butilamina hasta alcanzar la completa saturación de la muestra. Una vez saturada la muestra se purgó el reactor de desorción He durante 1 h para eliminar los restos de n-butilamina. Finalmente se realiza el ensayo de desorción térmica programada calentando hasta los 1000 ºC, a una velocidad de calentamiento de 10 ºC/min.

Para conocer la naturaleza Brönsted o Lewis predominante de los sitios ácidos se llevó a cabo el análisis FTIR de las muestras saturadas con n-butilamina, para lo cual 0.050 g de cada muestra, previamente secas a 110 ºC, se colocaron en un desecador que contiene una atmosfera saturada de n-butilamina a presión atmosférica y temperatura ambiente, hasta que se alcanzó el equilibrio (hasta pesada constante). Con las muestras saturadas se prepararon las pastillas con KBr, y se analizan de acuerdo con el procedimiento descrito en la sección 2.3.2.2. En los espectros de IR, se consideraron sitios ácidos de Lewis las señales situadas a 1630 cm^{-1}, y sitios Brönsted las situadas a 1500 cm^{-1}.[22]

2.4. HIDROGENACIÓN DE CITRAL

La hidrogenación de citral se llevó a cabo en un reactor de alta presión de la casa Parr, modelo 5500, de 300 mL de capacidad provisto de un sistema de agitación, una entrada de gas, y sistema de calefacción automatizados. Dicho reactor, mostrado en la Figura 2.3a, puede trabajar en unas condiciones máximas de presión y temperatura de 207 bares y 350 ºC, respectivamente.

Todos los experimentos de reacción realizados para la presente Tesis se llevaron a cabo en modo semi-continuo, es decir, manteniendo constante la presión de hidrógeno.

El protocolo de reacción realizado en todos los casos fue el siguiente: se introduce en el reactor 100 ml de disolución de citral en n-heptano con la concentración deseada y se elimina el O_2 burbujeando con N_2. Posteriormente, se añade la masa de catalizador pre-tratada y se fija la presión de trabajo con N_2. A continuación se purga con N_2 a dicha presión durante 25 min y tras este tiempo se termostatiza a la temperatura de reacción y comienza la agitación. Una vez alcanzada la temperatura de operación extrae el N_2 abriendo la válvula de salida y se presuriza con H_2 hasta la presión seleccionada, el cual burbujea dentro de la disolución; y considerándose éste momento como tiempo inicial de reacción. Durante los primeros 25 minutos se mantiene semi-abierta la salida del reactor a fin de poder evacuar y purgar todo el nitrógeno inicial. Tras estos 25 min se cierra la salida de H_2 y solo se mantiene abierta la entrada. Los químicos utilizados en la disolución son n-heptano 99% de Panreac y citral >97% de Merck.

Figura 2.3. a) Reactor de alta presión empleado en la reacción de hidrogenación de citral. b) Cromatógrafo de gases para la identificación de los productos de reacción.

Las alícuotas de reacción, tomadas periódicamente a diferentes tiempos del reacción, permitieron analizar la composición de reactivos y productos mediante cromatografía de gases, previa calibración con el uso de patrones comerciales de los productos hidrogenados de citral (Aldrich > 98%) en una concentración de 0,05 a 0,5 M.

El seguimiento de la reacción de hidrogenación del citral se efectuó en un cromatógrafo de gases Bruker 430-GC, equipado con un detector FID (Figura 2.3b). Se utilizó una columna Varian GC (25m x 0,32 mm x 0,45 μm), la cual se mantuvo isotérmicamente a 150 ºC. Las temperaturas del inyector y detector fueron de 250ºC y 275ºC respectivamente. Como gas de arrastre se empleó He.

El comportamiento catalítico fue evaluado mediante el cálculo de la conversión de citral (C), en base a la cantidad de reactivos y productos detectados, y mediante el cálculo de la selectividad (S) a cada uno de los productos, las cuales se detallan a continuación:

$$C(\%) = \frac{moles\ de\ citral\ o\ cinamaldehído\ consumidos}{moles\ iniciales\ citral\ o\ cinamaldehído} \cdot 100 \quad (5)$$

$$S_{UA}(\%) = \frac{moles\ alcohol\ insaturado\ detectados}{moles\ de\ citral\ o\ cinamaldehído\ consumidos} \cdot 100 \quad (6)$$

Siendo AU: alcoholes insaturados (nerol y geraniol o alcohol cinamílico),

Los productos detectados por cromatografía son nerol, geraniol, citronelol, citronelal, 3,7-dimetiloctanol, 3,7-dimetiloctanal, mentol e isopulegol, alcohol cinamílico, hidrocinamaldehído e hidrocinamilalcohol.

2.5. FOTO-DEGRADACIÓN DE ORANGE G

Para los experimentos de foto-degradación, se empleó una lámpara de luz visible de 10 W de potencia, 250 mL de disolución acuosa de Orange G (sal disódica del ácido 1-fenilazo-2-naftol-6,8-disulfónico, CAS 1936-15-8) de concentración inicial 10 mg/L, y una relación catalizador/disolución total de 1 mg/mL. El seguimiento de la foto-degradación se llevó a cabo tomando alícuotas del reactor cada cierto tiempo, y analizándolas mediante espectrofotometría UV a una λ= 487 nm.

Se determinó inicialmente la cinética de adsorción del Orange G sobre el material foto-catalítico obteniéndose el tiempo necesario para alcanzar el equilibrio de saturación. Para ello, 250 mg de material se introducen en 250 mL de una disolución de 20 mg/L de colorante en oscuridad (para evitar la foto-descomposición) y con agitación (para minimizar los problemas difusionales). Se toman alícuotas de solución cada cierto tiempo hasta que la concentración de Orange G (medida con espectroscopía UV) permanece constante.

También se obtuvo la isoterma de adsorción, para calcular la capacidad de adsorción del material, para lo cual 25 mg de muestra se introducen en 25 mL de soluciones de concentración comprendida entre 5 y 50 mg/mL de Orange G, en oscuridad y bajo agitación. Tras 2 h más del tiempo necesario para alcanzar el equilibrio, las soluciones se filtran y se mide la concentración final mediante espectroscopía UV. La cantidad adsorbida corresponde a la diferencia con la concentración inicial y estos datos se ajustan mediante la aplicación de la ecuación de Langmuir para obtener la capacidad de adsorción de la muestra.

Antes de proceder con la reacción de foto-degradación y con objeto de poder discriminar claramente los efectos cooperativos entre los fenómenos de adsorción y

catálisis, todos los foto-catalizadores pre-tratados se saturaron previamente con una disolución de Orange G.

La saturación de cada material se realiza en oscuridad y bajo agitación. Para ello, se adicionan 250 mg de muestra pre-tratada a 250 mL de una solución de concentración adecuada. Tras alcanzar la saturación del catalizador, la concentración se ajustó a 10 mg/mL.

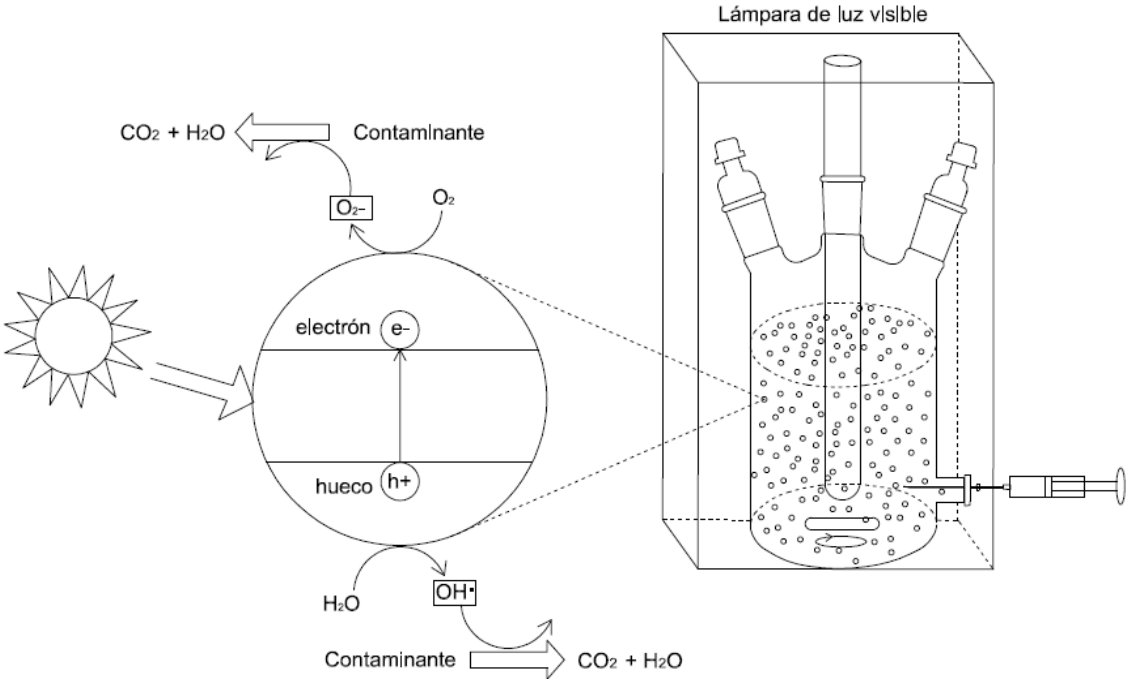

Figura 2.4. Esquema del dispositivo usado para la foto-degradación del Orange G.

En estas condiciones, se realiza la foto-degradación del Orange G bajo luz visible ó UV, siguiendo la evolución de la degradación mediante la toma de alícuotas cada cierto tiempo. Las concentraciones correspondientes se determinaron mediante espectroscopía UV (Figura 2.4), como se comentó anteriormente.

Simultáneamente se analiza la evolución del carbón orgánico total (TOC) presente en la disolución para evaluar el grado de mineralización (degradación total y eliminación como CO_2) del contaminante orgánico. Los valores de TOC se obtuvieron mediante un analizador Shimadzu V-CSH.

2.6. BIBIOGRAFÍA

[1] M. Bishop and D.L. Ward. The direct determination of mineral matter in coal, *Fuel* **37**, 191, 1958.

[2] R.W. Pekala. Organic aerogels from the polycondensation of resorcinol with formaldehyde, *Journal of Materials Science* **24**(9), 3221-3227, 1-9-1989.

[3] R.W. Pekala, C.T. Alviso, and J.D. LeMay. Organic aerogels: microstructural dependence of mechanical properties in compression, *Journal of Non-Crystalline Solids* **125**(1–2), 67, 1990.

[4] R.W. Pekala, C.T. Alviso, F.M. Kong, and S.S. Hulsey. Aerogels derived from multifunctional organic monomers, *Journal of Non-Crystalline Solids* **145**(0), 90, 1992.

[5] R.A. Dalla-Betta and M. Boudart. *Proceeding 5th International Congress on Catalysis* **1**, 1329, 1973.

[6] M.A. Richard and R.J. Pancirov. Thermal decomposition of tetraamineplatinum(II) chloride by simultaneous TG/DTG/DTA/MS and direct insertion probe mass spectrometry, *Journal of Thermal Analysis and Calorimetry* **32**(3), 825, 1987.

[7] S. Brunauer, P.H. Emmett, and E. Teller. Adsorption of Gases in Multimolecular Layers, *Journal of the American Chemical Society* **60**(2), 309-319, 1-2-1938.

[8] MM. Dubinin. Contemporary state of the theory of volume filling of micropores of adsorbents in the adsorption of gases and vapors on carbon adsorbents, *Russian Journal of Physical Chemestry* **39**, 1305, 1965.

[9] E.P. Barrett, L.G. Joyner, and P.P. Halenda. The Determination of Pore Volume and Area Distributions in Porous Substances. I. Computations from Nitrogen Isotherms, *Journal of the American Chemical Society* **73**(1), 373-380, 1-1-1951.

[10] F. Stoeckli, *porosity in carbons - characterization and applications* (Arnold, London, 1995).

[11] M.M. Dubinin. Generalization of the theory of volume filling of micropores to nonhomogeneous microporous structures, *Carbon* **23**(4), 373, 1985.

[12] E.W. Washburn. Note on a Method of Determining the Distribution of Pore Sizes in a Porous Material, *Proceedings of the National Academy of Sciences USA* **7**(4), 115-116, 1921.

[13] C.A. Leon, J.M. Solar, V. Calemma, and L.R. Radovic. Evidence for the protonation of basal plane sites on carbon, *Carbon* **30**(5), 797, 1992.

[14] J.S. Noh and J.A. Schwarz. Estimation of the point of zero charge of simple oxides by mass titration, *Journal of Colloid and Interface Science* **130**(1), 157, 1989.

[15] J.E. Benson and M. Boudart. Hydrogen-oxygen titration method for the measurement of supported platinum surface areas, *Journal of Catalysis* **4**(6), 704, 1965.

[16] G.R. Wilson and W.K. Hall. Studies of the hydrogen held by solids: XVIII. Hydrogen and oxygen chemisorption on alumina- and zeolite-supported platinum, *Journal of Catalysis* **17**(2), 190, 1970.

[17] C. Moreno-Castilla, M.A. Salas-Peregrín, and F.J. López-Garzón. Hydrogenation of carbon oxides by Ru/activated carbon catalysts obtained from $Ru_3(CO)_{12}$: effect of pretreatment on their dispersion, composition and activity, *Journal of Molecular Catalysis A: Chemical* **95**(3), 223, 1995.

[18] F. Rodríguez-Reinoso, J. de Dios López-González, C. Moreno-Castilla, A. Guerrero-Ruiz, and I. Rodríguez-Ramos. Porous carbon as support for iron and ruthenium catalysts, *Fuel* **63**(8), 1089, 1984.

[19] H. Kubicka. The specific activity of technetium, rhenium, ruthenium, platinum, and palladium in catalytic reactions of benzene with hydrogen, *Journal of Catalysis* **12**(3), 223, 1968.

[20] P. Reyes, M.C. Aguirre, G. Pecchi, and J.L.G. Fierro. Crotonaldehyde hydrogenation on Ir supported catalysts, *Journal of Molecular Catalysis A: Chemical* **164**(1-2), 245, 2000.

[21] N.G. Keats, G. Curthoys, and A.K. Ghosh. Temperature-programmed desorption of ammonia and n-butylamine on mordenites, *Journal of Catalysis* **96**(1), 288, 1985.

[22] D.M. Araújo Melo, J.A.C. Ruiz, M.A.F. Melo, E.V. Sobrinho, and A.E. Martinelli. Preparation and characterization of lanthanum palygorskite clays as acid catalysts, *Journal of Alloys and Compounds* **344**(1–2), 352, 2002.

[23] D.M.A. Melo, J.A.C. Ruiz, E.V. Sobrinho, M.A.F. Melo, A.E. Martinelli, and L.B. Zinner. Determination of relative acid strength of La/paligorskyte by n-butylamine, *Journal of Solid State Chemistry* **171**(1–2), 217, 2015.

Capítulo III

FITTING THE EXPERIMENTAL CONDITIONS AND CHARACTERISTICS OF Pt/C CATALYSTS FOR THE SELECTIVE HYDROGENATION OF CITRAL

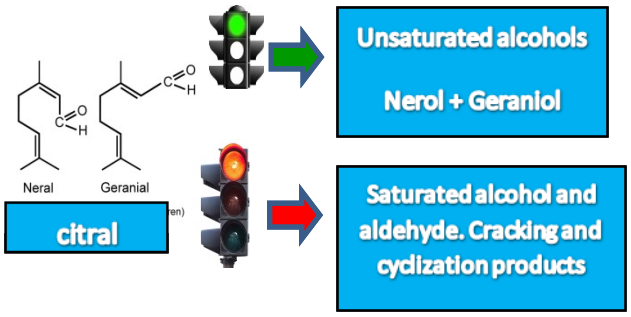

FITTING THE EXPERIMENTAL CONDITIONS AND CHARACTERISTICS OF Pt/C CATALYSTS FOR THE SELECTIVE HYDROGENATION OF CITRAL

Manuscript submitted to Catalysis Science & Technology

Highlights

- C/Pt catalysts for citral hydrogenation are developed.
- The influence of experimental conditions: P_{H_2}, T^a and stirring was studied.
- Mesoporosity of supports and high temperatures favours secondary reaction.
- The optimum Pt-particle size detected was around 8 nm
- Theoretical models reveal the absence of diffusional restrictions for citral.
- Cracking reactions are mainly observed by decarbonylation of previously formed UA.

Abstract

Two different carbon materials, a microporous carbon xerogel shaped by microspheres and a classical micro-mesoporous activated carbon were selected to develop supported Pt-catalysts. Both experimental conditions and catalysts characteristics were optimized. The influence of the support textural characteristics on the catalytic performance, based on the study of the internal and external diffusion limitations, is presented. Pt-dispersion and its distribution, strongly influence the activity and the obtained product distribution. The valuable unsaturated alcohols are favoured for catalysts with Pt-particle size around 8 nm working at high hydrogen pressure and moderate temperatures. Secondary reactions are favoured by increasing temperature and the presence of mesopores in the support.

3.1. INTRODUCTION

The selective hydrogenation of carbonyl groups of α,β-unsaturated aldehydes, and particularly citral, is a challenging process, either from a scientific and economic point of view[1]. The most valuable hydrogenation products are unsaturated alcohols. A survey of consumer products revealed that Geraniol and Nerol (citral derivatives) are present in the large part of cosmetic and domestic products of the European market[2]. Recent studies also revealed that geraniol exhibits pharmacological properties as a antimicrobial and anti-inflammatory agent[2,3]. Furthermore, these molecules are important intermediates in the synthesis of other organic molecules with high added value including vitamins A and E[4].

Citral has recently come to be produced petro-chemically in very large quantities, and the heterogeneously catalyzed selective-hydrogenation is one of the more feasible ways for obtaining its appreciated unsaturated-alcohols, nerol and geraniol[5]. But the selective hydrogenation of citral is not easy, because citral is an α,β-unsaturated aldehyde which possesses three double bonds that can be hydrogenated: an isolated C=C bond and the conjugated C=O and C=C bonds, being more favourable the C=C hydrogenation. Also, other secondary reactions such as cyclization, isomerization or cracking can take place (Figure 3.1).

The main challenge from a catalytic point of view is therefore the design of materials for the selective C=O hydrogenation. There are several important issues that influence on the product selectivity, related either with the catalysts properties as with the operational conditions[6].

Low selectivity values, around 50 % or less, are achieved using Pt or Ru monometallic catalyst supported on activated carbon[6-9]. Better selectivities are obtained using electron-donating supports as graphite or carbon nanotubes. The better selectivity described for monometallic graphite catalysts in the hydrogenation of citral was 65 % at 30% conversion[9]. This improved selectivity would be explained on the basis of an electron transfer from the graphitic support to the metal particles located at the edges of the basal planes. The increased charge density on the metal particles would decrease the probability of adsorption via the C=C bond, and therefore hindering its

hydrogenation[10]. A selectivity range from 30 to 95 was achieved[11-13] when using CNTs as supports. Several factors must be considered when analyzing these differences, mainly related with the CNT purity (presence of the metal used in the CNT synthesis)[11,13], obtaining bimetallic catalysts rather than the proposed monometallic one.

The porosity of the support can also influence the selectivity of the catalytic system. If hydrogenation takes place inside micropores or narrow mesopores, the product reaction is confined into the pore being further hydrogenated to secondary products due to internal diffusion problems[14,15]. The surface chemistry is also very important. The removal of oxygenated groups from the support increases the selectivity to unsaturated alcohols due to defects generated in the structure and/or higher exposure of the π-sites capable of acting as electron donors[16,17].

In this sense, carbon gels could be appropriate supports to develop selective catalysts for this reaction, due to its synthetic procedure it permits to fit the porous texture of the samples with high carbon purity, which can be modified by functionalization[18] or even partially graphitized[19]. In the previous manuscript[20,21], we showed a best performance of these materials in the citral hydrogenation regarding inorganic supports (SiO_2, TiO_2, Al_2O_3) or classical activated carbons when used as Pt-supports.

Experimental conditions (stirring, catalyst/citral ratio, etc) should also be fitted in order to avoid mass transfer limitations (internal or external). It is also well known that the higher the hydrogenation temperature is, the higher is the conversion because the hydrogen transfer from the catalytic site to the C=C or C=O bond is favoured by increasing temperature. However, secondary reactions of isomerization, cyclization and cracking are favoured at higher temperature[22]. The hydrogen pressure is also a very important factor to determine the hydrogen concentration in the employed solvent. Thus citral conversion is enhanced by increasing hydrogen pressure[22,23].

In this manuscript the behavior of Pt supported on an activated carbon or a nanostructured carbon xerogel is discussed on the basis of a deep textural and chemical characterization. Calculations of citral mass transfer limitations were correlated with

properties such as Pt-dispersion and localization in different porosity ranges. The operational conditions (stirring speed, amount of catalyst, initial concentration, pressure and temperature) were optimized in such a basis.

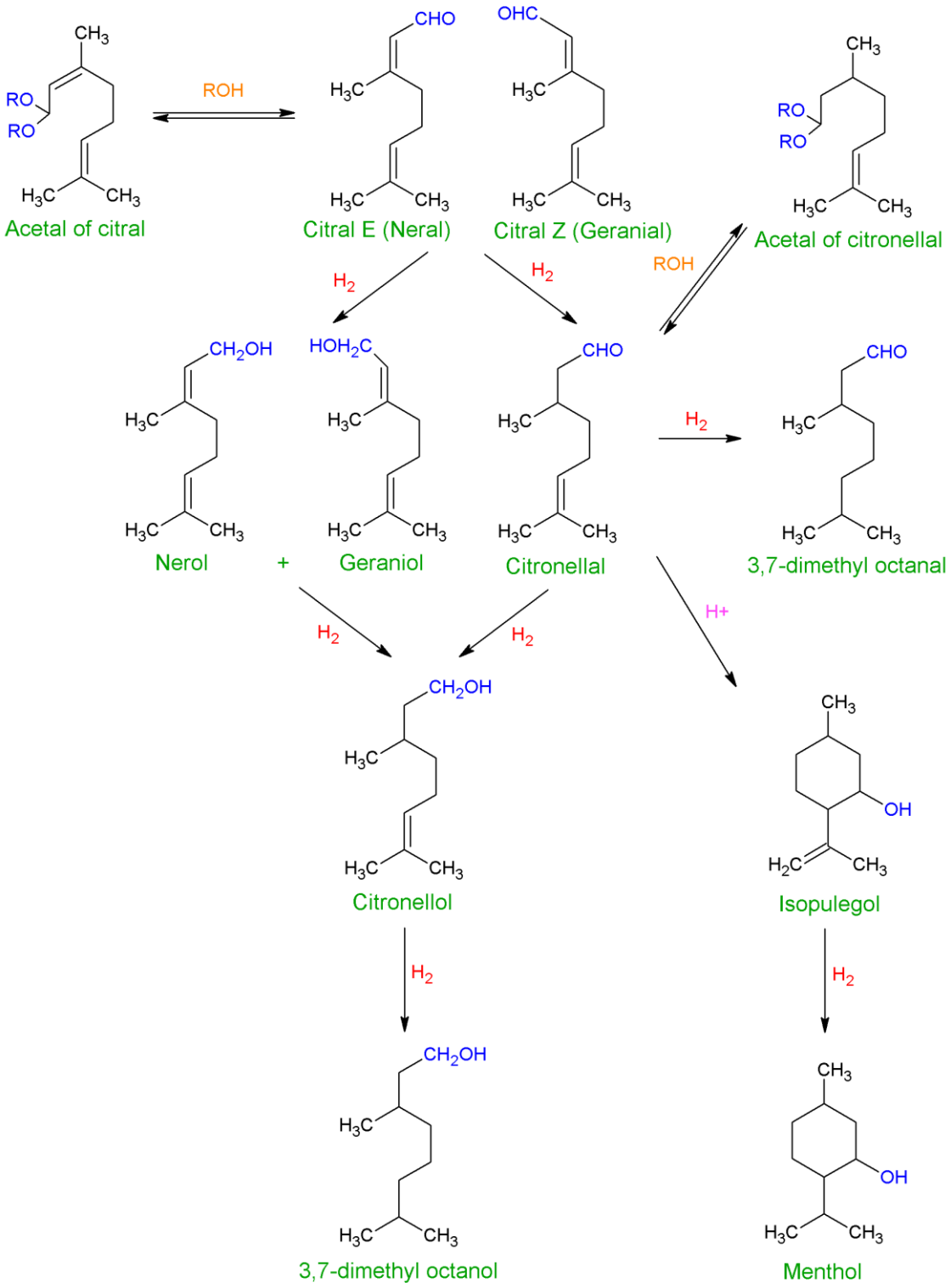

Figure 3.1. Reaction scheme of the citral hydrogenation. Adapted from[24].

3.2. EXPERIMENTAL

3.2.1. Preparation of the catalysts

The carbon xerogel (A8) was prepared by poly-condensation of resorcinol with formaldehyde in aqueous media, using Cs_2CO_3 as polymerization catalyst by modifying a previous synthesis procedure[25]. The molar rations composition of the mixture were R/F = 1/2, R/W = 3/500 and R/C = 800. Accordingly, the proper amounts were added to in a three-neck glass reactor provided with reflux, controlled temperature and stirring. Aqueous solutions of resorcinol and caesium carbonate in deionised water were mechanically stirred at the polymerization temperature (85 ºC) then, formaldehyde solution (Sigma, 37 wt. %) was added drop wise in the flask under agitation (250 rpm). The gel was aged at 85 °C for 24 hours, after which the suspension was filtered; the obtained gel shows an intense orange colour. After the curing cycle, the gel was placed in acetone for three days to exchange water inside the pores changing acetone twice a day in order to reduce porosity collapsing during the subsequent drying process[26]. The gel was dried by microwave using a Saivod MS-287W microwave oven under nitrogen atmosphere in periods of 1 minute at 384 W until constant weight. Pyrolysis of organic gel to obtain the corresponding carbon xerogel was carried out in a 100 cm^3/min N_2 flow and by heating to 900 °C at a 1°C/min heating rate and a 2 h soaking time. Finally, the carbon xerogel obtained was milled and sieved to a diameter smaller than 0.150 mm before impregnation.

Supported catalysts were prepared from $[(Pt(NH_3)_4]Cl_2$ (reagent grade supplied by Aldrich) dissolved in water. A solution of the salt was mixed with the appropriate amount of support and the solvent evaporated at 333 K. The catalysts were then dried at 373 K overnight and kept in a desiccator until use. Metal loading was ~3%; the exact amount of Pt was determined after burning off the support at 873 K in air flow.

Progressively more severe pre-treatment conditions (temperature between 300-400ºC and time between 3 and 12 h in He flow) were used to obtain different Pt-particle sizes in order to establish the influence of this parameter on the catalytic performance. Pt catalyst was also prepared using a commercial activated carbon SorboNorit (S) as support which previously was milled and sieved to a diameter smaller than 0.150 mm to

compare its catalytic performance with the carbon xerogel synthesized in our laboratory.

Catalysts were referred indicating the support followed by the Pt-loading and finally the Pt-particle size determined by H_2-chemisorption. For example, A8Pt3-8 was prepared with 3 % of Pt loading on A8 carbon xerogel as support and pretreated at the appropriate conditions to obtain a Pt particle size of 8 nm.

3.2.2. Characterization of the catalysts

The morphology of the supports was studied by scanning electron microscopy (SEM) using a LEO (Carl Zeiss) GEMINI-1530 microscope. Textural characterization was carried out by N_2 and CO_2 adsorption at −196 ºC and 0 ºC, respectively, with a Quantachrome Autosorb-1 equipment. The BET and Dubinin–Radushkevich equations were applied to determine the apparent surface area (S_{BET}) and the micropore volume (W_0), the average micropore width (L_0) and the microporous surface area (S_{mic}), respectively[27-30]. Furthermore, the BJH method was applied to the N_2 desorption branch in order to calculate the mesopore volume of the samples (V_{meso}) and pore size distributions[31]. The total pore volume was considered as the volume of N_2 adsorbed at $P/P_0 = 0.95$[32].

The chemical characterization of the catalysts was analyzed by elemental analysis, pH_{PZC} and Thermal Programmed Desorption (TPD) curves of carbon monoxide, carbon dioxide, water and hydrogen were registered. The integration of CO and CO_2-TPD profiles enabled us to determine quantitatively the total oxygen content and the different oxygenated groups. Experiments were carried out by heating 150 mg of samples at 50 ºC min^{-1} up to 1000 ºC using He as the carrier gas (60 cm^3 min^{-1}). The analysis of desorbed gases was performed with a Mass Spectrometer model Prisma (Pfeiffer). The calibrations for CO and CO_2 were carried out by analyzing these gases diluted in He (10 vol%) and the calibration for H_2O was performed by means of a TPD of $CuSO_4 \cdot 5H_2O$. The masses (uma) analyzed for these gases were: H_2O – 16, 17, 18; CO – 12, 16, 28; and CO_2, 12, 16, 28, 44. Consecutive TPD experiments were carried out in order to check that samples had not been oxidized by He impurities and the reproducibility of the results.

The pH_{PZC} (point of zero charge) of samples was determined according to the method proposed by Leon et al.[33] . For that, 250 mg of each sample were suspended on 4 mL of previously degasified distilled water. Suspensions were stirred and thermostated at 25 ºC measuring the pH periodically until the reading was constant. The final pH obtained in this way was considered as the pH_{PZC} for each sample.

Pt dispersion (D) and average particle size (d) were obtained by H_2-chemisorption and high-resolution transmission electron microscopy (HRTEM). The H_2-chemisorption isotherms were measured at 25 ºC. The Pt dispersion is obtained[34,35] from the amount of H_2-chemisorbed assuming a stoichiometric ratio H_2:Pt = 1:2 (dissociative chemisorption) and the average particle size was calculated as $d_{Pt}(H_2)$ = 1.08/D (nm). HRTEM experiments were carried out using a Phillips CM-20 microscope equipped with an EDAX microanalysis system and microphotograph analyzed by the appropriate software.

The chemical characterization of the catalysts was further analyzed by X-ray photoelectron spectroscopy (XPS). The spectra were obtained on a Kratos Axis Ultra-DLD X-ray photoelectron spectrometer equipped with a hemispherical electron analyzer connected to a detector DLD (delay-line detector).

3.2.3. Catalytic performance

The citral hydrogenation was carried out in 100 ml heptane solution at a constant hydrogen pressure of 8.3 bar and 90 ºC using a Parr reactor model 5500. The experimental conditions, being citral concentration, catalyst weight and agitation speed, were previously optimized in order to avoid mass transfer limitations and fixed in 0.05 M, 500 mg and 1500 rpm, respectively. A small volume of a sample (1 mL) was periodically withdrawn and analyzed by chromatography using a Bruker 430-GC equipped with a FID detector and a Varian GC Capillary Column CP7485 (25m x 0.32 mm x 0.45 μm). Both citral and any possible product were previously calibrated.

To analyze the influence of pressure and temperature in the catalytic system, the samples were fit in 1.1, 2.1 and 8.3 bar; and 90 and 110 ºC, respectively using SPt3-9 as catalyst.

3.3. RESULTS AND DISCUSSION

3.3.1. Textural and chemical properties

The textural characteristics of both supports are summarized in Table 3.1. Clearly, the commercial activated carbon (S) has a more developed porosity than carbon xerogel (A8). Thus higher micropore volume W_0 (either determined from N_2 or CO_2 adsorption isotherms) as mesopore volume (V_{meso}) were determined, which leads also to higher surface area values. The different porosity of A8 and S is clearly pointed out by the shape of their corresponding N_2-adsorption isotherms (Figure 3.2), being type I for A8, typical of microporous solids, and type IV, with an important hysteresis loop, characteristic of mesoporous solids. The N_2-isotherm also shows a very heterogeneous pore size distribution for S, as denoted by the large neck of the isotherms and the slope at relative pressures higher than 0.1, while A8 presents a closed neck and a flat plateau, indicating a more homogeneous microporosity and a practically null mesopore volume, as determined by BJH (Table 3.1).

Table 3.1. Textural characterization of carbon supports and their derivative catalysts.

Sample	S_{BET}	$W_0(N_2)$	$W_0(CO_2)$	L_0 (N_2)	L_0 (CO_2)	V_{meso}	L_{meso}	$S_{mic}(CO_2)$	$V_{0.95}$
	$m^2 \cdot g^{-1}$	$cm^3 \cdot g^{-1}$	$cm^3 \cdot g^{-1}$	nm	nm	$cm^3 \cdot g^{-1}$	nm	$m^2 \cdot g^{-1}$	$cm^3 \cdot g^{-1}$
S	1284	0.532	0.388	1.57	0.87	0.123	2.8	888	0.656
SPt3-9	535	0.224	0.114	1.69	1.28	0.080	2.8	179	0.286
A8	614	0.245	0.285	0.78	0.60	0.000	-	952	0.305
A8Pt3-8	531	0.210	0.278	0.62	0.58	0.000	-	960	0.219

It is well known that the CO_2 adsorption provides complementary information about the narrow microporosity, corresponding to micropores with a diameter lower than 0.7 nm, while the total microporosity is obtained from N_2 isotherm only in absence of diffusion restrictions[36]. The total pore volume was considered[32] as the volume of liquid N_2 adsorbed at $P/P_0 = 0.95$ determined from the N_2-adsorption isotherms ($V_{0.95}$). A8 shows $W_0(N_2) < W_0(CO_2)$ and $S_{mic} > S_{BET}$, denoting diffusional restrictions as consequence of a narrow porosity, as is also shown by the smaller L_0 values (Table 3.1). S shows the opposite trend, S presents $W_0(N_2) > W_0(CO_2)$ and $S_{mic} < S_{BET}$ denoting no diffusional restriction and a wide microporosity.

Textural characteristics of derivative catalysts with similar Pt-particle size were also included in Table 3.1. It is observed how the formation of Pt-nanoparticles partially blocks the porosity of the support, decreasing both pore volume and surface areas values. Nevertheless, the blockage of porosity seems to be deeper in the case of sample S. The formation of Pt-nanoparticles with a diameter of 8 nm is obviously impossible inside the narrower microporosity. Thus, in the case of A8, these nanoparticles should be formed exclusively on the external surface, and only a small decrease of L_0 and W_0 values are detected. However, in the case of sample S, the mesopore volume and the large size of micropores (see L_0 values) can stimulate the formation of Pt-nanoparticles inside these pores, as denoted by the significant decrease of V_{meso} and W_0, moreover, the increasing of the L_0 values denotes the preferential blockage of the narrowest microporosity. This means that despite the average Pt-particle size can be similar in both cases, the Pt-distribution (localization) is clearly different.

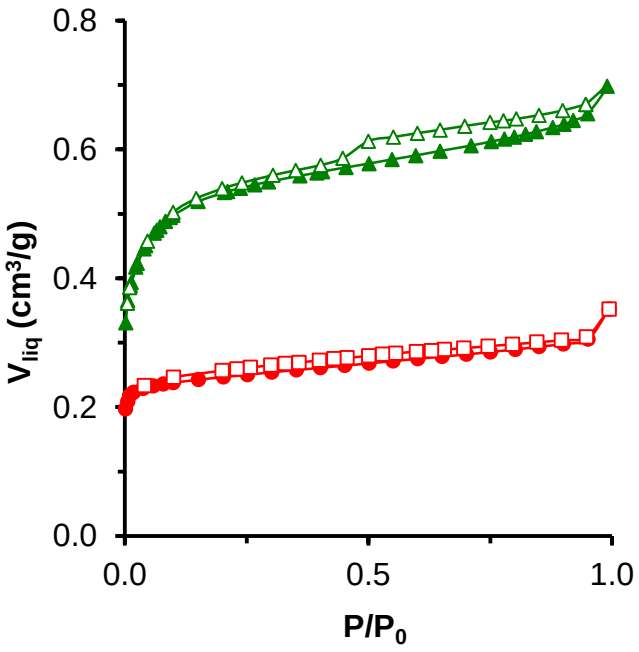

Figure 3.2. N_2-isotherm of S (▲) and A8 (■) supports; closed symbol adsorption and open symbol desorption branch.

The chemical characteristics of the supports are determined by their oxygen content and the oxygenated surface group (OSG) nature, thus elemental analysis, TPD and pH_{PZC} measurements were carried out and the results are collected in Table 3.2. The

oxygen content is also clearly smaller in the case of carbon xerogel, however, this difference does not influences strongly the pH_{PZC} values, which only varies from 9.4 to 10.9 being therefore both supports, basic supports. Some oxygenated surface groups (OSG) are acidic (carboxylic, lactones, anhydrides, phenol) while other such as chromene or pyrone groups are classified as basic centers[37]. The high pH_{PZC} of sample S and the preferential CO-desorption regarding the CO_2-desorption during TPD-experiments (Table 3.2) denote that in this sample the OSG present a basic character.

Table 3.2. Chemical characteristics of carbon supports.

Sample	CO	CO_2	O_2	CO/CO_2	pH_{PZC}	Elemental analysis (wt. %)			
	($\mu mol \cdot g^{-1}$)		%			C	O	H	N
S	1080	447	9.8	2.4	10.9	89.7	9.8	0.3	0.2
A8	303	81	0.8	3.7	9.4	95.1	4.3	0.6	0

The Pt-dispersion and chemical nature was determined by TEM, DRX, H_2-chemisorption and XPS, as described in the experimental section. These results are collected in Table 3.3. It is worth mentioning that although it was expected that Pt-dispersion was favoured by mesoporosity of the S support regarding the microporous A8[18], the Pt-particle size was around 8 ± 0.5 nm when pretreated in the selected conditions (400 ºC in He flow for 6 h), showing that the porosity of the samples is high enough to adequately disperse the Pt-nanoparticles, as shown by representative TEM micrographs (Figure 3.3), in both cases, Pt-particles between 3-6 nm are preferentially formed, although some big particles (up to 40 nm in diameter) were also detected. The catalyst A8Pt3 was pretreated in different experimental conditions to obtain a Pt-particle size between 3 – 10 nm (according to the H_2-chemisorption results) in order to optimize this parameter for citral hydrogenation. XPS results (Table 3.3) show a decrease in $\%Pt_{xps}/\%Pt_{Tot}$ ratio as a consequence of increasing the particle size. However, when comparing catalysts with a similar dispersion (A8Pt3-8 and SPt3-9), $\%Pt_{xps}/\%Pt_{Tot}$ is lower in the second one, which confirms the presence of Pt-nanoparticles inside the pores (not detected by XPS).

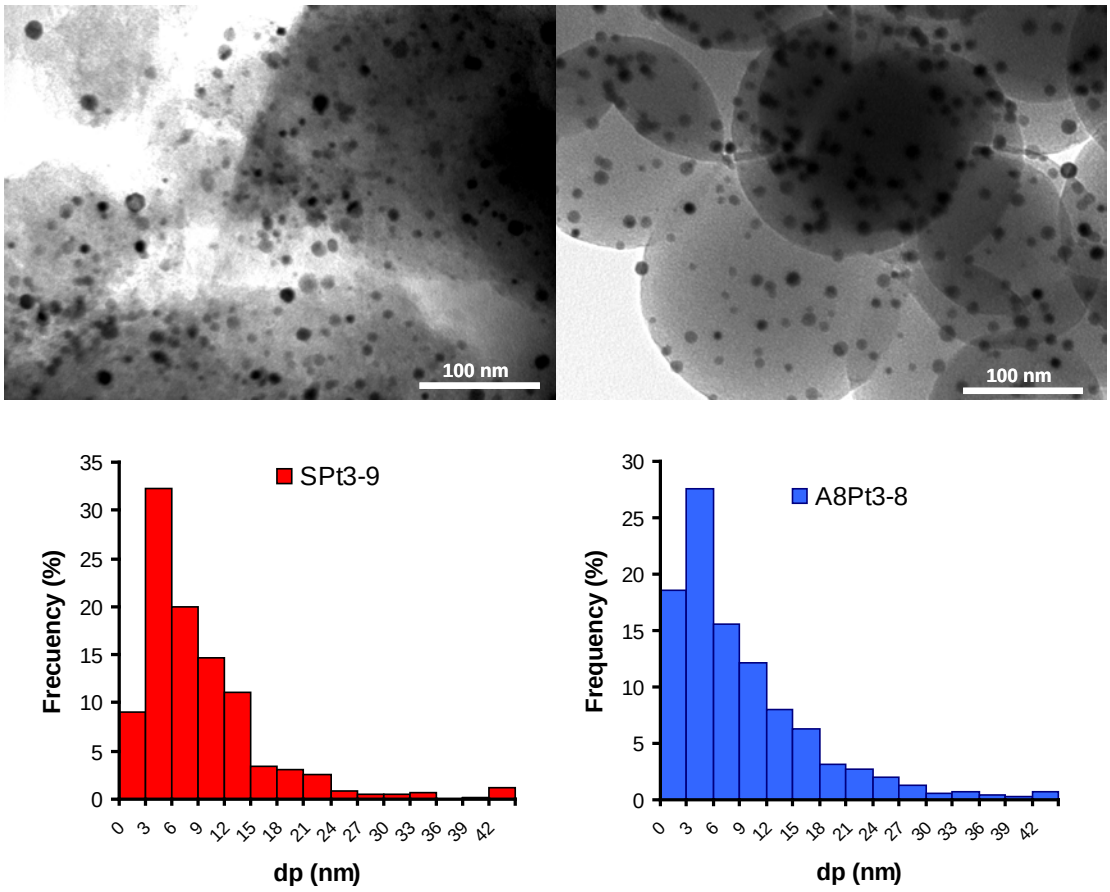

Figure 3.3. Representative HRTEM microphotographs of pretreated catalysts and their corresponding Pt-particle size histograms. Left: SPt3-9 and right: A8Pt3-8.

Table 3.3. Pt-particle size obtained by H_2-chemisorption ($\bar{d}_{H_2}$) or TEM ($\bar{d}_{TEM}$) and Pt-content determined by XPS.

Catalyst	Pre-treatment in He flow	$\bar{d}_{H_2}$ (nm)	$\bar{d}_{TEM}$ (nm)	Pt_{xps} (wt.%)	Pt_{xps}/Pt_{Tot}
A8Pt3-3	350ºC, 6 h	2.9	3.8	6.1	2.02
A8Pt3-5	350 ºC, 12 h	4.7	7.2	5.7	1.97
A8Pt3-8	400 ºC, 6 h	7.9	9.3	4.4	1.50
A8Pt3-10	400 ºC, 12 h	10.0	12.6	4.3	1.42
SPt3-9	400 ºC, 6 h	8.5	9.3	4.1	1.36

The experimental conditions of the reaction (stirring speed, temperature, P_{H2} and Pt/citral ratio) were optimized using the SPt3-9, because the presence of Pt-nanoparticles inside the porosity can favour certain mass transfer restrictions.

Additionally, as commented in the introduction, it is well known that citral hydrogenation is significantly influenced by factors such as the porosity and surface chemistry of supports or Pt-particle size[38,39] and thus, we have also studied the catalytic performance of A8Pt3 as a function of these variables. All results are shown below.

3.3.2. Evaluation of the external mass transfer limitations

The first role of agitation is to keep the catalyst particles uniformly dispersed in the reaction medium and facilitate the gas to liquid mass transfer. Moreover, an efficient stirring is needed to avoid external mass and heat transfer limitations from the liquid phase to the external surface of the solid catalyst particles.

A perfectly mixed reactor is gradient-less at the reactor scale, i.e., a global uniformity of concentrations and temperature throughout the reaction volume is realized. Thus in a perfectly mixed reactor there are no intra-reactor gradients. A simple procedure to assess the perfect mixing at the reactor scale is the agitation test. The aim of the test is to evaluate the minimum stirring rate needed to avoid segregation of both fluid and solid catalyst and to obtain perfect mixing[40]. So the conversion is measured while increasing the stirring rate and keeping constant any other variable. Perfect mixing is obtained when the conversion is independent on any further increasing in stirring speed. The agitation test is also useful to check the presence of interphase gradients. So in the case of gas-solid and liquid-solid systems, an operating regime practically free form interphase limitations is the one in which the reactant conversion does not vary with further increase in the stirring speed.

The case of three-phase systems is more complicated. In fact the overall reaction involves transport phenomena acting at both gas-liquid and liquid-solid interfaces. The basic approach to eliminate transport limitations is the same as in a two-phase operation, i.e., to provide effective stirring[40]. However, as stirring affects gas-liquid transport more than liquid-solid transport[41] the agitation test could be inadequate to evidence liquid-solid transport limitations. In order to evaluate which transport limitation is determining, an additional test can be performed by varying the amount of catalyst.

Therefore the stirring speed used was 750 and 1500 rpm using SPt3-9 as catalyst. Also two different catalyst weights were used. Results are shown in Figure 3.4 showing no difference between both stirring speeds regardless of catalyst weight, and therefore no external mass diffusion has been observed at stirring speed above 750 rpm due to conversion and even selectivity values (S_{UA}) are constant regardless of the stirring speed.

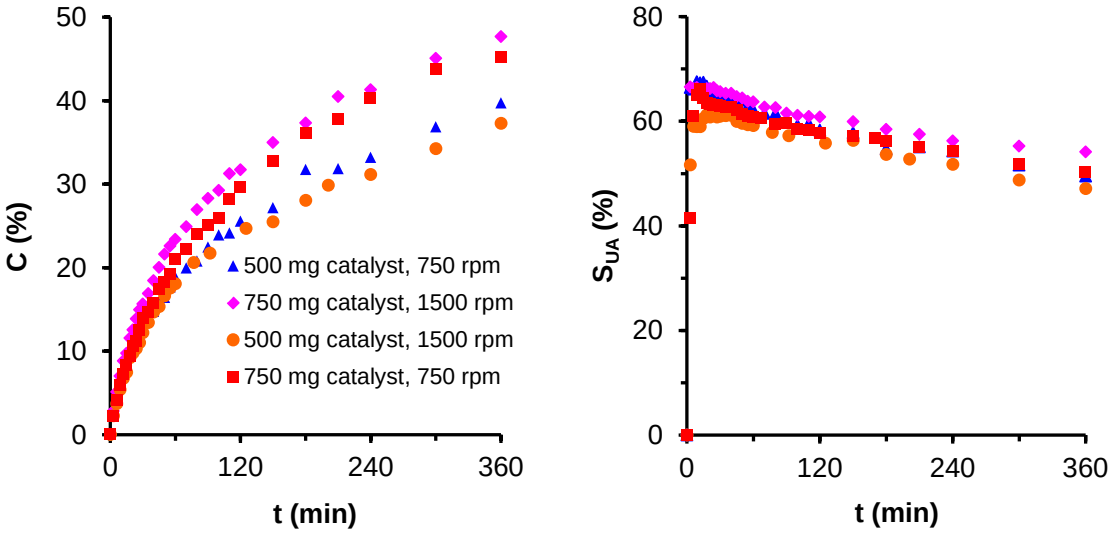

Figure 3.4. Influence of stirring speed on the catalytic performance of SPt3-9 catalyst.

To evaluate the extent of mass-transfer limitation related to diffusion from the liquid to the solid phase, the method introduced by Carberry has been adopted. The Carberry number, Ca, represents the extent of external mass-transfer limitation and ranges from zero to unity. A Carberry number smaller than 0.05 indicates that diffusion retardation by external mass transfer may be neglected[42].

$$Ca = \frac{r'^{0}_{Citral}}{k_{LS} \cdot \frac{6 \cdot w}{d_p \cdot \rho_p} \cdot C^{0}_{Citral}} < 0.05 \qquad (1)$$

r'^{0}_{Citral}= initial citral conversion rate (mol/s)

d_p= diameter of the largest catalyst particle (m)

k_{LS}= liquid-solid mass-transfer coefficient (m/s)

w= catalyst weight (Kg)

ρ_p= catalyst particle density (Kg/m^3)

C^0_{Citral}= initial citral concentration (mol/m^3)

The solid–liquid mass transfer coefficient required in Eq. (1) is calculated using the following correlation for batch stirred tank reactor[43,44]:

$$Sh = 2.0 + 0.6 \cdot (Re_p)^{0.5} (Sc)^{0.33} \quad (2)$$

Where $Sh = \frac{k_{LS} d_p}{D_{AB}}$, $Sc = \frac{\mu_L}{\rho_L \cdot D_{AB}}$ and $Re_p = \frac{\rho_L \cdot v_p \cdot d_p}{\mu_L}$

ρ_L= solvent density (Kg/m^3)

μ_L= solvent viscosity (Pa/s)

v_p= terminal velocity of the particles (m/s)

Carberry numbers for all catalysts are given in Table 3.4. The Carberry numbers are smaller than 0.05, indicating the absence of external liquid-solid diffusion limitations in all experiments.

The effect of the catalyst weight was studied using 300, 500 and 750 mg of SPt3-9 catalyst, while keeping constant the other experimental conditions (0.05 M, 1500 rpm, 90 ºC, 8.3 bar). It was found that conversion increased with the catalyst weight (Figure 3.5). This is because of the increase in number of active sites available for the substrate molecule. However, this increase in conversion is proportional to the increase of catalyst weight (number of active site available) when the catalysts weight increases from 300 mg to 500 mg but not increasing from 500 mg to 750 mg. Similarly, the increase of catalyst weight from 300 to 500 mg also favours the S_{UA} values, mainly with increasing conversion. However similar S_{UA} values were observed with 500 and 750 mg in all the conversion range. Clearly at high citral/catalyst ratio, active sites yielding UA are more easily deactivated.

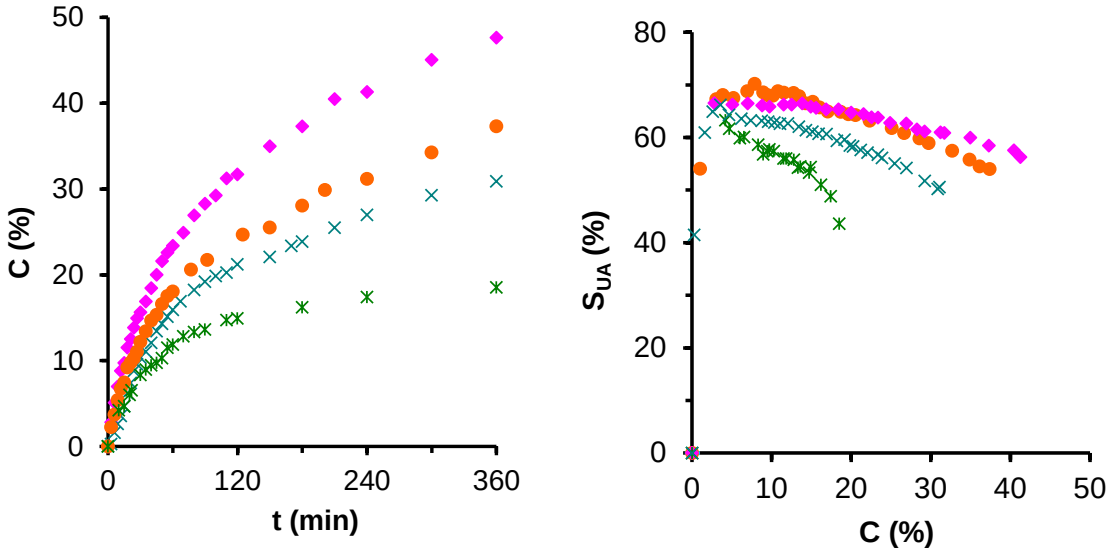

Figure 3.5. Influence of catalyst weight on the catalytic performance of SPt3-9 catalyst. 300 mg 0.05 M (✳), 500 mg 0.05 M (●), 750 mg, 0.05 M (◆) and 750 mg 0.1M (×). 1500 rpm, 8.3 Bar, 90 ºC

This fact indicates that using 750 mg there is an excess of catalyst. However, maintaining the catalysts weight but increasing the citral concentration from 0.05 to 0.1 M conversion values decreases in a similar proportion. This means that the number of active sites working at 0.05 M and 0.1 M is the same, i.e. citral is not the limiting reactant at 0.05 M. Because Carberry numbers indicate the absence of restrictions for citral molecules, the results described at different catalyst weight can be due to the low solubility of hydrogen in heptane. Thus, the hydrogen availability seems to be low and not all active centers present could work.

The initial reaction rate for citral consumption (r^0_{Citral}) was also calculated (Figure 3.6) for these experiments. Results are collected in Table 3.4 and presents the same evolution previously described for the conversion and selectivity values, i.e. strongly increases from 300 to 500 mg while only a small increase is observed when use 750 mg catalysts. It is also worth mentioning that A8Pt3-8 catalysts shows a smaller r^0_{Citral} values than SPt3-9 in the same experimental conditions, in spite that this sample presents Pt-particles only on the most external catalyst surface, avoiding in such a way any diffusion process of reactant or products. This fact will be deeply analyzed bellow.

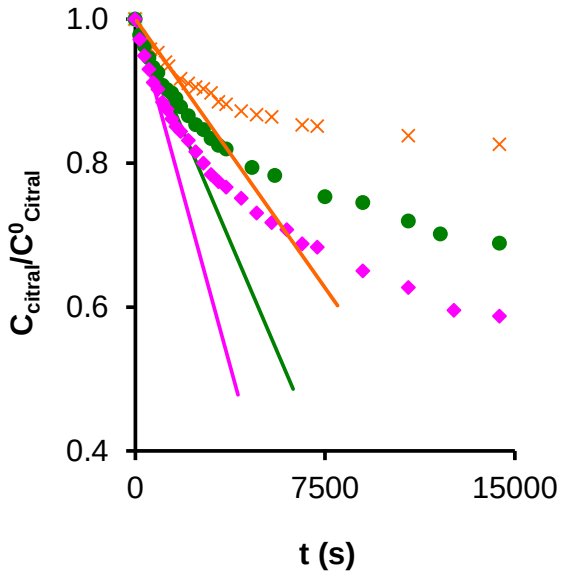

Figure 3.6. Calculation of initial rates (slope=-$r^0_{Citral}/C^0_{Citral}$) using SPt3-9 catalyst. (×) 300 mg, (●) 500 mg, (◆) 750 mg at 1500 rpm.

3.3.3. Internal mass transfer limitations

The absence of internal mass transfer limitations was confirmed by the criterion of Weisz-Prater[45-47].

$$\Phi = \eta\phi^2 = \frac{0.28 \cdot \rho_p \cdot r^0_{Citral} \cdot R_p^2}{D_{ef} \cdot C^0_{Citral}} \leq 1 \qquad (3)$$

η= effectiveness factor for catalyst particle

ϕ=Thiele modulus

Φ=dimensionless Weisz-Prater modulus

ρ_p= catalyst particle density (Kg/m^3)

r^0_{Citral}= initial Citral conversion rate (mol/s·Kg) (Figure 3.6)

R_p= radius of the largest catalyst particle (m)

D_{ef}= effective diffusion coefficient (m^2/s)

C^0_{Citral}= initial Citral concentration (mol/m^3)

The effective diffusivity of citral and Hydrogen were estimated using Eq. (4)[48]:

$$D_{ef} = \frac{D_{AB} \cdot \varepsilon_p}{\tau_p} \quad (4)$$

D_{AB}= molecular diffusivity of citral in Heptane (m^2/s)., ε_p= void fraction, τ= tortuosity factor of the carbon (3 for activated carbon[49]).

The void fraction was calculated using data obtained from mercury porosimetry as:

$$\varepsilon_p = 1 - \frac{\rho_{bulk}}{\rho_p} \quad (5)$$

ρ_{bulk} =bulk density, ρ_p= particle density and D_{AB} was calculated by using the Wilke–Chang equation (Eq. (6))[50]

$$D_{AB} = \frac{7.4 \cdot 10^{-8} \cdot (\Theta \cdot M_B)^{0.5} \cdot T}{\mu_{BV} \cdot V_A} \cdot 10^{-4} \quad (6)$$

where D_{AB} is m^2/s, Θ is the association parameter of heptane and has a value of 1, M_B is the molecular weight of heptane (100.2 g/mol), T is the temperature (363 K), μ_{BV} is viscosity of heptane (0.376 cp), and V_A is the molar volume of the solute at its boiling temperature (210 cm^3/mol). The value of VA was calculated using Schroeder's method[51]:

$$V_A = 7(N_C + N_H + N_O + N_N + N_{DB} + 2N_{TB}) + 31.5N_{Br} + 24.5N_{Cl} + 10.5N_F + 38.5N_I + 21N_S - 7^*$$

where N_i is the number of element i and subscripts DB and TB stand for double and triple bonds and the last value* is counted once if the compound has one or more rings.

In Table 3.4 the parameters used for the calculations are given, as well as the Weisz-Prater modulus for all experiments. Weisz–Prater numbers for all catalysts are

given in Table 3.4. The Weisz–Prater numbers are smaller than 1, indicating the absence of internal diffusion limitations in all experiments. Then, no diffusional limitations seem to be present under typical reaction conditions and the reaction takes place under kinetic control.

Table 3.4. Weisz–Prater (Φ) and Carberry numbers (Ca) for citral in the reaction performed under standard conditions (T = 363 K, C^0_{Citral}= 50 mol/m^3, 1500 rpm and P=8.3 Bar) and the parameters used for the calculations.

Parameter	SPt3-9 300 mg	SPt3-9 500 mg	SPt3-9 750 mg	A8Pt3-8 500 mg
$\rho_{p,}$ Kg/m^3	850	850	850	1475.6
$r^0_{Citral,}$ mol/(Kg m^3)	$7.7\cdot10^{-4}$	$8.7\cdot10^{-4}$	$8.9\cdot10^{-4}$	$2.2\cdot10^{-4}$
R_p, m	$7.5\cdot10^{-5}$	$7.5\cdot10^{-5}$	$7.5\cdot10^{-5}$	$7.5\cdot10^{-5}$
ε_p	0.69	0.69	0.69	0.59
τ	3	3	3	3
D_{AB}, m^2/s	$2.9\cdot10^{-9}$	$2.9\cdot10^{-9}$	$2.9\cdot10^{-9}$	$2.9\cdot10^{-9}$
D_{ef}, m^2/s	$6.6\cdot10^{-10}$	$6.6\cdot10^{-10}$	$6.6\cdot10^{-10}$	$6.6\cdot10^{-10}$
C^0_{Citral}, mol/m^3	50	50	50	50
Φ	0.031	0.035	0.036	0.018
Ca	0.029	0.034 (0.040)*	0.031 (0.035)*	0.005

*in parenthesis 750 rpm.

3.3.4. Effect of hydrogen pressure

Experiments at different pressures of hydrogen (1.1, 2.1 and 8.3 bar) were then performed maintaining the rest of experimental conditions. The conversion increases with the increase of the pressure (Figure 3.7) due to an increase of the hydrogen solubility in the solvent (heptane) and consequently, its concentration over the active sites. Thus conversion as well as the initial reaction rate (r^0_{Citral}), linearly increases with the hydrogen pressure. These results are in agreement with those observed by different authors[22,23]. However, concerning S_{UA}, only a slight increase in selectivity to unsaturated alcohol was observed by increasing the pressure (Table 3.5). Moreover, this percentages tend to decrease with increasing conversion values (and Figure 3.7b). Thus, there are certain active sites on the catalyst, wherein the hydrogenation of C=O double bond is favoured, which are progressively activated by raising the hydrogen pressure

probably because either in terms of localization on the support or by a greater coordination in the crystal structure, are less accessible or their interactions with H_2 are weaker.

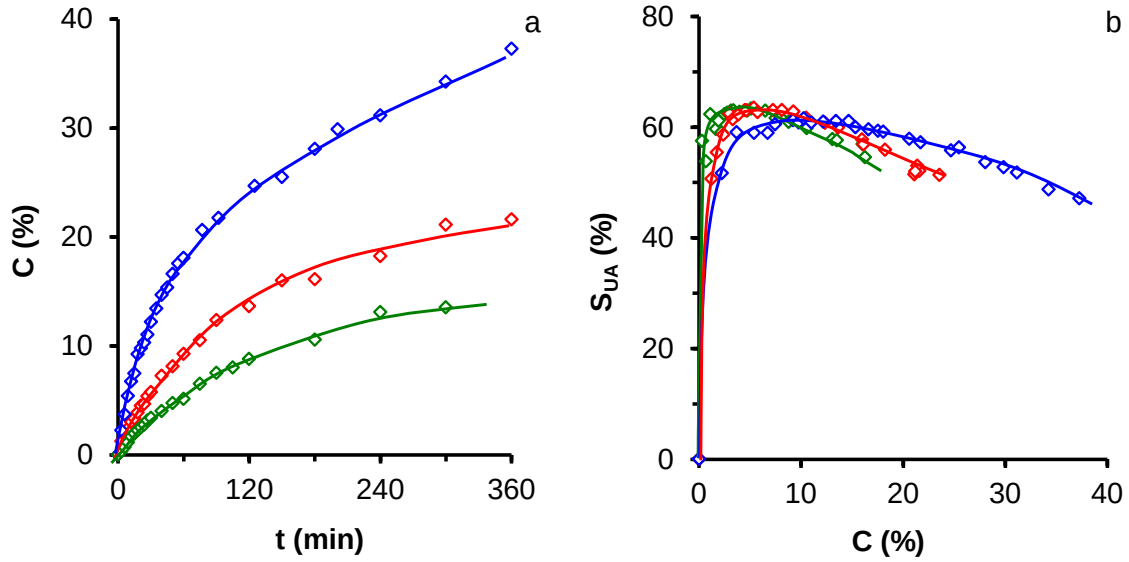

Figure 3.7. Evolution of conversion (a) and S_{UA} (b) at different H_2 pressure using SPt3-9 catalyst. 8.3 bar (△), 2.1 bar (□) and 1.1 bar (○).

Moreover, citral is a racemic mixture of neral and geranial (Figure 3.1). Comparing results at iso-conversion (Table 3.5), it seems that Neral is less reactive than Geranial, therefore appearing after reaction in a larger proportion (not consumed reactant) regarding to the composition of the initial raw citral. However, with increasing P_{H_2}, the amount of geranial increases while the neral one decreases, indicating that both isomers are therefore transformed on different active sites. Therefore, both conversion increase and selectivity increase, can be related with the greater transformation of neral with increasing P_{H_2}, suggesting that UA are formed preferentially from neral. Consequently, the higher the amount of Neral transformed is, the higher is the selectivity to unsaturated alcohol.

3.3.5. Effect of temperature

To check the effect of temperature, citral hydrogenation was developed at 90 ºC and 110 ºC at 8.3 Bar of hydrogen using SPt3-9 as catalyst. The results are shown in Figure 8. As can be observed, a temperature increase of 20 ºC produces an increase of

77 % in conversion (Figure 3.8a). However, this increase in conversion is not accompanied by an increase in selectivity to unsaturated alcohols, which decreases (Figure 3.8b). The product distribution obtained as a function of conversion is shown in Figure 3.8c and d. Figure 3.8c display the evolution of UA (nerol and geraniol) as primary products, and their possible derivative compounds citronellol and 3,7-dimethyl octanol (3-7 DMO). Similarly, Figure 3.8d shows the evolution of citronellal as primary products and their cyclization secondary products, isopulegol and menthol. Other citronellal secondary products (3,7 dimethyl octanal and acetal of citronellal) were not detected.

Table 3.5. Variation of initial reaction rates as function of H_2-pressure. Selectivity and detected products at isoconversion (16 %). Experimental conditions: 8.3 Bar, 0.05 M citral in heptane and 500 mg of SPt3-9. (Gol: geraniol, Nol: nerol, Col: citronellol, Cal: citronellal, 3-7DMO: 3,7-dimethyl octanol, Isop: isopulegol; Ment: menthol).

P	r^0	S_{UA}	Citral E (Geranial)	Citral Z (Neral)	Gol	Nol	Col	Cal	3-7DMO	Isop	Ment
Bar	mol/(l·s)	%	%	%	%	%	%	%	%	%	%
raw	citral		46.47	53.53							
1.1	$1.0\cdot10^{-6}$	56.9	37.10	46.86	6.08	3.05	2.04	3.41	0.85	0.48	0.14
2.1	$1.6\cdot10^{-6}$	57.7	37.63	46.39	6.10	3.42	1.88	3.42	0.84	0.47	0.14
8.3	$4.1\cdot10^{-6}$	59.9	38.47	45.53	6.17	3.43	1.41	3.32	0.84	0.70	0.13

It is observed that the development of secondary reaction, cyclization to menthol and cracking reactions, is favoured at higher temperature, which is also in agreement with previously published results[22,52]. Citronellal decreases by the formation of isopulegol and menthol by cyclization reactions. However, the stronger selectivity decrease is observed for both UA mainly for conversions greater than 15% (Figure 3.8c). Because the yield of their secondary hydrogenation products (citronellol and 3-7 DMO) remain almost constant independently of the temperature used, cracking products detected from these conversion values should come mainly from the breakage (decarbonylation) of nerol and geraniol, which is favoured with increasing temperature[53]. Thus, initially UA are preferentially formed which are thereafter cracked. It is also known that decarbonylation reaction is more probable via decarbonylation of unsaturated alcohols[22,53]. At low temperature (25 ºC) CO slowly

accumulates, poisoning Pt-active sites and eventually lead to a complete loss of activity. At higher reaction temperatures (100 ºC) alcohol decomposition is more rapid, but the CO desorption rate is also significantly enhanced and a pseudo-steady state is readily established which results in minimal inhibition and conventional Arrhenius behaviour.

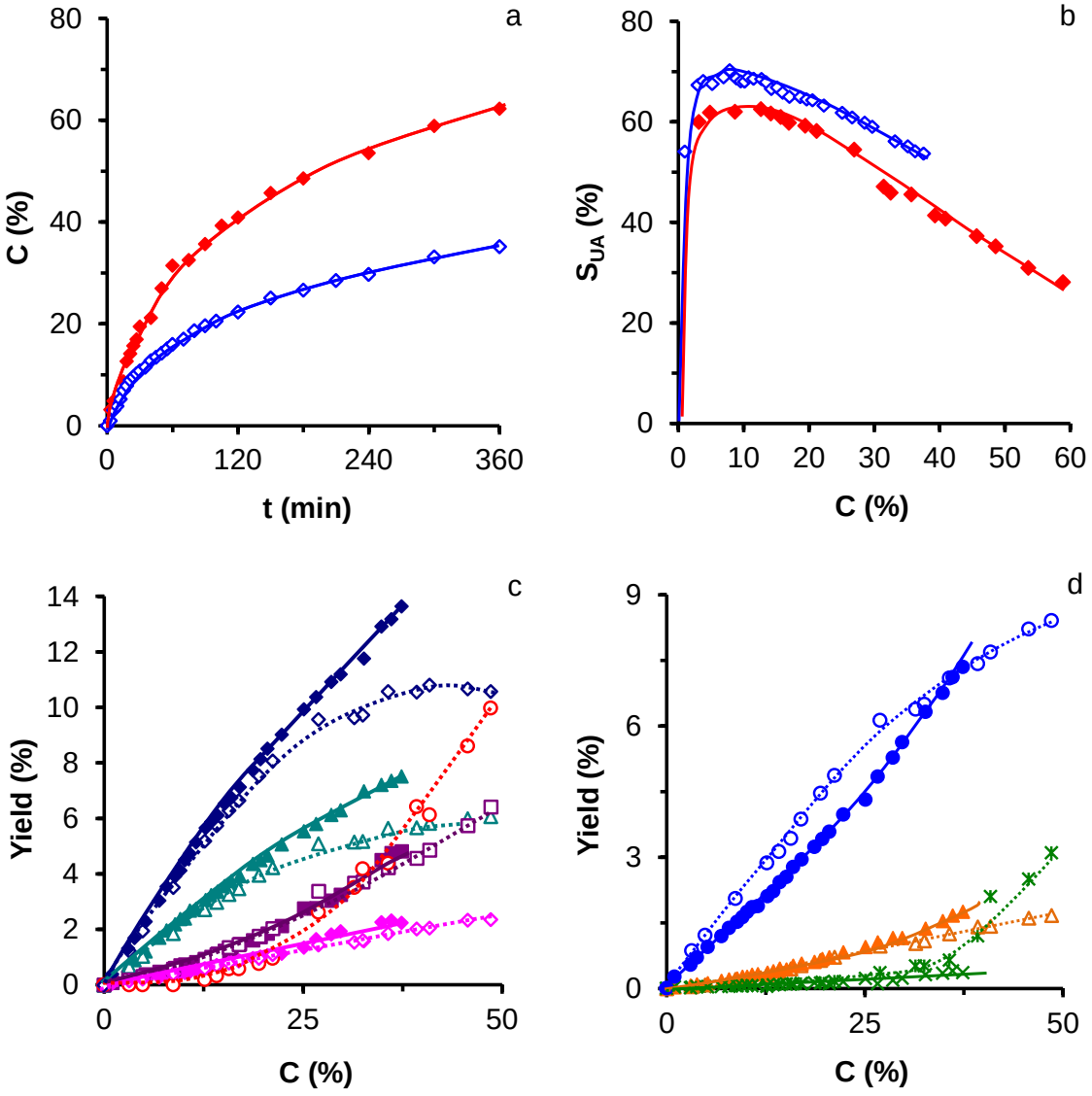

Figure 3.8. Influence of temperature in a) conversion and b) selectivity: 90 ºC (◇) and 110ºC (◆) and c), d) in yield: Open symbol (110ºC) and close symbol (90ºC): geraniol (◆), nerol (▲), citronellol (■), 3.7 DMO (◆), citronellal (●), isopulegol (▲), menthol (x: 90 ºC and ∗:110 ºC) and cracking products (○). SPt3-9 catalyst

3.3.6. Influence of the platinum particle size

One of the key aspects in the catalytic performance of the supported catalysts is the optimization of the particle size of the metallic phase. Usually, a good dispersion and a small particle size are desirable to maximize the exposed metallic phase fraction and so, maximize the number of active centres. However, the selective hydrogenation of α,β-unsaturated aldehydes is structure sensitive. The hindered adsorption of the olefinic bond of the α,β-unsaturated aldehyde by a steric repulsion between the metal surface in large metal particles and the aldehyde molecule was concluded to be responsible for the high selectivity toward C=O group hydrogenation in aldehyde like cinnamaldehyde[54,55].

In order to study the effect of this parameter, the particle size was modified changing the thermal treatment of the A8Pt3 catalyst as described in the experimental section. Thermal treatments and the obtained particle size are shown in Table 3.3. Pt-particle size ranges from 3 to 10 nm. In Figure 3.9 the influence of Pt particle size on the catalytic performance is shown. The selectivity to unsaturated alcohols increases as the particle size increases up to 8 nm and then decrease. The same trend has been obtained for the conversion. The optimal Pt particle size obtained is around 8 nm.

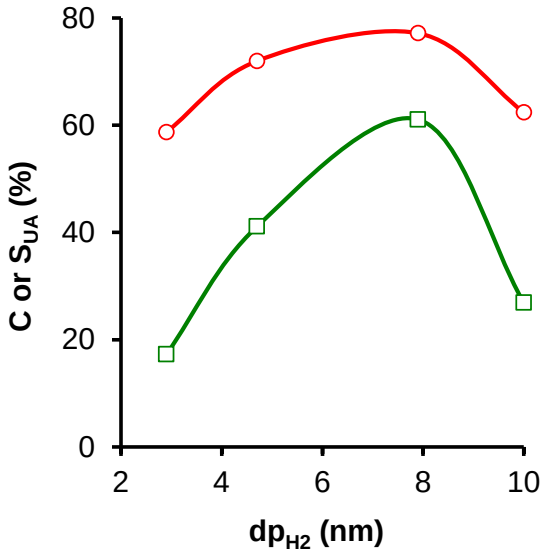

Figure 3.9. Influence of Pt particle size on the catalytic performance using A8Pt3 as catalyst, S_{UA}(○) and C(□). 0.05 M, 500 mg catalyst, 8.3 Bar, 90 ºC and 1500 rpm

Moreover, the increase in selectivity to unsaturated alcohol up to 8 nm was accompanied by an increase of the neral transformed and a decrease of the geranial (Table 3.6 and Figure 3.10), which suggests again that unsaturated alcohols come mainly from neral. Consequently, the higher the amount of neral transformed is, the higher is the selectivity to unsaturated alcohol. These results show the possibility to obtain selectively nerol or geraniol from their corresponding isomers (neral and geranial) by optimizing the Pt-particle size and working at low temperature and high hydrogen pressure.

Table 3.6. Selectivity and amount of detected products at isoconversion (26 %) as a function of particle size. Experimental conditions: 8.3 Bar, 0.05 M citral in heptane and 500 mg of A8Pt3. (Gol: geraniol, Nol: nerol, Col: citronellol, Cal: citronellal, 3-7DMO: 3,7-dimethyl octanol, Isop: isopulegol; Ment: menthol).

d_P	S_{UA}	Citral E (Geranial)	Citral Z (Neral)	Gol	Nol	Col	Cal	3-7 DMO	Isop	Ment
nm	%	%	%	%	%	%	%	%	%	%
raw	citral	46.47	53.53							
3	58.6	34.99	39.01	9.94	5.30	3.59	6.22	0.42	0.32	0.21
5	65.8	36.18	37.82	11.05	6.32	2.89	4.92	0.41	0.30	0.10
8	72.0	37.23	36.77	12.24	6.49	2.54	4.07	0.33	0.22	0.11
10	62.2	35.55	38.45	10.30	5.54	3.47	5.65	0.50	0.32	0.21

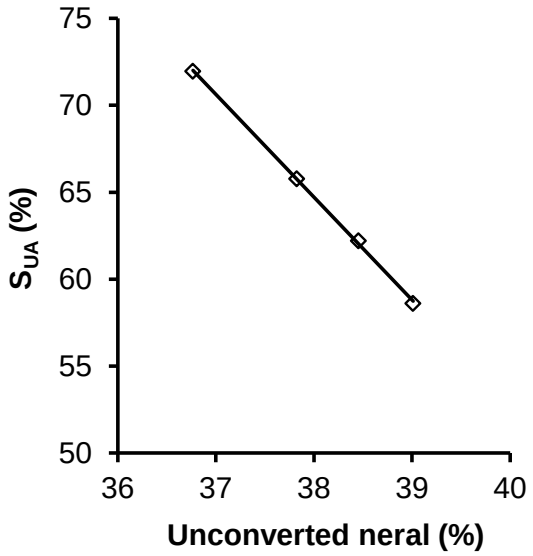

Figure 3.10. Relationship between the amount of neral converted and the S_{UA}. Experimental conditions: 8.3 Bar, 0.05 M citral in heptane and 500 mg of A8Pt3.

3.3.7. Influence of Pt - support

In order to check the effect of porous texture and surface chemistry of supports, the catalytic performance of A8Pt3 and SPt3 are compared using the optimized Pt-particle size and experimental conditions (Figure 3.11). Previously (Table 3.4) it was exposed that the initial reaction rate is high in the case of SPt3-9 catalysts than for A8Pt3-8. This is clearly observed also in Figure 3.11. Thus, the conversion values obtained during the two first hours of reactions are greater in the first case. However, after this time (at around 20 % of citral conversion), reaction rate strongly decrease, which is simultaneously accompanied by a S_{UA} decrease (Figure 3.11 b). On the contrary, after a short induction period of around 30 min, conversion increases more or less lineally during 6 h of reaction when A8Pt3-8 is used. Thus at this time the conversion reached is around 65 % for A8Pt3-8 and 40% for SPt3-9. It is also worth mentioning the different evolution of product distribution in each case (Figures 3.11 c, d). Thus, initially S_{UA} is also very high (at around 60 %) for SPt3-9 remaining below 10 % for A8Pt3-8. However, while S_{UA} tend to decrease with increasing reaction time (conversion values) becoming at around 40% after 6 h of reaction for SPt3-9, the opposite trend is observed for A8Pt3-8, reaching in this case S_{UA} values at around 80 %. After this time therefore, the batch experiments present a UA yield of 16 % for SPt3-9 and 48 % for A8Pt3-8, i.e. at around three times greater in the last case.

The smaller initial reaction rate observed for A8Pt3-8 can be related to the smaller surface area and porosity of A8 support. Thus, the adsorption of citral molecules is initially slower, but is maintained or even increased after the first minutes of reaction. A small amount of reactant and/or products remain permanently adsorbed on the catalyst surface blocking microporosity[20] and changing the catalysts surface from hydrophobic to hydrophilic, which favours also the citral adsorption by the C=O bond and the consequent increase of S_{UA}.

In the case of SPt3-9, conversion becomes finally smaller because a reaction is developed, at less partially, inside the mesopores where the Pt-particles are located. A smaller concentration of hydrogen inside the mesopores can occur, decreasing the activity of these Pt particles inside mesopores regarding those external ones. The selectivity decrease with increasing reaction time is also due to the presence of Pt-

particles inside mesopores, due to the development of secondary reactions faster than the diffusion of primary products from the mesopores. Cyclization reaction of citronellal to menthol and isopulegol and secondary hydrogenation to citronellol, 3,7 dimethyl octanol (DMO) or 3,7 dimethyl octanal (DMA) are favoured inside the mesopores because the residence time in this case is higher.

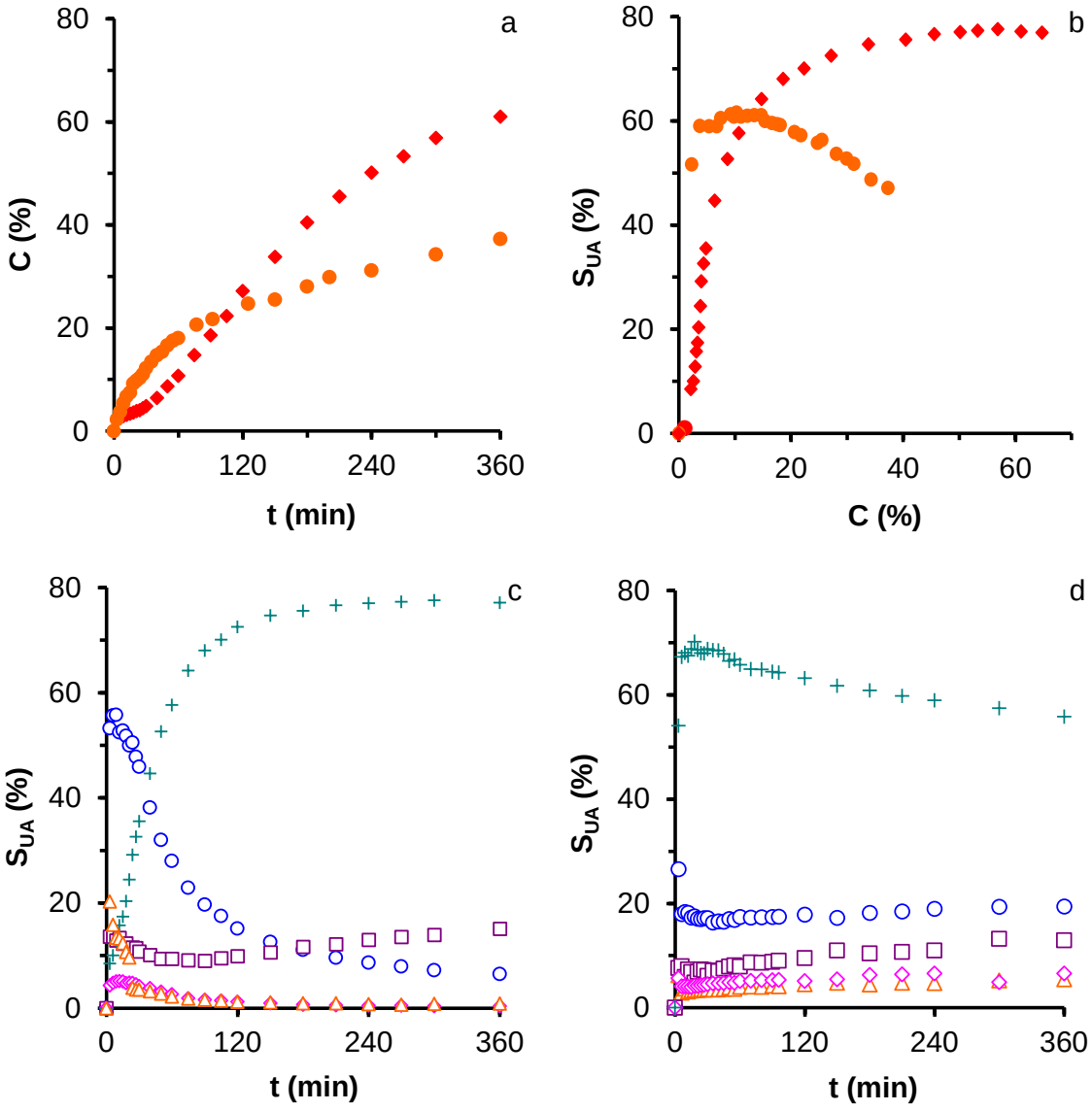

Figure 3.11. Influence of Pt-support on a) conversion b) selectivity for A8Pt3-8(◆) SPt3-9 (●), and products distribution of c) A8Pt3-8 and d) SPt3-9. UA (+), citronellol (□), 3.7 DMO (◇), citronellal (○), isopulegol and menthol (△),

3.4. CONCLUSIONS

The experimental conditions for citral hydrogenation and the characteristics of Pt/C supports were optimized, in such a manner that an unusual very high S_{UA} value (at around 80%) for monometallic Pt-catalysts is achieved in the case of Pt-supported on carbon xerogel.

The use of this microporous carbon support, structured in microspheres, permits to obtain a high and homogeneous distribution of Pt-nanoparticles on their external surface. The optimum Pt-particle size detected was around 8 nm.

In spite of that, the used models revealed the absence of diffusional restrictions for citral, neither internal nor external, when using mesoporous activated carbons, this pore range permits the formation of Pt-nanoparticles inside the pores, working like a pseudo-reactor. The increase of the residence time favours the development of secondary reactions on these active sites.

Similarly, secondary reactions are favoured by increasing temperature. Cracking reactions are mainly observed by decarbonylation of previously formed UA, while citronellal molecules are cycled to isopulegol and/or menthol.

However, increasing the hydrogen pressure both activity and selectivity are favoured, indicating that the progressively activated weaker sites are more selective to the C=O hydrogenation instead the C=C one.

3.5. REFERENCES

[1] F. Delbecq and P. Sautet. Competitive C=C and C=O Adsorption of α,β–Unsaturated Aldehydes on Pt and Pd Surfaces in Relation with the Selectivity of Hydrogenation Reactions: A Theoretical Approach, *Journal of Catalysis* **152**(2), 217, 1995.

[2] W. Chen and A.M. Viljoen. Geraniol: A review of a commercially important fragrance material, *South African Journal of Botany* **76**(4), 643, 2010.

[3] P. Ji, M.S. Si, Y. Podnos, and D.K. Imagawa. Monoterpene geraniol prevents acute allograft rejection, *Transplantation Proceedings* **34**(5), 1418, 2002.

[4] M. Eisenacher, S. Beschnitt, and W. Hölderich. Novel route to a fruitful mixture of terpene fragrances in particular phellandrene starting from natural feedstock geraniol using weak acidic boron based catalyst, *Catalysis Communications* **26**(0), 214, 2012.

[5] H. Surburg and J. Panten, *common fragrance and flavor materials: preparation, properties and uses*, 5th ed. (WILEY-VCH, Weinheim, Germany, 2006).

[6] E. Bailón-García, F.J. Maldonado-Hódar, A.F. Pérez-Cadenas, and F. Carrasco-Marín. Catalysts Supported on Carbon Materials for the Selective Hydrogenation of Citral, *Catalysts* **3**(4), 853, 2013.

[7] S. Galvagno, C. Milone, A. Donate, G. Neri, and R. Pietropaolo. Influence of metal particle size in the hydrogenation of citral over Ru/C, *Catalysis Letters* **18**(4), 349, 1993.

[8] G. Neri, C. Milone, S. Galvagno, A.P.J. Pijpers, and J. Schwank. Characterization of Pt-Sn/carbon hydrogenation catalysts, *Applied Catalysis A: General* **227**(1–2), 105, 2002.

[9] M. Steffan, F. Klasovsky, J. Arras, C. Roth, J. Radnik, H. Hofmeister, and P. Claus. Carbon-carbon double bond versus carbonyl group hydrogenation: Controlling the intramolecular selectivity with polyaniline-supported platinum catalysts, *Advanced Synthesis and Catalysis* **350**(9), 1337, 2008.

[10] A. Giroir-Fendler, D. Richard, and P. Gallezot. Selectivity in cinnamaldehyde hydrogenation of group-VIII metals supported on graphite and carbon, *Studies in Surface Science and Catalysis* **41**(C), 171, 1988.

[11] E. Asedegbega-Nieto, A. Guerrero-Ruiz, and I. Rodríguez-Ramos. Modification of the stereo selectivity in the citral hydrogenation by application of carbon nanotubes as support of the Pt particles, *Carbon* **44**(4), 804, 2006.

[12] F. Qin, W. Shen, C.C. Wang, and H.L. Xu. Selective hydrogenation of citral over a novel platinum/MWNTs nanocomposites, *Catalysis Communications* **9**(11-12), 2095, 2008.

[13] P.D. Zgolicz, J.P. Stassi, M.J. Yañez, O.A. Scelza, and S.R. de Miguel. Influence of the support and the preparation methods on the performance in citral hydrogenation of Pt-based catalysts supported on carbon nanotubes, *Journal of Catalysis* **290**(0), 37, 2012.

[14] J. Zhu, M. Lu, M. Li, J. Zhu, and Y. Shan. Selective hydrogenation of citral over a carbon-titania composite supported palladium catalyst, *Chinese Journal of Chemistry* **29**(4), 655, 2011.

[15] J. Zhu, M. Lu, M. Li, J. Zhu, and Y. Shan. Synthesis of carbon-titania composite and its application as catalyst support, *Materials Chemistry and Physics* **132**(2-3), 316, 2012.

[16] Z. Guo, Y. Chen, L. Li, X. Wang, G.L. Haller, and Y. Yang. Carbon nanotube-supported Pt-based bimetallic catalysts prepared by a microwave-assisted polyol

reduction method and their catalytic applications in the selective hydrogenation, *Journal of Catalysis* **276**(2), 314, 2010.

[17] B.F. Machado, S. Morales-Torres, A.F. Pérez-Cadenas, F.J. Maldonado-Hódar, F. Carrasco-Marín, A.M.T. Silva, J.L. Figueiredo, and J.L. Faria. Preparation of carbon aerogel supported platinum catalysts for the selective hydrogenation of cinnamaldehyde, *Applied Catalysis A: General* **425–426**(0), 161, 2012.

[18] S. Morales-Torres, F.J. Maldonado-Hódar, A.F. Pérez-Cadenas, and F. Carrasco-Marín. Design of low-temperature Pt-carbon combustion catalysts for VOC's treatments, *Journal of Hazardous Materials* **183**(1-3), 814, 2010.

[19] F.J. Maldonado-Hódar, C. Moreno-Castilla, J. Rivera-Utrilla, Y. Hanzawa, and Y. Yamada. Catalytic Graphitization of Carbon Aerogels by Transition Metals, *Langmuir* **16**(9), 4367, 2000.

[20] E. Bailón-García, F. Carrasco-Marín, A.F. Pérez-Cadenas, and F.J. Maldonado-Hódar. Development of carbon xerogels as alternative Pt-supports for the selective hydrogenation of citral, *Catalysis Communications* **58**, 64, 2014.

[21] E. Bailón-García, F. Carrasco-Marín, A.F. Pérez-Cadenas, and F.J. Maldonado-Hódar. Microspheres of carbon xerogel: an alternative Pt-support for the selective hydrogenation of citral, *Applied Catalysis A: General* **482**, 318, 2014.

[22] D. Manikandan, D. Divakar, and T. Sivakumar. Selective hydrogenation of citral over noble metals intercalated montmorillonite catalysts, *Catalysis Letters* **123**(1-2), 107, 2008.

[23] M. Chatterjee, Y. Ikushima, T. Yokoyama, and M. Sato. Density-dependent formation of the pure trans-isomer of the unsaturated alcohol by selective hydrogenation of citral in supercritical carbon dioxide, *Advanced Synthesis & Catalysis* **350**(4), 624, 2008.

[24] T. Ekou, A. Vicente, G. Lafaye, C. Especel, and P. Marecot. Bimetallic Rh-Ge and Pt-Ge catalysts supported on TiO_2 for citral hydrogenation II. Catalytic properties, *Applied Catalysis A-General* **314**(1), 73, 2006.

[25] S. Morales-Torres, F.J. Maldonado-Hódar, A.F. Pérez-Cadenas, and F. Carrasco-Marín. Textural and mechanical characteristics of carbon aerogels synthesized by polymerization of resorcinol and formaldehyde using alkali carbonates as basification agents, *Phys. Chem. Chem. Phys.* **12**(35), 10365, 2010.

[26] E. Gallegos-Suárez, A.F. Pérez-Cadenas, F.J. Maldonado-Hódar, and F. Carrasco-Marín. On the micro- and mesoporosity of carbon aerogels and xerogels. The role of the drying conditions during the synthesis processes, *Chemical Engineering Journal* **181–182**(0), 851, 2012.

[27] S. Brunauer, P.H. Emmett, and E. Teller. Adsorption of Gases in Multimolecular Layers, *Journal of the American Chemical Society* **60**(2), 309-319, 1-2-1938.

[28] M.M. Dubinin. Generalization of the theory of volume filling of micropores to nonhomogeneous microporous structures, *Carbon* **23**(4), 373, 1985.

[29] MM. Dubinin. Contemporary state of the theory of volume filling of micropores of adsorbents in the adsorption of gases and vapors on carbon adsorbents, *Russian Journal of Physical Chemestry* **39**, 1305, 1965.

[30] F. Stoeckli, *porosity in carbons - characterization and applications* (Arnold, London, 1995).

[31] E.P. Barrett, L.G. Joyner, and P.P. Halenda. The Determination of Pore Volume and Area Distributions in Porous Substances. I. Computations from Nitrogen Isotherms, *Journal of the American Chemical Society* **73**(1), 373-380, 1-1-1951.

[32] R. Ubago-Pérez, F. Carrasco-Marín, D. Fairén-Jiménez, and C. Moreno-Castilla. Granular and monolithic activated carbons from KOH-activation of olive stones, *Microporous and Mesoporous Materials* **92**(1–3), 64, 2006.

[33] C.A. Leon, J.M. Solar, V. Calemma, and L.R. Radovic. Evidence for the protonation of basal plane sites on carbon, *Carbon* **30**(5), 797, 1992.

[34] J.E. Benson and M. Boudart. Hydrogen-oxygen titration method for the measurement of supported platinum surface areas, *Journal of Catalysis* **4**(6), 704, 1965.

[35] G.R. Wilson and W.K. Hall. Studies of the hydrogen held by solids: XVIII. Hydrogen and oxygen chemisorption on alumina- and zeolite-supported platinum, *Journal of Catalysis* **17**(2), 190, 1970.

[36] D. Cazorla-Amorós, J. Alcañiz-Monge, and A. Linares-Solano. Characterization of Activated Carbon Fibers by CO_2 Adsorption, *Langmuir* **12**(11), 2820, 1996.

[37] M.A. Montes-Morán, D. Suárez, J.A. Menéndez, and E. Fuente. On the nature of basic sites on carbon surfaces: an overview, *Carbon* **42**(7), 1219, 2004.

[38] F. Klasovsky and P. Claus, "Chapter 8 - Metal Nanoclusters in Catalysis: Effects of Nanoparticle Size, Shape, and Structure",in *Metal Nanoclusters in Catalysis and Materials Science,* edited by B. Corain, G. Schmid, and N. Toshima (Elsevier, Amsterdam, 2008), pp.167-181.

[39] U.K. Singh and M.A. Vannice. Kinetics of liquid-phase hydrogenation reactions over supported metal catalysts- a review, *Applied Catalysis A: General* **213**(1), 1, 2001.

[40] C.N. Satterfield, *mass transfer in heterogeneous catalysis* (MIT Press, Cambridge, 1970).

[41] G. Roberts, *catalysis in organic synthesis* (Academic Press, New York, 1976).

[42] S.P. Lee and Y.W. Chen. Nitrobenzene hydrogenation on Ni–P, Ni–B and Ni–P–B ultrafine materials, *Journal of Molecular Catalysis A: Chemical* **152**(1–2), 213, 2000.

[43] Y. Sano, N. Yamaguchi, and T. Adachi. Mass Transfer Coefficients for Suspended Particles in Agitated Vessels and Bubble Columns, *Journal of Chemical Engineering of Japan* **7**(4), 255, 1974.

[44] G. Trubiano, D. Borio, and A. Errazu. Influence of the operating conditions and the external mass transfer limitations on the synthesis of fatty acid esters using a Candida antarctica lipase, *Enzyme and Microbial Technology* **40**(4), 716, 2007.

[45] P.B. Weisz and C.D. Prater, "Interpretation of Measurements in Experimental Catalysis",in *Advances in Catalysis*, Volume 6 ed. edited by W.G. Frankenburg (Academic Press, 1954), pp.143-196.

[46] M.L. Toebes, T. exander Nijhuis, J. Hájek, J.H. Bitter, A. Jos van Dillen, D.Y. Murzin, and K.P. de Jong. Support effects in hydrogenation of cinnamaldehyde over carbon nanofiber-supported platinum catalysts: Kinetic modeling, *Chemical Engineering Science* **60**(21), 5682, 2005.

[47] C.A. Ferretti, R.N. Olcese, C.R. Apesteguía, and J.I. Di Cosimo. Heterogeneously-Catalyzed Glycerolysis of Fatty Acid Methyl Esters: Reaction Parameter Optimization, *Industrial & Engineering Chemistry Research* **48**(23), 10387-10394, 16-9-2009.

[48] Z.P. Xu and K.T. Chuang. Effect of internal diffusion on heterogeneous catalytic esterification of acetic acid, *Chemical Engineering Science* **52**(17), 3011, 1997.

[49] R. Leyva-Ramos and C.J. Geankoplis. Diffusion in liquid-filled pores of activated carbon. I. Pore volume diffusion, *The Canadian Journal of Chemical Engineering* **72**(2), 262-271, 1-4-1994.

[50] C.R. Wilke and P. Chang. Correlation of diffusion coefficients in dilute solutions, *AIChE Journal* **1**(2), 264-270, 1-6-1955.

[51] R.C. Reid, J.M. Prausnitz, and B.E. Poling, *the properties of gases and liquids*, 4th ed. (McGraw- Hill, New York, 1987).

[52] P. Maki-Arvela, N. Kumar, K. Eranen, T. Salmi, and D.Y. Murzin. Inverse temperature dependence due to catalyst deactivation in liquid phase citral hydrogenation over Pt/Al_2O_3, *Chemical Engineering Journal* **122**(3), 127, 2006.

[53] U.K. Singh and M. Albert Vannice. Liquid-Phase Hydrogenation of Citral over Pt/SiO_2 Catalysts: I. Temperature Effects on Activity and Selectivity, *Journal of Catalysis* **191**(1), 165, 2000.

[54] P. Beccat, J.C. Bertolini, Y. Gauthier, J. Massardier, and P. Ruiz. Crotonaldehyde and methylcrotonaldehyde hydrogenation over Pt(111) and $Pt_{80}Fe_{20}$(111) single crystals, *Journal of Catalysis* **126**(2), 451, 1990.

[55] A. Giroir-Fendler, D. Richard, and P. Gallezot. Chemioselectivity in the catalytic hydrogenation of cinnamaldehyde. Effect of metal particle morphology, *Catalysis Letters* **5**(2), 175, 1990.

Capítulo IV

MICROSPHERES OF CARBON XEROGEL: AN ALTERNATIVE Pt-SUPPORT FOR THE SELECTIVE HYDROGENATION OF CITRAL

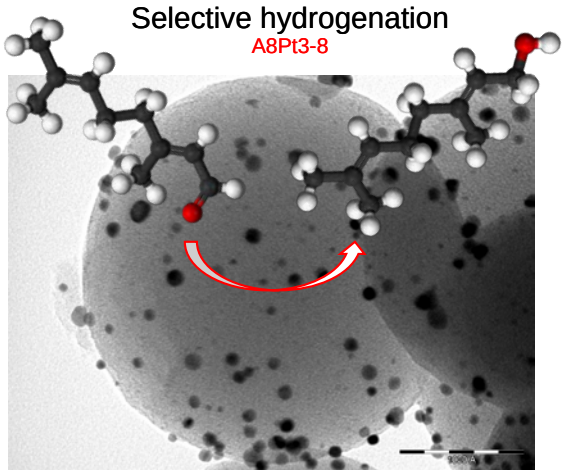

MICROSPHERES OF CARBON XEROGEL: AN ALTERNATIVE Pt-SUPPORT FOR THE SELECTIVE HYDROGENATION OF CITRAL

Article published in Applied Catalysis A: General, 482 (2014) 318-326, doi:10.1016/j.apcata.2014.06.011

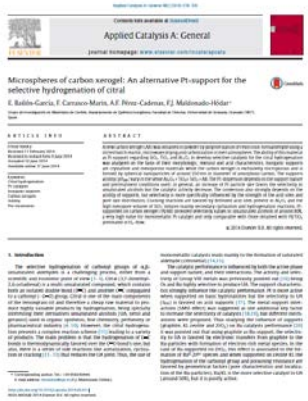
Applied Catalysis A: General

Microspheres of carbon xerogel: An alternative Pt-support for the selective hydrogenation of citral

Highlights

- Carbon xerogel is prepared as microporous spheres.
- Inorganic supports are mesoporous and acidic materials.
- The performance of Pt-catalysts is related with the acidity and porosity of supports.
- Pt/carbon xerogels are highly selective and stable catalysts.

Abstract

A new carbon xerogel (A8) was obtained in powder by polymerization of resorcinol-formaldehyde using a stirred batch reactor, microwave drying and carbonization in inert atmosphere. The ability of this material as Pt-support regarding SiO_2, TiO_2 and Al_2O_3 to develop selective catalysts for the citral hydrogenation was analyzed on the basis of their morphologic, textural and acid characteristics. Inorganic supports are crystalline and mesoporous materials while the carbon xerogel is exclusively microporous and is formed by spherical nanoparticles of around 250 nm in diameter of amorphous carbon. The supports acidity (pH_{pzc}) vary in the sense Al_2O_3>TiO_2> SiO_2>A8. The Pt-dispersion depends on the support nature and pretreatment conditions used; in general, an increase of Pt-particle size favors the selectivity to unsaturated alcohols but the catalytic activity decrease. The conversion also strongly depends on the acidity of supports, but selectivity is more specifically influenced by the strength of the acid sites and pore size distribution. Cracking reactions are favored by Brönsted acid sites present in Al_2O_3 and the high mesopore volume of SiO_2 induces mainly secondary cyclization and hydrogenation reactions. Pt-supported on carbon xerogel (Pt/A8) provided selectivity values to unsaturated alcohols of around 80%, a very high value for monometallic Pt-catalyst and only comparable with those obtained with Pt/TiO_2 pretreated in H_2-flow.

4.1. INTRODUCTION

The selective hydrogenation of carbonyl groups of α,β-unsaturated aldehydes is a challenging process, either from a scientific and economic point of view[1-3]. Citral (3,7-dimethyl-2,6-octadienal) is a multi-unsaturated compound, which contains both an isolated double bond (C=C) and another C=C conjugated to a carbonyl (–C=O) group. Citral is one of the main components of the lemongrass oil and therefore a cheap raw material to produce highly valuable products by hydrogenation, being specially interesting their derivatives unsaturated alcohols (UA, nerol and geraniol) used in organic synthesis, fine chemistry, perfumery or pharmaceutical industry[4-10]. However, the citral hydrogenation presents a complex reaction scheme[11] leading to a variety of products. The main problem is that the hydrogenation of C=C bonds is thermodynamically favored over the C=O bond's one, but also, there is a series of side reactions like acetalization, cyclization or cracking[11-13] that reduces the UA yield. Thus, the use of monometallic catalysts leads mainly to the formation of saturated aldehyde (citronellal)[14,15].

The catalytic performance is influenced by both the active phase and support nature, and their interactions. The activity and selectivity of Group VIII metals was previously pointed out[16] being Os and Ru highly selective to produce UA. The support characteristics strongly influence the catalytic performance. Pt is more active when supported on basic hydrotalcites but the selectivity to UA (S_{UA}) is favored on acid supports[17]. The metal-support interactions (SMSI effect) was suggested as one additional key factor to increase the selectivity of catalysts[18,19], but different mechanisms were proposed. Thus studying the influence of supports (graphite, KL zeolite and ZrO_2) on Ru-catalysts performance [20] it was pointed out that using graphite as Ru-support, the selectivity to UA is favored by electronic transfers from graphite to the Ru-particles with formation of electron-rich metal species. In the case of Ru-supported on ZrO_2, this effect is associated to the formation of Ru^0-Zr^{n+} species and when supported on zeolite KL the hydrogenation of the carbonyl group and poisoning resistance are favored by geometrical factors (pore characteristics and localization of the Ru-particles). Ru/KL is the more selective catalyst to UA (around 50%), but it is poorly active.

Alternatively, bimetallic catalysts have been also developed trying to increase the selectivity to UA[21-23]. Using Pt-Co/C catalysts S_{UA} depend on the Pt/Co ratio and activation conditions, in the best case, S_{UA} ranges between 70-80%[24]. The S_{UA} increase is due to electronic transfer from Co to Pt atoms. Similar results and conclusions were obtained with other supported catalytic system as Rh-Ge, Pt-Ge, Pt-Sn, etc[1,11].

Carbon aerogels and xerogels are a new type of carbon materials synthesized with controllable porosity and surface chemistry and therefore with large perspectives in catalysis[25-27]. No information about the use of microporous carbon xerogels for the development of catalysts for the selective citral hydrogenation is available in the bibliography. In this manuscript we prepare a microporous carbon xerogel in microspheres and study its performance as Pt-support in comparison with mesoporous inorganic oxides (SiO_2, Al_2O_3 and TiO_2). Hydrogenation of citral was selected as model reaction and the catalytic performance was analyzed as a function of the catalysts physicochemical characteristics.

4.2. EXPERIMENTAL

4.2.1. Preparation of the catalysts

Commercial inorganic oxides (SiO_2, Al_2O_3 and TiO_2) and a carbon xerogel (A8) synthesized in our laboratory were used as Pt-supports. SiO_2 (Silica Gel 100, Merck), Al_2O_3 (Aluminum oxide acidic, Merck), TiO_2 (anatase, Alfa Aesar) were used without additional treatments.

The carbon xerogel was prepared by polycondensation of resorcinol (R) with formaldehyde (F) in aqueous (W) media, using Cs_2CO_3 as polymerization catalyst (C) by modifying a previous synthesis procedure[28]. The composition of the mixture (molar ratios) was R/F = 1/2, R/W = 3/500 and R/C = 800. Accordingly, the proper amount of resorcinol and cesium carbonate were dissolved to deionised water in a three-necks glass reactor provided of reflux, controlled temperature and stirring. The temperature of this solution was increased to the polymerization temperature (85 °C) and then, formaldehyde solution (Sigma, 37 wt.%) was added dropwise in the flask under agitation (250 rpm). After aging for 24 h, the gel formed presents an intense orange

color and is recovered by filtration. The solid obtained was placed in acetone for 3 days, changing acetone twice daily, in order to exchange water within the pores by acetone. This exchange procedure reduces the porosity collapse during the subsequent drying step[29]. The gel was dried by microwave heating using a Saivod MS-287W microwave oven under nitrogen atmosphere in periods of 1 minute at 384 W until constant weight. The organic xerogel obtained was then pyrolyzed for 2h at 900 °C in N_2 flow (150 cm^3min^{-1}), using a tubular furnace and a slow heating rate (1 °C/min), in order to allow a soft removing of pyrolysis gases, and soaking time of 2 h. The carbon xerogel obtained will be referred to as A8 sample.

All supports were milled and sieved to a diameter smaller than 0.150 mm before impregnation. Platinum catalysts were prepared by impregnation at 3 wt.% Pt-loading. For that, the appropriate amount of $[Pt(NH_3)_4]Cl_2$ was dissolved in the minimum amount of water (according to the salt solubility) and then slowly dropped on the support under constant homogenization by shaking. Impregnated supports were dried at room temperature for 1 day and at 110 °C in an oven for additional 24 h and stored in a desiccator in the lab. Before reaction, samples were pretreated in He or H_2 flow at 400 °C (heating rate of 5 °C/min) for 12 h. Catalysts were referred indicating the support, the Pt-content and the final mean Pt-particle size determined by H_2-chemisorption. Thus, as an example, A8Pt3-8 indicates that Pt was deposited on the carbon support with a 3wt.% - loading and presents, after pretreatment, a particle size of 8 nm.

4.2.2. Textural and chemical characterization

The morphology of supports was studied by scanning electron microscopy (SEM) using a LEO (Carl Zeiss) GEMINI-1530 microscope. Textural characterization was carried out by N_2 and CO_2 adsorption at −196 °C and 0 °C, respectively, using a Quantachrome Autosorb-1 equipment. The BET equation was applied to the N_2-adsorption isotherms to determine the apparent surface area (S_{BET}) and the Dubinin–Radushkevich and Stoeckli equations applied to both N_2 and CO_2-adsorption isotherms to determine the micropore volume (V_{mic}), the mean micropore width (L_0) and the microporous surface (S_{mic}), respectively[30-33]. Furthermore, the BJH method was used to calculate the mesopore volume of the samples (V_{meso}) and the mean mesopore width

(L_{meso}). Pore size distributions (PSD) were also obtained by applying the BJH method[34]. The total pore volume (V_{Total}) was considered as the volume of N_2 adsorbed at P/P_0 = 0.95[35].

Pt dispersion (D) and mean particle size (d) were obtained by H_2-chemisorption and high-resolution transmission electron microscopy (HRTEM). The H_2-chemisorption isotherms were measured at 25 °C. The Pt dispersion (D) is obtained[36,37] from the amount of H_2-chemisorbed assuming a stoichiometric ratio H_2:Pt = 1:2 (dissociative chemisorption) and the average particle size was calculated as $d_{Pt}(H_2)$ = 1.08/D (nm). HRTEM experiments were carried out using a Phillips CM-20 microscope equipped with EDAX microanalysis system and microphotographs were analyzed by the appropriate software (IJ.JAR, from Java). A minimum of 1000 particles were analyzed from different microphotographs and their diameter calculated by the program assuming spherical shape, finally results were compiled and treated using a spreadsheet (Excel), obtaining the frequency factor (%) for each particle size interval and the corresponding histograms.

The chemical characterization of the catalysts was further analyzed by X-ray photoelectron spectroscopy (XPS). The spectra were obtained on a Kratos Axis Ultra-DLD X-ray photoelectron spectrometer equipped with a hemispherical electron analyzer connected to a detector DLD (delay-line detector). The Pt_{4f} spectral region was scanned several times to obtain good signal-to-noise ratios. In addition, the spectral region Pt_{4d} was also scanned in the case of Al_2O_3 supported catalysts to avoid overlapping effects of the Pt_{4f} and Al_{2p} spectral regions.

Information about the support acidity was obtained by measuring the pH_{pzc}, according to the methodology previously described[38], n-butylamine adsorption/desorption (TPD) process and FTIR analysis. The IR absorption spectra were recorded on a Nicolet 20SXB FTIR spectrometer using KBr/saturated sample pellets. Adsorption/desorption tests were carried out in a quartz microreactor at atmospheric pressure with 0.2 g sample using a He/Ar flow saturated with n-butylamine at 0 °C. The total flow rate was 60 cm^3min^{-1} and the partial pressure of n-butylamine 28.92 Torr. Analyses were carried out on-line with a Mass Spectometer model Prisma (Pfeiffer). Samples were heated in pure He flow up to the adsorption temperature (90 or

150 °C) and after stabilization, the He flow was turned by the saturated He/Ar flow up to sample saturation (the n-butylamine concentration is recovered). After that, the saturated sample was purged in pure He for 1 h to remove rest of trapped n-butylamine, and then, TPD-n-butylamine was recorded by heating at 10 °C/min.

4.2.3. Catalytic performance

The citral hydrogenation was carried out in 100 ml heptane solution at a constant hydrogen pressure of 8.3 bar and 90 °C using a Parr reactor model 5500. The experimental conditions: citral concentration, catalyst weight and agitation speed were previously optimized in order to avoid mass transfer limitations (results not showed) and fixed in 0.05 M, 500 mg and 1500 rpm, respectively. A small volume of sample (1 ml) was periodically withdrawn and analyzed by chromatography using a Bruker 430-GC equipped with a FID detector and a Varian GC Capillary Column CP7485 (25m x 0.32 mm x 0.45 μm). Both citral and any possible product were previously calibrated.

4.3. RESULTS AND DISCUSSION

4.3.1. Characterization of the supports and catalysts

In Table 4.1, there are summarized the results obtained from CO_2 and N_2 adsorption showing a great variation of the textural properties of supports. It is well known that the CO_2 adsorption provides the information about the narrow microporosity, corresponding to micropores with diameter lower than 0.7 nm, while the total microporosity is determined from N_2 isotherm only in absence of diffusion restrictions[39]. All inorganic oxides present a low micropore volume independently of the adsorbate (N_2 or CO_2) used. The pore size distribution (PSD) obtained by application of the BJH method to the N_2 desorption isotherm showed that these samples are eminently mesoporous materials (Figure S.4.1). The mesopore volume (V_{meso}) and the mean mesopore width (L_{meso}) clearly decreases in the sense $SiO_2 > TiO_2 > Al_2O_3$. For these samples, even the mean micropore width (L_0) determined from the N_2 adsorption isotherms are close to the mesopore range, thus, in the case of the SiO_2 support $S_{BET} > S_{mic}$, as consequence of the great contribution of the external surface associated to the strong mesopore volume (V_{meso}). Silica presents a total porosity

(V_{Total}) significantly higher than the rest of supports, and also a more homogeneous PSD of mesopores at around 10 nm in diameter (Figure S.4.1). On the contrary, TiO_2 presents a wide PSD. The greater BET surface area was detected for carbon xerogel, however, A8 is a support exclusively microporous with a null mesopore volume (V_{meso}), and narrower micropores (L_0) than those detected for inorganic supports, in such a way that there is an important difference between V_{mic} and surface area values determined by CO_2 and N_2-adsorption, showing in this case that N_2-adsorption presents significant diffusional restrictions to accede into the A8 porosity.

Table 4.1. Textural characteristics and pH_{pzc} values of supports.

Support	pH_{pzc}	S_{BET}	$S_{mic}(CO_2)$	$V_{mic}(N_2)$	$V_{mic}(CO_2)$	V_{meso}	V_{Total}	$L_0(N_2)$	L_{meso}
		$m^2 \cdot g^{-1}$	$m^2 \cdot g^{-1}$	$cm^3 \cdot g^{-1}$	$cm^3 \cdot g^{-1}$	$cm^3 \cdot g^{-1}$	$cm^3 \cdot g^{-1}$	nm	nm
SiO_2	7.58	241	144	0.094	0.056	0.974	0.983	1.78	10.0
TiO_2	4.90	116	159	0.047	0.054	0.405	0.493	1.89	6.11
Al_2O_3	4.39	121	131	0.047	0.051	0.240	0.244	1.61	4.62
A8	8.73	614	952	0.245	0.285	0.000	0.305	0.78	-

In order to determine the accessibility of the reactant solution to the porosity, samples were recovered after reaction, dried at room temperature for at least a week and analyzed by thermogravimetry (TG) in N_2 flow. The weight loss observed was associated to heptane desorption (taking into account the low proportion of citral or reaction products) and the results obtained (Figure S.4.2) showed that the volume of heptane desorbed (heptane density = 0.785 $cm^3 \cdot g^{-1}$) correctly matches the total pore volume (V_{Total}) of the samples, which indicates that all the porosity is accessible to the reactant solution in the experimental conditions used independently of the support.

The determined pH_{pzc} values of supports are also included in Table 4.1, being also noteworthy the great acidity difference observed: Al_2O_3 and TiO_2 are acid, SiO_2 present a neutral surface and A8 is clearly a basic material. The acidity of oxides was previously evaluated by different authors and their conclusions are clearly in agreement with the described tendency. As an example Gervasini *et al.*[40] pointed out a similar acidity of TiO_2 and Al_2O_3 by NH_3-adsorption and isopropanol decomposition. No NH_3-adsorption or catalytic activity was obtained for SiO_2, denoting the non-acidity character. Walker *et al.*[41] pointed out that Al_2O_3 mostly comprises of Brönsted sites

while Lewis sites dominates on TiO_2 surface. Recently, the TiO_2, Al_2O_3 and SiO_2 acidity was extensively studied by NH_3 chemisorption, titration and IR spectroscopy of adsorbed probe molecules[42]. Authors found that the NH_3 uptake was in the order TiO_2 > Al_2O_3>>SiO_2, but the Brönsted acidity vary as: Al_2O_3>TiO_2 > SiO_2.

The acid characteristics of pretreated catalysts were evaluated by n-butylamine adosorption/desorption experiments, and the nature of the acid sites (Lewis or Brönsted acid sites) by FTIR[43,44]. TPD-results, obtained by integration of the TPD-profiles shown in Figure 4.1, are summarized in Table 4.2. At low adsorption temperature (90 °C) results are clearly influenced by the porous texture of supports, thus, n-butylamine desorption, even after purging the sample in pure He-flow, vary according to the S_{BET} values (Table 4.1), indicating a significant influence of the physisorbed product. With increasing adsorption temperature (up to 150°C) this effect is avoided, in such a manner that the amount of n-butylamine desorbed vary according to the acidity of supports described by other authors[40-42], and previously commented. Thus, the catalyst acidity decreases progressively when Pt is supported on Al_2O_3, TiO_2, SiO_2 and A8. Melo *et al.*[43] considered the amount of n-butylamine desorbed below 110 °C as physisorbed species, and established three ranges (weak, medium and strong acid sites) for n-butylamine desorbed between 110 and 210 °C, 210 and 330 °C and after 330 °C, respectively. This acid site distribution is obviously influenced by the temperature treatment. In our case, all the samples were pretreated at the same temperature, but changing the pretreatment atmosphere. When pretreated in He-flow, in the case of Pt/Al_2O_3 the main desorption peak occurs at 190 °C, showing a large tail up to high temperature with a shoulder at around 300 °C, thus the n-butylamine desorption is higher than for the rest of samples in all the temperature range, indicating that this sample present the higher acid site content in all the acid strength range. Among the inorganic supports, silica presents the smaller amount of acid sites (amount of n-butylamine desorbed), and desorption takes place mainly at low temperature, indicating that weak acid sites are predominant in this case. The acidity of some catalysts after H_2-pretreatment was also examined. Results obtained for Pt/TiO_2 catalysts were compared in Figure 4.1.b, as an example. The acidity of the samples significantly decreases after H_2-pretreatment regarding the He-pretreatment.

Table 4.2. Amounts of n-butylamine desorbed by He-pretreated catalysts after saturation at 90 or 150 °C.

Catalysts	Desorbed after saturation at 90 ºC	Desorbed after saturation at 150 ºC
	µmol/g_{cat}	
SiO_2Pt3-8	411.7	23.0
A8Pt3-5	434.8	17.4
Al_2O_3Pt3-10	232.8	95.1
TiO_2Pt3-7	184.0	43.8

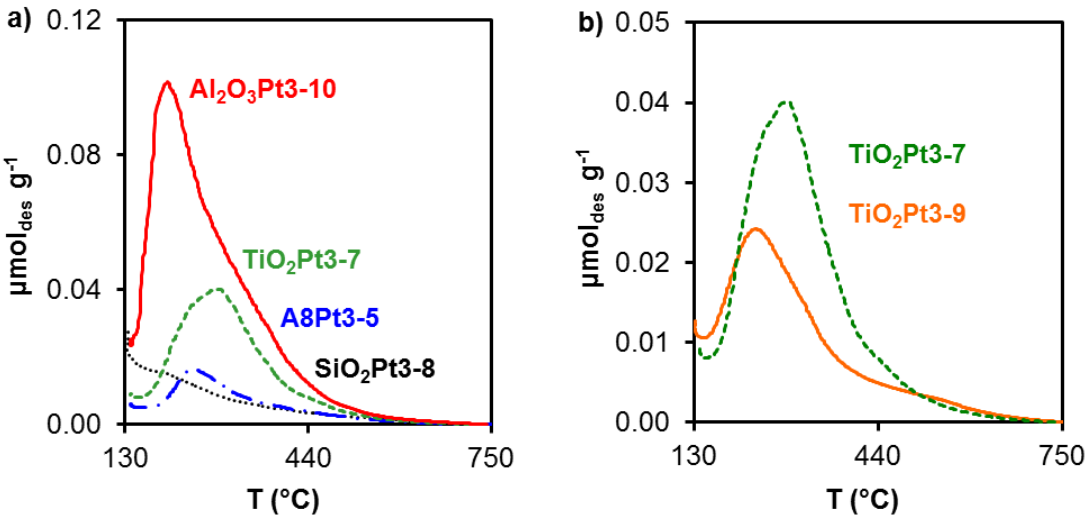

Figure 4.1. TPD-nbutylamine profiles obtained after saturation of He-pretreated catalysts at 150 °C and desorption in a) He flow at 10 °C/min and b) He or H_2 flow at 10 °C/min.

Results obtained by FTIR of n-butylamine saturated catalysts are summarized in Figure 4.2. According to the bibliography[45], the n-butylamine adsorbed on Lewis and Brönsted acid sites generates bands at 1630 and 1500 cm^{-1}, respectively. While the first one is observed in all catalysts, being significantly developed in the Pt/A8 catalysts by H_2-pretreatment, the presence of Brönsted acid sites were only observed in the case of Pt/Al_2O_3 catalysts, mainly when pretreated in He-flow. The weaker influence of pretreatment on the spectra profile was observed in the case of Pt/SiO_2 catalysts.

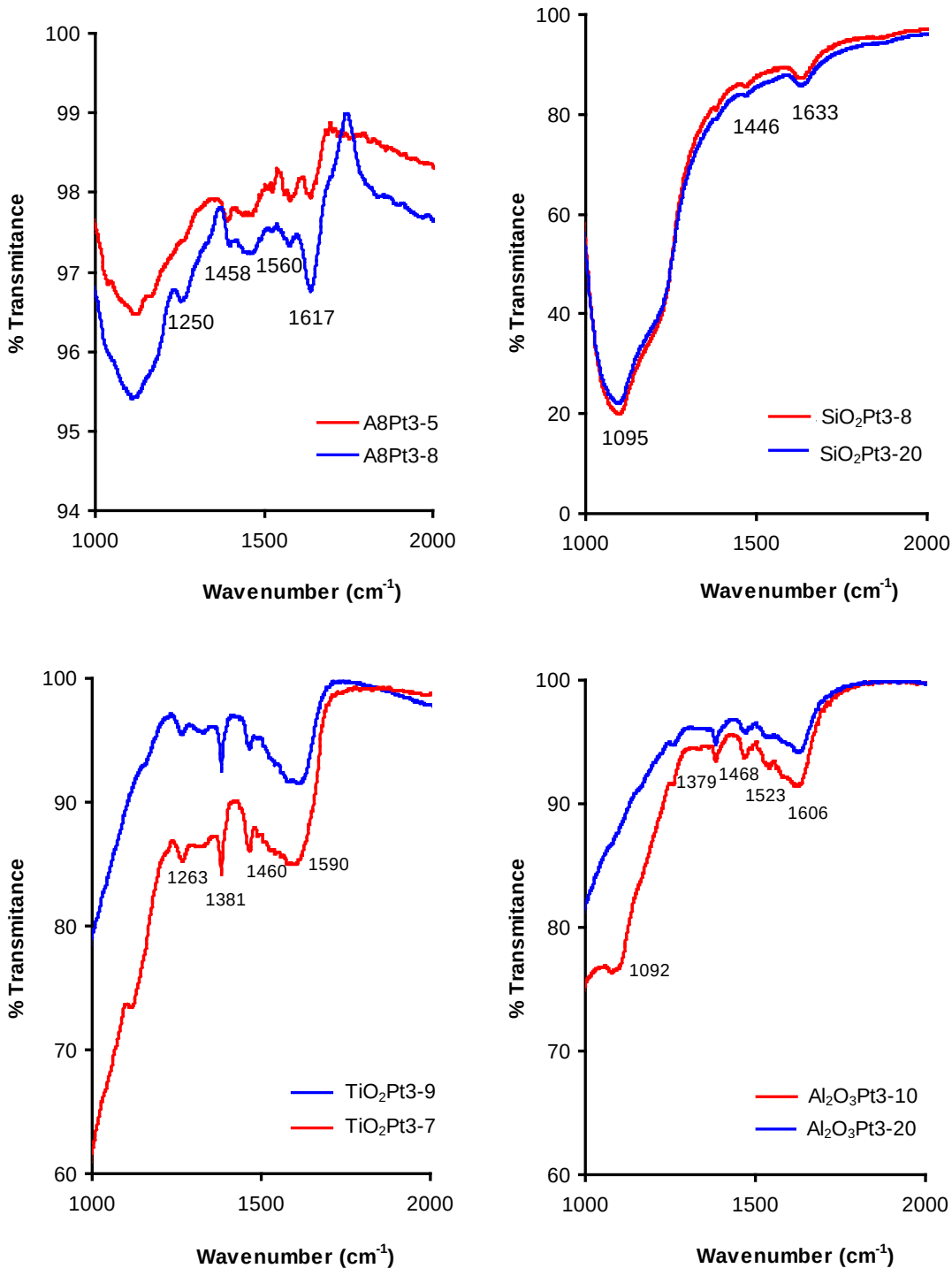

Figure 4.2. FTIR spectra of n-butylamine saturated catalysts. Red: He pretreatments; Blue: H_2 pretreatments.

As previously commented, after impregnation with the precursor salt, samples were pretreated at 400 °C/12 h in He or H_2 flow and Pt-dispersion analyzed by H_2-chemisorption and TEM measurements. Results are summarized in Table 4.3 and some

representative micrographs shown in Figure 4.3. In all cases (Table 4.3), smaller Pt-particle sizes were obtained after He-pretreatment. These results are in agreement with those previously observed[46] and seem to be due to the formation of an intermediate Pt-hydride in H_2 flow, $[Pt(NH_3)_2H_2]$, which favors the Pt-mobility on the support surface. Pt-dispersion is also strongly influenced by the porous texture of the supports. Thus, it was expected according to previous studies[47] that the mesopore volume showed by inorganic support contributes to a higher Pt-dispersion. However, the best Pt-dispersion was obtained using microporous A8 support (Table 4.3). Moreover, the influence of the pretreatment atmosphere is stronger for inorganic supports: H_2-pretreatment at 400 °C provokes in these samples (except for TiO_2) a strong sintering.

Table 4.3. Experimental conditions of catalysts pretreatment mean Pt-particle size ($\bar{d}_{H_2}$) determined from the amount of H_2 chemisorbed (Q_{H_2}), total Pt-surface concentration (Pt_{XPS}, wt.%) and nature and proportion (%) of the Pt-species detected by XPS.

Catalyst	Pretreatment	Q_{H_2} (µmol/g)	$\bar{d}_{H_2}$ (nm)	Pt^0 BE (eV)	Pt^0 (%)	Pt^{II} BE (eV)	Pt^{II} (%)	Pt_{XPS} (wt.%)
A8Pt3-5	400 °C He 12h	16.5	5.1	71.31	72.4	72.48	27.6	6.98
A8Pt3-8	400 °C H_2 12 h	10.5	7.9	71.27	70.4	72.33	29.6	4.38
SiO_2Pt3-8	400 °C He 12h	10.5	7.9	71.30	73.0	72.48	26.8	1.80
SiO_2Pt3-20	400 °C H_2 12h	4.1	20.4	71.41	71.7	72.43	28.3	1.10
TiO_2Pt3-7	400 °C He 12h	12.1	6.8	70.89	67.7	71.52	32.3	2.00
TiO_2Pt3-9	400 °C H_2 12h	9.0	9.2	71.45	72.8	72.03	27.2	1.95
Al_2O_3Pt3-10	400 °C He 12h	8.5	9.8	70.95 (313.20)	61.9	71.78 (315.28)	38.2	2.94
Al_2O_3Pt3-20	400 °C H_2 12h	4.0	20.0	71.02 (313.03)	72.8	71.82 (315.18)	27.2	0.75

* Spectral region Pt_{4f}, except values in parenthesis, corresponding to BE of Pt_{4d} spectral region

* Pt_{XPS} (wt.%) indicates the total Pt-concentration (wt.%) detected by XPS, while % Pt^0 and Pt^{II} indicate the proportion of each species.

The analysis by TEM (Figure 4.3) pointed out the ability of microporous A8 support to stabilize small and well distributed Pt-nanoparticles. A8 sample is morphologically quite different to oxide supports: spherical carbon particles of about

250 nm homogenously coated by also nearly spherical Pt-nanoparticles were observed. The particle size distribution obtained after He-pretreatment (Figure S.4.3) is more homogeneous than after H_2-pretreatment, the Pt-sintering induced is pointed out by the large tail observed in the particle size distribution, although the large part of Pt-particles are also very small.

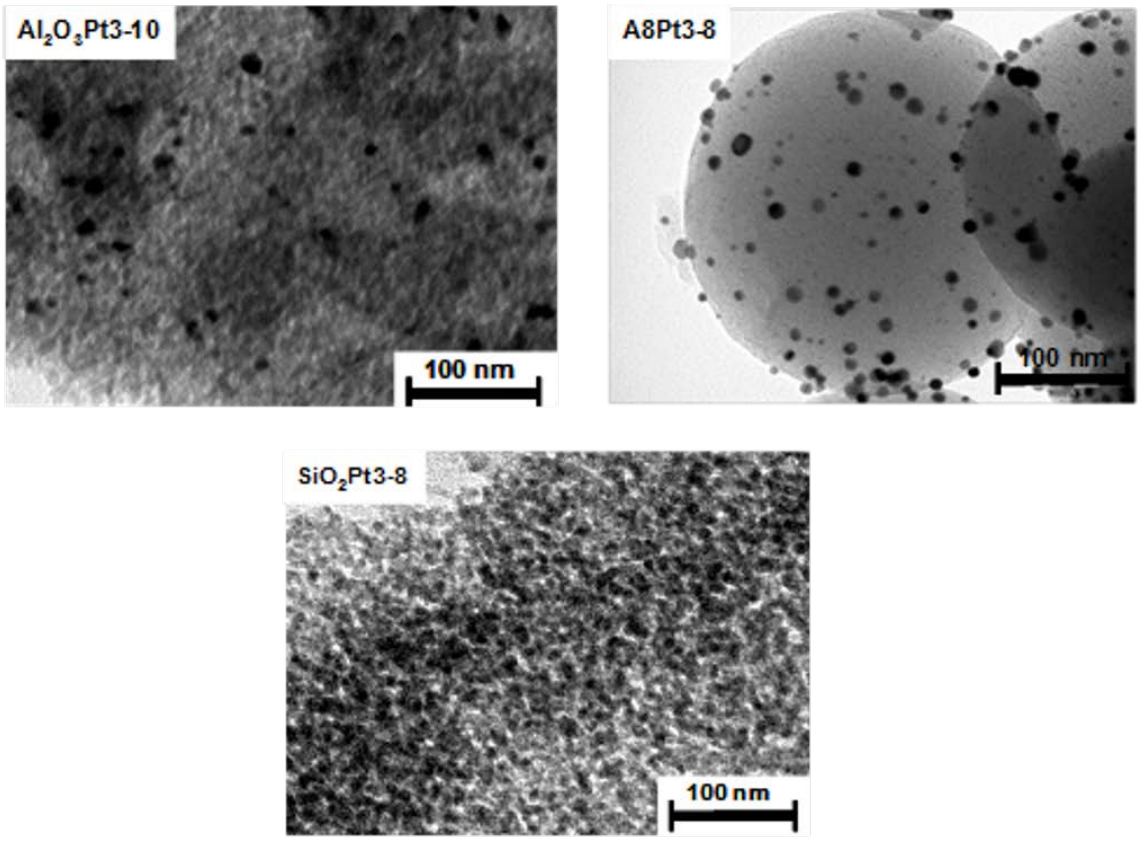

Figure 4.3. Representative TEM images of supported Pt-catalysts.

In Table 4.3 are collected the results obtained from the XPS analysis of pretreated catalysts. In all cases there is a fraction of Pt^{II} which could correspond to unreduced precursor or could be formed by reoxidation during the storage in air before the analysis. For Pt/Al_2O_3 catalysts, the 4d spectral region of Pt was also analyzed to avoid interferences of the Al_{2p} region on the Pt-results, showing nevertheless a similar tendency. After He-pretreatment the BE of Pt^0 supported on acidic oxides (Al_2O_3 and TiO_2) is around 0.4 eV smaller than when supported on neutral (SiO_2) or basic (A8) supports, being also greater the Pt^{II} ratio observed. The BE values are in general quite similar after treatment in H_2, except in the case of TiO_2 that significantly increases,

which can be due to a partial reduction of the TiO_2 support[11]. The BE variations can be associated to the different Pt-support interactions[48,49].

Regarding Pt-distribution it is noteworthy that in all cases, the surface Pt concentration (Pt_{XPS} %) decreases after the H_2-pretreatment, as consequence of the greater Pt-particle size obtained (Table 4.3). Therefore, it is important to compare catalysts at similar Pt-dispersion (at around 9 nm of Pt-particle size), where variations on Pt_{XPS} (%) are related only to the Pt-distribution inside the pores. In such a way Pt_{XPS} (%) varies linearly with V_{meso} according the sequence: SiO_2Pt3-8 ≤ TiO_2Pt3-9 < Al_2O_3Pt3-10 < A8Pt3-8. Thus, for inorganic oxides, but mainly in the case of SiO_2, some of the Pt-particles are located inside mesopores being not detected by XPS. However, in the case of A8Pt3 catalysts, Pt_{XPS} (%) > Pt loading (%), indicating a Pt-concentration on the external surface as denoted also by HTREM images. This support is exclusively microporous and the Pt-particles of 8 nm size cannot be located inside micropores (<2nm).

4.3.2. Catalytic performance

It is well known that the hydrogenation of α-β unsaturated aldehydes is strongly dependent of Pt-dispersion[2,50,51], i.e. citral hydrogenation is a structure sensitive reaction. The effect of the catalysts pretreatment on the conversion and S_{UA} attached is shown in Figure 4.4. After pretreatment in He flow, the Pt-particle size vary from 5 to 10 nm (Table 4.3) being conversion higher for the catalyst with larger Pt-particles. The strong sintering after H_2-pretreatment previously described for catalysts supported on silica and alumina leads to a strong loss of activity (from 100% to 35% for Pt/SiO_2 after 6 h of reaction) although favors S_{UA} values. However, sintering caused by H_2-pretreatment is smaller when Pt is supported on TiO_2 or A8, in both cases the Pt-particle size increase slowly which favors both conversion and S_{UA} (Figure 4.4). These means that both conversion and S_{UA} are not directly proportional to Pt dispersion but there is an optimum Pt-particle size at around 10 nm. The influence of the support on the S_{UA} is also evident, very high S_{UA} (around 80 %) is obtained when Pt is supported on A8 carbon xerogel independently of the catalysts pretreatment. These S_{UA} values are only reached with Pt-supported on TiO_2 and pretreated in H_2 flow. This behavior was previously described for Pt/TiO_2 catalysts and was associated to the partial reduction of

the support with the formation of oxygen vacancies or $TiO_{(2-x)}$ moieties[11,52], which can be in agreement with the XPS results previously commented.

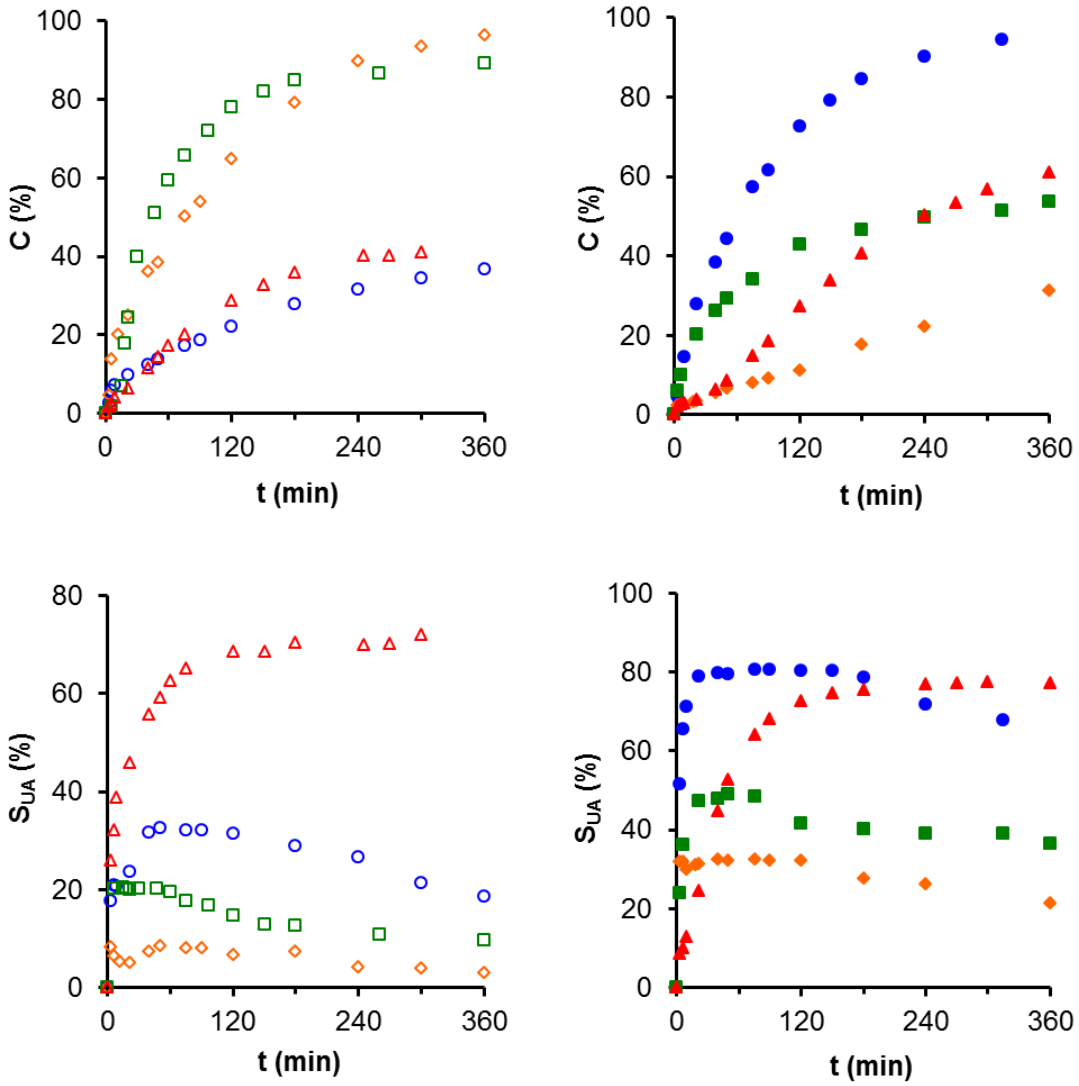

Figure 4.4. Influence of the He or H_2 pretreatment on the activity (C %) and selectivity to UA (S_{UA} %) of Pt-supported catalysts. Open symbol: He pretreated catalysts. Close symbol: H_2 pretreated catalysts. Pt/A8 (△), Pt/TiO_2 (○), Pt/Al_2O_3 (□) and Pt/SiO_2 (◇). Reaction conditions: citral in heptane solution (0.05M), 500 mg of catalyst, 1500 rpm, 90 ºC and P_{H_2} = 8.3 bar.

Therefore, to determine the influence of the support, catalysts were compared at similar Pt-particle size, in such a way that differences should be related to the porosity and surface chemistry of supports, the SMSI effect and/or the citral adsorption

modes on the catalyst surface. The performance of catalysts with similar Pt-dispersion (SiO_2Pt3-8; TiO_2Pt3-9; Al_2O_3Pt3-10; A8Pt3-8) is compared in Figure 4.5. The activity of catalysts (conversion values) is quite similar in all cases when use inorganic supports, reaching total conversion after 6 h of reaction. Reaction is slower for Pt-supported on the carbon xerogel, reaching at this time only around 60% of conversion. However, as commented, A8Pt3-8 catalyst presents the best behavior in terms of S_{UA}, only comparable to TiO_2Pt3-9. The worse S_{UA} was detected for SiO_2Pt3-8. To evaluate the contribution of supports on these results, they were pretreated and tested in the same experimental conditions that their corresponding Pt-catalysts. The results are summarized in Table 4.4.

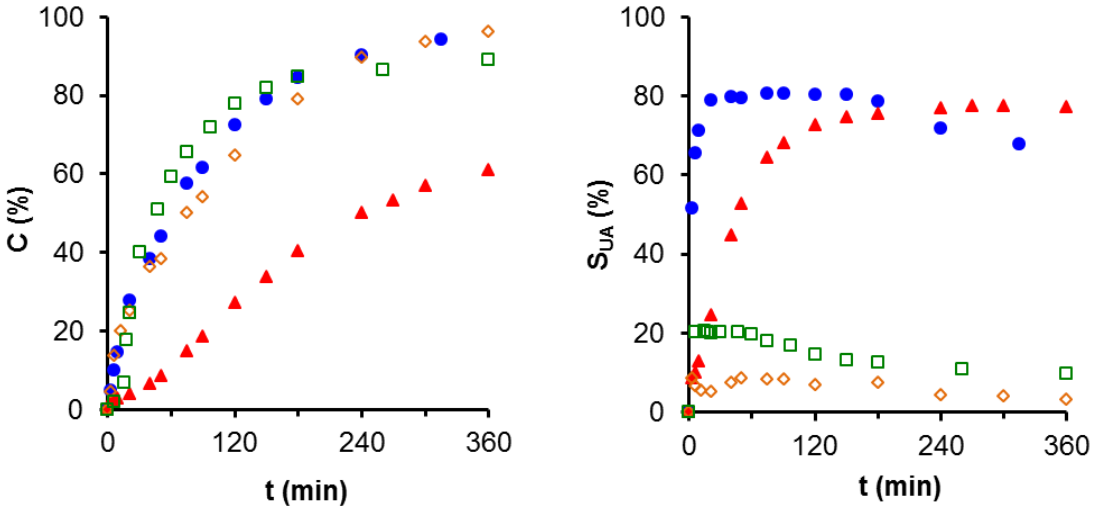

Figure 4.5. Conversion and S_{UA} obtained with 3% Pt-catalysts on different supports with Pt-particle size of 8.7 ± 1.2 nm. A8Pt3-8 (▲), TiO_2Pt3-9 (●), Al_2O_3Pt3-10 (□) and SiO_2Pt3-8 (◇). Reaction conditions: citral in heptane solution (0.05M), 500 mg of catalyst, 1500 rpm, 90 ºC and P_{H_2} = 8.3 bar.

Catalytically Al_2O_3 is the most active support, but its hydrogenation ability is too low: this sample generates mainly cracking products (different cracking compounds were formed and detected at low retention time on the corresponding chromatograms; they were collected in column 8 as "cracking"). Using TiO_2, conversion decreases around 50% and although S_{UA} increases three times regarding Al_2O_3, consecutive hydrogenation reactions are favored in such a way that citronellol is obtained as the main reaction product; nevertheless, it is also noteworthy that cracking products were

not detected. Conversion and S_{UA} decrease again using SiO_2 regarding TiO_2. The lowest activity was found for A8 xerogel, which presents however the higher S_{UA} obtained for pure supports.

Table 4.4. Conversion and products distribution after 6 h of reaction using the pretreated supports as catalysts.

Catalyst	C (%)	S_{UA} (%)	S_{Cal} (%)	S_{Col} (%)	$S_{isop+ment}$ (%)	S_{DMO} (%)	$S_{cracking}$ (%)
A8-H_2	4.8	25.1	39.1	28.6	7.1	0.0	0.0
Al_2O_3-He	49.0	5.8	5.4	-	3.7	6.5	78.6
SiO_2-He	11.5	14.2	25.6	23.9	34.6	1.7	0.0
TiO_2-H_2	24.2	18.8	23.8	33.2	23.0	1.2	0.0

*UA-Unsaturated alcohols, Cal – Citronellal, Col-citronellol, isop – isopulegol, ment – menthol, DMO – dimetlhyl octanol, Cracking products. Reaction conditions: citral in heptane solution (0.05M), 500 mg of support, 1500 rpm, 90 ºC and P_{H_2} = 8.3 bar.

According to these results, it is clear that the acid characteristics of supports are the main parameter (but not unique) determining their catalytic performance. In the case of Al_2O_3, Brönsted acid sites are strong enough to favor the cracking of citral molecules and/or their hydrogenated products. Conversion decreases for TiO_2 in spite that presents a pH_{pzc} slightly higher than Al_2O_3 and a similar surface area. The TiO_2 Lewis acid sites are weaker than those Brönsted groups present in the Al_2O_3, being unable to induce cracking reactions. However, these Lewis acid sites also favor the catalytic activity, as deduced when compare the catalytic performance of TiO_2 and SiO_2. This means that the critical factor to develop cracking reactions is the strength of the acid sites, and not the total acidity of the sample. In the same sense, conversion decreases again for SiO_2 because pH_{pzc} increases to values around neutrality. The low S_{UA} detected for SiO_2 should be related to textural characteristics and a weaker acidity. The large mesopore volume favors the development of secondary reactions, thus as observed, mainly secondary cyclization reactions of citronellal to isopulegol and menthol takes place inside the pores (Table 4.4) favored by acid sites. Similarly, the low activity of carbon xerogel can be related to the basic character of its surface and the narrower porosity. The low activity obtained with A8 pointed out the weaker interaction of the carbon support with citral molecules. In fact, we have detected that

the citral concentration remain constant in the reactor after several hours if pressurization is carried out with N_2 instead H_2, i.e. citral is not adsorbed (in spite that the citral solution fills the complete microporosity, (Figure S.4.2) not transformed under these experimental conditions). The hydrogenation of C=C bonds to citronellal is also preferred even in this case regarding the C=O ones, being also citronellal the main hydrogenation product. However, this support provides the higher S_{UA}, showing that can be an appropriate candidate to prepare selective hydrogenation Pt-catalysts.

Analyzing the evolution of products distribution obtained for the different Pt-catalysts as a function of the reaction time (Figure 4.6) it is observed that the most stable product distribution is obtained for Al_2O_3Pt3-10 catalyst, where the cracking selectivity is around 80% in all the conversion range (i.e. near to the product distribution obtained with the pure support). This means that cracking reactions developed on the Brönsted acid sites of the alumina surface are faster than the hydrogenation on Pt-active sites. Moreover, Brönsted acid sites do not deactivated after 6 h of reaction, on the contrary, $S_{cracking}$ tends to increase at the expense of S_{UA} and S_{Cal}, (Figure 4.6) by the consumption of the hydrogenated products previously formed. High S_{UA} values are obtained for TiO_2Pt3-9 catalyst. This parameter increases quickly at the reaction beginning but also decreases at high conversion values, in this case with formation of citronellol by hydrogenation of both UA and citronellal.

Using low acidic and mesoporous silica as Pt-support, the main product is citronellal in a large conversion range, obtained as primary reaction product. With increasing conversion values, citronellal is thereafter transformed into isopulegol and menthol by secondary cyclization reactions due to the conversion of citronellal to menthol involves two steps: cyclization of citronellal to isopulegol and hydrogenation of isopulegol to menthol. The first step is catalyzed by acid sites and the second one by metal sites. Secondary hydrogenations to citronellol and 3,7 DMO are also favored with time on reaction because these reactions are faster than the diffusion of citronellal from the mesopores. Citronellal was also initially the main product using A8Pt3 catalyst, but most active centers leading to the C=C hydrogenation are quickly deactivated, favoring the C=O hydrogenation to UA that become the main reaction products (S_{UA} progressively increases up to around 80% with increasing conversion values). The deactivation of Pt-hydrogenation centers by formation of carbon-like deposits or

irreversibly chemisorbed CO, formed by decomposition of citral molecules, on the most active Pt-sites was previously reported[19,53,54].

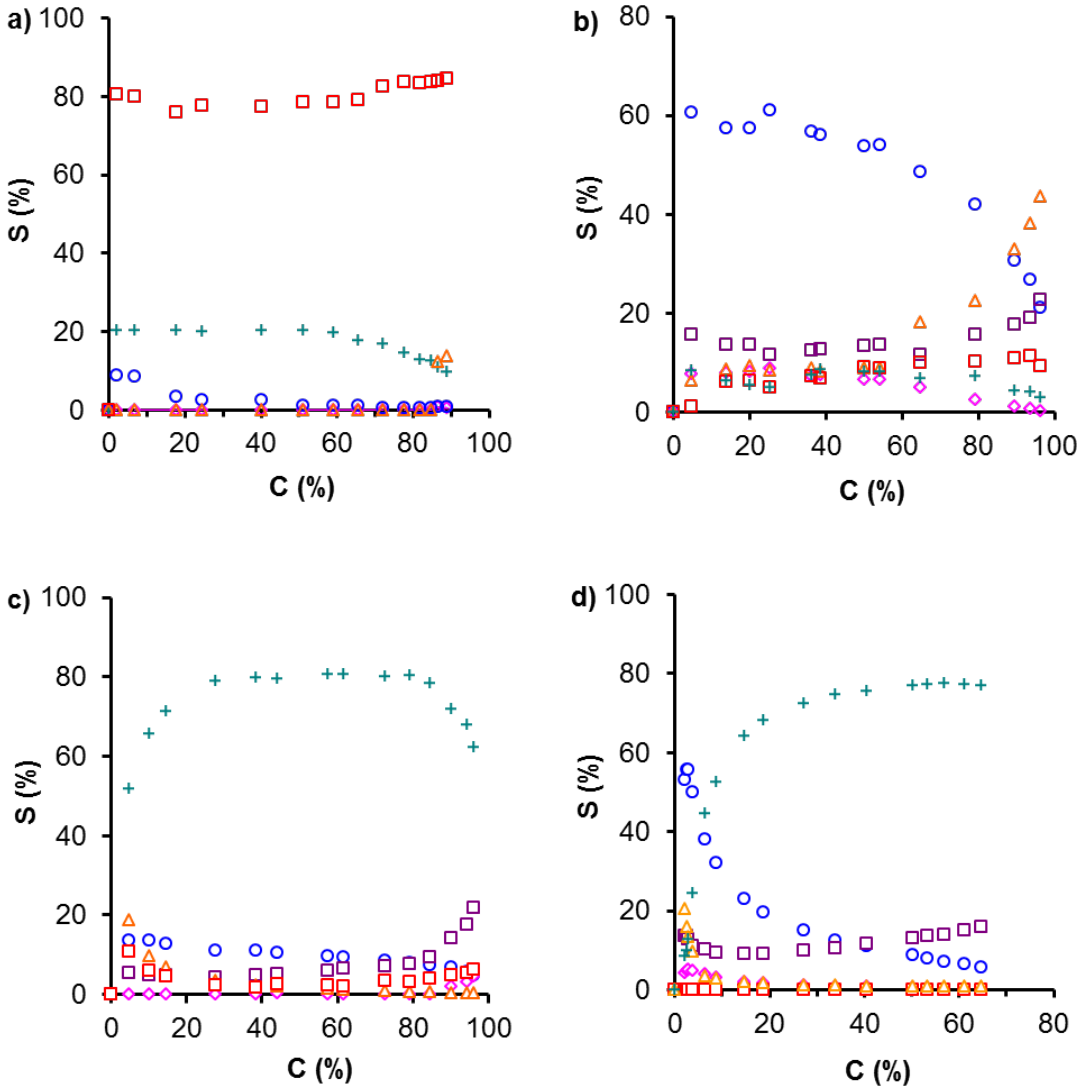

Figure 4.6. Product distribution along the reaction development: a) Al_2O_3Pt3-10, b) SiO_2Pt3-8, c) TiO_2Pt3-9 and d) A8Pt3-8**.** Citronellal (○), S_{UA} (+), Cyclization = isopulegol + menthol (△), citronellol (□), 3,7 DMO (◇), cracking (□). Reaction conditions: citral in heptane solution (0.05M), 500 mg of catalyst, 1500 rpm, 90 ºC and P_{H_2} = 8.3 bar.

There is therefore a change in the citral adsorption mode on the A8 surface with the reaction development. Because A8 presents the smaller external surface area due to the absence of mesopores, initially citral is slowly adsorbed close to the Pt-sites,

where H_2 molecules are adsorbed and dissociated, forming citronellal because the hydrogenation of C=C bonds is thermodynamically favored. With this, the catalysts surface chemistry changes due to more or less permanently adsorbed reactant and/or products, and, transforms the catalysts surface from hydrophobic to hydrophilic because the oxygen content increase. These changes occur progressively but slowly, as denoted by the conversion and product distribution evolution (Figures 4.5 and 4.6). The change from hydrophobic to hydrophilic surfaces favors the citral adsorption through C=O bond and consequently the UA formation[55]. The C=O adsorption mode can be also favored by the microporous character of the support: the confinement effect of citral into micropores was previously suggested for Ru/KL catalysts[20,56]. Finally, it is necessary to remember that we used Cs_2CO_3 as polymerization catalysts in the synthesis of the raw aerogel. Thus, Cs remained in solution being incorporated to the xerogel structure and influencing the xerogel morphology[28]. Thus, the highly electropositive Cs can act as a "doping" agent leading to certain electronic enrichment of Pt-particles that together the electron-donor character of the carbon surface, can favor the formation of species Pt (δ^-) which also favor the hydrogenation of the C=O bond in the citral molecule[20,24].

4.4. CONCLUSIONS

The catalytic performance of Pt supported on inorganic oxides (SiO_2, TiO_2 and Al_2O_3) and carbon xerogel (A8) was studied. The optimal Pt-particle size was found to be at between 7 and 10 nm; the stronger Pt-sintering detected on silica and alumina causes a significant activity loss but favors the S_{UA}. To study the influence of support, catalysts were compared at similar Pt-dispersion. The results obtained point out different correlations between porosity and surface chemistry of supports with their catalytic performance. The great mesopore volume of non–acidic SiO_2, where Pt-particles are located, favors the development of secondary hydrogenation and cyclization reactions. Brönsted acid sites present on Al_2O_3 lead to highly active Pt-catalysts, but poorly selective because they mainly induce cracking reactions. Using TiO_2 as support high S_{UA} values are obtained only after reduction in H_2 atmosphere, probably by formation of oxygen vacancies acting as specific adsorption sites. The use of microporous carbon xerogels is an interesting alternative to the use of TiO_2 supports. Unusually high S_{UA} values (greater than 80%) are obtained for this monometallic

catalyst by the combination of an appropriate spherical shape, porous texture, basic character (avoiding cracking) of the carbon surface and the external distribution of highly dispersed Pt-nanoparticles (avoiding secondary reactions) which are electronically enriched by Cs and carbon support. The adsorption of citral molecules through the C=O bonds seem to be determined by the pore size distribution of the support and favored by the increasing oxygen content of the carbon surface. Both parameters, the pore size distribution and surface chemistry of the carbon support, can be easily fitted by the appropriate treatment. These results open new opportunities in the preparation of highly selective hydrogenation catalysts.

4.5. SUPPORTING INFORMATION

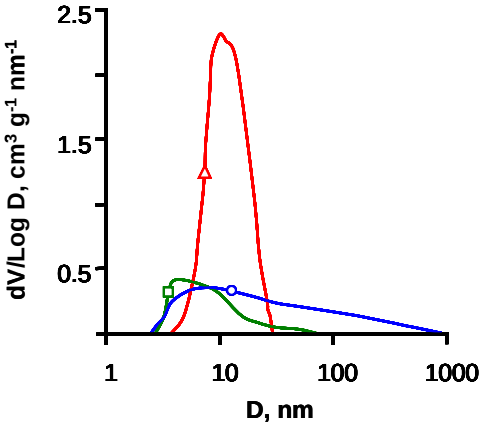

Figure S.4.1. Pore size distribution obtained by application of the BJH method to the N_2-adsorption isotherms. TiO_2 (—○—), SiO_2 (—△—) and Al_2O_3 (—□—).

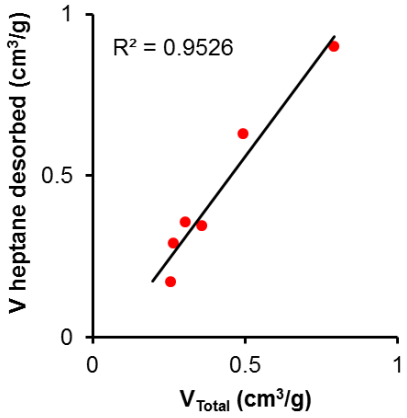

Figure S.4.2. Relationship between the total pore volume detected by N_2 adsorption and the solvent volume evolved after reaction for some supports and catalysts.

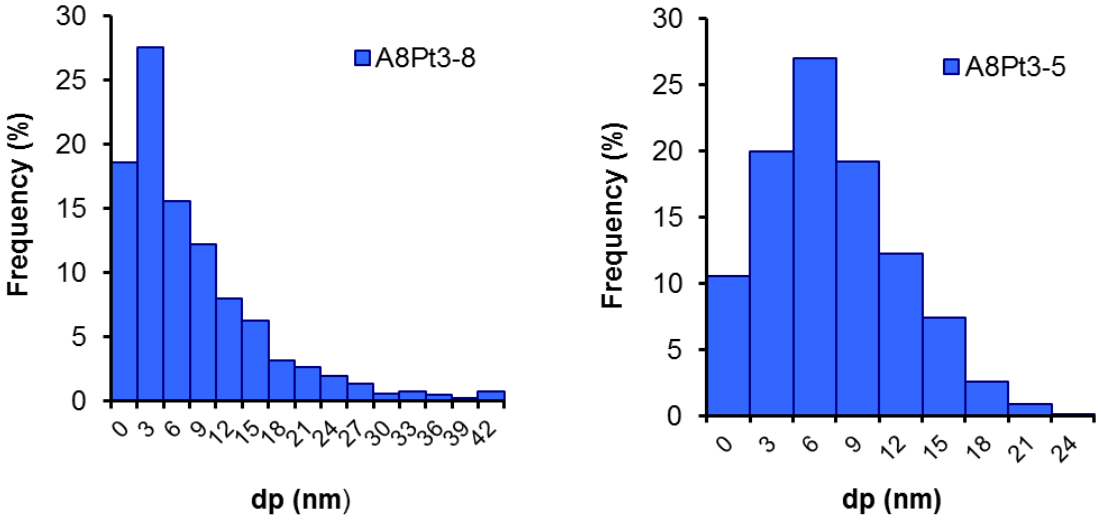

Figure S.4.3. Pt-particle size distribution obtained from TEM images after pretreatment of A8Pt3 catalysts in H_2 flow (A8Pt3-8) and He flow (A8Pt3-5).

4.6. REFERENCES

[1] T. Ekou, A. Vicente, G. Lafaye, C. Especel, and P. Marecot. Bimetallic Rh-Ge and Pt-Ge catalysts supported on TiO_2 for citral hydrogenation I. Preparation and characterization of the catalysts, *Applied Catalysis A-General* **314**(1), 64, 2006.

[2] F. Delbecq and P. Sautet. Competitive C=C and C=O Adsorption of α,β–Unsaturated Aldehydes on Pt and Pd Surfaces in Relation with the Selectivity of Hydrogenation Reactions: A Theoretical Approach, *Journal of Catalysis* **152**(2), 217, 1995.

[3] T. Ekou, L. Ekou, A. Vicente, G. Lafaye, S. Pronier, C. Especel, and P. Marecot. Citral hydrogenation over Rh and Pt catalysts supported on TiO_2: Influence of the preparation and activation protocols of the catalysts, *Journal of Molecular Catalysis A-Chemical* **337**(1-2), 82, 2011.

[4] A.E. Edris. Pharmaceutical and therapeutic potentials of essential oils and their individual volatile constituents: A review, *Phytotherapy Research* **21**(4), 308, 2007.

[5] M. Eisenacher, S. Beschnitt, and W. Hölderich. Novel route to a fruitful mixture of terpene fragrances in particular phellandrene starting from natural feedstock geraniol using weak acidic boron based catalyst, *Catalysis Communications* **26**(0), 214, 2012.

[6] J. Groling, *ullmann's encyclopedia of industrial chemistry*, Seven ed. (Electronic Release, Weinheim, 2003).

[7] S.C. Rastogi, J.D. Johansen, and T. Menné. Natural ingredients based cosmetics. Content of selected fragrance sensitizers, *Contact Dermatitis* **34**(6), 423, 1996.

[8] S.C. Rastogi, J.D. Johansen, P. Frosch, T. Menne, M. Bruze, J.P. Lepoittevin, B. Dreier, K.E. Andersen, and I.R. White. Deodorants on the European market: quantitative chemical analysis of 21 fragrances, *Contact Dermatitis* **38**(1), 29, 1998.

[9] S.C. Rastogi, S. Heydorn, J.D. Johansen, and D.A. Basketter. Fragrance chemicals in domestic and occupational products, *Contact Dermatitis* **45**(4), 221, 2001.

[10] K. Sato, S. Krist, and G. Buchbauer. Antimicrobial effect of vapours of geraniol, (R)-(−)-linalool, terpineol, γ–terpinene and 1,8-cineole on airborne microbes using an airwasher, *Flavour and Fragrance Journal* **22**(5), 435-437, 2007.

[11] T. Ekou, A. Vicente, G. Lafaye, C. Especel, and P. Marecot. Bimetallic Rh-Ge and Pt-Ge catalysts supported on TiO_2 for citral hydrogenation II. Catalytic properties, *Applied Catalysis A-General* **314**(1), 73, 2006.

[12] P. Barbaro and F. Liguori, *heterogenized homogeneous catalysts for fine chemicals production: materials and processes* (Springer, 2010).

[13] J. Aumo, S. Oksanen, J.P. Mikkola, T. Salmi, and D.Y. Murzin. Hydrogenation of citral over activated carbon cloth catalyst, *Industrial & Engineering Chemistry Research* **44**(14), 5285-5290, 6-7-2005.

[14] E. Bailón-García, F.J. Maldonado-Hódar, A.F. Pérez-Cadenas, and F. Carrasco-Marín. Catalysts Supported on Carbon Materials for the Selective Hydrogenation of Citral, *Catalysts* **3**(4), 853, 2013.

[15] A. Giroir-Fendler, D. Richard, and P. Gallezot. Selectivity in cinnamaldehyde hydrogenation of group-VIII metals supported on graphite and carbon, *Studies in Surface Science and Catalysis* **41**(C), 171, 1988.

[16] U.K. Singh and M.A. Vannice. Liquid-phase citral hydrogenation over SiO_2-supported group VIII metals, *Journal of Catalysis* **199**(1), 73, 2001.

[17] S. Santiago-Pedro, V. Tamayo-Galván, and T. Viveros-García. Effect of the acid–base properties of the support on the performance of Pt catalysts in the partial hydrogenation of citral, *Catalysis Today* **213**(0), 101, 2013.

[18] T. Ekou, C. Especel, and S. Royer. Catalytic performances of large pore Ti-SBA15 supported Pt nanocomposites for the citral hydrogenation reaction, *Catalysis Today* **173**(1), 44, 2011.

[19] T. Ekou, A. Flura, L. Ekou, C. Especel, and S. Royer. Selective hydrogenation of citral to unsaturated alcohols over mesoporous Pt/Ti-Al_2O_3 catalysts. Effect of the reduction temperature and of the Ge addition, *Journal of Molecular Catalysis A-Chemical* **353**, 148, 2012.

[20] J. Alvarez-Rodríguez, I. Rodríguez-Ramos, A. Guerrero-Ruiz, E. Gallegos-Suarez, and A. Arcoya. Influence of the nature of support on Ru-supported catalysts for selective hydrogenation of citral, *Chemical Engineering Journal* **204-205**, 169, 2012.

[21] G. Neri, L. Mercadante, C. Milone, R. Pietropaolo, and S. Galvagno. Hydrogenation of citral and cinnamaldehyde over bimetallic Ru-Me/Al_2O_3 catalysts, *Journal of Molecular Catalysis A: Chemical* **108**(1), 41, 1996.

[22] G. Neri, C. Milone, A. Donato, L. Mercadante, and A.M. Visco. Selective Hydrogenation of Citral Over Pt-Sn Supported on Activated Carbon, *Journal of Chemical Technology and Biotechnology* **60**(1), 83, 1994.

[23] V. Ponec. On the role of promoters in hydrogenations on metals; α,β−unsaturated aldehydes and ketones, *Applied Catalysis A: General* **149**(1), 27, 1997.

[24] N.M. Bertero, A.F. Trasarti, B. Moraweck, A. Borgna, and A.J. Marchi. Selective liquid-phase hydrogenation of citral over supported bimetallic Pt-Co catalysts, *Applied Catalysis A-General* **358**(1), 32, 2009.

[25] C. Moreno-Castilla and F.J. Maldonado-Hódar. Carbon aerogels for catalysis applications: An overview, *Carbon* **43**(3), 455, 2005.

[26] F.J. Maldonado-Hódar. Advances in the development of nanostructured catalysts based on carbon gels, *Catalysis Today* **218–219**(0), 43, 2013.

[27] B.F. Machado, S. Morales-Torres, A.F. Pérez-Cadenas, F.J. Maldonado-Hódar, F. Carrasco-Marín, A.M.T. Silva, J.L. Figueiredo, and J.L. Faria. Preparation of carbon aerogel supported platinum catalysts for the selective hydrogenation of cinnamaldehyde, *Applied Catalysis A: General* **425–426**(0), 161, 2012.

[28] S. Morales-Torres, F.J. Maldonado-Hódar, A.F. Pérez-Cadenas, and F. Carrasco-Marín. Textural and mechanical characteristics of carbon aerogels synthesized by polymerization of resorcinol and formaldehyde using alkali carbonates as basification agents, *Physical Chemistry Chemical Physics* **12**(35), 10365, 2010.

[29] E. Gallegos-Suárez, A.F. Pérez-Cadenas, F.J. Maldonado-Hódar, and F. Carrasco-Marín. On the micro- and mesoporosity of carbon aerogels and xerogels. The role of the drying conditions during the synthesis processes, *Chemical Engineering Journal* **181–182**(0), 851, 2012.

[30] S. Brunauer, P.H. Emmett, and E. Teller. Adsorption of Gases in Multimolecular Layers, *Journal of the American Chemical Society* **60**(2), 309-319, 1-2-1938.

[31] M.M. Dubinin. Generalization of the theory of volume filling of micropores to nonhomogeneous microporous structures, *Carbon* **23**(4), 373, 1985.

[32] MM. Dubinin. Contemporary state of the theory of volume filling of micropores of adsorbents in the adsorption of gases and vapors on carbon adsorbents, *Russian Journal of Physical Chemestry* **39**, 1305, 1965.

[33] F. Stoeckli, *porosity in carbons - characterization and applications* (Arnold, London, 1995).

[34] E.P. Barrett, L.G. Joyner, and P.P. Halenda. The Determination of Pore Volume and Area Distributions in Porous Substances. I. Computations from Nitrogen Isotherms, *Journal of the American Chemical Society* **73**(1), 373-380, 1-1-1951.

[35] R. Ubago-Pérez, F. Carrasco-Marín, D. Fairén-Jiménez, and C. Moreno-Castilla. Granular and monolithic activated carbons from KOH-activation of olive stones, *Microporous and Mesoporous Materials* **92**(1–3), 64, 2006.

[36] J.E. Benson and M. Boudart. Hydrogen-oxygen titration method for the measurement of supported platinum surface areas, *Journal of Catalysis* **4**(6), 704, 1965.

[37] G.R. Wilson and W.K. Hall. Studies of the hydrogen held by solids: XVIII. Hydrogen and oxygen chemisorption on alumina- and zeolite-supported platinum, *Journal of Catalysis* **17**(2), 190, 1970.

[38] C.A. Leon, J.M. Solar, V. Calemma, and L.R. Radovic. Evidence for the protonation of basal plane sites on carbon, *Carbon* **30**(5), 797, 1992.

[39] D. Cazorla-Amorós, J. Alcañiz-Monge, and A. Linares-Solano. Characterization of Activated Carbon Fibers by CO_2 Adsorption, *Langmuir* **12**(11), 2820, 1996.

[40] A. Gervasini and A. Auroux. Acidity and basicity of metal oxide surfaces II. Determination by catalytic decomposition of isopropanol, *Journal of Catalysis* **131**(1), 190, 1991.

[41] G.S. Walker, E. Williams, and A.K. Bhattacharya. Preparation and characterization of high surface area alumina-titania solid acids, *Journal of Materials Science* **32**(21), 5583, 1997.

[42] S. Nair, A.H.M. Shahadat Hussain, and B.J. Tatarchuk. The role of surface acidity in adsorption of aromatic sulfur heterocycles from fuels, *Fuel* **105**(0), 695, 2013.

[43] D.M.A. Melo, J.A.C. Ruiz, E.V. Sobrinho, M.A.F. Melo, A.E. Martinelli, and L.B. Zinner. Determination of relative acid strength of La/paligorskyte by n-butylamine, *Journal of Solid State Chemistry* **171**(1–2), 217, 2015.

[44] J. Zawadzki. Infrared studies on the adsorption of n-butylamine on carbon films, *Carbon* **26**(2), 183, 1988.

[45] D.M. Araújo Melo, J.A.C. Ruiz, M.A.F. Melo, E.V. Sobrinho, and A.E. Martinelli. Preparation and characterization of lanthanum palygorskite clays as acid catalysts, *Journal of Alloys and Compounds* **344**(1–2), 352, 2002.

[46] F.J. Maldonado-Hódar, C. Moreno-Castilla, and A.F. Pérez-Cadenas. Catalytic combustion of toluene on platinum-containing monolithic carbon aerogels, *Applied Catalysis B: Environmental* **54**(4), 217, 2004.

[47] S. Morales-Torres, F.J. Maldonado-Hódar, A.F. Pérez-Cadenas, and F. Carrasco-Marín. Design of low-temperature Pt-carbon combustion catalysts for VOC's treatments, *Journal of Hazardous Materials* **183**(1-3), 814, 2010.

[48] B.M. Reddy, B. Chowdhury, E.P. Reddy, and A. Fernández. An XPS study of dispersion and chemical state of MoO_3 on Al_2O_3-TiO_2 binary oxide support, *Applied Catalysis A: General* **213**(2), 279, 2001.

[49] T. Zheng, J. He, Y. Zhao, W. Xia, and J. He. Precious metal-support interaction in automotive exhaust catalysts, *Journal of Rare Earths* **32**(2), 97, 2014.

[50] P. Claus. Selective hydrogenation of α,β–unsaturated aldehydes and other C=O and C=C bonds containing compounds, *Topics in Catalysis* **5**(1), 51, 1998.

[51] A. Giroir-Fendler, D. Richard, and P. Gallezot. Chemioselectivity in the catalytic hydrogenation of cinnamaldehyde. Effect of metal particle morphology, *Catalysis Letters* **5**(2), 175, 1990.

[52] M. Englisch, A. Jentys, and J.A. Lercher. Structure Sensitivity of the Hydrogenation of Crotonaldehyde over Pt/SiO_2 and Pt/TiO_2, *Journal of Catalysis* **166**(1), 25, 1997.

[53] U.K. Singh, M.N. Sysak, and M.A. Vannice. Liquid-Phase Hydrogenation of Citral over Pt/SiO_2 Catalysts: II. Hydrogenation of Reaction Intermediate Compounds, *Journal of Catalysis* **191**(1), 181, 2000.

[54] S. Nishiyama, T. Hara, S. Tsuruya, and M. Masai. Infrared Spectroscopy Study of Aldehydes Adsorbed on Rh–Sn Bimetallic Systems: Selective Activation of Aldehydes by Tin, *The Journal of Physical Chemistry B* **103**(21), 4431, 1999.

[55] H.J. Jiang, H.B. Jiang, D.M. Zhu, X.L. Zheng, H.Y. Fu, H. Chen, and R.X. Li. Cooperation between the surface hydroxyl groups of the support and organic additives in the highly selective hydrogenation of citral, *Applied Catalysis A: General* **445-446**, 351, 2012.

[56] J. Alvarez-Rodríguez, A. Guerrero-Ruiz, I. Rodríguez-Ramos, and A. Arcoya-Martin. Surface and structural effects in the hydrogenation of citral over RuCu/KL catalysts, *Microporous and Mesoporous Materials* **97**(1-3), 122, 2006.

Capítulo V

THE INFLUENCE OF THE PRETREATMENT CONDITIONS ON THE DEVELOPMENT AND PERFORMANCE OF ACTIVE SITES OF Pt/TiO_2 CATALYSTS USED FOR THE SELECTIVE HYDROGENATION OF CITRAL

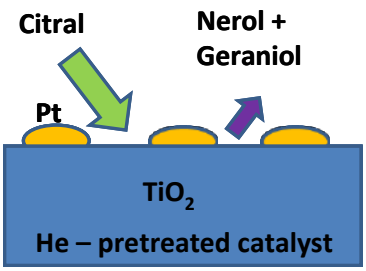

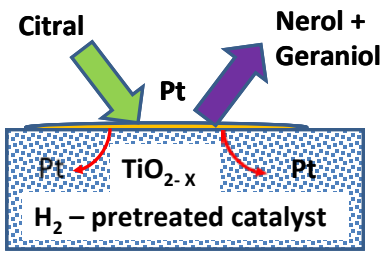

THE INFLUENCE OF THE PRETREATMENT CONDITIONS ON THE DEVELOPMENT AND PERFORMANCE OF ACTIVE SITES OF Pt/TiO_2 CATALYSTS USED FOR THE SELECTIVE HYDROGENATION OF CITRAL

Manuscript submitted to Journal of Catalysis

Highlights

- Pretreatment conditions determine the performance of Pt/TiO_2 catalysts
- Pretreatment in H_2-flow enhances both activity and selectivity
- The stronger Pt-sintering occurs in He-flow, leading to a low performance.
- H_2-pretreatment induces the formation of oxygen vacancies and Pt-nanoparticles
- Active and selective sites for citral hydrogenation are formed during H_2-pretreatment.

Abstract

The influence of pretreatment conditions of Pt/TiO_2 catalysts was analyzed by different techniques and changes in the textural and chemical properties correlated with the catalytic performance in citral hydrogenation. After H_2-pretreatment the formation of two-dimensional Pt-nanoparticles and oxygen vacancies favours the diffusion of Pt-species into the TiO_2 structure, while three-dimensional Pt-crystallites are formed after He-pretreatment. The coupled effect of Pt-2D nanoparticles and oxygen vacancies strongly enhances the catalytic activity and the selective hydrogenation of citral to unsaturated alcohols by favouring the citral adsorption on the reduced surface through the terminal C=O groups in an environment rich in hydrogen provided by the highly dispersed Pt-nanoparticles. These coupled metal – vacancy active sites are formed also after a combined He/H_2-pretreatment, nevertheless, the formation of 3-dimensional Pt-particles during the previous He treatment strongly reduces the extent of TiO_2-Pt interface and consequently the surface site concentration and the catalytic activity.

5.1. INTRODUCTION

Citral (3,7-dimethyl-2,6-octadienal) is an isomeric mixture of the acyclic aldehydes geranial (citral E) and neral (citral Z). The demand of their derivatives unsaturated alcohols (UA), geraniol and nerol by chemical, pharmaceutical or perfumery industries, progressively increases. Citral is found in plants and citrus fruits but very recently comes to be produced petrochemically in very large quantities[1]. Although geraniol can be isolated from palmarosa oil and nerol was obtained from the oil of nerol[2,3], the selective hydrogenation of citral is one of the more feasible ways to obtain these unsaturated alcohols at large scale.

Nevertheless, in the selective hydrogenation of α,β-unsaturated aldehydes thermodynamic and kinetic factors favour the hydrogenation of the conjugated C=C over the C=O bond[4], and thus, the saturated aldehyde or alcohol are mainly obtained. In addition, secondary reactions of hydrogenation, isomerization, cyclization or cracking also take place leading to a complex reaction pathway[5]. The challenge is to selectively enhance the hydrogenation of the C=O bond to UA, which can only be achieved by an optimal design of the catalyst. Different approaches for this objective were previously published, by studying the influence of supports[6-8], active phases[9,10] and the interactions between them[6,11,12].

The nature and effect of the strong metal-support interactions (SMSI) were early shown by Tauster and Fung[13] and related with the support reducibility. Nevertheless, SMSI is even today a matter of discussion and generates a field of great research interest in the development of selective hydrogenation catalysts. In this sense, recently the influence of impregnation procedures and pre-treatments at different temperatures (300 vs 500 ºC) in H_2 flow of Pt/TiO_2 and Rh/TiO_2 catalysts used in the citral hydrogenation was described[14]. It is suggested that with increasing temperature, conversion decreases but selectivity to UA increases as a consequence of the formation of TiO_{2-X} species (no identified), because these effects were not observed using the same active phases on non-reducible Al_2O_3 as support[15]. It was also suggested[16] that the improved hydrogenation performance of Pt-catalysts using TiO_2/SiO_2 composite as support regarding pure TiO_2 is due to a stronger SMSI effect in the first case, because

the formation of anatase nano-crystallites facilitates the interactions with Pt after reduction.

These works are focused mainly on catalytic results but there is a lack of information about the chemical and structural modifications caused by pretreatments, the identification of Pt-species on reduced TiO_2 surfaces and the influence of such species on the catalytic performance. In this manuscript, we analyze by different techniques Pt/TiO_2 catalysts before and after pre-treatments in different experimental conditions. The structural and chemical changes detected are related with the catalytic performance obtained.

5.2. EXPERIMENTAL

5.2.1. Preparation of the catalysts

Commercial TiO_2 (anatase, Alfa Aesar) without additional treatments was milled and sieved to a diameter smaller than 0.150 mm before impregnation. Platinum catalysts were prepared by impregnation at 3 wt % Pt-loading using an aqueous solution containing the appropriate amount of $[Pt(NH_3)_4]Cl_2$, dried and finally pre-treated in He or H_2 flow at 400 °C (heating rate of 5 °C/min) for 12 h. An alternative pre-treatment where the precursor salt is decomposed initially for 2 h at 400 °C in He and after that treated in H_2 flow for additional 10 h was also carried out. Catalysts were referred indicating the reduction treatment. Thus, as an example, Pt/TiO_2-He indicates that Pt was deposited on TiO_2 support and pretreated in He flow.

5.2.2. Textural and chemical characterization

Textural characterization was carried out by N_2 adsorption at −196 °C using a Quantachrome Autosorb-1 equipment. The BET equation was applied to the N_2-adsorption isotherms to determine the apparent surface area (S_{BET}) and the Dubinin–Radushkevich and Stoeckli equations[17-20] applied to determine the micropore volume (W_0) and the average micropore width (L_0). The total pore volume (V_{Total}) was considered[21] as the volume of N_2 adsorbed at $P/P_0 = 0.95$ and the mesopore volume (V_{meso}) consequently calculated by difference.

Pt dispersion (D) and average particle size (d) were obtained by x-ray diffraction (XRD), H_2-chemisorption and high-resolution transmission electron microscopy (HRTEM). Chemisorption isotherms were measured in conventional volumetric equipment. Equilibrium pressure was measured with a precision of 0.1 mbar. 0.250 g of the supported catalyst was pretreated as described above and outgassed at 350 °C for 1 h. Subsequently, it was cooled down to 25 °C and a H_2 adsorption isotherm was measured between 70 and 350 mbar. H_2 uptake was determined from the intercept of the linear adsorption isotherm. Platinum dispersion, *D*, namely the ratio between surface (M_S) and total metal atoms (M_T), and the average Pt-particle size, $\bar{d}(\text{nm}) = \frac{1.08}{D}$, were obtained from the H_2 uptake assuming respectively a stoichiometric ratio H_2:Pt = 1:2 (dissociative chemisorption) and the formation of spherical particles[22,23].

HRTEM images were recorded using a FEI TITAN G2 80 - 300 microscope equipped with a scanning transmission electron microscopy (STEM) detector type HAADF (high-angle annular dark-field detector), corrector of spherical aberration (CEOS) and EDX microanalysis system (Super X). This equipment has a maximum resolution of 0.8 Å (TEM) or 1.4 Å (STEM); working with an acceleration voltage of 300 kV. A small amount of well milled catalysts is dispersed in ethanol under ultrasound and mounted on a 300 mesh carbon-coated cooper grid. Always more than 100 Pt-particles were analyzed by the appropriate software in order to obtain the particle size distributions and the average particle size.

X-ray diffraction (XRD) pattern were recorded using a Bruker D8 Advance X-ray diffractometer with Cu Kα radiation. The 2θ angles were scanned from 10 to 90°. The average Pt crystallite sizes (D) were estimated by the application of the Debye-Scherer formula, $D = 0.95\lambda/\beta \cos\theta$ to the {111} peak of platinum, where θ is the diffraction angle and β is the full width at half-maximum (fwhm). The fwhm was determined with an extrapolated baseline between the beginning (low angle side) and the end (high-angle side) of a diffraction peak with the highest intensity.

The chemical characterization of the catalysts was further analyzed by X-ray photoelectron spectroscopy (XPS). The spectra were obtained on a Kratos Axis Ultra-

DLD X-ray photoelectron spectrometer equipped with a hemispherical electron analyser connected to a detector DLD (delay-line detector). For these measurements, the binding energy (BE) values were referred to the C_{1s} peak at 284.6 eV and the Pt_{4f}, O_{1s} and Ti_{2p} spectral regions were scanned several times to obtain good signal-to-noise ratios. The spectra obtained after a background signal correction were fitted to Lorentzian and Gaussian curves in order to obtain the number of components, the position of each peak and the peak areas. Finally, all the components were assigned according to the bibliography[24-27].

Information about the support acidity was obtained by measuring the pH_{pzc}, according to the methodology previously described[28] and the strength and amount of acid sites of pretretated catalyst studied by n-butylamine adsorption/desorption (TPD) experiments. Dynamic adsorption / desorption tests (TPD) were carried out in a quartz microreactor at atmospheric pressure with 0.2 g of sample using a He/Ar flow (total flow rate 60 cm^3 min^{-1}) saturated with n-butylamine at 0 °C (partial pressure of n-butylamine 28.92 Torr). Analyses were carried out on-line with a Mass Spectometer model Prisma (Pfeiffer). Samples were heated in pure He flow up to the adsorption temperature (150 °C) and after stabilization, the He flow was turned up by the saturated He/Ar flow to sample saturation (the n-butylamine concentration is recovered). After that, the saturated sample was purged in pure He for 1 h to remove the rest of trapped n-butylamine, and then, TPD-n-butylamine was recorded by heating at 10 °C/min.

5.2.3. Catalytic performance

The citral hydrogenation was carried out in 100 ml heptane solution at a constant hydrogen pressure of 8.3 bar and 90 °C using a Parr reactor model 5500. The experimental conditions: citral concentration, catalyst weight and agitation speed were previously optimized in order to avoid mass transfer limitations (results not shown) and fixed in 0.05 M, 500 mg and 1500 rpm, respectively. A small volume of sample (1 mL) was periodically withdrawn and analysed by chromatography using a Bruker 430-GC equipped with a FID detector and a Varian GC Capillary Column CP7485 (25 m x 0.32 mm x 0.45 μm). Citral and any possible product were previously calibrated.

5.3. RESULTS AND DISCUSSION

The catalytic performance after reduction of Pt/TiO_2 in pure He or H_2 flow, and the combined reduction cycle (He/H_2), is compared in Figure 5.1. Clearly, both activity and selectivity are strongly favoured after H_2-pretreatment, in such a manner that a total conversion is achieved after 6 h of reaction with unusual high values of selectivity to UA (S_{UA}, at around 80%) for monometallic Pt-catalysts, which normally do not exceed S_{UA} values of 50-55%[5]. Selectivity values only decay at conversions greater than 80%, where secondary hydrogenations are favoured. On the contrary, the smallest activity and selectivity values are detected after pre-treatment in He-flow. Moreover, in this case, S_{UA} decreases even at significantly low conversion values (Figure 5.1), indicating that secondary reactions are favoured. In the case of the combined He/H_2-pretreatment, while the catalytic activity is similar to one the obtained after the He-pretreatment, the selectivity values are quite similar those obtained after H_2-pretreatment. This combined pretreatment points out that, while the number of active sites (activity) is determined by the previous He-pretreatment, the nature of the selective hydrogenation sites is determined by the H_2-pretreatment. This means that H_2-pretreatment generates some transformations that activate specifically the catalyst surface favouring the hydrogenation of citral to UA.

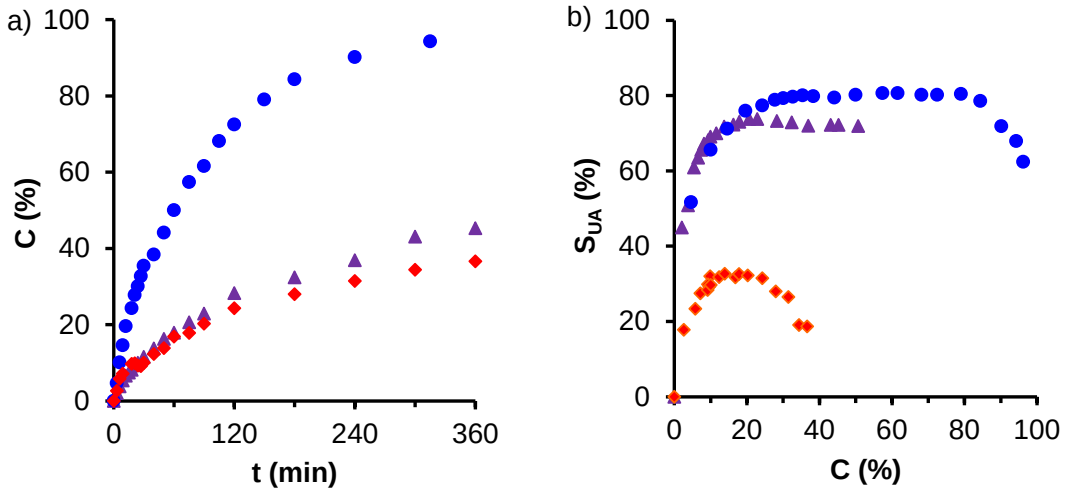

Figure 5.1. Influence of pretreatment conditions on the catalytic performance of Pt/TiO_2 catalysts a) Evolution of the conversion with reaction time b) selectivity to unsaturated alcohols with increasing conversion values. Pt/TiO_2-He, (◆), Pt/TiO_2-H_2 (●) and Pt/TiO_2-He, H_2 (▲).

It is noteworthy that S_{UA} initially increases independently of the pretreatment used (Figure 1b), this means that there is always an induction period where the active sites are progressively accommodated to the reaction development. This fact can be related with the total product distribution obtained in each case (Figure 5.2). Thus it is observed that after He-pretreatment, initially the stronger active sites produce the preferential hydrogenation of C=C bonds (to citronellal) and cracking of the citral molecules, but these sites are progressively deactivated. Cracking reactions are induced by the support acidity[29]. Simultaneously, citronellal is transformed by secondary hydrogenation or cyclization reactions to citronellol or menthol and isopulegol respectively. After 2h of reaction also the S_{UA} decreases because they are also transformed into citronellol. However, after H_2-pretreatment, UA are always the main reaction product obtained, denoting the different nature of the active sites and the different interaction of the catalyst surface with the citral molecules, that in this case are hydrogenated through the C=O bonds. The increase of S_{UA} during the induction period is also due to the deactivation of the C=C hydrogenation sites, while cracking are significantly reduced, because this preatreament also leads to an acidity decrease, as shown below. After that, the product distribution becomes very stable and only citronellol slowly increases at high conversion values by hydrogenation of UA. However, it is noteworthy that these secondary processes develop in a smaller proportion than in the previous case, denoting the weak interaction of the C=C bonds with these active sites. The products distribution obtained after He-H_2 pretreatment is quite similar to that obtained after H_2-pretreatment, in spite that the catalytic activity is considerably smaller. Thus, as commented, the nature of active sites seems to be similar but they are present in a smaller proportion.

Different factors can influence this catalytic behaviour; thus, textural properties and acidity of catalysts, and Pt-nature and dispersion, were carefully analyzed. Textural parameters can influence the citral adsorption mode and/or the adsorption capacity. In a previous paper[30] it was suggested that in order to increase the selectivity towards unsaturated alcohols, geometrical effects derived from the zeolite pore size and shape and location of ruthenium particles in the KL structure are more effective than the electronic modifications induced by electron-donor supports. Textural parameters obtained from the analysis of the N_2 adsorption isotherms are summarized in Table 5.1. The BET surface area of pre-treated catalysts are quite similar to the BET surface of the

support, but the total pore volume ($V_{0.95}$) slightly decreases by certain porous blockage caused by the Pt-nanoparticles loaded. This blockage takes place mainly in the mesopore range (V_{meso} decreased) where Pt-nanoparticles should be located, although this also leads to more narrow micropores (L_0). Nevertheless, the textural parameters determined for pretreated catalysts show similar values between them, and therefore the variations of the catalytic behaviour seem not to be due to textural changes after the different pretreatments. Moreover, the mesoporous character of the support avoids the development of steric restriction that could favour a preferential adsorption mode.

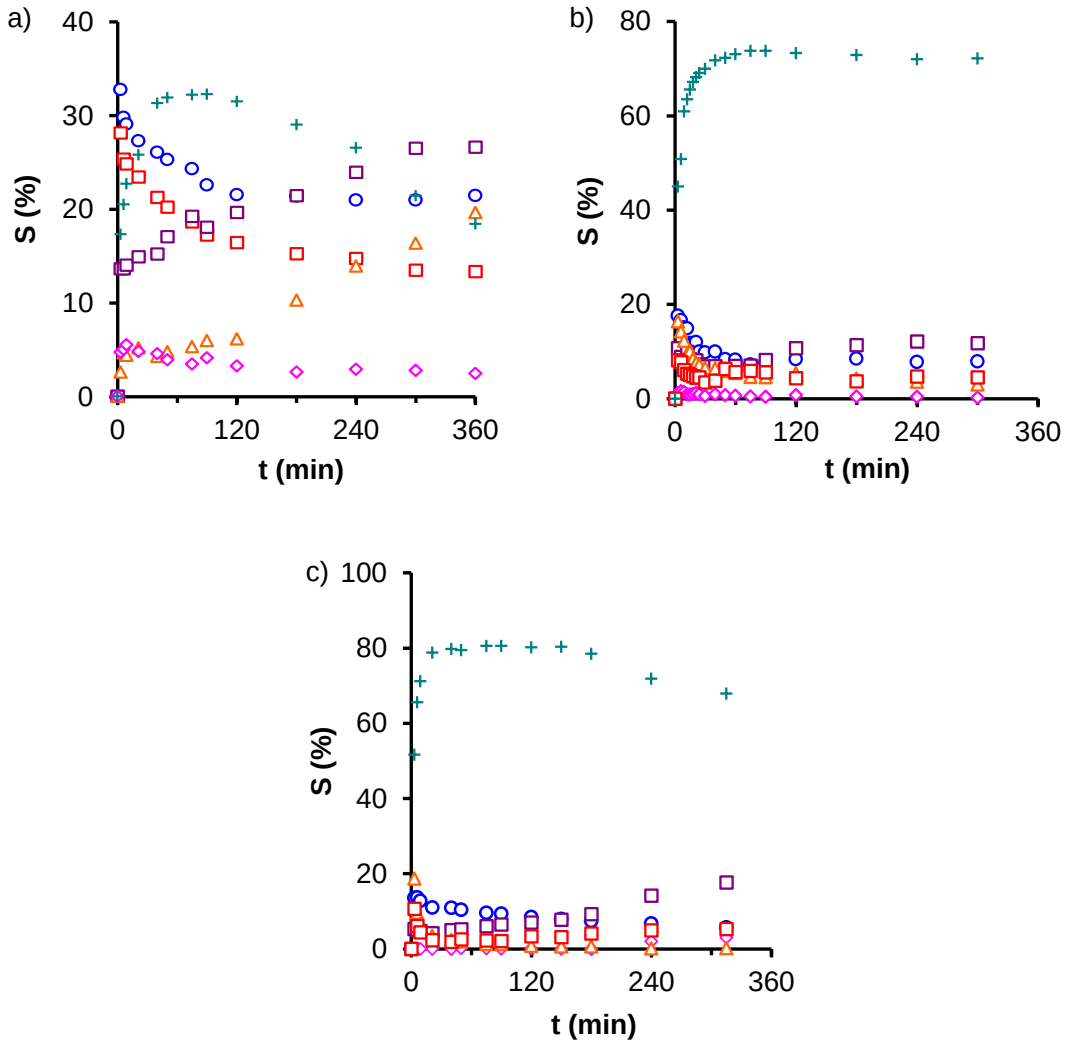

Figure 5.2. Product distribution along the reaction development: a) Pt/TiO_2-He, b) Pt/TiO_2-He,H_2 and c) Pt/TiO_2-H_2 **.** Citronellal (○), S_{UA} (+), Cyclization = isopulegol + menthol (△), citronellol (□), 3,7 DMO (◇), cracking (□). Reaction conditions: citral in heptane solution (0.05M), 500 mg of catalyst, 1500 rpm, 90 ºC and P_{H_2} = 8.3 bar.

Table 5.1. Textural parameters of pretreated Pt/TiO_2 catalysts obtained from N_2-adsorption isotherms.

Catalyst	S_{BET}	W_0	L_0	V_{meso}	$V_{0.95}$
	m^2g^{-1}	cm^3g^{-1}	nm	cm^3g^{-1}	
TiO_2	116	0.047	1.89	0.446	0.493
Pt/TiO_2 -He	115	0.040	1.65	0.397	0.437
Pt/TiO_2 –He-H_2	94	0.032	1.64	0.412	0.444
Pt/TiO_2 –H_2	111	0.045	1.62	0.397	0.442

S_{BET}: BET surface area, W_0: micropore volume, L_0: micropore width, V_{meso}: mesopore volume and $V_{0.95}$: Total pore volume.

The catalytic performance is also related with the catalysts acidity and the strength of the acid sites. We have pointed out that the strong Brönsted acidity of Al_2O_3 favours the activity at the expense of a very high cracking selectivity regarding other inorganic supports[29]. However, recently it was also found that basic catalysts are more active and more selective to citronellal, while acid sites favour the formation of U[31].

To analyze the influence of Pt-precursor decomposition conditions on the acidity of the samples both TiO_2 support and impregnated catalysts were pre-treated in identical conditions. The pH_{pzc} of TiO_2 pretreated in He-flow remain practically constant regarding the untreated sample (Table 5.2), but this parameter increases significantly after pretreatment in H_2 showing the release of some acid sites. This effect is similar for samples pretreated under consecutive He/H_2-flows. Pre-treated catalysts are stronger acid materials than their supports pretreated in identical experimental conditions, indicating that Pt-loading generate new acid sites. This behaviour was previously observed by others authors[32]. Moreover, pretreatment atmosphere also influences the precursor decomposition and sintering[33]. Because in this study only TiO_2 is used as support and $[Pt(NH_3)_4]Cl_2$ as metal precursor, changes on the catalyst acidity only depend on the pretreatment conditions. The acidity of materials therefore is favoured by the presence of Pt and decreases in all cases after H_2-pretreatments, which is in agreement with the evolution of the products distribution previously discussed.

Results obtained from TPD of n-butylamine provide similar conclusions (Figure 5.3). In this experimental conditions (after saturation at 150 ºC to avoid physical adsorption of n-butylamine), it is observed that He-pretreated catalyst presents a higher acidity and a greater number of acid sites in all the temperature range (in all the range of acid strength), but moreover the position of the maximum shifted to lower desorption temperatures after pretreatment in H_2 (to weaker acid sites) which is also in agreement to conclusions obtained from pH_{pzc} measurements. The smaller acidity after H_2-pretreatment should favour the formation of citronellal[31], however, we obtained the most selective catalyst to UA in these conditions.

Table 5.2. Values of the pH_{pzc} of pretreated supports and catalysts.

Pretreatment	TiO_2 support	Pt/TiO_2 catalyst
none	4.90	-
400 ºC 12 h He	4.87	2.44
400 ºC 2 h He, 10 h H_2	6.48	3.92
400 ºC 12 h H_2	6.36	3.62

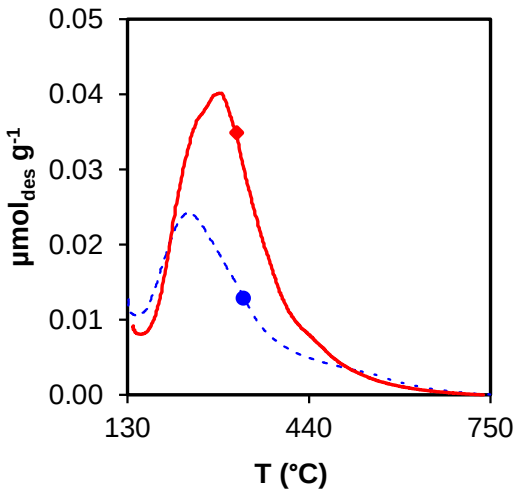

Figure 5.3. TPD of n-butylamine after saturation at 150 ºC. (●) Pt/TiO_2-H_2 (♦)Pt/TiO_2-He

The chemical characteristics of the catalysts surface were analyzed also by XPS. Some of the results obtained for TiO_2 and Pt characterization are summarized in Tables 5.3 and 5.4, respectively. Regarding TiO_2 (Table 5.3), the deconvolution of the Ti_{2p}

spectral region of untreated and He-pretreated samples only show a component at binding energy BE = 459.5 eV, corresponding to Ti^{+4} species while two components, at 530.8 and 532.5 eV were used to fit the O_{1s} spectral region. The major component of O_{1s} spectral region corresponds to the 'bulk' oxygen atom in the stoichiometric TiO_2 form, while the high BE component could correspond to various oxygen-containing surface functional groups[25]. Mainly hydroxyl (–OH) or bridge surface oxygen (Ti-O-Ti) groups were described[27]. It is noteworthy that in spite of the surface oxygen content is maintained after the He-pretreatment regarding untreated support (Table 5.3), the component at high BE significantly decreases regarding the untreated catalysts, which is consistent with the hydroxyl removal from TiO_2 by heating[26]. However, after the H_2-pretreatment, the oxygen content of the support significantly decreases (around 25% of the initial value) and simultaneously, new components are needed to fit both the O_{1s} and Ti_{2p} spectral regions (Table 5.3 and Figure 5.4). In both cases BE are shifted to lower values indicating an electronic enrichment (reduction). The Ti_{2p} component at 457.9 eV and 456.5 eV were assigned to the presence of Ti^{+3} and even Ti^{+2} species respectively (Figure 5.4), in agreement to the BE values previously published[24]. These results are also in agreement with the release of acid sites previously described and the formation of oxygen vacancies. However, and although different authors use the FTIR analysis to point out the release of hydroxyl groups from TiO_2 or their location in different environment[34,35] our FTIR spectra (data not shown) of pretreated catalysts are similar between them and do not permit the establishment of conclusions.

The XPS analysis also shows the chemical state and surface concentration of Pt-species. The results from the analysis of the Pt_{4f} spectral region are collected in Table 5.4. Before pre-treatment, the Pt concentration determined is greater than the total Pt-loading (3% wt), showing certain Pt-enrichment on TiO_2 surface. In this case, only Pt^{2+} is detected, indicating that there is not auto-reduction of the precursor salt during impregnation. On the contrary, a similar mixture of Pt^0 and Pt^{+2} was detected after any catalyst pre-treatment. This fact can be due to the reoxidation of Pt species during storage, but also, can indicate that pretreatments are not strong enough to guarantee the total precursor reduction. After pretreatments, Pt-content (Pt_{XPS}) significantly decreases (around 50%) which can be related with Pt-sintering. Sintering seems to be slightly favoured by H_2-pretreatment, also in agreement with previous observations[33]. It is however noteworthy that the BE of both Pt^0 and Pt^{+2} species after H_2-pretreatment

appeared at BE around 0.5 eV higher than in the case of He-pretreated samples, showing therefore the contrary behaviour described for Ti and O species. This behaviour probably indicates some electronic transfer from Pt-particles to the support (a smaller electron density on the Pt-particles).

Table 5.3. Influence of pretreatments on the surface oxygen content, binding energy and percentage of the components used to fit the XPS Ti_{2p} and O_{1s} spectral regions of Pt/TiO_2 catalysts.

Catalyst	BE (eV) Ti_{2p}	Peak %	BE (eV) O_{1s}	Peak %	% O_{xps}
Pt/TiO_2	459.5	100	530.8	80	40.33
			532.5	20	
Pt/TiO_2-He	459.5	100	530.8	92	41.02
			532.2	8	
Pt/TiO_2-H_2	456.5	9	527.9	15	30.02
	457.9	21	529.3	21	
	459.2	69	530.7	57	
			532.2	7	

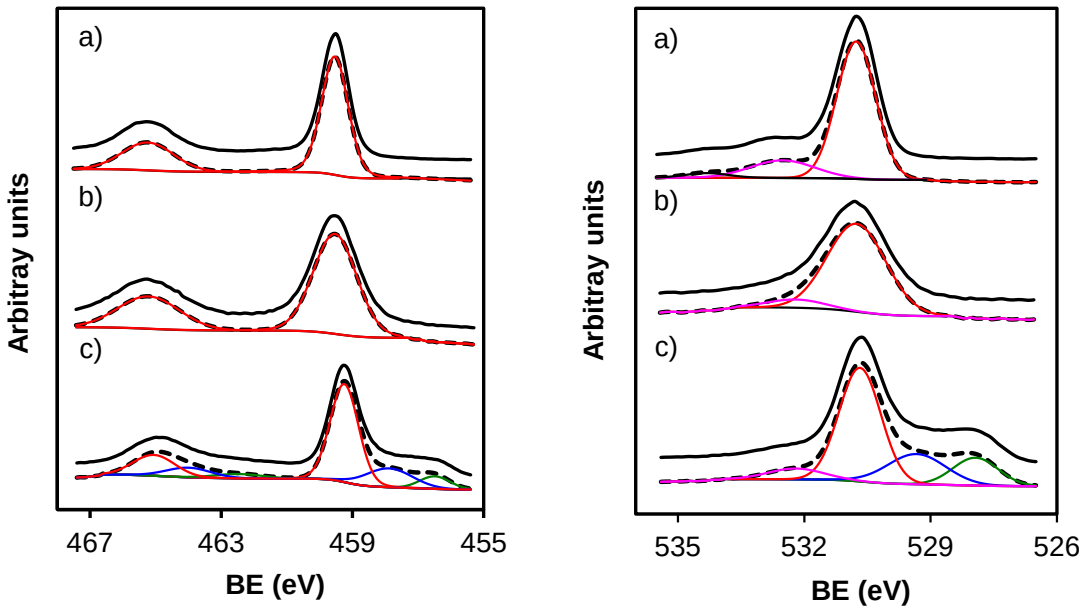

Figure 5.4. Survey and deconvolution of the XPS Ti_{2p} (left) and O_{1s} (right) spectral regions a) un-pretreated catalyst (Pt/TiO_2), b) He-pretreated catalyst (Pt/TiO_2-He) and c) H_2-pretreated catalyst (Pt/TiO_2-H_2).

These results are quite interesting, because in general, the opposite behaviour is assumed. Thus, the electronic enrichment of Pt-particles by electron-donor supports like graphite favours the UA selectivity of Pt-catalysts[9,36,37]. Thus, the active sites on Pt/TiO_2 catalyst generated during H_2-pretreatment and responsible of the S_{UA} enhanced have obviously a different nature than the exclusively metallic ones.

Table 5.4. Pt-surface concentration and distribution of Pt-species determined by XPS.

Catalyst	BE (eV) Pt^0	Pt (0) %	BE (eV) Pt^{2+}	Pt (II) %	Pt/Ti	Pt_{XPS} %Wt
Pt/TiO_2	-	-	72.9	100	0.019	4.2
Pt/TiO_2-He	70.9	68	71.5	32	0.007	2.0
Pt/TiO_2-H_2	71.5	73	72.0	27	0.007	1.9

*Pt/Ti atomic ratio; Pt_{xps} = surface Pt-concentration

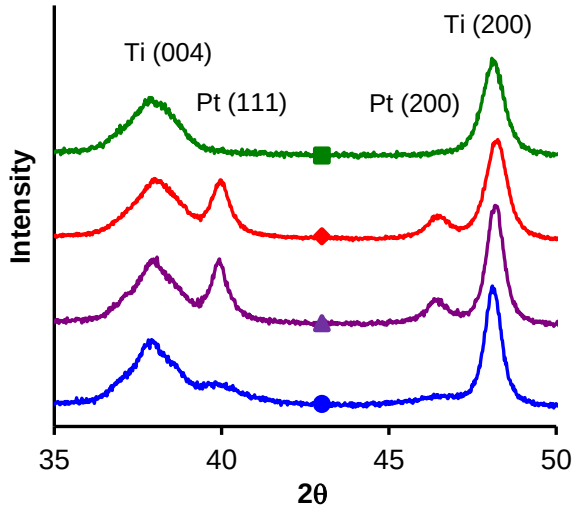

Figure 5.5. XRD patterns of TiO_2 support and pretreated Pt/TiO_2 catalysts. TiO_2 (■), Pt/TiO_2-He (◆), Pt/TiO_2-He,H_2 (▲) and Pt/TiO_2-H_2 (●).

When analyzing the pre-treated catalysts by XRD (Figure 5.5), it is noteworthy that the diffraction peaks corresponding to the TiO_2 phase do not present significant changes in both intensity and position, indicating that the surface reduction degree observed by XPS (Table 5.3) is not strong enough to significantly influence the crystallinity of the support. The major differences in the XRD patterns were observed for peaks at 39.7 and 46.3º corresponding to the Pt^0 (111) and (200) diffractions,

respectively. These peaks present a similar relative intensity and width after He or He/H_2 pretreatments, however both are broadened in such a way that only a small shoulder is appreciated after H_2-pretreatment. Because no additional diffraction peaks were detected, these results indicate smaller and/or no-crystalline Pt-particles. This fact must influence the catalytic performance shown in Figure 1.

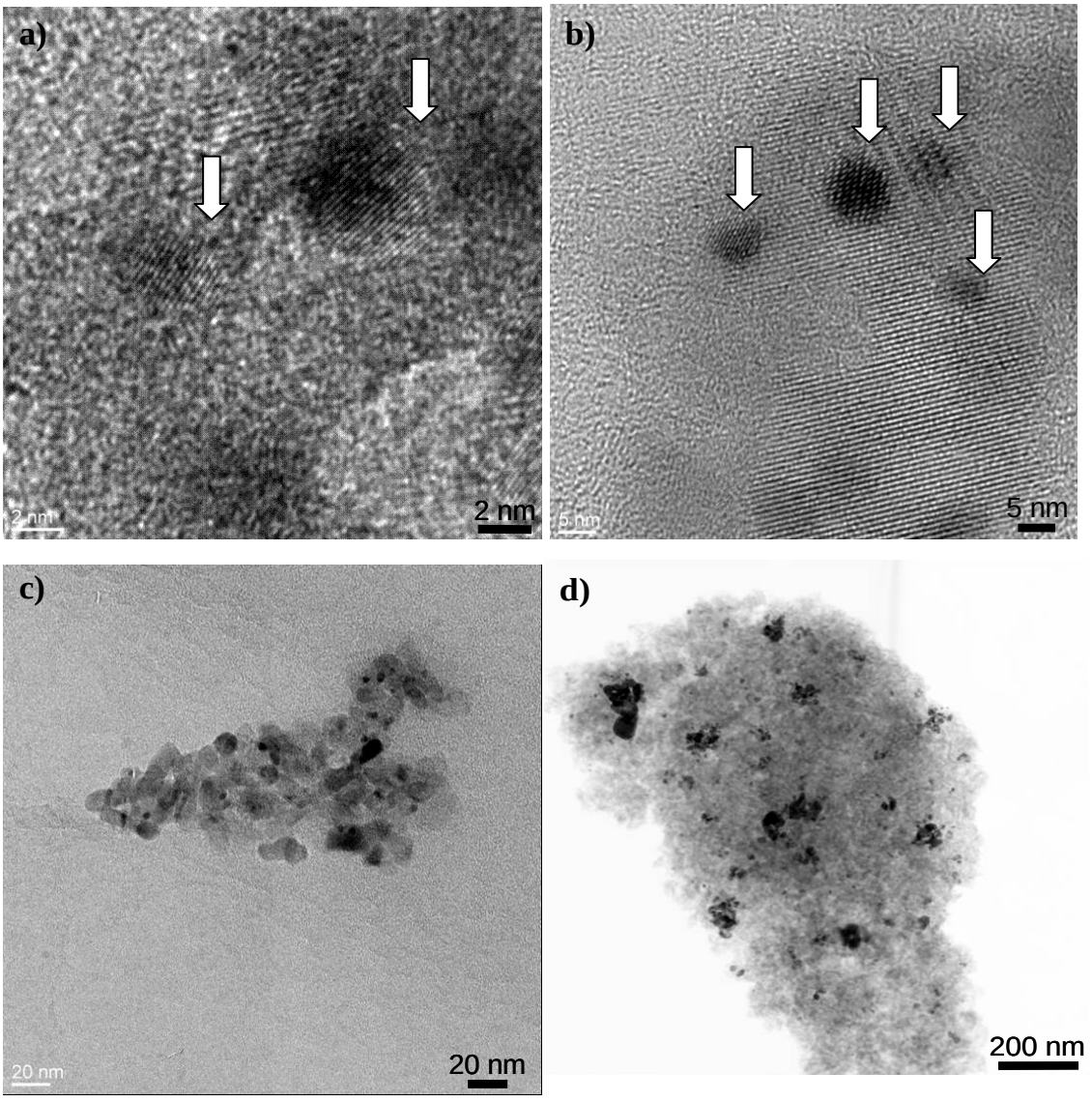

Figure 5.6. HRTEM images of Pt/TiO_2 catalyst; a,b) after H_2-pretreatment; Pt-particles marked with an arrow c) after He-pretreatment d) after He/H_2 pretreatment

This behaviour was also pointed out by HRTEM. The high resolution images obtained (Figure 5.6) permit describing significant structural differences after the corresponding treatments. This technique confirms a higher Pt-dispersion (smaller Pt-particle size) after reduction in pure H_2. In this case, very small Pt-nanoparticles of

around 2 nm were detected, while after reduction in He or even He/H_2 cycle, large Pt-particles, reaching some tens of nm are detected. Moreover, it is also noteworthy how the small Pt-nanoparticles obtained after H_2-pretreatments seem to be eminently two-dimensional particles, i.e. Pt is mainly coating the TiO_2 surface forming thin films in such a manner that the TiO_2 crystallographic layers remain visible and clearly differentiated from the Pt-ones (Figure 5.6). The formation of this type of 2-D raft Pt-particles were previously detected on different supports[38,39].There is nevertheless a miss orientation between the crystallographic planes of TiO_2 support and Pt-nanoparticles generating a high degree of imperfections and vacancies mainly in the surrounding interface area.

It is well known that the citral hydrogenation is a structure sensitive reaction, strongly dependent on the Pt-particle size[40-42]. Thus, we use complementary techniques (XRD, H_2-chemisorption and TEM) to determine the evolution of this parameter as described in the experimental section. Results are summarized in Table 5.5.

Table 5.5. Amount of H_2 chemisorbed (Q_{H_2}) and average particle size ($\overline{d}$) determined by XRD, TEM or H_2-chemisorption.

Catalyst	Q_{H_2}	$\overline{d}_{XRD}$	$\overline{d}_{TEM}$	$\overline{d}_{H_2}$
	µmol/g		**nm**	
Pt/TiO_2 -He	12.1	10.6	9.1	6.8
Pt/TiO_2 –He-H_2	11.7	12.6	11.6	7.7
Pt/TiO_2 –H_2	9.0	-	3.6	9.2

The average Pt-nanoparticle size determined by H_2-chemisorption is very similar after any pre-treatment, thus, although slightly increases in the case of H_2-pretreatment, Pt-particle size only varies from 6.8 to 9.2 nm. The combined He/H_2 reduction cycle presents an intermediate behaviour. This behaviour is in agreement with the XPS results previously discussed. A good agreement among the average particle size values determined by the different techniques is also observed when catalysts are pretreated in He or He/H_2-flow. However, in the case of H_2-pretreated catalysts there is a great difference between the values determined by TEM and H_2-chemisorption (XRD showed very low intensity to be used). Moreover, while H_2-chemisorption provides the higher

values of the series, TEM provides the smaller ones. In Figure 5.7 the Pt-particle size distribution obtained in each case is compared.

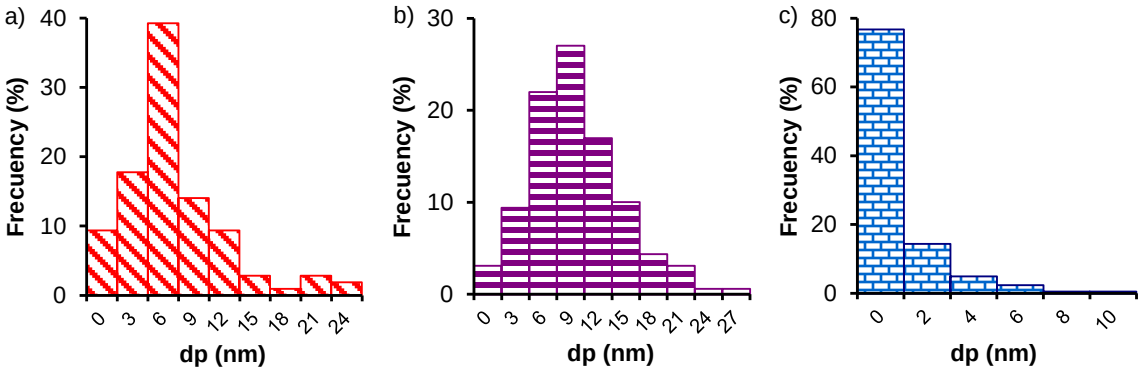

Figure 5.7. Pt-particle size distribution obtained by analysis of the HRTEM micrographs of pretreated catalysts: Pt/TiO_2-He (a) Pt/TiO_2-He/H_2 (b) and Pt/TiO_2-H_2 (c)

Taking into account the characteristics of each technique, they can provide significantly different average Pt-size values. Thus, XRD tends to provide an overestimated value, related mainly to the big crystalline particles while the smaller ones cannot be detected. On the contrary, in the case of H_2-chemisorption the amount adsorbed is greater on well dispersed catalysts, favouring consequently the determination of the smaller particles. H_2-chemisorption calculations [d_{H2} = 1.08/D (nm)] also assume the spherical shape of particles. In the case of flat particles, dispersion (D) tends to unity as decreases the particle height, increasing progressively the area / volume ratio until the formation of a monolayer. In this sense, the particle size determined for H_2-pretreated catalysts by applying this equation progressively underestimates the average particle size (even thus provides very high values). However, the different values obtained is not based on the error induced by this assumption, because the amount of chemisorbed H_2 (Table 5.5, Q_{H2}) is really smaller than after He-pretreatment, i.e. there is a smaller amount of surface Pt-atoms after H_2-pretreatment in spite of the flat shape and the smaller size of these particles.

Due to the different mobility of the Pt-species during He or H_2 pre-treatment[33] different structures can be formed. The mobility of metallic atoms (Pt, Rh, Ni) showing SMSI effects on defective titanium oxide lattices was previously described[24]. The role

of H_2 in the mobilization of the metallic active phase was associated to the incorporation of hydrogen into oxygen vacancies at the reduced support, forming hydride-like species [i.e., $(Ti\text{-}H)^{3+}$] that may be responsible for the enhancement of the Pt-mobility[43,44]. Thus, a different behaviour is expected under He and H_2-pretreatment.

In our case, after He-pretreatment the formation of 3D crystalline Pt-particles was pointed out unequivocally by XRD and TEM, and results are in agreement with the average Pt-particle size obtained by H_2-chemisorption. Only small and flat Pt-nanoparticles are obtained after H_2-pretreatment, this morphology does not produce XRD peaks, but contrary to the expected, the H_2-uptake (surface Pt-atoms) decreases even regarding large 3-D Pt-particles. In these experimental conditions the support reduction and the formation of oxygen vacancies were also unequivocally pointed out by XPS. Taking into account these results, Pt^{+2} species should diffuse into the TiO_2 structure in agreement with the SMSI model proposed by Sanchez *et al*.[45] for reducible oxides. They describe the SMSI effects in terms of a "burial" of metallic particles that diffuse through the defective metal oxide lattice filling with metal atoms the oxygen vacancies favoured by the hydrogen spillover and with elimination of oxygen of the anionic sub-lattice around them. The diffusion of Pt atoms through the oxygen vacancies of the TiO_2 structure favoured by hydride-like species, as commented, provoking smaller Pt-concentration and H_2-uptake values than those expected according to the Pt-loading and Pt-particle size observed by HRTEM. Recently, Ekou *et al*.[14] propose that defective TiO_{2-X} moieties migrates and decorates the three-dimensional Rh or Pt-particles. However, the opposite behaviour is found: the migration of metallic species into the supports. If the loss of H_2-uptake was due to Pt-sintering and mobile TiO_{2-x} moieties decorating the Pt-crystals, as proposed by Ekou[14], XRD peaks of the Pt-phase should be detected also in this case.

Correlating all the characterization results with the catalytic performance shown in Figure 5.1 it is clear that the formation of the active sites, selective to the UA formation, needs the presence of H_2 during pretreatment to produce a synergetic effect between the reduced TiO_2 support and the Pt nanoparticle. It is clear that the metallic Pt-nanoparticles generated after He-pretreatment, are less selective without the cooperation of oxygen vacancies on the support. Thus, similar S_{UA} is obtained after He/H_2 and H_2 pre-treatment (Figure 5.1), due to the similar nature of the active sites generated.

However, the catalytic activity is clearly smaller in the first case, which is related with a smaller active site concentration by formation of 3D Pt-nanocrystals. When $[Pt(NH_3)_4]Cl_2$ precursor is previously decomposed in He-flow the amount of active sites generated is strongly limited (and consequently the catalytic activity), because in this case the absence of oxygen vacancies constrain the mobility of Pt-species that can move only on the support surface favouring sintering processes. An ulterior H_2-pretreatment strongly modifies the Pt-support interactions and generates oxygen vacancies on the support (as shown by XPS) that enhance the citral adsorption through the C=O group and the consequently hydrogenation to UA. However, the greater the Pt-sintering, leads to a smaller support/Pt-crystallite interphase. The higher activity and selectivity obtained after H_2-pretreatment is due to a better Pt-dispersion and support reduction, very small Pt-particles surrounded by a high concentration of oxygen vacancies. This pretreatment also produces an acidity decrease, avoiding in a large extent the development of cracking reactions, which also favours the S_{UA} increase regarding the He-pretreatment.

Probably, both activity and selectivity can be improved by fitting the experimental conditions of treatment in H_2 (temperature and time) to balance where possible the positive effect TiO_2 reduction (concentration of vacancies) and the negative effect of Pt-sintering and Pt diffusion into the TiO_2 structure, because internal Pt should be catalytically inactive. The use of thermal treatment under vacuum[35] or alternative reductants like $NaBH_4$[46] were also suggested to generate oxygen vacancies in TiO_2, and permit to obtain very high Pt-dispersion regarding thermal treatments[47].

5.4. CONCLUSIONS

The influence of pretreatment conditions of Pt/TiO_2 catalysts was analyzed by different techniques. The activity and selectivity to unsaturated alcohols are favoured after H_2-pretreatments regarding the He-ones in the same experimental conditions. This fact is related with a partial reduction of TiO_2 under H_2-flow that favours a strong metal support interaction and the mobility of Pt species, avoiding the formation of three-dimensional Pt-nanoparticles during pretreatment. Active and selective sites were ascribed to the synergetic effect of oxygen vacancies on the TiO_2 support and Pt-metallic particles favouring the adsorption of citral through the C=O bond and a high

availability of atomic hydrogen on highly dispersed Pt-nanoparticles. However, if the decomposition of the precursor salt is carried out under He-flow, a posterior H_2-treatment leads to an increase of selectivity but does not favour the catalytic activity.

5.5. REFERENCES

[1] H. Surburg and J. Panten, *common fragrance and flavor materials: preparation, properties and uses*, 5th ed. (WILEY-VCH, Weinheim, Germany, 2006).

[2] G.S. Clark. Geraniol, *Perfumer & Flavorist* **23**, 19, 1998.

[3] W. Chen and A.M. Viljoen. Geraniol: A review of a commercially important fragrance material, *South African Journal of Botany* **76**(4), 643, 2010.

[4] P. Barbaro and F. Liguori, *heterogenized homogeneous catalysts for fine chemicals production* (Springer, London, 2010).

[5] E. Bailón-García, F.J. Maldonado-Hódar, A.F. Pérez-Cadenas, and F. Carrasco-Marín. Catalysts Supported on Carbon Materials for the Selective Hydrogenation of Citral, *Catalysts* **3**(4), 853, 2013.

[6] E. Asedegbega-Nieto, A. Guerrero-Ruiz, and I. Rodríguez-Ramos. Modification of the stereo selectivity in the citral hydrogenation by application of carbon nanotubes as support of the Pt particles, *Carbon* **44**(4), 804, 2006.

[7] G. Borda, H. Rojas, J. Murcia, J.L.G. Fierro, P. Reyes, and M. Oportus. Hydrogenation of citral on Ir/SiO_2 catalysts. Effect of the addition of Nb_2O_5 on surface and catalytic properties, *Reaction Kinetics and Catalysis Letters* **92**(2), 369, 2007.

[8] I.M.J. Vilella, S.R. Miguel, C.S.-M.d.L. Lecea, Á. Linares-Solano, and O.A. Scelza. Catalytic performance in citral hydrogenation and characterization of PtSn catalysts supported on activated carbon felt and powder, *Applied Catalysis A: General* **281**(1–2), 247, 2005.

[9] A. Giroir-Fendler, D. Richard, and P. Gallezot. Selectivity in cinnamaldehyde hydrogenation of group-VIII metals supported on graphite and carbon, *Studies in Surface Science and Catalysis* **41**(C), 171, 1988.

[10] U.K. Singh and M.A. Vannice. Liquid-phase citral hydrogenation over SiO_2-supported group VIII metals, *Journal of Catalysis* **199**(1), 73, 2001.

[11] S.A. Ananthan and V. Narayanan. Liquid phase selective hydrogenation of citral over Ru/TiO_2 and Pt/TiO_2 nano catalysts, *Proceedings of the International Conference on Nanoscience, Engineering and Technology, ICONSET 2011* , 23-29, 2011.

[12] S.A. Ananthan, N. Vengidusamy, K. Giribabu, and R. Suresh. Carbon nanotunes supported Pt and Pt-Ru catalysts for selective hydrogenation of citral: Effect of

promoters and thermal activation of catalysts, *Advanced Materials Research* **584**, 229, 2012.

[13] S.J. Tauster and S.C. Fung. Strong metal-support interactions: Occurrence among the binary oxides of groups IIA–VB, *Journal of Catalysis* **55**(1), 29, 1978.

[14] T. Ekou, L. Ekou, A. Vicente, G. Lafaye, S. Pronier, C. Especel, and P. Marecot. Citral hydrogenation over Rh and Pt catalysts supported on TiO_2: Influence of the preparation and activation protocols of the catalysts, *Journal of Molecular Catalysis A-Chemical* **337**(1-2), 82, 2011.

[15] G. Lafaye, T. Ekou, C. Micheaud-Especel, C. Montassier, and P. Marecot. Citral hydrogenation over alumina supported Rh-Ge catalysts - Effects of the reduction temperature, *Applied Catalysis A-General* **257**(1), 107, 2004.

[16] M. Bidaoui, C. Especel, N. Bouchenafa-Saib, D. Duprez, O. Mohammedi, and S. Royer. Citral hydrogenation on high surface area mesoporous TiO_2-SiO_2 supported Pt nanocomposites: Effect of titanium loading and reduction temperature on the catalytic performances, *Applied Catalysis A: General* **445-446**, 14, 2012.

[17] S. Brunauer, P.H. Emmett, and E. Teller. Adsorption of Gases in Multimolecular Layers, *Journal of the American Chemical Society* **60**(2), 309-319, 1-2-1938.

[18] M.M. Dubinin. Generalization of the theory of volume filling of micropores to nonhomogeneous microporous structures, *Carbon* **23**(4), 373, 1985.

[19] MM. Dubinin. Contemporary state of the theory of volume filling of micropores of adsorbents in the adsorption of gases and vapors on carbon adsorbents, *Russian Journal of Physical Chemestry* **39**, 1305, 1965.

[20] F. Stoeckli, *porosity in carbons - characterization and applications* (Arnold, London, 1995).

[21] J.F. Vivo-Vilches, E. Bailón-García, A.F. Pérez-Cadenas, F. Carrasco-Marín, and F.J. Maldonado-Hódar. Tailoring the surface chemistry and porosity of activated carbons: Evidence of reorganization and mobility of oxygenated surface groups, *Carbon* **68**(0), 520, 2014.

[22] J.E. Benson and M. Boudart. Hydrogen-oxygen titration method for the measurement of supported platinum surface areas, *Journal of Catalysis* **4**(6), 704, 1965.

[23] G.R. Wilson and W.K. Hall. Studies of the hydrogen held by solids: XVIII. Hydrogen and oxygen chemisorption on alumina- and zeolite-supported platinum, *Journal of Catalysis* **17**(2), 190, 1970.

[24] A.R. González-Elipe, A. Fernández, J.P. Espinós, and G. Munuera. Role of hydrogen in the mobility of phases in Ni–TiO_x systems, *Journal of Catalysis* **131**(1), 51, 1991.

[25] M.E. Nagassa, A.E. Daw, W.G. Rowe, A. Carley, D.W. Thomas, and R. Moseley. Optimisation of the hydrogen peroxide pre-treatment of titanium: surface characterisation and protein adsorption, *Clinical Oral Implants Research* **19**(12), 1317, 2008.

[26] A. Orendorz, J. Wüsten, C. Ziegler, and H. Gnaser. Photoelectron spectroscopy of nanocrystalline anatase TiO_2 films, *Applied Surface Science* **252**(1), 85, 2005.

[27] A. Samokhvalov, E.C. Duin, S. Nair, and B.J. Tatarchuk. An in situ temperature-programmed XPS study of the surface chemical reactions of thiophene with Ag/titania, *Surface and Interface Analysis* **42**(9), 1476-1482, 1-9-2010.

[28] C.A. Leon, J.M. Solar, V. Calemma, and L.R. Radovic. Evidence for the protonation of basal plane sites on carbon, *Carbon* **30**(5), 797, 1992.

[29] E. Bailón-García, F. Carrasco-Marín, A.F. Pérez-Cadenas, and F.J. Maldonado-Hódar. Microspheres of carbon xerogel: an alternative Pt-support for the selective hydrogenation of citral, *Applied Catalysis A: General* **482**, 318, 2014.

[30] J. Alvarez-Rodríguez, I. Rodríguez-Ramos, A. Guerrero-Ruiz, E. Gallegos-Suarez, and A. Arcoya. Influence of the nature of support on Ru-supported catalysts for selective hydrogenation of citral, *Chemical Engineering Journal* **204-205**, 169, 2012.

[31] S. Santiago-Pedro, V. Tamayo-Galván, and T. Viveros-García. Effect of the acid–base properties of the support on the performance of Pt catalysts in the partial hydrogenation of citral, *Catalysis Today* **213**(0), 101, 2013.

[32] J.L. Dong, J.H. Zhu, and Q.H. Xu. Influence of structure and acidity-basicity of zeolites on platinum supported catalysts of n-C6 aromatization, *Applied Catalysis A: General* **112**(2), 105, 1994.

[33] F.J. Maldonado-Hódar, C. Moreno-Castilla, and A.F. Pérez-Cadenas. Catalytic combustion of toluene on platinum-containing monolithic carbon aerogels, *Applied Catalysis B: Environmental* **54**(4), 217, 2004.

[34] M.D. Hernández-Alonso, A.R. Almeida, J.A. Moulijn, and G. Mul. Identification of the role of surface acidity in the deactivation of TiO_2 in the selective photo-oxidation of cyclohexane, *Catalysis Today* **143**(3–4), 326, 2009.

[35] M. Xing, J. Zhang, F. Chen, and B. Tian. An economic method to prepare vacuum activated photocatalysts with high photo-activities and photosensitivities, *Chemical Communications* **47**(17), 4947-4949, 2011.

[36] P. Gallezot and D. Richard. Selective Hydrogenation of α, β-Unsaturated Aldehydes, *Catalysis Reviews* **40**(1-2), 81, 1998.

[37] M. Steffan, F. Klasovsky, J. Arras, C. Roth, J. Radnik, H. Hofmeister, and P. Claus. Carbon-carbon double bond versus carbonyl group hydrogenation: Controlling the intramolecular selectivity with polyaniline-supported platinum catalysts, *Advanced Synthesis and Catalysis* **350**(9), 1337, 2008.

[38] S.D. Jackson, M.B.T. Keegan, G.D. Mclellan, P.A. Meheux, G. Webb, R.B. Moyes, P.B. Wells, R. Whyman, and J. Willis, "Preparation and Properties of a Pt/Silica and Its Comparison With Europt-1",in *Studies in Surface Science and Catalysis. Preparation of Catalysts V Scientific Bases for the Preparation of Heterogeneous Catalysts Proceedings of the Fifth International Symposium,* Volume 63 ed. edited by G. Poncelet (Elsevier, Amsterdam, 1991), pp.135-144.

[39] O.K. Ezekoye, A.R. Drews, H.W. Jen, R.J. Kudla, R.W. McCabe, M. Sharma, J.Y. Howe, L.F. Allard, G.W. Graham, and X.Q. Pan. Characterization of alumina-supported Pt and Pt–Pd NO oxidation catalysts with advanced electron microscopy, *Journal of Catalysis* **280**(1), 125, 2011.

[40] P. Claus. Selective hydrogenation of α,β–unsaturated aldehydes and other C=O and C=C bonds containing compounds, *Topics in Catalysis* **5**(1), 51, 1998.

[41] F. Delbecq and P. Sautet. Competitive C=C and C=O Adsorption of α,β–Unsaturated Aldehydes on Pt and Pd Surfaces in Relation with the Selectivity of Hydrogenation Reactions: A Theoretical Approach, *Journal of Catalysis* **152**(2), 217, 1995.

[42] A. Giroir-Fendler, D. Richard, and P. Gallezot. Chemioselectivity in the catalytic hydrogenation of cinnamaldehyde. Effect of metal particle morphology, *Catalysis Letters* **5**(2), 175, 1990.

[43] J.C. Conesa, P. Malet, G. Munuera, J. Sanz, and J. Soria. Magnetic resonance studies of hydrogen-reduced rhodium/titanium dioxide catalysts, *The Journal of Physical Chemistry* **88**(14), 2986-2992, 1-7-1984.

[44] A.R. Gonzalez-Elipe, P. Malet, J.P. Espinos, A. Caballero, and G. Munuera. Effect of Water in the Encapsulation of the Metallic Phase During Smsi Generation in Pt/TiO_2 Catalysts, *Studies in Surface Science and Catalysis* **48**, 427, 1989.

[45] M.G. Sanchez and J.L. Gazquez. Oxygen vacancy model in strong metal-support interaction, *Journal of Catalysis* **104**(1), 120, 1987.

[46] W. Fang, M. Xing, and J. Zhang. A new approach to prepare Ti^{3+} self-doped TiO_2 via $NaBH_4$ reduction and hydrochloric acid treatment, *Applied Catalysis B: Environmental* **160–161**(0), 240, 2014.

[47] J.L. Figueiredo, M.F.R. Pereira, P. Serp, P. Kalck, P.V. Samant, and J.B. Fernandes. Development of carbon nanotube and carbon xerogel supported catalysts for the electro-oxidation of methanol in fuel cells, *Carbon* **44**(12), 2516, 2006.

Capítulo VI

DEVELOPMENT OF CARBON XEROGELS AS ALTERNATIVE Pt-CARBON SUPPORTS FOR THE SELECTIVE HYDROGENATION OF CITRAL

CITRAL

Backhousia citriodora

Catalyst

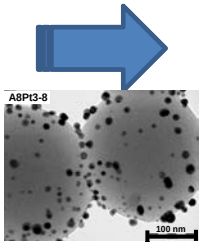

Nerol / Geraniol

Fragrances, chemicals

DEVELOPMENT OF CARBON XEROGELS AS ALTERNATIVE Pt-SUPPORTS FOR THE SELECTIVE HYDROGENATION OF CITRAL

Article published in Catalysis Communications, 58 (2015) 64-69, doi:10.1016/j.catcom.2014.09.001

Highlights

- Pure carbon xerogels with fitted porosity were prepared by sol-gel technology.
- Activated carbons contain mineral matter in different proportion and nature.
- The developed mesoporosity and acid impurities favor secondary reactions.
- Secondary reactions are avoided using microporous spherical carbon xerogels.

Abstract

The role of activated carbons and carbon xerogels as Pt-supports for the selective citral hydrogenation is compared. The influence of porosity and inorganic matter impurities in activated carbons determines the performance of their derivative catalysts. The presence of Pt-particles inside mesopores and acid mineral matter favors secondary reactions decreasing the unsaturated alcohols (UA) yield. Highly active and selective monometallic Pt-catalysts were obtained using pure carbon xerogels structured in microspheres as support.

6.1. INTRODUCTION

The selective hydrogenation of carbonyl groups of α,β-unsaturated aldehydes is a challenging process, either from a scientific and economic point of view[1]. Among them, citral is a cheap raw material obtained from different natural sources being their derivative unsaturated-alcohols (UA), nerol and geraniol, highly demanded by pharmaceutical and chemical industries. The design and development of catalysts for the selective citral hydrogenation are influenced by several factors determining the catalysts performance: the active metal phase and support nature[2], metal particle size[3], bimetallic catalysts[1,4] and factors related with the preparation method and metal-support interactions[5,6]. All these factors and the evolution of the designed catalysts were recently reviewed[7].

Carbon materials are very interesting catalyst supports due to their ability to fit their chemical and textural properties. Doing a bibliography review[8], it can be seen that three types of carbon materials have been used in the selective hydrogenation of citral: activated carbons[9,10], graphite[10,11] and carbon nanotubes or nanofibers[11-13], being the best selectivity achieved around 65% at 30% conversion obtained with monometallic Pt-supported on electron-donor graphite[14].

It is noteworthy that no reference has been found in which carbon aerogels or xerogels were used as support, in spite of the benefits that these kinds of materials show in very different catalysed reactions[15]. In this manuscript we have prepared two nanostructured carbon xerogels and their performance as Pt-support was compared to activated carbons on the basis of the different textural properties and purity.

6.2. EXPERIMENTAL

Two carbon xerogels (A1, A8) were prepared by polycondensation of resorcinol (R) with formaldehyde (F) in aqueous (W) media, using Cs_2CO_3 as polymerization catalyst (C). Briefly, the appropriate amounts of resorcinol (24.7 g) and Cs_2CO_3 (0.72 or 0.09 g) were dissolved in deionizedwater (670 mL) using a three-neck glass reactor (2 L) provided of reflux, controlled temperature and stirring. The temperature of this solution was fitted to 85 °C under stirring (250 rpm) and then, 36.3

g of formaldehyde solution (Sigma, 37 wt.%) was added dropwise. Thus, the composition of the mixture (molar ratio) was R/F = 1/2, R/W = 3/500 for both samples and R/C was 100 and 800, for A1 and A8 respectively. The gel formed was aged at 85 °C for 24 h, filtered and placed in acetone for 3 days, in order to reduce the porosity collapse during the subsequent drying process by microwave[16]. The gel was dried by microwave heating using a Saivod MS-287W microwave oven under nitrogen atmosphere in periods of 1 minute at 384 W until constant weight. Pyrolysis of organic xerogel was carried out at 900 °C for 2 h in N_2 flow (300 cm^3min^{-1}). An activated carbon (EG) was also prepared in our laboratories by chemical activation of olive stones with KOH following the experimental procedure previously published[17]. Olive stones were milled and sieved to 1.0–2.0 mm, treated with sulphuric acid (1 N) to remove the rest of pulp and washed until all sulfates had been removed. An initial carbonization was carried out by heating at 10 °C min^{-1} to 400 °C and a soak time of 2 h under a nitrogen flow of 300 cm^3 min^{-1} using a tubular furnace (from Heraeus). Chemical activation was carried out using a mixture of this carbonized material and KOH in a 1:7 mass ratio. This mixture was treated under nitrogen flow for two hours at 350 °C followed by three hours at 850 °C. Cooling to ambient temperature was performed by keeping the sample under nitrogen atmosphere. Additionally, a commercial activated carbon from Norit (Sorbo, S) was also used as reference material. Platinum-catalysts were prepared by impregnation of supports at 3 wt.% Pt-loading, using an aqueous solution of $[Pt(NH_3)_4]Cl_2$. Catalysts were pre-treated at 400 °C for 6 hours in Helium flow and referred indicating support, Pt-loading and Pt-particle size determined by H_2-chemisorption. For example, A8Pt3-8 was prepared with 3% of Pt using A8 carbon xerogel as support and after pre-treatment a Pt-particle size of 8 nm is obtained.

The samples morphology was studied by scanning electron microscopy (SEM) using a LEO (Carl Zeiss) GEMINI-1530 microscope. Textural characterization was carried out by N_2 and CO_2 adsorption at −196 °C and 0 °C, respectively, using a Quantachrome Autosorb-1 equipment. The BET and Dubinin–Radushkevich equations were applied to determine the apparent surface area (S_{BET}) and the micropore volume (W_0), the mean micropore width (L_0) and the microporous surface (S_{mic}), respectively. The total pore volume was considered as the volume of N_2-adsorbed at $P/P_0 = 0.95$ and the BJH method was used to calculate the mesopore volume of the samples (V_{meso})[18-21].

The macropore volume (V_3) and a fraction (pores larger than 6.5 nm) of the mesopore volume (V_2) of the samples were determined by mercury porosimetry.

The chemical characterization of supports and catalysts was carried out by elemental analysis, XPS, DRX and thermal programmed desorption (TPD). Determination of the pH_{zpc} values was performed according to the method proposed by Leon *et al.*[22]. Pt dispersion (D) and mean particle size (d) were obtained by H_2-chemisorption and the analysis of images from high-resolution transmission electron microscopy (HRTEM), obtained using a Phillips CM-20 microscope.

The citral hydrogenation was carried out in 100 mL heptane solution at a constant hydrogen pressure of 8.3 bar and 90 °C using a Parr reactor model 5500. The experimental conditions: citral concentration, catalyst weight and stirring speed were previously optimized in order to avoid mass transfer limitations (results not showed) and fixed in 0.05 M, 500 mg and 1500 rpm, respectively. A small volume of sample (1 mL) was periodically withdrawn and analysed by chromatography using a Bruker 430-GC equipped with a FID detector and a Varian GC Capillary Column CP7485 (25m x 0.32 mm x 0.45 μm). Both citral and any possible product were previously calibrated.

6.3. RESULTS AND DISCUSSIONS

The textural characteristics of supports and their respective Pt-catalysts are summarized in Table 6.1. Only the support A8 is an exclusively microporous material; the rest of supports present a certain mesopore volume that increases in the sense S<A1<EG. When V_2 and V_{meso} values (Table 6.1) were compared, it is observed that the large part of mesopores are smaller than 6.5 nm for both S and A1 support, while both parameters are quite similar in the case of EG, indicating a very opened mesoporosity as shown by mercury porosimetry (Figure 6.1). In this case, large mesopores of around 10 nm in diameter, together with a wide distribution of macropores, were observed. Carbon xerogels, but specifically A8, present a narrower microporosity (L_0 values) than activated carbons. The A8 microporous carbon xerogel also exhibits a significant macropore volume (Figure 6.1), probably located between primary particles [9,10]. All pretreated catalysts present smaller pore volumes and surface

areas than their corresponding supports, denoting a certain pore blockage by the deposition of Pt-particles.

Table 6.1. Textural characteristics of carbon supports and derivatives Pt-catalysts.

	N_2-adsorption					CO_2-adsorption			Mercury porosimetry	
Sample	**S_{BET}** $m^2 \cdot g^{-1}$	**W_0** $cm^3 \cdot g^{-1}$	**L_0** nm	**V_{meso}** $cm^3 \cdot g^{-1}$	**$V_{0.95}$** $cm^3 \cdot g^{-1}$	**W_0** $cm^3 \cdot g^{-1}$	**S_{mic}** $m^2 \cdot g^{-1}$	**L_0** nm	**V_2** $cm^3 \cdot g^{-1}$	**V_3** $cm^3 \cdot g^{-1}$
S	1284	0.53	1.57	0.12	0.66	0.39	888	0.87	0.014	0.481
SPt3-9	535	0.22	1.69	0.08	0.29	0.11	179	1.28	-	-
EG	2219	1.05	1.59	1.22	2.17	0.38	704	1.09	1.141	7.732
EGPt3-9	2065	0.843	1.37	1.53	2.16	0.422	696	1.21	-	-
A1	526	0.20	0.86	0.24	0.40	0.19	611	0.62	0.038	0.834
A1Pt3-8	503	0.20	0.87	0.12	0.29	0.21	781	0.55	-	-
A8	614	0.25	0.78	0.00	0.31	0.29	952	0.60	0.002	3.914
A8Pt3-8	531	0.21	0.62	0.00	0.22	0.28	960	0.58	-	-

* S_{BET}= BET surface area, W_0 = micropore volume, L_0 = micropore wide, V_{meso}= BJH mesopore volume, $V_{0.95}$ = total pore volume, S_{mic} = microporous surface, V_2, V_3 = meso and macropore volume.

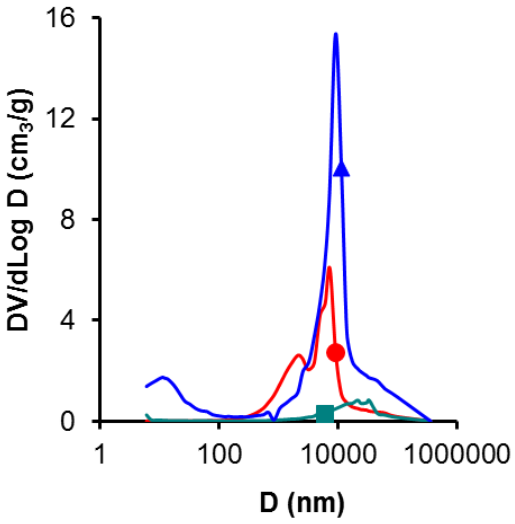

Figure 6.1. Pore size distribution obtained by mercury porosimetry of supports A1 (■), A8 (●) and EG (▲).

The chemical characteristics of carbon supports are summarized in Table 6.2. All samples behave as basic materials due to the very low oxygen contents, but the pH_{pzc} values increases from 7.3 to 11.0. In general, this parameter decreases with increasing the oxygen content, because in this sense the formation of acid oxygenated surface groups (OSG) is favored evolving as CO_2 (carboxylic acid, anhydrides, lactones, etc) during TPD experiments, while those OSG that evolve as CO (semiquinone, carbonyl, etc) behave as basic groups[23]. The pH_{pzc} is also influenced by the inorganic content, both carbon xerogels are pure carbon supports because they are synthesized from pure organic reactants (using Cs_2CO_3 as polymerization catalyst); however, AC precursors contain always different inorganic fractions. The total ash content of S and EG is 6.9 and 3.7, respectively, determined by burning of a fraction of these samples. The XRD analysis (Figure 6.2) points out that S-support contains mainly basic compounds like anhydrite ($CaSO_4$), while the inorganic matter of EG-support is formed by different types of acid iron oxides; the more intense diffraction peaks correspond to hematites (α-Fe_2O_3), but also maghemite (γ-Fe_2O_3) and magnetite (Fe_3O_4) forms were detected, which clearly contribute to the pH_{pzc} values observed for these samples.

Table 6.2. Chemical characteristics of carbon supports

Sample	CO	CO_2	O_2	CO/CO_2	pHpzc	Elemental analysis		
	($\mu mol \cdot g^{-1}$)		%			C(%)	O(%)	H(%)
S	1080	447	3.2	2.4	11.0	89.7	9.8	0.3
EG	1156	148	2.3	7.8	7.3	-	-	-
A1	388	230	1.4	1.7	10.3	94.5	5.0	0.5
A8	303	81	0.8	3.7	9.4	95.1	4.3	0.5

*CO and CO_2 evolved during TPD runs.

The morphology was studied by SEM and representative microphotographs are shown in Figure 6.3 for carbon xerogels. The variation on the R/C ratio strongly influence the morphology [24]. Sample A1 presents the typical structure of carbon gels, i.e. a three-dimensional network of agglomerated primary particles (Figure 6.3). These particles leaves between them a significant mesopore volume[24] as denoted in Table 6.1. With increased R/C ratio, bigger primary particles are formed in A8, in such a way that

in this case interparticle voids are also bigger; thus, macropores are formed instead mesopores, in agreement also to the porosimetry results (Figure 6.1).

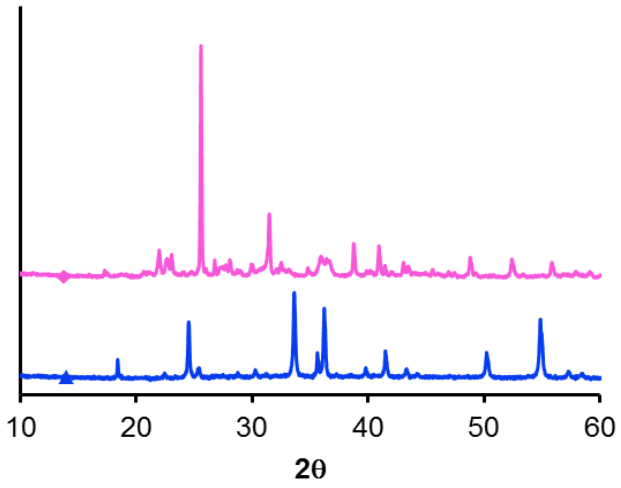

Figure 6.2. XRD-patterns of the inorganic matter present in activated carbons. EG (▲) and S (◆).

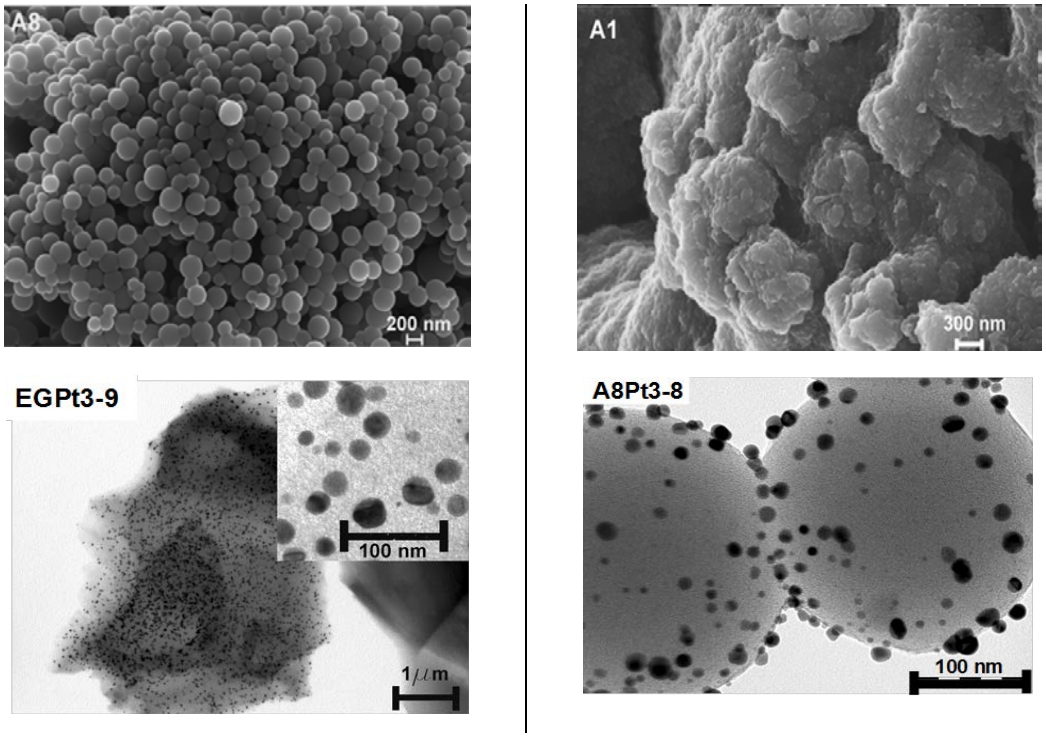

Figure 6.3. Influence of the R/C ratio on the morphology of carbon xerogels (SEM images of A1 and A8) and Pt-dispersion on activated carbon (TEM images of EGPt3-9) and carbon xerogels (A8Pt3-8).

Catalysts were also extensively characterized. The concentration of Pt species, particle size and dispersion results are collected in Table 6.3 and some representative HRTEM micrographs are shown in Figure 6.3. As expected [25] mesoporosity favors a very homogenous particle distribution on EG sample, but this behavior was observed even for microporous A8Pt3-8 catalyst. Moreover, the Pt-particle size determined by H_2-chemisorption was in all cases 8.6 ± 0.7 nm, showing that the porosity of the samples is high enough to adequately disperse the Pt-nanoparticles formed. Nevertheless, the Pt-localization is influenced by the support porosity. Analyzing the $\%Pt_{xps}/Pt_{Tot}$ ratio, it is observed that this parameter is closer to the unity for mesoporous EG support, indicating a homogeneous distribution of Pt-particles along the material, i.e. some of Pt-particles are formed inside the mesopores. However, the highest value of this parameter was observed for microporous A8 support, because Pt-particles cannot be formed inside the narrow microporosity (Table 6.1) and consequently they are distributed only on the external surface of the support spherical particles (Figure 6.3). Probably, this external localization can also favor the reduction of Pt(II) to Pt^0 (Table 6.3), while certain electronic enrichment of the Pt-particles seems occur when deposited on carbon xerogels regarding activated carbons, because in these cases the BE of Pt-species appeared at around 0.5 eV shifted to lower BE values.

Table 6.3. Pt-particle size obtained by H_2-chemisorption ($\bar{d}_{H_2}$) or TEM ($\bar{d}_{TEM}$), Pt-content determined by XPS (Pt_{xps}) and B.E. and concentration (in parenthesis) of Pt-species.

Catalyst	$\bar{d}_{H_2}$	$\bar{d}_{TEM}$	**B.E (e.v)**		**Pt_{xps}**	**$\%Pt_{xps}/\%Pt_{Tot}$**
	(nm)	**(nm)**	**$Pt^0 4f_{7/2}$**	**$Pt^{II} 4f_{7/2}$**	**%**	
SPt3-9	8.5	9.3	71.7 (61)	72.8 (39)	4.1	1.36
EGPt3-9	9.3	13.1	71.6 (56)	72.9 (44)	3.2	1.12
A1Pt3-8	7.9	8.2	71.3 (57)	72.4 (43)	3.0	1.01
A8Pt3-8	7.9	9.3	71.3 (76)	72.4 (24)	4.4	1.50

In order to study the contribution of the carbon support to the catalytic performance, the A8 carbon xerogel, a pure carbon material, was first used as catalysts in the experimental conditions previously exposed. The conversion obtained is very low (bellow 5%) being preferential the C=C hydrogenation to citronellal (39%) and their

derivative products, citronellol (29%), menthol and isopulegol (8%), although also a significant hydrogenation of C=O bonds (25%) to unsaturated alcohols (UA) was also detected.

The performance of Pt-catalysts is therefore mainly due to the role of Pt; for that, the chemical state, dispersion, localization and stability of Pt-species on the carbon surface were analyzed. The citral hydrogenation is a structure sensitive reaction, being strongly influenced by the Pt-particle size[26]. Thus, the similar Pt-dispersion obtained permits to correlate the support characteristics with the catalytic performance. The obtained results are summarized in Figures 6.4 and 6.5. It is noteworthy that when Pt is supported on carbon xerogels, it generates both the most active catalyst (microporous) as the less active catalyst (mesoporous). However, initially, microespheres-shaped A8Pt3-8 catalyst provides the smaller reaction rate and is clearly activated during the first hours of reaction (Figure 6.4). This fact is related with the absence of mesoporous surface in this support, leading initially to a smaller citral concentration on surface; however, after saturation, reaction becomes faster favored by the external localization of the Pt-particles.

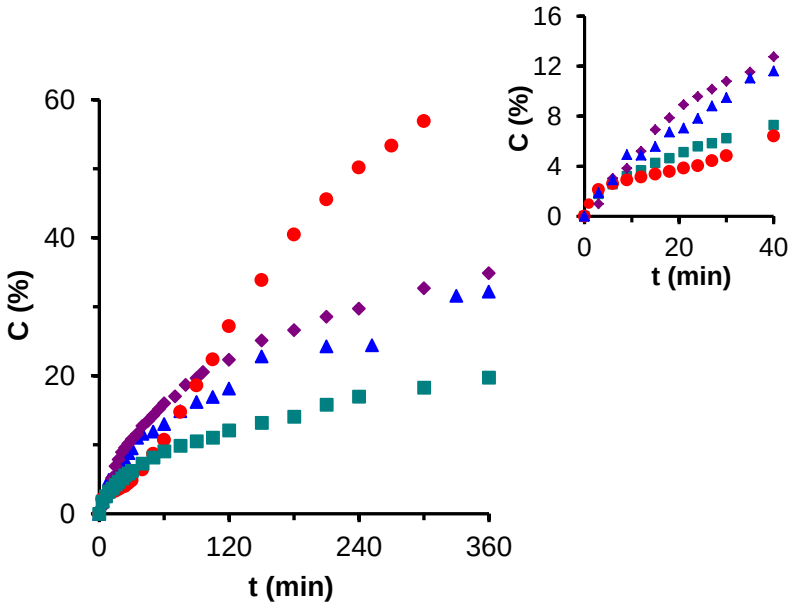

Figure 6.4. Comparison of the catalytic activity of Pt-supported on carbon xerogels a function of the reaction time. A1Pt3-8 (■), A8Pt3-8 (●), EGPt3-9 (▲) and SPt3-9(◆) (500 mg of catalysts, 1500 rpm, 0.05 M citral, PH_2 = 8 bar, 90 ºC).

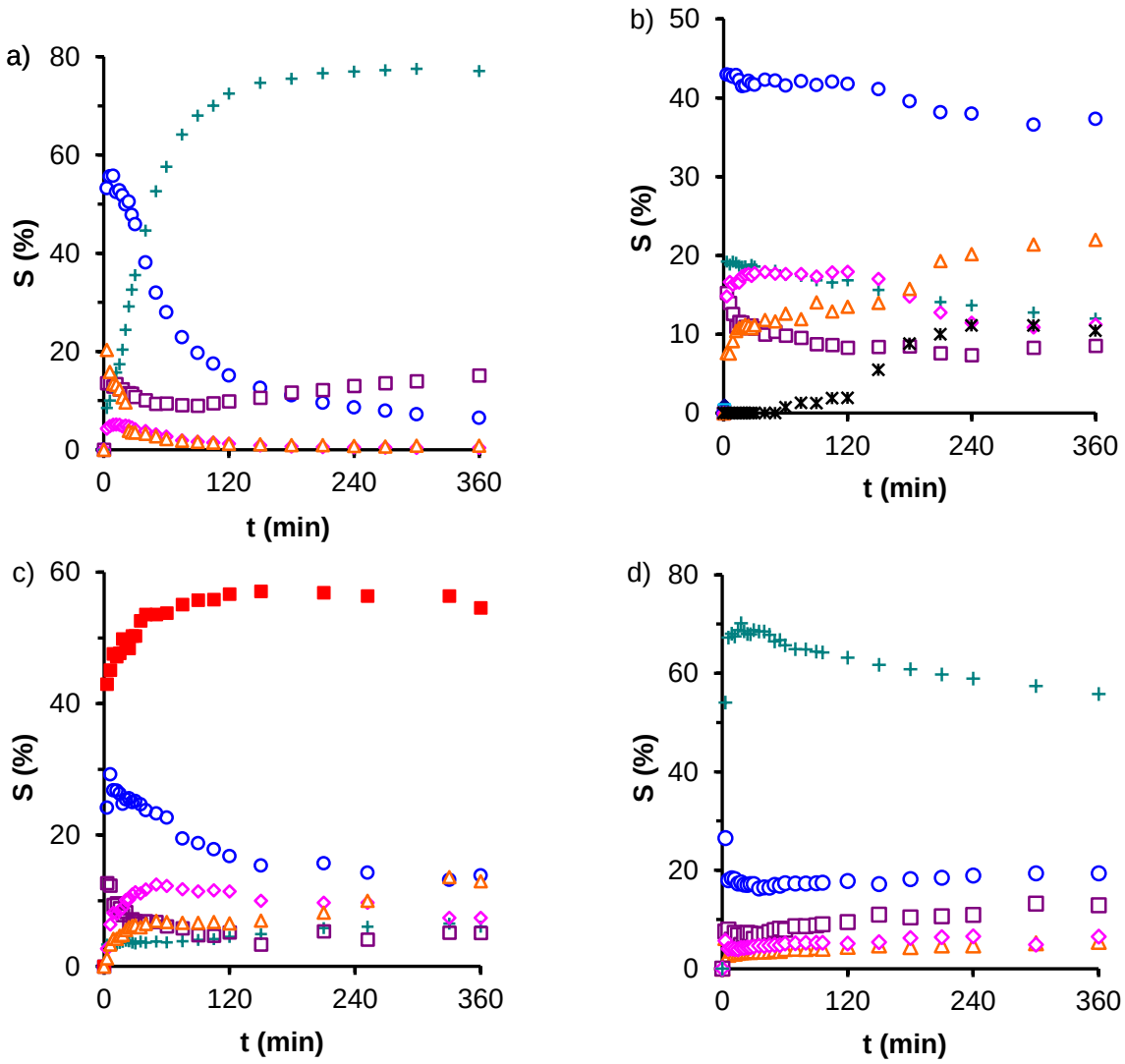

Figure 6.5. Products distribution as a function of the reaction time (500 mg of catalyst, 1500 rpm, 0.05 M citral, P_{H_2} =8 bar, 90 °C): Isopulegol+Menthol(△), Others (■), Citronellal (○) Citronellol (□), 3,7 DMO (◇) , S_{UA} (+) and 3,7 DMA (∗). a) A8Pt3-8, b) A1Pt3-8, c) EGPt3-9 and d) SPt3-9.

The evolution of the products distribution along the reaction is also strongly influenced by the support characteristics (Figure 6.5). At the beginning of the reaction A8Pt3-8 catalyst is not only less active but also less selective than A1Pt3-8. Citronellal is initially the main reaction product obtained in both cases; however, during the first 2 h of reaction the product distribution deeply changes using A8Pt3-8: the citronellal selectivity strongly decays favoring the formation of UA, reaching S_{UA} values at around 80% even at high conversion degrees. This S_{UA} value is very high regarding those described in the bibliography for monometallic Pt-catalysts[8]. On the contrary, using the mesoporous carbon xerogel (Figure 6.5b), the product distribution does not change

significantly during the first 2 h of reaction, and then, both citronellal and UA selectivity decreases favoring the development of secondary reactions. Cyclization reaction of citronellal to menthol and isopulegol and secondary hydrogenation to 3,7 dimethyl octanol (DMO) or 3,7 dimethyl octanal (DMA) are favored inside the mesopores because the residence time in this case is higher.

When activated carbons are used as supports, together with the influence of porosity, the catalytic performance is also determined by the presence of inorganic matter. When EG is used as support, cracking reactions are catalyzed by acid iron oxides being the main reaction products obtained in all the conversion range. Secondary hydrogenation reactions leading to DMO and cyclization products are favored at the expense of citronellal during the first 2 h of reaction (Figure 6.5c) induced by the great mesopore volume of this support. Consequently, this catalyst provides the lowest UA yields of this catalysts series in all the conversion range.

When the activated carbon S is used as Pt-support, the S_{UA} is significantly high in all the conversion range, but tends to decrease favoring mainly the citronellol formation. The products distribution is quite stable along the reaction time. This fact can be related with the smaller mesopore volume of this support and the presence of basic sites, that can induce the interaction with the citral molecule through the C=O bond favoring the formation of UA[5]; however the conversion degree reached with this catalysts is significantly smaller than those obtained using microporous xerogels structured in microspheres, which showed the best performance between the supports studied.

After reaction, Pt was undetected in solution by atomic absorption experiments, while XPS experiments of the used catalyst showed only a certain modification of the Pt/Pt^{2+} ratio and a significant increase of the oxygen content, pointing out the adsorption of oxygenated compounds (citral or their derivative products) on the catalyst surface. As an example, the O_{XPS} content increases for A8Pt3-8 catalyst from 1.5 to 2.4%. These groups fixed more or less permanently to the carbon surface favor the hydrophilic character of the catalysts. The change from hydrophobic to hydrophilic surfaces favors the citral adsorption through C=O bond and consequently the UA formation[27]. Nevertheless, in spite of the increase in the oxygen content, the distribution

of oxygenated surface groups (OSG) on the carbon surface is practically unchanged (these results avoid the possibility to know if reactant or hydrogenated products are fixed preferentially), as denoted by XPS from the analysis of the C_{1s} spectral region (Fig. 6.6a). The following functions[28] were considered (with binding energies) in the curve-fitting of the C_{1s} spectrum: aromatic and aliphatic carbon (284.9 eV), single C-O bonds (286.2 eV), double C=O bonds (288.0 eV), carboxyl groups (289.1 eV) and carbonate groups (290.6 eV). While the increase of hydrophilicity of the carbon surface can favor the selectivity to UA, these deposits can also favor the catalyst deactivation by covering the Pt-particles or blocking the porosity of supports, as denoted by the corresponding N_2-adsorption isotherms (Fig. 6.6b). Additional effort regarding the possibility of reuse catalysts in consecutive reaction cycles is therefore needed to clarify these aspects.

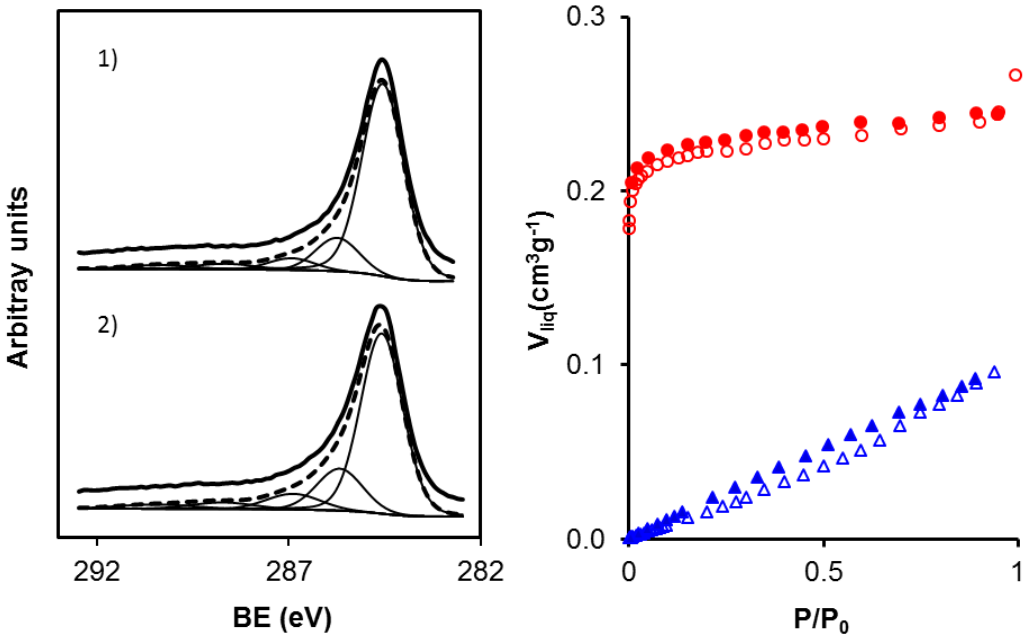

Figura 6.6. Chemical and porous transformation of A8Pt3-8 catalyst during reaction. a) Curve-Fitted C1s core level spectra of 1) fresh and 2) used catalysts. b) N2-adsorption isotherms of frech (○) and used (△) catalysts. Open symbol-adsorption; close symbols-desorption branch.

6.4. CONCLUSIONS

Carbon xerogels are a very interesting alternative as Pt-support because the porosity and chemical characteristics can be fitted to improve the UA yield. The purity

of these support avoid interferences of the mineral matter present on classical ACs. The worse UA yield was obtained using highly mesoporous activated carbons containing acid mineral matter, which favors the development of secondary and cracking reactions. Basic sites can favor however the S_{UA} values, opening news doping possibilities. Very high UA yields were obtained by using a microporous xerogels obtained as microspheres shaped as Pt-support.

6.5. REFERENCES

[1] T. Ekou, A. Vicente, G. Lafaye, C. Especel, and P. Marecot. Bimetallic Rh-Ge and Pt-Ge catalysts supported on TiO_2 for citral hydrogenation I. Preparation and characterization of the catalysts, *Applied Catalysis A-General* **314**(1), 64, 2006.

[2] U.K. Singh and M.A. Vannice. Liquid-phase citral hydrogenation over SiO_2-supported group VIII metals, *Journal of Catalysis* **199**(1), 73, 2001.

[3] F. Delbecq and P. Sautet. Competitive C=C and C=O Adsorption of α,β–Unsaturated Aldehydes on Pt and Pd Surfaces in Relation with the Selectivity of Hydrogenation Reactions: A Theoretical Approach, *Journal of Catalysis* **152**(2), 217, 1995.

[4] G. Lafaye, C. Micheaud-Especel, C. Montassier, and P. Marecot. Characterization of bimetallic rhodium-germanium catalysts prepared by surface redox reaction, *Applied Catalysis A-General* **230**(1-2), 19, 2002.

[5] S. Santiago-Pedro, V. Tamayo-Galván, and T. Viveros-García. Effect of the acid–base properties of the support on the performance of Pt catalysts in the partial hydrogenation of citral, *Catalysis Today* **213**(0), 101, 2013.

[6] A. Vicente, T. Ekou, G. Lafaye, C. Especel, P. Marecot, and C.T. Williams. Influence of the nature of the precursor salts on the properties of Rh-Ge/TiO_2 catalysts for citral hydrogenation, *Journal of Catalysis* **275**(2), 202, 2010.

[7] A. Stolle, T. Gallert, C. Schmoger, and B. Ondruschka. Hydrogenation of citral: a wide-spread model reaction for selective reduction of α,β-unsaturated aldehydes, *RSC Advances* **3**(7), 2112, 2013.

[8] E. Bailón-García, F.J. Maldonado-Hódar, A.F. Pérez-Cadenas, and F. Carrasco-Marín. Catalysts Supported on Carbon Materials for the Selective Hydrogenation of Citral, *Catalysts* **3**(4), 853, 2013.

[9] J. Aumo, S. Oksanen, J.P. Mikkola, T. Salmi, and D.Y. Murzin. Novel woven active carbon fiber catalyst in the hydrogenation of citral, *Catalysis Today* **102**, 128, 2005.

[10] B. Bachiller-Baeza, A. Guerrero-Ruiz, P. Wang, and I. Rodríguez-Ramos. Hydrogenation of citral on activated carbon and high-surface-area graphite-

supported ruthenium catalysts modified with iron, *Journal of Catalysis* **204**(2), 450, 2001.

[11] E. Asedegbega-Nieto, A. Guerrero-Ruiz, and I. Rodríguez-Ramos. Modification of the stereo selectivity in the citral hydrogenation by application of carbon nanotubes as support of the Pt particles, *Carbon* **44**(4), 804, 2006.

[12] J. Khanderi, R.C. Hoffmann, J. Engstler, J.J. Schneider, J. Arras, P. Claus, and G. Cherkashinin. Binary Au/MWCNT and Ternary Au/ZnO/MWCNT Nanocomposites: Synthesis, Characterisation and Catalytic Performance, *Chemistry-A European Journal* **16**(7), 2300, 2010.

[13] F. Qin, W. Shen, C.C. Wang, and H.L. Xu. Selective hydrogenation of citral over a novel platinum/MWNTs nanocomposites, *Catalysis Communications* **9**(11-12), 2095, 2008.

[14] M. Steffan, F. Klasovsky, J. Arras, C. Roth, J. Radnik, H. Hofmeister, and P. Claus. Carbon-carbon double bond versus carbonyl group hydrogenation: Controlling the intramolecular selectivity with polyaniline-supported platinum catalysts, *Advanced Synthesis and Catalysis* **350**(9), 1337, 2008.

[15] F.J. Maldonado-Hódar. Advances in the development of nanostructured catalysts based on carbon gels, *Catalysis Today* **218–219**(0), 43, 2013.

[16] E. Gallegos-Suárez, A.F. Pérez-Cadenas, F.J. Maldonado-Hódar, and F. Carrasco-Marín. On the micro- and mesoporosity of carbon aerogels and xerogels. The role of the drying conditions during the synthesis processes, *Chemical Engineering Journal* **181–182**(0), 851, 2012.

[17] J.F. Vivo-Vilches, E. Bailón-García, A.F. Pérez-Cadenas, F. Carrasco-Marín, and F.J. Maldonado-Hódar. Tailoring the surface chemistry and porosity of activated carbons: Evidence of reorganization and mobility of oxygenated surface groups, *Carbon* **68**(0), 520, 2014.

[18] S. Brunauer, P.H. Emmett, and E. Teller. Adsorption of Gases in Multimolecular Layers, *Journal of the American Chemical Society* **60**(2), 309-319, 1-2-1938.

[19] M.M. Dubinin. Generalization of the theory of volume filling of micropores to nonhomogeneous microporous structures, *Carbon* **23**(4), 373, 1985.

[20] MM. Dubinin. Contemporary state of the theory of volume filling of micropores of adsorbents in the adsorption of gases and vapors on carbon adsorbents, *Russian Journal of Physical Chemestry* **39**, 1305, 1965.

[21] F. Stoeckli, *porosity in carbons - characterization and applications* (Arnold, London, 1995).

[22] C.A. Leon, J.M. Solar, V. Calemma, and L.R. Radovic. Evidence for the protonation of basal plane sites on carbon, *Carbon* **30**(5), 797, 1992.

[23] U. Zielke, K.J. Hüttinger, and W.P. Hoffman. Surface-oxidized carbon fibers: I. Surface structure and chemistry, *Carbon* **34**(8), 983, 1996.

[24] S.A. Al-Muhtaseb and J.A. Ritter. Preparation and Properties of Resorcinol–Formaldehyde Organic and Carbon Gels, *Advanced Materials* **15**(2), 101-114, 16-1-2003.

[25] S. Morales-Torres, F.J. Maldonado-Hódar, A.F. Pérez-Cadenas, and F. Carrasco-Marín. Textural and mechanical characteristics of carbon aerogels synthesized by polymerization of resorcinol and formaldehyde using alkali carbonates as basification agents, *Physical Chemistry Chemical Physics* **12**(35), 10365-10372, 2010.

[26] U.K. Singh and M.A. Vannice. Kinetics of liquid-phase hydrogenation reactions over supported metal catalysts- a review, *Applied Catalysis A: General* **213**(1), 1, 2001.

[27] H.J. Jiang, H.B. Jiang, D.M. Zhu, X.L. Zheng, H.Y. Fu, H. Chen, and R.X. Li. Cooperation between the surface hydroxyl groups of the support and organic additives in the highly selective hydrogenation of citral, *Applied Catalysis A: General* **445-446**, 351, 2012.

[28] A. Pérez-Cadenas, F.J. Maldonado-Hódar, and C. Moreno-Castilla. On the nature of surface acid sites of chlorinated activated carbons, *Carbon* **41**(3), 473, 2003.

Capítulo VII

ABOUT THE ACTIVE PHASE SELECTION IN DESIGNING SELECTIVE HYDROGENATION CATALYSTS SUPPORTED ON CARBON XEROGEL MICROSPHERES

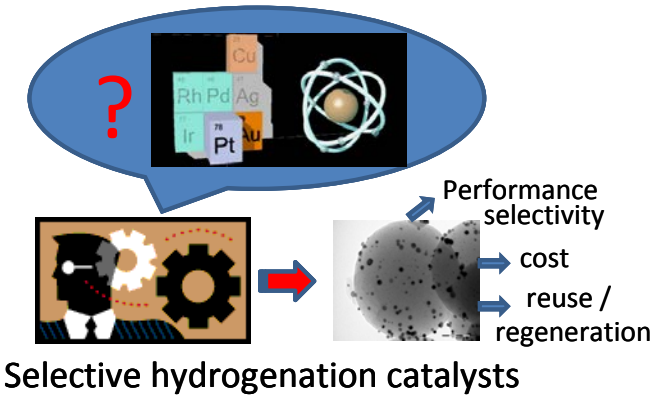

Selective hydrogenation catalysts

ABOUT THE ACTIVE PHASE SELECTION IN DESIGNING SELECTIVE HYDROGENATION CATALYSTS SUPPORTED ON CARBON XEROGEL MICROSPHERES

Manuscript submitted to RSC Advances

Highlights

- Metal-supported catalysts were prepared on microporous spheres of carbon xerogel.
- The selection of the active phase strongly determines the catalytic performance and the economy of the process.
- The performance of Ir, Pt and Ru-supported catalysts is compared.
- The best performance was obtained using Pt-catalysts.
- In terms of reusing catalysts, with Ir catalyst the best behaviour was observed.
- Deactivation was related with the chemical nature of the deposit generated along reactions.

Abstract

A series of monometallic Pt, Ir and Ru-catalysts supported on carbon xerogel microspheres was prepared, exhaustively characterized and used for the selective hydrogenation of citral. The metal particle size was similar in all cases after He-pre-treatment and the catalytic activity increases in the sense Ir < Ru < Pt, however the sintering was stronger after H_2-flow pre-treatment for Ru-catalysts leading to an important activity loss. Pt and Ir-catalysts were also more selective than Ru-catalysts, reaching selectivity values to unsaturated alcohols of around 80%. Thus, in terms of yields to these valuable products, Pt-catalyst seems to be the most appropriate active phase. Nevertheless, reutilization experiments showed that Ir-catalyst maintained a good performance, while Pt-catalyst was strongly deactivated. This fact was related with the different nature of the deposits formed during reaction.

7.1. INTRODUCTION

The selective hydrogenation of carbonyl groups of α,β-unsaturated aldehydes, to produce unsaturated alcohols, is a challenging process either from a scientific or economic point of view[1-3]. The selective hydrogenation of citral is one of the more feasible ways to obtain nerol and geraniol, molecules with a high demand for the pharmaceutical or chemical industry. Furthermore, citral has very recently come to be produced petrochemically in very large quantities, and partial hydrogenation of citral has become a very interesting economical route as it would be a single step synthesis in contrast with the actual long and complicated synthesis procedure[4]. Therefore, the hydrogenation of citral is attracting the attention of a large number of scientists worldwide.

Nevertheless, the selective hydrogenation of citral is not easy, because citral possesses three potentially hydrogenable double bonds: an isolated C=C bond in addition to conjugated C=O and C=C bonds. Thermodynamic and kinetic reasons favour the hydrogenation of the C=C over the C=O group and thus even in the presence of most of conventional hydrogenation catalysts, the saturated aldehyde or alcohol (instead the unsaturated ones) are obtained as main reaction products[5,6].

In the catalyst design for the hydrogenation of α,β-unsaturated aldehydes there are several important issues which affect on the catalysts performance and product distribution including the nature of the active metal and supports used[7,8], the catalyst preparation method (catalyst precursor, pretreatments, etc)[9,10], dispersion of the active phase and interaction with the support, the addition of a second metal[9,11,12], as well as other factors relating to the operating conditions as solvent (which is important in the formation of acetals), stirring, temperature, H_2-pressure and initial reactant / catalyst concentration.

Regarding the catalytic phase, not only the performance but also economic factors related with the stability, regeneration and price, should be considered. In general, transition metals are used as active phase. Vannice and Singh[6] show that the catalytic activity in citral hydrogenation varies as: Pd> Pt> Ir> Os> Ru> Rh> Ni> Co >> Fe. Catalysts based in Os showed a high selectivity to unsaturated alcohols (88%),

Ru and Co showed a moderate selectivity (55%) but, Pt, Ir, Rh, Ni and Pd were more selective to citronellal and isopulegol (0% unsaturated alcohols).

Several studies show also the importance of the support[7,13,14] on the catalyst performance. In previous manuscripts, we conclude that carbon xerogels offers several advantages as Pt-support regarding inorganic oxides[13] and even other carbon materials [14] on the basis of purity, absence of acidity and a defined morphology and porous texture. Moreover, the catalytic performance clearly is based on the combination of the support / active phase characteristics and their interactions. This fact was early studied by Sokol'skii[15] and Giroir-Fendler *et al.*[16] in the crotonaldehyde and cinnamaldehyde hydrogenation, respectively. They described a high selectivity to crotyl alcohol when Pt and Os are supported on Fe_2O_3. However, using carbon supports only obtained a similar selectivity value (around 75%) using Ir, but selectivity is moderate with Pt and Ru and poor using Rh and Pd. The S_{UA} of Pt and Ru-catalysts dramatically increased when supported on graphite regarding activated carbons, while iridium has a high intrinsic selectivity which is not modified by the carbon nature.

On the contrary, strong variations in the performance of Ir-catalysts were described by different authors[5,7]. Thus, using Ir/TiO_2, S_{UA} reached values as high as 91%–100%[17,18] while others authors get only a moderate selectivity of 60%[19] with the same catalyst and operating conditions. Similarly, using Ir/SiO_2 catalysts very different selectivity values, among 100%[17], 40%[20] or 15%[8], were obtained. Nevertheless, all of these studies agree with the poor activity of Ir-catalysts, where conversion values typically present values smaller than 15%[7].

These variations in the S_{UA} depending on the nature of supports / active phase were attributed to electronic transfers. The S_{UA} seem to be correlated with the metal d-band width, according to theoretical calculations of Delbecq and Soutet and semi-empirical calculations of Hückel[2,21]. With increasing electron density and hence d-orbital population, the repulsive electron interaction of the metal with the C=C double bond increases and the interaction of the metal surface with the C=O π-system is favoured[5,22]. Thus, in general it is described that independently of the support, Pd, Rh and Ni-catalysts are unselective to unsaturated alcohol, moderate selectivity values are achieved using Ru-catalysts while those based in Os are highly selective. As

commented, there is however a great dispersion of results regarding the behaviour of Pt and Ir-catalysts.

In previous manuscripts[13,14] we have prepared different Pt/C catalysts for the citral hydrogenation. The morphology and porosity of these supports were optimized regarding other carbon and inorganic supports, concluding that the preparation of microporous microspheres present the best combination of chemical and porous properties to enhance the catalytic performance of Pt-catalysts deposited on non-graphitic carbon supports. In this manuscript, we analyze de influence of the active phase dispersed on such optimized support, studying the characteristics of Pt, Ir and Ru catalysts obtained by the same preparation procedure and establishing relationships between these properties and the catalytic performance.

7.2. EXPERIMENTAL

The carbon xerogel (A8) was prepared by polycondensation of resorcinol with formaldehyde in aqueous media, using Cs_2CO_3 as a polymerization catalyst by modifying a previous synthesis procedure[23]. This synthesis procedure has been described in another publication[13,14]. In brief, the proper amount of resorcinol and cesium carbonate were added to deionised water in a three-neck glass reactor provided of reflux, controlled temperature (85 ºC) and stirring. Then, formaldehyde solution (Sigma, 37 wt.%) was added dropwise in the flask under agitation (250 rpm) and the gel formed was aged at 85°C for 24 hours. Finally, the suspension was filtered and placed in acetone (3 days, changing acetone twice a day) to exchange water within the pores by acetone, in order to reduce the porosity collapse during the subsequent drying process[24]. The gel was dried by microwave using a Saivod MS-287W microwave oven under nitrogen atmosphere in periods of 1 minute at 384 W until constant weight and carbonized to obtain the corresponding carbon xerogel in N_2 flow at 150 cm^3/min, heating to 900 ºC at a heating rate of 1 ºC/min, in order to allow a soft removing of pyrolysis gases, and soaking time of 2 h.

The support was milled and sieved to a diameter smaller than 0.150 mm before impregnation. Platinum, Iridium and Rutenium catalysts were prepared by impregnation at 3 wt.% Metal-loading using an aqueous solution that contains the

appropriate amount of $[Pt(NH_3)_4]Cl_2$, $IrCl_4$ and $RuCl_3$, respectively and pretreated in He or H_2 flow at 400 ºC (heating rate of 5 ºC/min) for 12 h. Catalysts were refereed indicating the support, the metal-content and the final average metal-particle size determined by H_2-chemisorption. Thus, as an example, A8Pt3-8 indicates that Pt was deposited on the carbon support and presents a particle size of 8 nm.

The morphology of the support was studied by scanning electron microscopy (SEM) using a LEO (Carl Zeiss) GEMINI-1530 microscope. Textural characterization was carried out by N_2 and CO_2 adsorption at −196 ºC and 0º C, respectively, with a Quantachrome Autosorb-1 equipment. The BET and Dubinin–Radushkevich equations were applied to determine the apparent surface area (S_{BET}) and the micropore volume (W_0), the average micropore width (L_0) and the microporous surface (S_{mic}), respectively[25-28]. The total pore volume was considered as the volume of N_2 adsorbed at $P/P_0 = 0.95$[29].

Pt dispersion (D) and average particle size (d) were obtained by H_2-chemisorption. The H_2-chemisorption isotherms were measured at 25 ºC. The metal dispersion is obtained from the amount of H_2-chemisorbed assuming a stoichiometric ratio H_2:Metal = 1:2 (dissociative chemisorption) and the average particle size was calculated as $d_M(H_2) = k/D$ (nm) (k=1.08 for Pt, 0.91 for Ru and 1.11 for Ir)[30-35]. HRTEM experiments were carried out using a Phillips CM-20 microscope equipped with an EDAX microanalysis system and microphotograph analyzed by the appropriate software.

The chemical characterization of the catalysts was further analyzed by X-ray photoelectron spectroscopy (XPS). The spectra were obtained on a Kratos Axis Ultra-DLD X-ray photoelectron spectrometer equipped with a hemispherical electron analyzer connected to a detector DLD (delay-line detector).

Thermogravimetric experiments of used catalysts were carried out in N_2-flow with coupled-FTIR analysis of the evolved gases (TPD) in order to obtain information about the amount and nature of organic compound deposits. In this sense, desorbed gases (CO, CO_2, H_2O and aliphatic rest, CH_4) were simultaneously analyzed.

The citral hydrogenation was carried out in 100 ml heptane solution at a constant hydrogen pressure of 8.3 bar and 90 ºC using a Parr reactor model 5500. The experimental conditions, being citral concentration, catalyst weight and agitation speed, were previously optimized in order to avoid mass transfer limitations (results not shown) and fixed in 0.05 M, 500 mg and 1500 rpm, respectively. A small volume of a sample was periodically withdraw and analyzed by chromatography using a Bruker 430-GC equipped with a FID detector and a Varian GC (25m x 0.32 mm x 0.45 μm) column. Both citral and any possible product were previously calibrated.

7.3. RESULTS AND DISCUSSION

7.3.1. Morphology and textural characterization

In previous manuscripts the textural and morphological properties of different carbon supports including carbon xerogels were optimized. The best performance in the citral hydrogenation was obtained using microporous materials structured in microspheres[14], Figure 7.1a. This material was selected now to develop a catalysts series based on different metals (M= Pt, Ru, Ir). The textural characteristics of the support and their respective pretreated M-catalysts are summarized in Table 7.1. The volume of N_2 adsorbed close to saturation (P/P_0 = 0.95; $V_{0.95}$) was considered as the total pore volume of the samples[29]. All the N_2-adsorption isotherms obtained corresponding to type I, and the results obtained from them (Table 7.1), point out that A8-support is a microporous material, with a null mesopore volume (V_{meso}), but that exhibits an important macropore volume as detected by mercury porosimetry (V_{macro} = 3.91 cm^3g^{-1}). Microporosity is intrinsic of the carbon microspheres, being mainly formed during carbonization by the release of gases[36], while large interparticle voids (macropores) are generated between them. The PSD (Figure 7.1b) obtained in this case, shows two maxima clearly located at the micrometer range. Catalysts present smaller micropore volumes and surface areas than their corresponding supports, denoting a certain micropore blockage after the deposition of metal-particles. The total pore volume detected by N_2-adsorption ($V_{0.95}$) progressively decreases with increasing the metal-particle size detected. However macroporosity does not change, confirming the interparticle character of this porosity range.

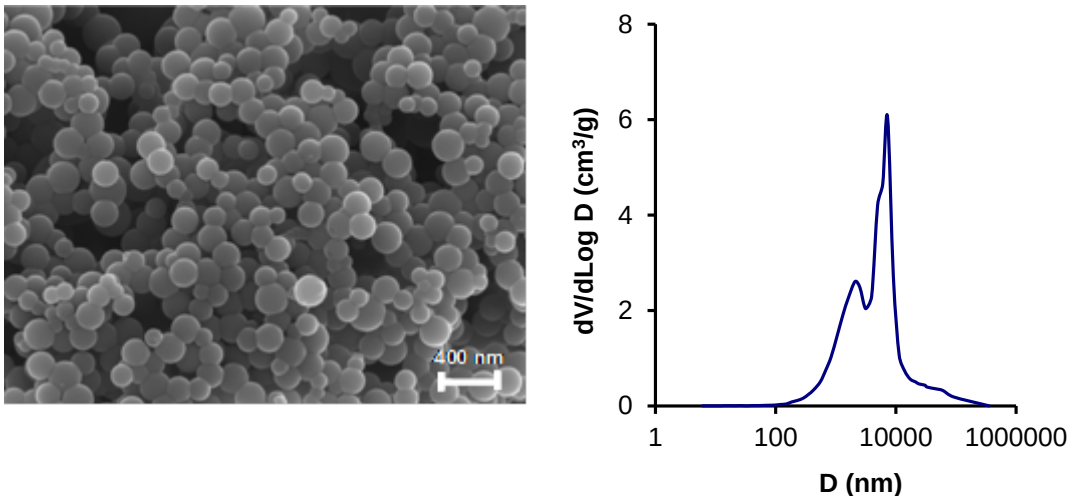

Figure 7.1. SEM image showing the morphology of A8-support and the pore size distribution obtained by mercury porosimetry.

Table 7.1. Textural characteristics of carbon support and derivatives Pt-catalysts.

		N_2-adsorption					CO_2-adsorption		
Sample	**Pretreatment conditions**	**S_{BET} $m^2 \cdot g^{-1}$**	**W_0 $cm^3 \cdot g^{-1}$**	**L_0 nm**	**V_{meso} $cm^3 \cdot g^{-1}$**	**$V_{0.95}$ $cm^3 \cdot g^{-1}$**	**W_0 $cm^3 \cdot g^{-1}$**	**S_{mic} $m^2 \cdot g^{-1}$**	**L_0 nm**
A8	-	614	0.25	0.78	0.00	0.31	0.29	952	0.60
A8Pt3-5	He/400ºC	553	0.22	0.64	0.00	0.25	0.28	965	0.58
A8Pt3-8	H_2/400ºC	521	0.21	0.60	0.00	0.22	0.28	960	0.58
A8Ir3-4	He/400ºC	578	0.23	0.73	0.00	0.32	0.29	933	0.62
A8Ir3-5	H_2/400ºC	595	0.24	0.50	0.00	0.31	0.30	997	0.61
A8Ru3-5	He/400ºC	573	0.23	0.72	0.00	0.31	0.28	913	0.62
A8Ru3-13	H_2/400ºC	404	0.15	0.91	0.00	0.26	0.24	749	0.63

7.3.2. Metal-characterization: nature and dispersion

It is well known that the hydrogenation of α-β unsaturated aldehydes is strongly dependent of metal dispersion[2,12,22]. In this catalyst series, the metal dispersion was tentatively modified by changing the pretreatment atmosphere. As commented in the experimental section, catalysts were pretreated at 400 ºC/12h in He or H_2 flow. The metal nature and dispersion were analyzed by XPS, DRX, H_2-chemisorption and TEM measurements. Results are summarized in Table 7.2, some representative TEM micrographs are shown in Figure 7.2 and the Pt-particle distribution calculated from

them in Figure 7.3. TEM images show in all cases a very high density of metal-nanoparticles on the spherical particles of the carbon support although sintering is favoured after H_2-pretreatment and mainly in the case of Ru-catalyst (Figure 7.2). In general there is a good agreement between the metal-particle size values obtained by TEM and H_2-chemisorption. Some large particles are always observed by TEM together with a majority of smaller ones, but this fact is not pointed out by H_2-chemisorption that only provides an average particle size. However, even this technique clearly points out the conclusion previously commented: H_2-pretretament favours the metal sintering regarding the He one being this effect stronger in the sense Ir<Pt<Ru. This is also pointed out by the significant shifting of the particle size distribution measured for Ru-catalysts after each pretreatment (Figure 7.3).

Table 7.2. Average metal-particle size ($\bar{d}_{H_2}$) determined by H_2-chemisorption and HRTEM ($\bar{d}_{TEM}$). XPS results: metal-surface concentration (M_{XPS}, % Wt.), B.E. of metal-species detected (M^0 and M^{II}) and their proportions (%).

Catalyst	$\bar{d}_{H_2}$ (nm)	$\bar{d}_{TEM}$ (nm)	M_{XPS} (% Wt)	M^0 BE (eV)	M^0 (%)	M^{II} BE (eV)	M^{II} (%)
A8Pt3-5	5.1	7.2	7.0	71.3	72	72.5	28
A8Pt3-8	7.9	9.3	4.4	71.3	70	72.3	30
A8Ir3-4	4.4	3.0	6.1	61.2	64	62.2	36
A8Ir3-5	5.2	3.4	5.8	61.3	66	62.2	34
A8Ru3-5	5.0	5.4	7.4	462.5	69	464.8	31
A8Ru3-13	13.4	7.5	5.1	462.2	70	464.2	30

Similarly, XPS results show that in all cases the surface metal content (M_{XPS} %) is greater than the theoretical loading (3%), indicating the metal concentration on the external surface. This parameter decreases after the H_2-pretreatment regarding the He-one, as a consequence of the greater Pt-particle size obtained. Due to the absence of mesoporosity in the support, and because always the metal particle size exceeds the micropore size (2 nm) these particles should be formed preferentially on the outer surface of the carbon microspheres, as is also denoted by the HRTEM images.

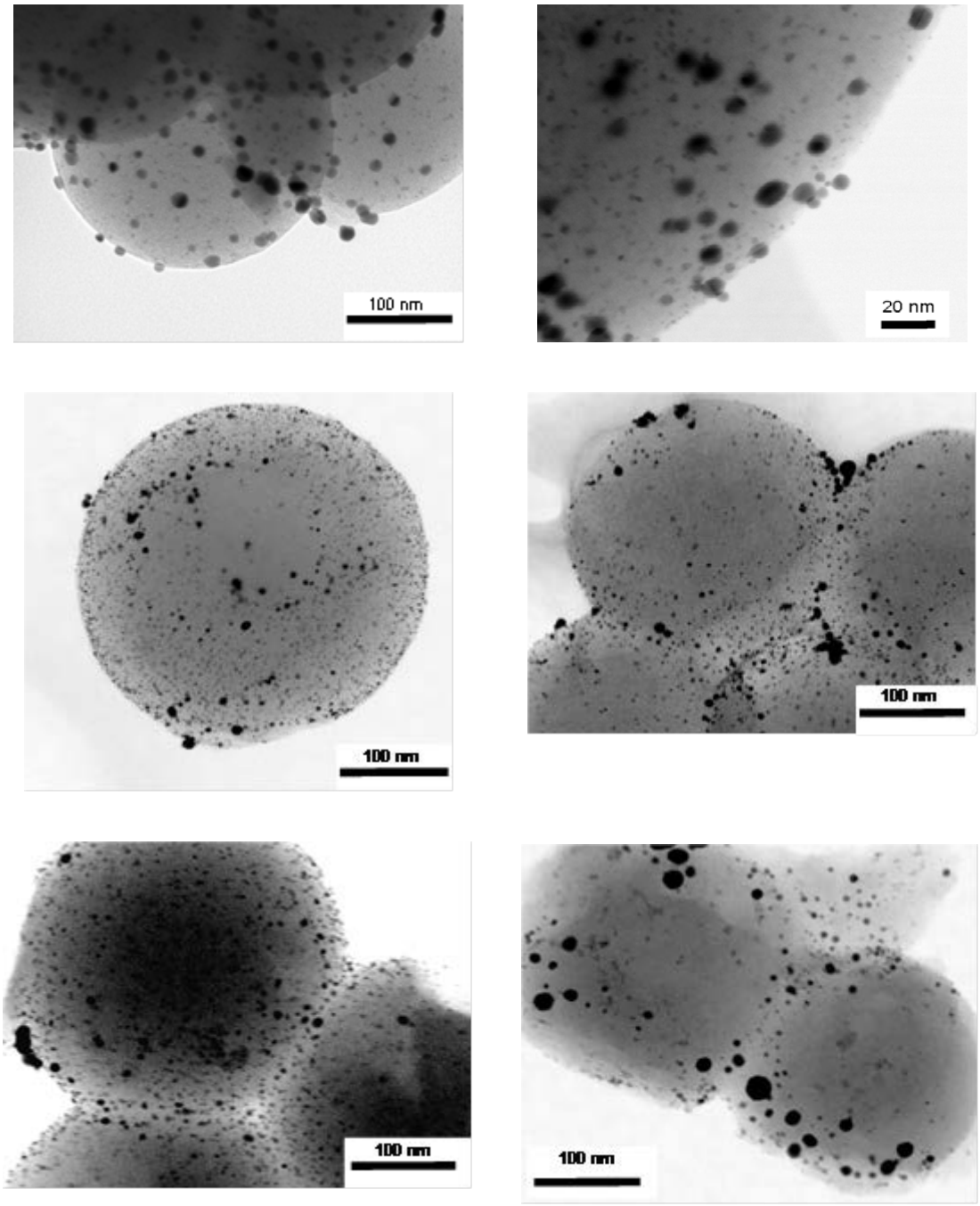

Figure 7.2. HRTM images of catalysts after He (left) or H_2-pretreatment (right). a) Pt, b) Ir and c) Ru-catalysts.

The different metal-particle size and distribution is also influencing the final porous texture and surface area of the catalysts. Thus, it is noteworthy that the S_{BET} decreases linearly with increasing the metal particle size (Figure 7.4). Metal particles are blocking or partially filling the larger micropores, as denoted by the reduction of both W_0 (N_2) and L_0 (N_2) values (Table 7.1), however, these parameters remains

constant regarding A8 support for all the pretreated catalysts for the narrower microporosity (micropores smaller than 0.7 nm) determined by CO_2 adsorption. These results mean that the larger micropores (0.7-2 nm of diameter) are related with the high and homogeneous distribution of metal particles on the carbon microspheres surface observed by HRTEM, but no the narrowest ones.

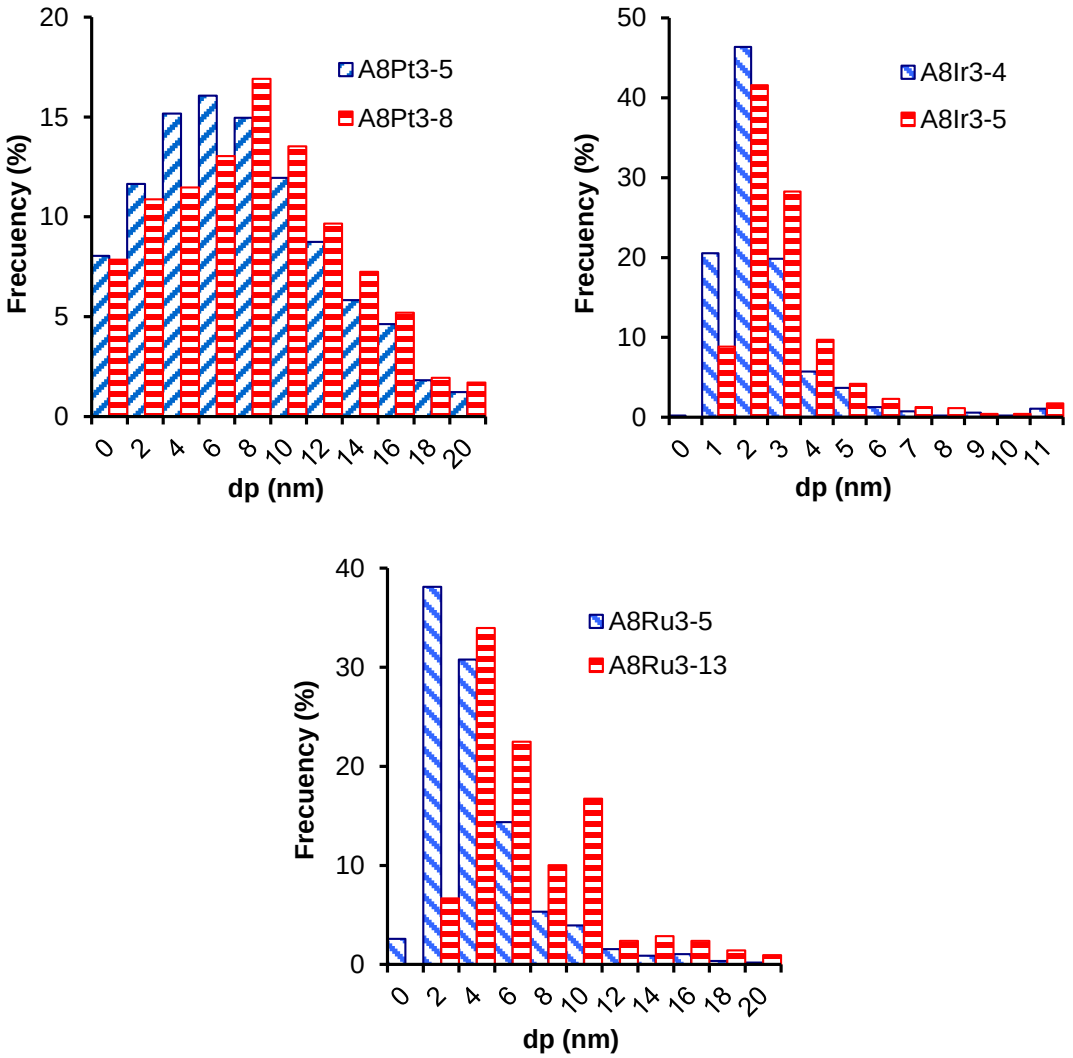

Figure 7.3. Pt-particle size distribution obtained from TEM images.

Regarding the chemical state of the different metals it was pointed out a mixture of M(0)/M(II) species in all the catalysts, this ratio is more or less independent of the metal and pretreatment used. In all cases there is a fraction of reduced metal around 70%, the oxidized phase can be formed during the storage in air before the analysis. However, XRD only showed peaks corresponding to the M^0 – species, indicating that the oxidized one can be amorphous particles or be formed on the more

reactive parts of the M^0 – nanoparticles (imperfections, borders, grain limits, etc) either by interaction with the air or with the oxygen content of the carbon surface.

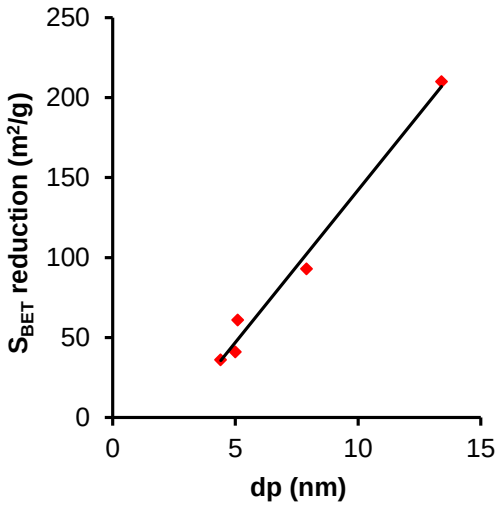

Figure 7.4. Relationship between the surface area blockage of catalysts and the average metal-particle size formed after each pretreatment.

7.3.3. Catalytic performance

Because all catalysts present a similar metal particle size after He-pretreatment (4.7 ± 0.4 nm, Table 7.2), the influence of the active phase can be pointed out directly by analyzing the evolution of the conversion and selectivity values along the reaction (Figure 7.5). Clearly, the catalytic activity increases in the sense Ir < Ru < Pt (Figure 7.5a). As commented, the low activity of Ir-catalysts is in agreement with previous studies[7]. Initially, the selectivity to the most valuable unsaturated alcohols varies as Ir>Ru>Pt, i.e. shows the opposite tendency than the catalytic activity (Figure 7.5b). However, the S_{UA} only presents constant values (at around 40%) in all the conversion range obtained when using Ru-catalyst, but increases during the reaction for Ir and Pt-catalysts. This increase is slower in the case of the Ir-catalyst and stronger and faster for Pt-catalyst, although the S_{UA} reaches in both cases a constant value around 70%.

After H_2-pretreatment, sintering is favoured in the sense Ir<Pt<Ru. The catalytic performance changes are directly related with the sintering degree regarding He-pretreatment. Thus, the slow increase in the metal particle size of Ir-catalyst mainly favours the activity without influencing selectivity values, the moderate sintering of Pt

favours both activity and selectivity, however, in the case of the Ru-catalyst, where sintering is stronger (Table 7.2), conversion clearly decreases 50% with a simultaneous decrease of the S_{UA} values. These results pointed out that both activity and selectivity present an optimum for a metal-particle size at around 8 nm, which is in agreement with previous studies[37]. Thus, probably the catalytic performance (mainly activity) of Ir-catalyst could be enhanced by increasing slowly the metal particle size obtained in these experimental conditions, while the selectivity values for Ru-catalyst seem to be always around 40%.

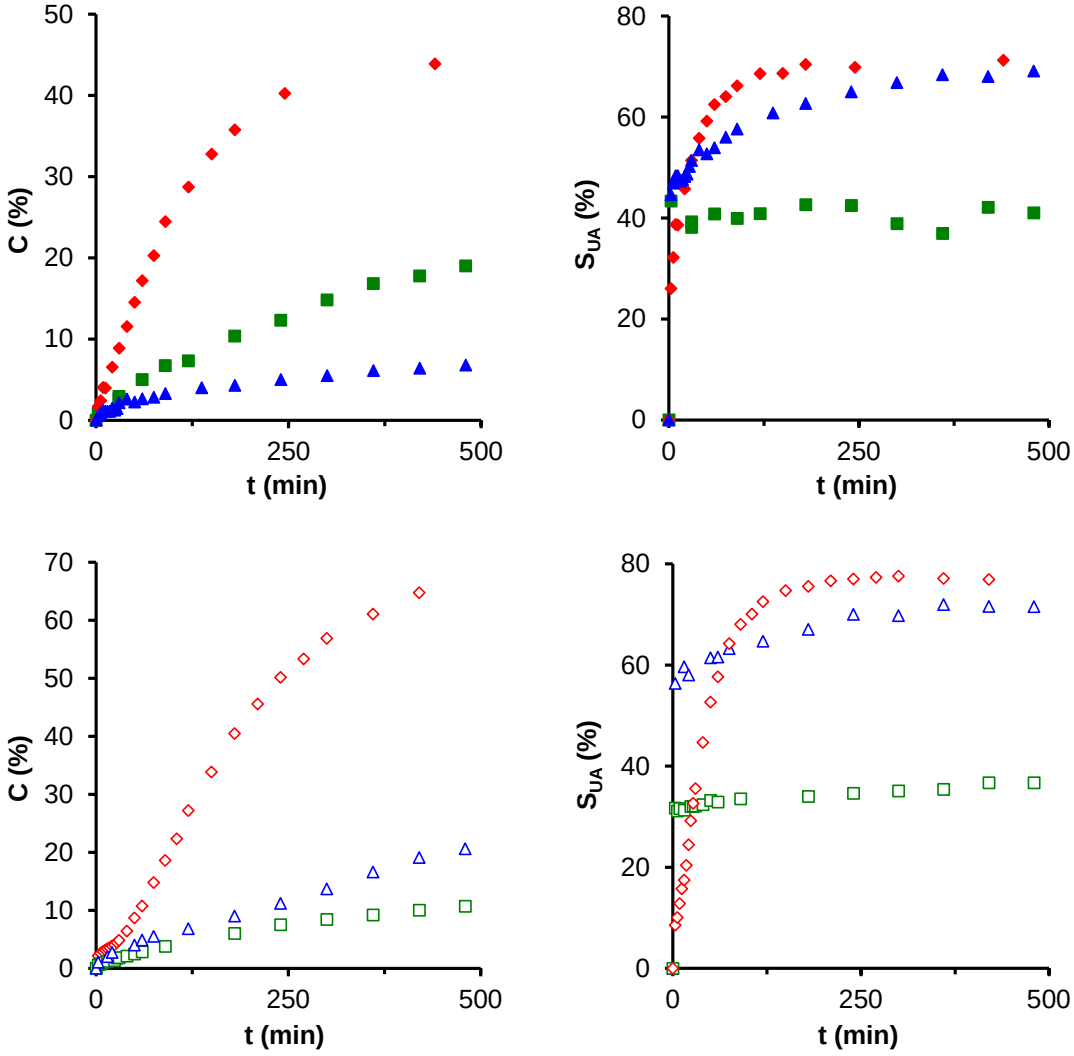

Figure 7.5. Conversion and S_{UA} obtained with 3% metal-loading catalysts (▲ Ir, ◆ Pt, ■ Ru) supported on carbon xerogel after a) He-pretreatment (closed symbols) and b) H_2-pretreatment: open symbols.

It is noteworthy that when Pt is supported on carbon xerogel, it generates both the most active and the most selective catalyst. Ir-supported catalyst provides similar selectivity to unsaturated alcohol than Pt-catalyst but the yield to these products is smaller by the smaller activity of this catalyst. Yield in UA still decrease using Ru-catalysts (A8Ru3-5), which shows an intermediate activity and selectivity.

The significant differences in activity between Pt and Ir can be explained on the basis of the d-character, which is an empirical indicator of the electronic structure of the metal, and refers to the contribution of the d-electrons to the spd hybrid orbitals assumed in Pauling's resonance valence band theory[8] and electronic effects[2,21]. The correlation of the TOF with percentage of d-character was made by Singh and Vannice[8] obtaining volcano plot results where Pd and Pt have the higher activity and Ru and Ir have similar low activity in term of TOF. The electrostatic interactions of metal particles with the double bonds of the reactant molecules also determine their selectivity. Increasing electron density and hence d-orbital population, the repulsive four electron interaction of the metal with the C=C double bond increase while with the C=O π-system is favoured[5,22].

When analysing the complete product distribution obtained in each case (Figure 7.6) it is observed that UA are formed preferentially at the initial of the reaction only in the case of Ir-catalysts, while citronellal is a main product obtained using either Pt or Ru-catalysts. The S_{UA} remains constant along reaction when using Ru-catalyst, independently the pretreatment used. In this case, with increasing conversion, secondary hydrogenation processes from citronellal to citronellol are favoured, but the complete hydrogenation to 3,7 DMO is not observed. In the case of Pt-catalyst, the strong increase of S_{UA} is accompanied by a simultaneous decrease of selectivity values to citronellal, and progressive hydrogenation to citronellol and 3,7 DMO also decreases, probably because secondary hydrogenation of citronellal are favoured regarding UA. Nevertheless, the selectivity to citronellol slowly increases at high conversion values, indicating that the formation of this product from UA is not completely avoided. A similar but slower evolution of product distribution can be described for Ir-catalyst. UA are formed instead of citronellal, increasing slowly the citronellol at high conversion values by hydrogenation of UA.

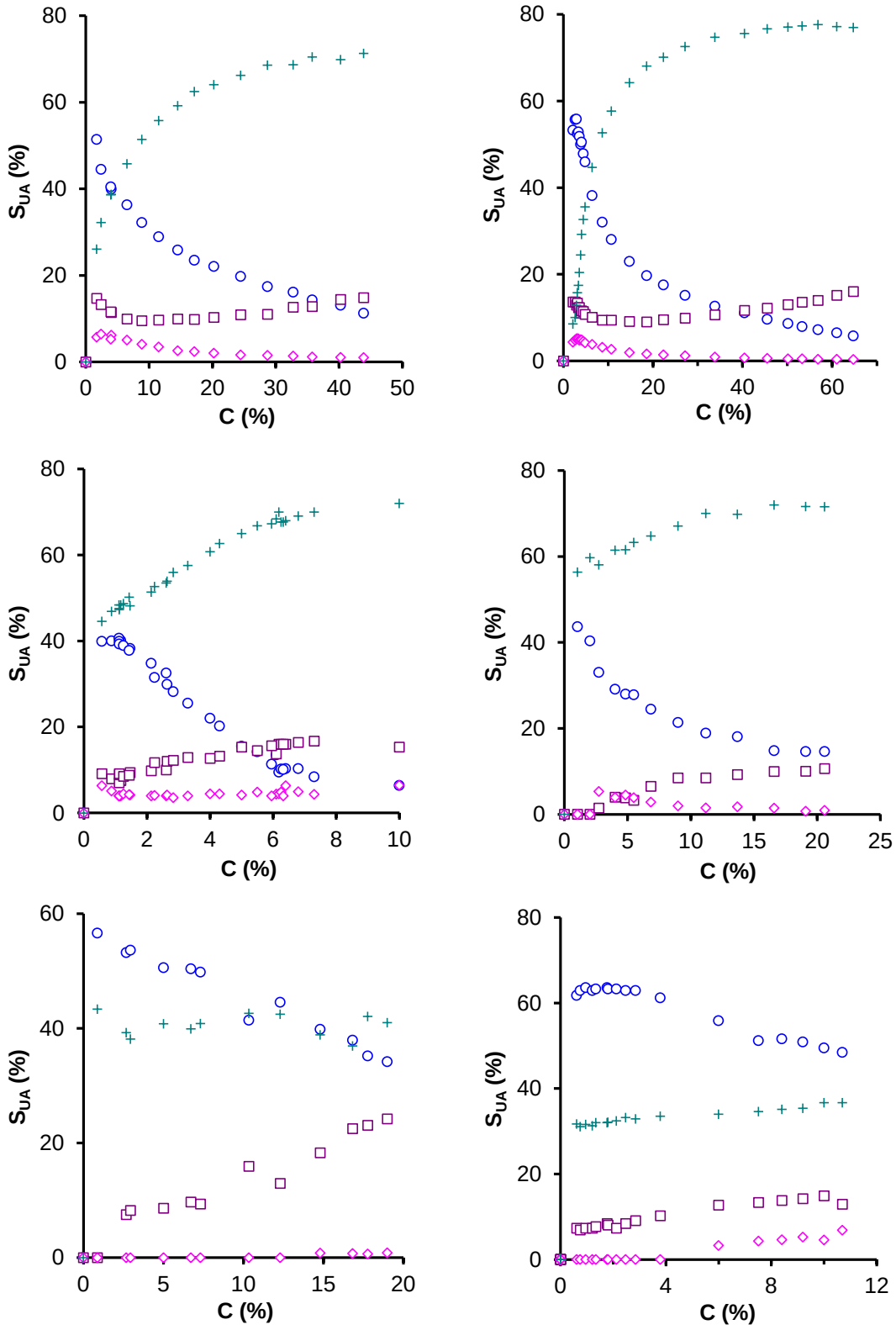

Figure 7.6. Products distribution as a function of the conversion reached (500 mg of catalyst, 1500 rpm, 0.05 M citral, P_{H_2} =8 bar, 90 °C): Citronellal (○) Citronellol (□), 3,7 DMO (◇) , S_{AU} (+). a) A8Pt3, b) A8Ir3, c) A8Ru3. Left: He-pretreatments, right: H_2-pretreatments.

These changes in the product distributions means that at the initial of the reaction some transformations in Pt and Ir-catalysts are produced that deactivate the more active centres where the C=C hydrogenation occurs, favouring the hydrogenation of the C=O bonds forming UA. In such a basis, used Ir and Pt-catalysts could be consequently more selective to UA than their corresponding fresh samples and therefore, the reuse of these samples seems to be quite interesting. Ru-catalyst is not included in this study due to the lower performance detected. The results obtained after a second hydrogenation cycle are compared in Figure 7.7.

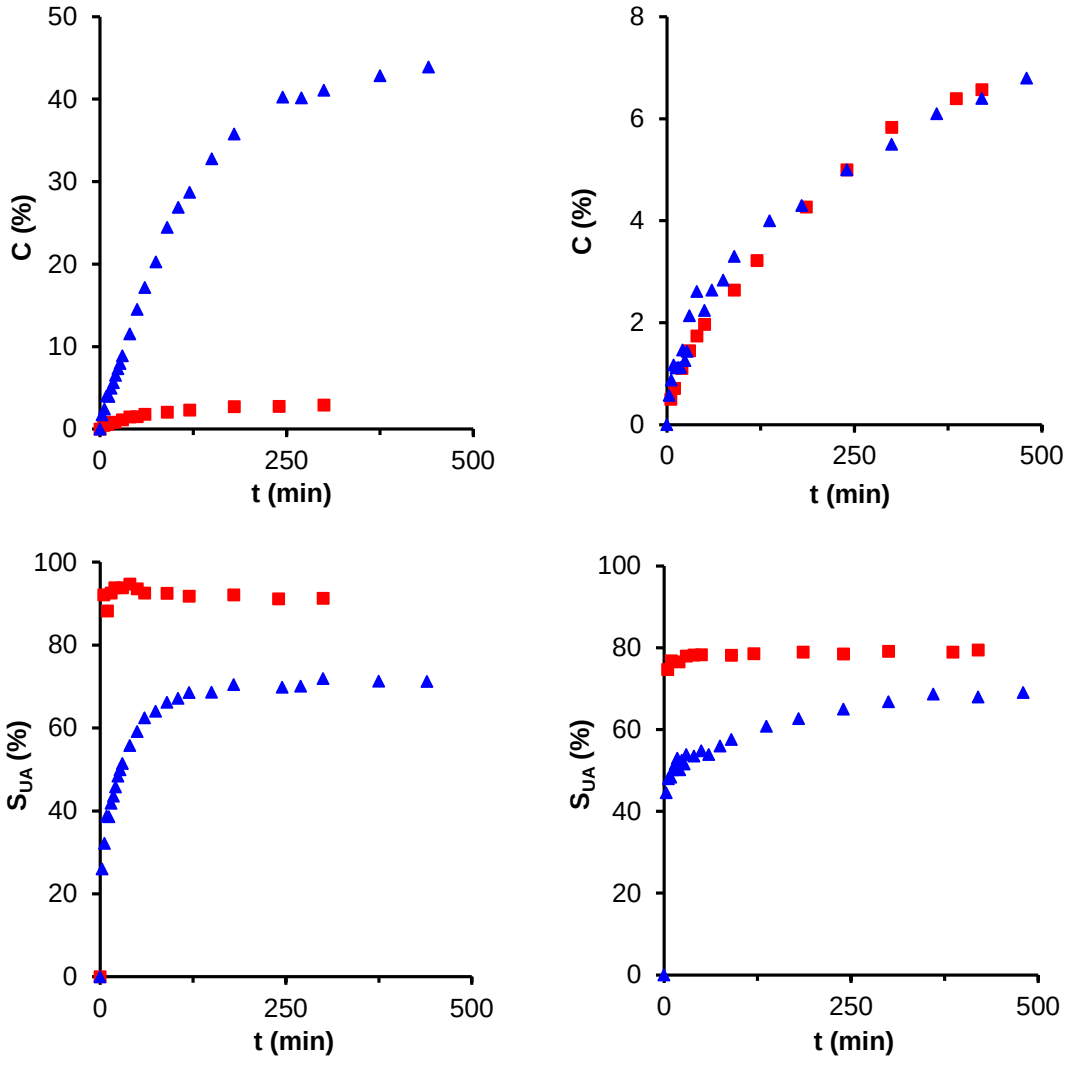

Figure 7.7. Evolution of conversion and selectivity values in two consecutive reaction cycles. Left A8Pt3-5, right A8Ir3-5. (▲) First cycle, (■) second cycle.

It is observed that the performance of Ir-catalyst is improved; the activity is maintained regarding the first hydrogenation cycle and the selectivity, as expected,

increase showing very high S_{UA} values (S_{UA} > 80 %). However, in the case of Pt-samples, catalyst is clearly deactivated, conversion values become very low in spite of UA being practically the only products obtained.

To elucidate this behaviour, the used catalysts were analyzed from a textural and chemical point of view. These changes should be associated to modification in the chemical and porous characteristics of supports, because no metal-leaching or sintering was observed by analysing both the liquid reaction media and the recovered solid catalysts.

The first question is to determine the amount of possible deposits formed more or less permanently on the catalyst surface but due to the carbon support nature, it is impossible to determine the exact content of these organic deposits by burning. Because the mass balances indicate a good agreement between the amount of reactants and reaction products, the amount of these deposits should be low. Nevertheless, a pore blockage of the support porosity was observed analyzing the N_2 isotherm of the used catalysts from 580 m^2g^{-1} to around 10 m^2g^{-1}. Nevertheless, this fact occurs in both Ir and Pt-catalysts after the first cycle of reaction, and the microporosity blockage does not influence the catalytic performance, as occurs in the case of Ir-samples, because metal particles are located on the external surface as previously described.

Therefore, Pt-deactivation should be related with chemical aspects. TG-experiments carried out in N_2-flow with coupled-FTIR analysis of the evolved gases (TPD) can provide some information about the amount and nature of such deposits. In this case, desorbed gases (CO, CO_2, H_2O and aliphatic rest, CH_4) were simultaneously analyzed. In Figure 7.8 the weight loss (WL) detected for Pt and Ir-catalysts after the first reaction cycle are shown. Fresh Ir-catalyst is used as a blank sample. It is observed that in both samples used, the WL increases regarding the fresh one. The used Ir-catalyst shows higher WL than the Pt-ones bellow 600 ºC, while from this temperature range this parameter quickly increases in the last case. These results indicate that both metals induce the formation of deposits with a different chemical nature.

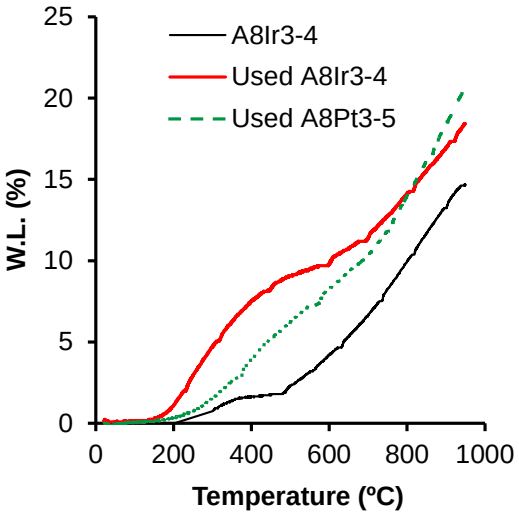

Figure 7.8. Thermogravimetric analysis of fresh and used catalysts.

These differences are also noticed by analyzing the nature of the gases evolved during the TG experiments. The formation of CO and CO_2 by decomposition of oxygenated groups located on the carbon surface is well documented[38,39]. Thus, CO_2 can be evolved from carboxylic acid groups that decompose at low temperature (typically bellow 400 ºC) while lactones can be stable up to 700 ºC. Other oxygenated structures like phenols, ether or quinones are evolved as CO and they are in general thermally more stable than those evolved as CO_2, typically evolving from 600 ºC. In our case, because supports are obtained at high temperature and catalysts were previously reduced, oxygenated surface groups should be generated mainly during citral reactions, being mainly associated to an adsorbed rest of citral or their derivatives products. As commented, the deposit generated on Ir-catalysts presents a smaller thermal stability than those formed on Pt-catalyst, as demonstrated by the WL observed by TG. This fact is also accompanied by a greater amount of CO_2 evolved (Figure 7.9). CO-desorption was only observed at high temperature, i.e. this is due to the decomposition of more stable oxygenated species. In this case, the amount of CO-evolved is higher in the case of used Pt-catalysts.

The enrichment of the support surface with oxygenated deposits changes the nature of this surface from hydrophobic to hydrophilic, which favours the citral adsorption through C=O bond and consequently the UA formation[13].This fact is observed for both Ir-and Pt-catalysts (Figures 7.6 and 7.7), while the Ru-one seems to be unaffected by this fact. Nevertheless, the importance of the nature of these deposits

plays an important role on the stability of the catalyst. Thus, while the activity of Ir-catalyst is maintained, the deactivation of Pt-hydrogenation centres by formation of carbon-like deposits was observed. This fact was also previously described by different authors[40,41], showing that irreversibly chemisorbed CO, formed by decomposition of citral molecules, can deactivate the active Pt-sites.

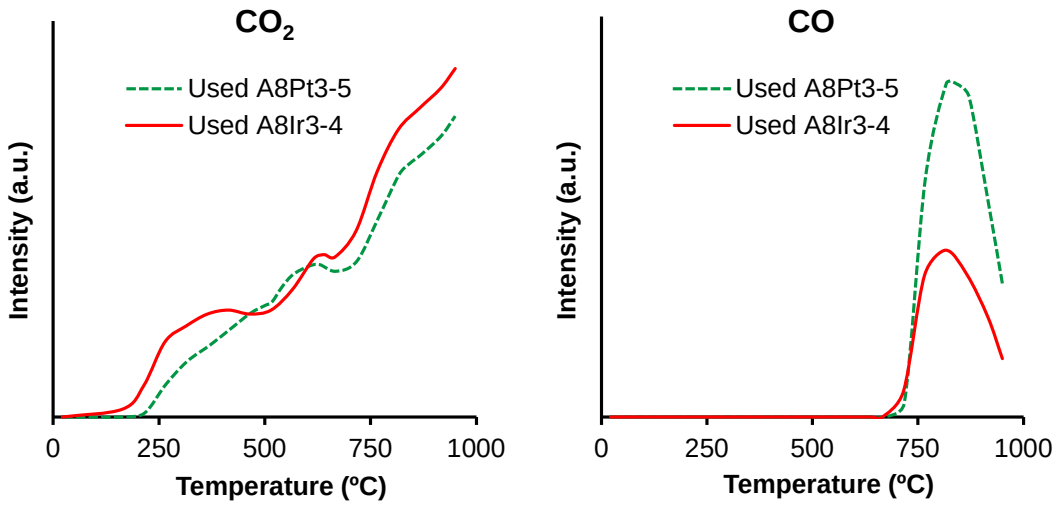

Figure 7.9. TPD-profiles of CO_2 and CO evolved from Ir and Pt-catalysts after a first cycle of citral hydrogenation.

7.4. CONCLUSIONS

A series of supported catalysts was obtained by impregnation of a carbon xerogel shaped in microspheres with different metal active phases (Pt, Ru, Ir). The pre-treatment in He-flow leads to a similar metal-dispersion, however the sintering increases after H_2-pretreatment mainly in the case of Ru-catalyst. In all cases, metal particles were formed exclusively on the external surface of microspheres because of the microporous character of the support.

The catalytic activity vary in the sense Pt>Ru>Ir, while the most selective catalysts were obtained with Pt and Ir. Thus the higher UA yield was obtained using Pt-catalyst. The catalytic performance was favoured by increasing the metal-particle size below 10 nm. The large sintering detected for Ru-catalyst provokes a decrease of both activity and selectivity. An intrinsic selectivity of around 40% was detected for Ru-

catalyst along the reaction, while this parameter clearly increased during the reaction for both Pt and Ir-catalysts, suggesting an interesting reuse of samples.

The reutilization experiments point out that a reutilization process is possible for the Ir-catalyst but a strong deactivation is found in the case of the Pt-catalyst. This is related with the formation of highly stable CO-species poisoning the Pt-active sites.

7.5. REFERENCES

[1] T. Ekou, A. Vicente, G. Lafaye, C. Especel, and P. Marecot. Bimetallic Rh-Ge and Pt-Ge catalysts supported on TiO_2 for citral hydrogenation I. Preparation and characterization of the catalysts, *Applied Catalysis A-General* **314**(1), 64, 2006.

[2] F. Delbecq and P. Sautet. Competitive C=C and C=O Adsorption of α,β–Unsaturated Aldehydes on Pt and Pd Surfaces in Relation with the Selectivity of Hydrogenation Reactions: A Theoretical Approach, *Journal of Catalysis* **152**(2), 217, 1995.

[3] T. Ekou, L. Ekou, A. Vicente, G. Lafaye, S. Pronier, C. Especel, and P. Marecot. Citral hydrogenation over Rh and Pt catalysts supported on TiO_2: Influence of the preparation and activation protocols of the catalysts, *Journal of Molecular Catalysis A-Chemical* **337**(1-2), 82, 2011.

[4] H. Surburg and J. Panten, *common fragrance and flavor materials: preparation, properties and uses*, 5th ed. (WILEY-VCH, Weinheim, Germany, 2006).

[5] P. Claus and Y. Önal, "Regioselective Hydrogenations",in *Handbook of Heterogeneous Catalysis,* Second ed. edited by G. Ertl, H. Knözinger, F. Schüth, and J. Weitkamp (WILEY-VCH, Weinheim (Germany), 2008), pp.3311-3312.

[6] A. Vannice and U.K. Singh. Citral hydrogenation over Pt and other group VIII metals, *Abstracts of Papers of the American Chemical Society* **223**, U437, 2002.

[7] E. Bailón-García, F.J. Maldonado-Hódar, A.F. Pérez-Cadenas, and F. Carrasco-Marín. Catalysts Supported on Carbon Materials for the Selective Hydrogenation of Citral, *Catalysts* **3**(4), 853, 2013.

[8] U.K. Singh and M.A. Vannice. Liquid-phase citral hydrogenation over SiO_2-supported group VIII metals, *Journal of Catalysis* **199**(1), 73, 2001.

[9] B. Coq, P.S. Kumbhar, C. Moreau, P. Moreau, and M.G. Warawdekar. Liquid phase hydrogenation of cinnamaldehyde over supported ruthenium catalysts: Influence of particle size, bimetallics and nature of support, *Journal of Molecular Catalysis* **85**(2), 215, 1993.

[10] V. Ponec. On the role of promoters in hydrogenations on metals; α,β–unsaturated aldehydes and ketones, *Applied Catalysis A: General* **149**(1), 27, 1997.

[11] S. Galvagno, C. Milone, A. Donato, G. Neri, and R. Pietropaolo. Hydrogenation of Citral Over Ru-Sn/C, *Catalysis Letters* **17**(1-2), 55, 1993.

[12] A. Giroir-Fendler, D. Richard, and P. Gallezot. Chemioselectivity in the catalytic hydrogenation of cinnamaldehyde. Effect of metal particle morphology, *Catalysis Letters* **5**(2), 175, 1990.

[13] E. Bailón-García, F. Carrasco-Marín, A.F. Pérez-Cadenas, and F.J. Maldonado-Hódar. Microspheres of carbon xerogel: an alternative Pt-support for the selective hydrogenation of citral, *Applied Catalysis A: General* **482**, 318, 2014.

[14] E. Bailón-García, F. Carrasco-Marín, A.F. Pérez-Cadenas, and F.J. Maldonado-Hódar. Development of carbon xerogels as alternative Pt-supports for the selective hydrogenation of citral, *Catalysis Communications* **58**, 64, 2014.

[15] D. Sokolskii, N. Anisimova, A. Zharmagambetova, S. Mukhamedzhanova, and L. Edygenova. Pt-Fe_2O_3 catalytic system for hydrogenation reactions, *Reaction Kinetics and Catalysis Letters* **33**(2), 399, 1987.

[16] A. Giroir-Fendler, D. Richard, and P. Gallezot, "Heterogeneus Catalysis and Fine Chemicals",in *Studies in surface science and catalysis*, edited by M. Guisnet, J. Barrault, C. Bouchoule, D. Duprez, C. Montassier, and G. Perot (Elsevier, Amsterdam, 1988), p.171.

[17] P. Reyes, H. Rojas, G. Pecchi, and J.L.G. Fierro. Liquid-phase hydrogenation of citral over Ir-supported catalysts, *Journal of Molecular Catalysis A-Chemical* **179**(1-2), 293, 2002.

[18] H. Rojas, G. Borda, P. Reyes, J.J. Martinez, J. Valencia, and J.L.G. Fierro. Citral hydrogenation over Ir/TiO_2 and Ir/TiO_2/SiO_2 catalysts, *Catalysis Today* **133**, 699, 2008.

[19] P. Chen, J.Q. Lu, G.Q. Xie, G.S. Hu, L. Zhu, L.F. Luo, W.X. Huang, and M.F. Luo. Effect of reduction temperature on selective hydrogenation of crotonaldehyde over Ir/TiO2 catalysts, *Applied Catalysis A: General* **433–434**(0), 236, 2012.

[20] G. Borda, H. Rojas, J. Murcia, J.L.G. Fierro, P. Reyes, and M. Oportus. Hydrogenation of citral on Ir/SiO_2 catalysts. Effect of the addition of Nb_2O_5 on surface and catalytic properties, *Reaction Kinetics and Catalysis Letters* **92**(2), 369, 2007.

[21] F. Delbecq and P. Sautet. A Density Functional Study of Adsorption Structures of Unsaturated Aldehydes on Pt(111): A Key Factor for Hydrogenation Selectivity, *Journal of Catalysis* **211**(2), 398, 2002.

[22] P. Claus. Selective hydrogenation of α,β–unsaturated aldehydes and other C=O and C=C bonds containing compounds, *Topics in Catalysis* **5**(1), 51, 1998.

[23] S. Morales-Torres, F.J. Maldonado-Hódar, A.F. Pérez-Cadenas, and F. Carrasco-Marín. Textural and mechanical characteristics of carbon aerogels synthesized by

polymerization of resorcinol and formaldehyde using alkali carbonates as basification agents, *Physical Chemistry Chemical Physics* **12**(35), 10365, 2010.

[24] E. Gallegos-Suárez, A.F. Pérez-Cadenas, F.J. Maldonado-Hódar, and F. Carrasco-Marín. On the micro- and mesoporosity of carbon aerogels and xerogels. The role of the drying conditions during the synthesis processes, *Chemical Engineering Journal* **181–182**(0), 851, 2012.

[25] S. Brunauer, P.H. Emmett, and E. Teller. Adsorption of Gases in Multimolecular Layers, *Journal of the American Chemical Society* **60**(2), 309-319, 1-2-1938.

[26] M.M. Dubinin. Generalization of the theory of volume filling of micropores to nonhomogeneous microporous structures, *Carbon* **23**(4), 373, 1985.

[27] MM. Dubinin. Contemporary state of the theory of volume filling of micropores of adsorbents in the adsorption of gases and vapors on carbon adsorbents, *Russian Journal of Physical Chemestry* **39**, 1305, 1965.

[28] F. Stoeckli, *porosity in carbons - characterization and applications* (Arnold, London, 1995).

[29] R. Ubago-Pérez, F. Carrasco-Marín, D. Fairén-Jiménez, and C. Moreno-Castilla. Granular and monolithic activated carbons from KOH-activation of olive stones, *Microporous and Mesoporous Materials* **92**(1–3), 64, 2006.

[30] J.E. Benson and M. Boudart. Hydrogen-oxygen titration method for the measurement of supported platinum surface areas, *Journal of Catalysis* **4**(6), 704, 1965.

[31] G.R. Wilson and W.K. Hall. Studies of the hydrogen held by solids: XVIII. Hydrogen and oxygen chemisorption on alumina- and zeolite-supported platinum, *Journal of Catalysis* **17**(2), 190, 1970.

[32] C. Moreno-Castilla, M.A. Salas-Peregrín, and F.J. López-Garzón. Hydrogenation of carbon oxides by Ru/activated carbon catalysts obtained from Ru3(CO)12: effect of pretreatment on their dispersion, composition and activity, *Journal of Molecular Catalysis A: Chemical* **95**(3), 223, 1995.

[33] F. Rodriguez-Reinoso, J. de Dios López-González, C. Moreno-Castilla, A. Guerrero-Ruiz, and I. Rodriguez-Ramos. Porous carbon as support for iron and ruthenium catalysts, *Fuel* **63**(8), 1089, 1984.

[34] H. Kubicka. The specific activity of technetium, rhenium, ruthenium, platinum, and palladium in catalytic reactions of benzene with hydrogen, *Journal of Catalysis* **12**(3), 223, 1968.

[35] P. Reyes, M.C. Aguirre, G. Pecchi, and J.L.G. Fierro. Crotonaldehyde hydrogenation on Ir supported catalysts, *Journal of Molecular Catalysis A: Chemical* **164**(1-2), 245, 2000.

[36] C. Moreno-Castilla and F.J. Maldonado-Hódar. Carbon aerogels for catalysis applications: An overview, *Carbon* **43**(3), 455, 2005.

[37] E. Bailón-García, F.J. Maldonado-Hódar, A.F. Pérez-Cadenas, and F. Carrasco-Marín. Fitting the experimental conditions and characteristics of Pt/C catalysts for the selective hydrogenation of citral, *Catalysis Science & Technology* , 2015.

[38] C. Moreno-Castilla, F. Carrasco-Marín, F.J. Maldonado-Hódar, and J. Rivera-Utrilla. Effects of non-oxidant and oxidant acid treatments on the surface properties of an activated carbon with very low ash content, *Carbon* **36**(1–2), 145, 1998.

[39] J.L. Figueiredo, M.F.R. Pereira, M.M.A. Freitas, and J.J.M. Órfão. Modification of the surface chemistry of activated carbons, *Carbon* **37**(9), 1379, 1999.

[40] D. Manikandan, D. Divakar, and T. Sivakumar. Selective hydrogenation of citral over noble metals intercalated montmorillonite catalysts, *Catalysis Letters* **123**(1-2), 107, 2008.

[41] U.K. Singh and M. Albert Vannice. Liquid-Phase Hydrogenation of Citral over Pt/SiO_2 Catalysts: I. Temperature Effects on Activity and Selectivity, *Journal of Catalysis* **191**(1), 165, 2000.

Capítulo VIII

DESARROLLO DE NUEVOS MATERIALES COMPUESTOS DE XEROGEL DE CARBÓN Y ÓXIDO INORGÁNICO

PATENTES EN TRÁMITE

CHAPTER OVERVIEW

This Chapter collects the synthesis of composites materials carbon xerogel – inorganic oxides and their applications in the selective hydrogenation of α,β-unsaturated compounds and/or photo-catalytic reactions. Actually, these materials are being patented and for this reason only an adequate resume of the patent applications should be included in this book.

The preparation of these materials has been carried out by the establishment of new and optimized one pot methods of synthesis in which the polymerization of resorcinol and formaldehyde takes place in organic media together with the hydrolysis of a metallic alkoxide, and where the alkoxide is the precursor compound of the TiO_2, SiO_2 or ZrO_2 phases in the new composites.

Therefore, section 8.1 collects the synthesis methods of carbon xerogel – TiO_2 and carbon xerogel – SiO_2 composites as well as the preparation of the corresponding platinum and iridium supported catalysts. These catalysts have shown a very high performance in the selective hydrogenation of α,β-unsaturated aldehydes, with selectivities higher than 95% (Table 8.1). The synthesis method of the composites consists in a very efficient methodical sequence where some specific steps determine the final excellent catalytic properties of these materials, for example: the use of some surfactant compounds, a strict control of the polymerization temperature during a very slow addition of some solutions, the stirring speed or the use of microwaves during the drying step. In these conditions a very high dispersion of the metal oxide phase is achieved on the carbon xerogel matrix, maximizing the metal-support interactions in the supported catalysts, which permits to obtain very high activities and selectivities in relative soft reaction conditions, avoiding the use of supercritical solvents or bimetallic catalysts and therefore making possible cheaper catalytic processes.

Section 8.2 collects the synthesis methods of carbon xerogel – ZrO_2 composites which show excellent catalytic behaviour in the photo-degradation of organic pollutant using visible light (Figure 8.1). The synthesis method of the composites also consists in a very efficient new methodology which allows obtaining carbon xerogels doped with high zirconia loadings very well dispersed on the carbon

matrix, reaching a synergic effect which permits the use of visible light for pollutant degradation. The results obtained with these zirconia composites are at the same level or better than the equivalent ones reported for different optimized titanium composites.

Table 8.1. Selectivity to unsaturated alcohols obtained using Pt supported catalysts (3 wt.% metal loading) at 50% of conversion in the selective hydrogenation of citral.

Catalizador	**t (min)**	**S_{UA} (%)**
A8Pt3-8	270	77.3
TiPt3-9	60	79.5
CTi10Pt3-8	60	73.6
CTi20Pt3-7	26	85.7
CTi30Pt3-9	18	90.5
CTi40Pt3-9	12	95.2
CTi50Pt3-10	27	88.3
CTi80Pt3-10	150	77.3
SiPt3-20	-	19.6 (al 36% C)
CSi30Pt3-22	90	92.2

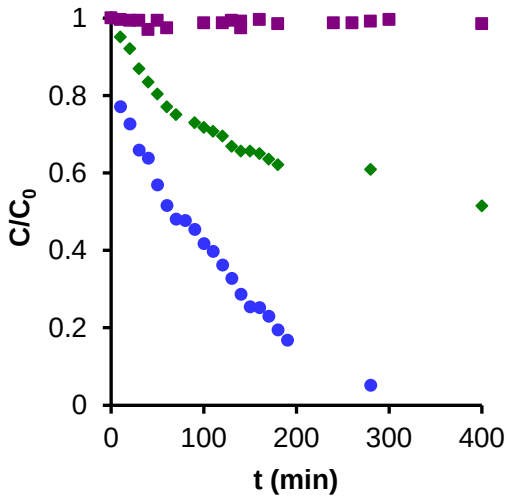

Figure 8.1. Photocatalytic degradation kinetics of Orange G using zirconia-carbon composite under visible light. P25 (◆), CZr40 (●) and photolysis (■).

Finally, Section 8.3 collects a synthesis method modified with respect to the method described in Section 8.1 for the carbon xerogel – TiO_2 composite preparation which permits to obtain carbon xerogel microspheres coated with TiO_2 (Figure 8.2). This TiO_2 coating is stable enough to use in the tested catalytic conditions. A pre-gelation step of the resorcinol – formaldehyde phase is crucial to obtain this type of composite. This new materials have been tested in the photo-degradation of Orange G using visible light with very good results (Figure 8.3). On the other side, the special hydrophobic/hydrophilic character of this composite allows its precipitation in aqueous solutions making possible an easy separation from the media after reaction (Figure 8.4), which is a very important advantage for real applications.

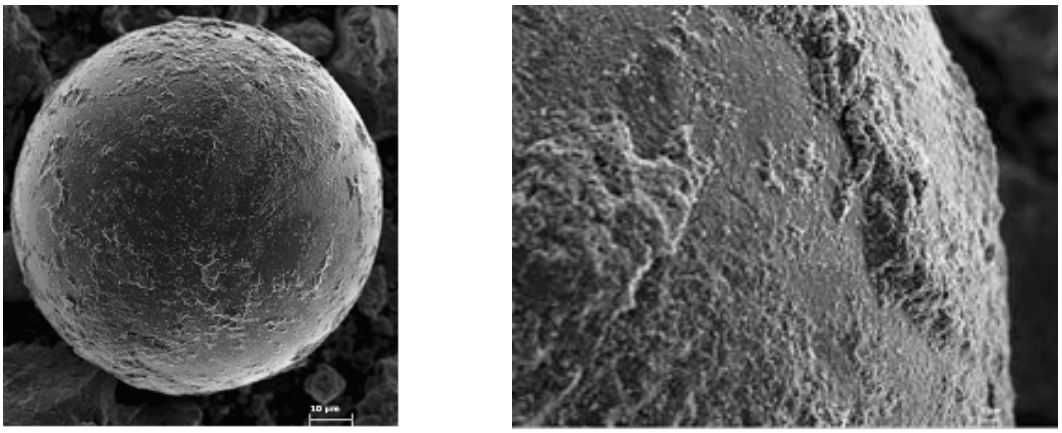

Figure 8.2. SEM images of carbon xerogel microspheres coated with TiO_2. b) Surface detail.

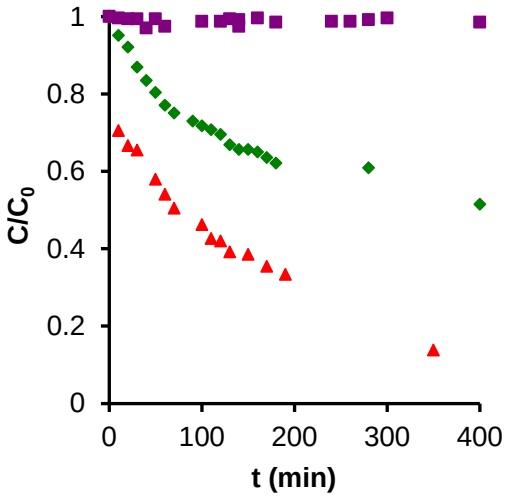

Figure 8.3. Photocatalytic degradation kinetics of Orange G using carbon xerogel microspheres coated with TiO_2 (CTi40S2h) under visible light. P25 (◆), CTi40S2h (▲) and Photolysis (■).

Figure 8.4. Suspensions of the photo-catalysts after reaction. Left (CTi40S2h); right (P25).

8.1. MÉTODO DE PREPARACIÓN DE MATERIALES COMPUESTOS ÓXIDO INORGÁNICO - CARBÓN Y SUS APLICACIONES EN EL DESARROLLO DE CATALIZADORES ESPECÍFICOS PARA LA HIDROGENACIÓN SELECTIVA DE α,β INSATURADOS

D. JUAN ANTONIO MUÑOZ ORELLANA, TÉCNICO DE LA OFICINA DE TRANSFERENCIA DE RESULTADOS DE INVESTIGACION DE LA UNIVERSIDAD DE GRANADA

INFORMA: Que según nuestros archivos, Dña. Ester María José Bailón García figura como inventora en la invención "M***étodo de preparación de materiales compuestos óxido inorgánico – carbón y sus aplicaciones en el desarrollo de catalizadores específicos para la hidrogenación selectiva de α,β–insaturados***",** para la que se ha solicitado protección mediante patente y a la que esta oficina le ha asignado la referencia interna **IPR- 523**.

Y que en estos momentos se está preparando la correspondiente solicitud de patente ante la Oficina Española de Patentes y Marcas por lo que **toda la información relativa a esta invención debe ser considerada confidencial** para salvaguardar la patentabilidad de la misma.

Granada, a 20 de febrero de 2015.

Fdo.: Juan Antonio Muñoz Orellana

Universidad de Granada

Ref. Interna: IPR-523

MÉTODO DE PREPARACIÓN DE MATERIALES COMPUESTOS ÓXIDO INORGÁNICO – CARBÓN Y SUS APLICACIONES EN EL DESARROLLO DE CATALIZADORES ESPECÍFICOS PARA LA HIDROGENACIÓN SELECTIVA DE α,β-INSATURADOS

INFORMACIÓN PARA LA VALORIZACIÓN DE LA INVENCIÓN

El cuestionario que sigue a continuación pretende proporcionar a la OTRI elementos para evaluar la patentabilidad de la invención y agilizar su posible transferencia, si ésta no está ya comprometida. Trate de responder a los apartados que pueda, pero deje en blanco los que no sepa responder para rellenarlos, junto con el personal técnico de la OTRI, en los contactos que está previsto mantener al efecto.

1.- ORIGEN DE LA INVENCIÓN

La invención es resultado de:

☒ proyecto de investigación *(citar título, entidad financiadora y código de referencia):*

Control estructural de materiales avanzados de carbón para la optimización de su comportamiento como filtros, membranas y soportes de catalizadores. Ministerio de Ciencia e Innovación - FEDER ref. CTM2010-18889

☐ un contrato de investigación (*citar nombre de la empresa/entidad*):

☐ un proyecto de Investigación con participación empresarial (*citar código de referencia, entidad financiadora y empresa*):

☐ otros (explicar):

¿La titularidad de la posible patente debe ser compartida con otra entidad?

SI ☐ NO ☒

En caso afirmativo,

¿qué entidad?

¿en qué % debe ser propietario la UGR? %

¿hay documento contractual que así lo acredita ? SI ☐ NO ☐

Universidad de Granada

Ref. Interna: IPR-523

2.- GRADO DE DIFUSIÓN DE LA INVENCIÓN

¿Se ha difundido previamente el objeto de la invención?

☐ SI ☒ NO

En caso afirmativo, indique medio de difusión, fecha y contenido (depósito y defensa de tesis, publicaciones, congresos, proyectos fin de carrera, medios de comunicación,…)

3.- ESTADO DE LA TÉCNICA

Describa el estado del arte del campo de su invención. Incluya referencias conocidas cercanas a su tecnología (artículos, patentes, páginas webs, proyectos, etc.). Si es necesario, anexe los citados documentos a este impreso.

Los aldehídos α,β-insaturados son moléculas que contienen al menos dos dobles enlaces potencialmente hidrogenables, un doble enlace C=C y un doble enlace C=O conjugados. La hidrogenación selectiva de estos aldehídos α,β-insaturados hacia el alcohol insaturado (producto deseado) tiene gran importancia tanto a nivel industrial (para la producción de sustancias químicas específicas o farmacéuticas) como a nivel científico. Se plantea pues el reto científico de desarrollar catalizadores selectivos hacia la formación de alcoholes insaturados, ya que la obtención del aldehído saturado o el alcohol saturado es termodinámica y cinéticamente más favorable que la obtención del alcohol insaturado. Además, es un reto económico, pues estos últimos son de mayor valor añadido. Actualmente, en presencia de la mayoría de los catalizadores monometálicos convencionales (Pt, Rh, Pd, Ru o Co) soportados tanto sobre soportes inorgánicos clásicos como sílice o alúmina, o sobre carbón activado, se obtiene mayoritariamente el aldehído o alcohol saturado[1-3].

Dos de estos aldehídos α,β-insaturados de gran importancia a nivel industrial son el citral y el cinamaldehído dada las aplicaciones de sus alcoholes insaturados[4-12]. De este modo la hidrogenación selectiva de estas moléculas ha atraído la atención de un gran número de grupos de investigación a nivel internacional[13,14].

La hidrogenación selectiva de citral hacia nerol y geraniol es complicada. Este aldehído contiene dos dobles enlaces C=C y un doble enlace C=O y, además, dos

estero-isómeros (geranial (E) y neral (Z)) de modo que su esquema de reacción es bastante complejo (Figura 8.1.1) por la gran cantidad de productos que pueden obtenerse, así como otras reacciones no deseadas como ciclación, reacciones con el disolvente, cracking, etc, que pueden tener lugar. De este modo, el objetivo es aumentar selectivamente la hidrogenación del enlace C=O para producir nerol y geraniol, disminuyendo paralelamente la hidrogenación del enlace C=C para reducir la formación de citronelal, y lo que es aún más difícil, para evitar hidrogenaciones consecutivas hacia el alcohol o aldehído saturado (citronelol, 3,7-dimetiloctanol y 3,7-dimetiloctanal), así como evitar rutas de ciclación que darían lugar al isopulegol, y su alcohol saturado, el mentol.

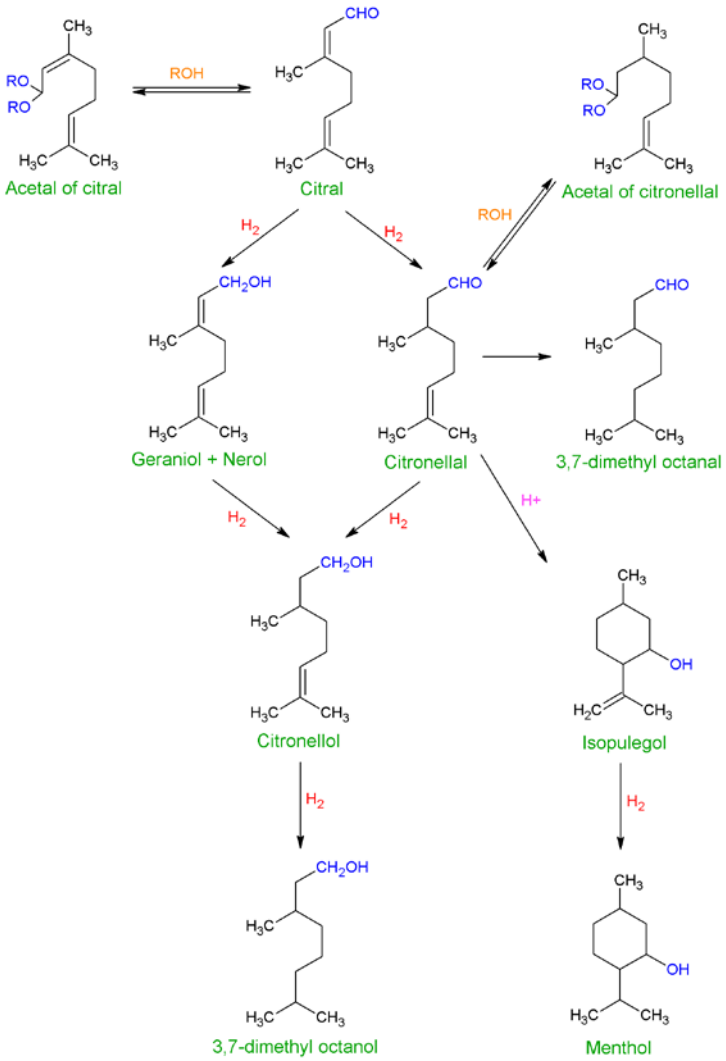

Figura 8.1.1. Esquema de reacción de hidrogenación del citral.

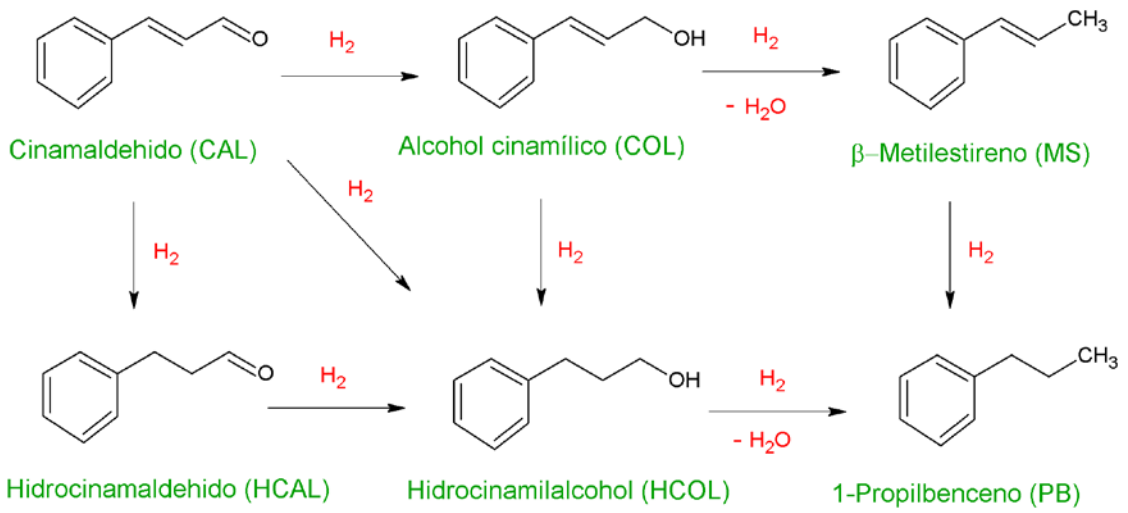

Figura 8.1.2. Esquema de reacción de hidrogenación del cinamaldehído.

Igual ocurre con el cinamaldehído (Figura 8.1.2). Este posee un doble enlace C=C conjugado con el C=O y su hidrogenación produce el alcohol insaturado (alcohol cinamílico) mediante la hidrogenación del doble enlace C=O, el aldehído saturado (hidrocinamaldehído) mediante la hidrogenación del doble enlace C=C o bien el alcohol saturado (Hidrocinamilalcohol) por hidrogenación de ambos dobles enlaces. Por otra parte también pueden darse reacciones de deshidratación del alcohol insaturado o del alcohol saturado, obteniéndose el β-metilestireno o el 1-propilbenceno, respectivamente

De este modo, la obtención selectiva de los correspondientes alcoholes insaturados se ve dificultada tanto por cuestiones termodinámicas como por la multitud de rutas de reacción existentes que conllevan a una gran variedad de productos. La obtención de alcoholes insaturados puede lograrse únicamente mediante un diseño óptimo del catalizador heterogéneo y la optimización de las condiciones de operación, de modo que se activen los modos de adsorción a través grupo C=O y/o se dificulten los modos de adsorción del enlace C=C[15].

Con el empleo de catalizadores mono-metálicos en la hidrogenación selectiva de cinamaldehído y citral se obtiene generalmente el alcohol insaturado con una selectividad inferior al 60%[14,16-32]. Se han realizado grandes esfuerzos para mejorar esta

selectividad mediante el empleo de catalizadores bimetálicos[14,33-48], empleo de soportes no convencionales como nanotubos[49-58], grafenos[59], mezclas de óxidos inorgánicos o con la adicción de sustancias básicas que modifiquen la interacción de la molécula con el catalizador[60-62]. No obstante, en el mejor de los casos solo se obtienen selectividades **(S_{UA})** entorno al 85% para el cinamaldehído, siendo superior (95%) para el citral, pero a conversiones no muy elevadas, por lo que el rendimiento es bajo. Para obtener rendimientos mayores se debe recurrir al empleo de condiciones más extremas como sería con el uso de disolventes no convencionales como CO_2 supercrítico o líquidos iónicos[63-71], aumentando con ello el coste del proceso y de los equipos necesarios pues deben trabajar a altas presiones[67]. Otro modo de obtener selectividades mayores con altas conversiones sería con la combinación de varios factores como son la preparación de catalizadores bi-metálicos, el uso de soportes más específicos como los nanotubos y el empleo de altas presiones de H_2 (>25 Bar)[72-74], lo cual también aumenta el coste de obtención del alcohol insaturado.

Así pues, no solo es de importancia la selección y diseño del catalizador, sino que también la optimización de las condiciones de operación. Según bibliografía, un aumento en la temperatura produce un aumento en la conversión pues se favorece la transferencia de hidrogeno desde el sitio catalítico al doble enlace. En cuanto a la selectividad, es algo más contradictorio pues hay autores que observan un descenso en la selectividad, dado que se favorecen las hidrogenaciones sucesivas así como otras reacciones secundarias de ruptura (cracking)[75,76] y otros que observan un aumento[77,78]. Por otro lado, un aumento en la presión produce un aumento en la conversión manteniéndose la selectividad constante cuando las presiones son moderadas[75,79-81] y un aumento en selectividad para presiones más elevadas[68,77] aunque depende del disolvente empleado. Fundamentalmente se usan alcoholes como etanol, isopropanol o 2-propanol, no obstante éstos pueden dar lugar a reacciones de condensación con los alcoholes producidos por lo que alternativamente se usan olefinas como el hexano, heptano, etc. De este modo, el rango de condiciones experimentales usado es muy amplio, la temperatura varía entre 25-200 ºC y la presión entre 1-75 Bar, así como diversos disolventes, velocidades de agitación, cargas de catalizador, etc.

Universidad de Granada

Ref. Interna: IPR-523

4- OBJETO DE LA INVENCIÓN

Por favor, defina su resultado (elija una o varias opciones):

- ☒ un nuevo producto (considerar 'producto' en sentido general)
- ☐ un nuevo procedimiento de invención
- ☐ mejora de un producto existente
- ☒ mejora de un proceso existente
- ☐ una idea
- ☐ un servicio nuevo o mejorado

Por favor, enumere los productos alternativos a su invención que ya existen en el mercado actualmente:

En la preparación de catalizadores de hidrogenación el inconveniente de los soportes inorgánicos es su baja área superficial ya que en este tipo de catalizadores es deseable una mayor área superficial que facilite la dispersión de la fase activa. Las interacciones metal – soporte se favorecen también mediante el uso de óxidos parcialmente reducibles, fundamentalmente TiO_2. De este modo, materiales como sílice o carbón se emplean como soportes para depositar estos óxidos parcialmente reducibles con el objetivo de aumentar el área del mismo en contacto con la fase activa. Analizada la bibliografía, algunos de los resultados catalíticos obtenidos con este tipo de soportes en la hidrogenación selectiva de cinamaldehído y citral se muestran en la Tabla 8.1.1 y 8.1.2, respectivamente. Se observa que a pesar de intentar mejorar el rendimiento de los catalizadores mono-metálicos usando la estrategia anteriormente descrita, no se logran altos rendimientos hacia los alcoholes insaturados con el empleo de mezclas óxido inorgánico-óxido parcialmente reducido e incluso, en el caso de mezclas óxido parcialmente reducible-carbón el rendimiento es inferior al 20 % [82-84].

Tabla 8.1.1. Hidrogenación selectiva de cinamaldehído sobre materiales compuestos.

Catalizador	P Bar	Tª ºC	Disolvente	C %	S_{UA} %	Ref.
Pt/SiO_2-V_2O_5	1	150	-	-	32.1	85
Pt/SiO_2-TiO_2	1	150	-	-	38.3	
Pt/TiO_2-V_2O_5	1	150	-	-	40.3	
Pt/TiO_2-ZrO_2	1	150	-	-	41.7	
Pt/MgO-TiO_2	1	150	-	-	44.2	
Pt/MgO-V_2O_5	1	150	-	-	50.8	
Pt/SiO_2	1	150	-	-	3.9	
Pt/TiO_2	1	150	-	-	19.9	
Pt/CeO_2-ZrO2	20	100	Isopropanol	63.4	71.1	86

Tabla 8.1.2. Hidrogenación selectiva de citral sobre materiales compuestos.

Catalizador	P Bar	Tª ºC	Disolvente	C, %	S_{UA} %	Ref.
Pt/SiO_2	20	100	Isopropanol	50	7	87
Pt/SiO_2-TiO_2	20	100	Isopropanol	50	46	
Pt/SiO_2-ZrO_2	20	100	Isopropanol	45	75	82-84
Pd/C-TiO_2	30	90	Isopropanol	90	0	
Pt/C-CeO_2	70	70	Isopropanol	75	16	88
Pt/TiO_2	70	70	Isopropanol	70	45	
Pt/Al_2O_3	70	70	Isopropanol	90	5	89
$Pt/10\%TiO_2$–Al_2O_3	70	70	Isopropanol	40	10	
$Pt/20\%TiO_2$–Al_2O_3	70	70	Isopropanol	40	35	
$Pt/33\%TiO_2$–Al_2O_3	70	70	Isopropanol	40	50	
$Pt/25\%TiO_2$-SiO_2	70	70	Isopropanol	90	25	
$Pt/40\%TiO_2$-SiO_2	70	70	Isopropanol	80	30	90
Pt/SiO_2	70	70	Isopropanol	95	2	
Pt/TiO_2	70	70	Isopropanol	100	20	
Ir/SiO_2	6.2	90	Heptano	5	63	91
Ir/Nb_2O_5	6.2	90	Heptano	15	21	
Ir/SiO_2-Nb_2O_5	6.2	90	Heptano	5	100	

Tabla 8.1.2. Hidrogenación selectiva de citral sobre materiales compuestos. (Continuación)

Catalizador	P Bar	Tª ºC	Disolvente	C, %	S_{UA} %	Ref.
Pt/SiO_2	70	70	Isopropanol	100	4	92
$Pt/2\%TiO_2\text{-}SiO_2$	70	70	Isopropanol	77	10	
$Pt/8\%TiO_2\text{-}SiO_2$	70	70	Isopropanol	71	20	
$Pt/12\%TiO_2\text{-}SiO_2$	70	70	Isopropanol	61	32	
$Pt/18\%TiO_2\text{-}SiO_2$	70	70	Isopropanol	88	13	
$Pt/25\%TiO_2\text{-}SiO_2$	70	70	Isopropanol	90	12	
Pt/TiO_2	70	70	Isopropanol	100	10	

Indique qué ventajas técnicas y beneficios económicos tiene la invención respecto a los citados productos:

- ✓ En los materiales compuestos gel de carbón - óxido inorgánico existe un claro sinergismo comparado con sus respectivos óxidos metálicos puros obteniendo selectividades y actividades mejoradas cuando se usan los materiales compuestos.
- ✓ La selectividad alcanzada con el empleo de materiales compuestos óxido inorgánico-carbón son muy superiores (entorno 95 %)
- ✓ El rendimiento está entorno al 80 % con una conversión superior al 90%.
- ✓ No se requiere del empleo de condiciones extremas de presión y temperatura, ni de condiciones supercríticas (CO_2 supercrítico como disolvente) lo cual hace más económico el proceso.
- ✓ No precisa del uso de catalizadores bimetálicos lo cual encarece el proceso.
- ✓ En estos nuevos materiales compuestos, el óxido inorgánico se encuentra altamente disperso de modo que se maximiza las interacciones metal – soporte (efecto SMSI) obteniéndose actividades y selectividades mejoradas.

- ✓ El tiempo de reacción necesario para alcanzar el rendimiento máximo es inferior a 40 min, (en la mayoría de los sistemas se necesitan tiempos superiores a 3-4 h) lo cual hace más económico el proceso debido al menor gasto energético.

La invención se considera nueva porque:

☒ no se ha encontrado nada igual en bancos de datos de patentes
☒ no se ha encontrado nada igual en la bibliografía científica consultada
☒ no se ha encontrado nada igual en un informe de búsqueda completo

5.- APLICACIONES DE LA INVENCIÓN

Describa las aplicaciones industriales de la invención

Los nuevos materiales compuestos propuestos son geles de carbón dopados con óxido de titanio u óxido de silicio obtenidos empleando nuevas rutas de síntesis. Presentamos la utilización de estos materiales compuestos en base a sus prestaciones como soporte de catalizadores metálicos, tales como: Pt e Ir. Los catalizadores soportados resultantes hacen posible que las reacciones de hidrogenación de aldehídos α,β-insaturados, en fase líquida, transcurran selectivamente hacia la obtención de los correspondientes alcoholes insaturados, productos muy apreciados en la industria química y farmacéutica. Por lo tanto los sectores técnicos relacionados con esta invención son el químico e industrial.

Universidad de Granada

Ref. Interna: IPR-523

SECTOR INDUSTRIAL

Indique los sectores a los que va dirigida (señale el sector que la produciría y el que la utilizaría):

SECTOR	Producción	Utilización
A. ACUICULTURA Y PESCA	☐	☐
B. ADMINISTRACIÓN PÚBLICA	☐	☐
C. AERONÁÚTICO	☐	☐
D. ALIMENTACIÓN	☐	☐
E. AUTOMOCIÓN, TRANSPORTE Y LOGÍSTICA	☐	☐
F. BIOTECNOLOGÍA	☐	☐
G. CERÁMICA Y MATERIALES	☐	☒
H. CONSTRUCCIÓN	☐	☐
I. CONSULTORÍA, GESTIÓN Y SERVICIOS EMPRESARIALES	☐	☐
J. EDUCACIÓN Y FORMACIÓN	☐	☐
K. ELECTRÓNICA, INFORMÁTICA Y TELECOMUNICACIONES (TIC)	☐	☐
L. ENERGÍA	☐	☐
M. FARMACIA Y COSMÉTICA	☒	☐
N. MADERA Y MUEBLES	☐	☐
O. MAQUINARÍA, AUTOMATIZACIÓN Y EQUIPAMIENTO INDUSTRIAL	☐	☐
P. MEDIO AMBIENTE	☐	☐
Q. MINERÍA	☐	☐
R. QUÍMICA Y PLÁSTICOS	☒	☐
S. SALUD	☐	☐
T. AGRICULTURA Y GANADERÍA	☐	☐
U. SEGURIDAD Y DEFENSA	☐	☐
V. TEXTILES Y CALZADO	☐	☐
W. TURISMO	☐	☐
X. OTROS:	☐	☐

6.- DESCRIPCIÓN GENERAL DE LA INVENCIÓN

Describa con detalle el objeto de la invención, en qué consiste, qué problema técnico resuelve y qué ventajas aporta respecto al estado de la técnica actual. Si es necesario, incluya dibujos, figuras o esquemas.

El sistema propuesto pretende utilizar catalizadores metálicos (Pt e Ir) soportados y bien anclados sobre los nuevos materiales compuestos desarrollados óxido de titanio-carbón y óxido de silicio-carbón para la obtención de alcoholes insaturados. Por ejemplo: nerol (CAS nº 106-25-2) y geraniol (CAS nº 106-24-1) o alcohol cinamílico (CAS nº 104-54-1) mediante la hidrogenación selectiva de sus

correspondientes aldehídos α,β-insaturados citral (CAS nº 5392-40-5) y cinamaldehído (CAS nº 104-55-2), respectivamente.

En un aspecto la invención se relaciona con un método para la preparación de materiales compuestos carbón-óxido de titanio y carbón-óxido de silicio, dónde la fase carbón será un xerogel de carbón obtenido a partir de la polimerización de resorcinol y formaldehído, y la fase inorgánica corresponderá a los óxidos de titanio o silicio obtenidos por hidrólisis de sus correspondientes alcóxidos. Este método optimizado para la obtención de los materiales compuestos se caracteriza tanto por la eficacia de la secuencia metodológica utilizada como por la particularidad de algunos de sus pasos, como son, la utilización de heptano como medio de reacción; la adicción lenta gota a gota de una solución que contiene la mezcla polimérica resorcinol-formaldehído sobre una disolución en heptano que contiene al compuesto precursor de la fase inorgánica; la temperatura de reacción (70 ºC), tiempo de reacción y envejecimiento (24 horas), y velocidad de agitación (470 rpm); el empleo de microondas para la etapa de secado; una rampa de velocidad de carbonización muy lenta (1 ºC/min) hasta 900 ºC en atmósfera de nitrógeno y mantenida dicha temperatura durante 2 horas.

Dicho método, en adelante método de la invención, comprende las siguientes etapas:

(i) Obtención de un hidrogel compuesto (gel orgánico dopado con un óxido metálico) a partir de un compuesto fenólico (R), un surfactante (S), un aldehído, (F) y un alcóxido metálico (A)
(ii) Curado del hidrogel compuesto resultante de la etapa (i)
(iii) Secado del hidrogel compuesto resultante de la etapa (ii) mediante microondas en atmósfera de argón dando lugar a un gel seco.
(iv) Carbonización del gel seco resultante de la etapa (iii).

La obtención del hidrogel compuesto de la etapa (i) se lleva acabo a su vez a través de las siguientes etapas según se trate del hidrogel compuesto gel orgánico-óxido de titanio o hidrogel compuesto gel orgánico-óxido de silicio:

(i)-1. Obtención del hidrogel compuesto gel orgánico - óxido de titanio

a) Preparar una solución de surfactante en un disolvente orgánico.
b) Calentar la solución (a) por debajo del punto de ebullición del disolvente orgánico, bajo agitación.
c) Preparar una solución acuosa que contenga un compuesto fenólico y un aldehído.
d) Adicionar gota a gota la solución acuosa del apartado (c) sobre la solución de surfactante (b).
e) Adicionar a la solución obtenida durante la etapa (d) la cantidad adecuada de un alcóxido metálico.
f) Gelificación de la solución obtenida en el apartado (e) a temperatura constante hasta la obtención del hidrogel.

(i)-2. Obtención del hidrogel compuesto gel orgánico-óxido de silicio.

a) Preparar una solución del alcóxido metálico en un disolvente orgánico
b) Calentar la solución (a) por debajo del punto de ebullición del disolvente orgánico, bajo agitación.
c) Preparar una solución acuosa que contenga un compuesto fenólico y un aldehído.
d) Adicionar gota a gota la solución acuosa del apartado (c) sobre la solución de alcóxido obtenido en el apartado (b).
e) Hidrólisis del alcóxido metálico contenido en la solución preparada en el apartado (d) forzando un cambio de pH de la solución.
f) Gelificación de la solución obtenida en el apartado (e) a temperatura constante hasta la obtención del hidrogel.

PALABRAS CLAVE

Indique las palabras clave para efectuar búsquedas en bases de datos (en español y en inglés):

Universidad de Granada

Ref. Interna: IPR-523

7.- GRADO DE DESARROLLO DE LA INVENCIÓN.

Elija las opciones que más se aproximen al grado de desarrollo de la invención:

☒ se ha realizado en laboratorio, exclusivamente.
☐ se ha realizado ensayo en planta piloto.
☐ existe prototipo preparado para su desarrollo y comercialización.
☐ habría que realizar desarrollos para su comercialización o implantación industrial

Si fuera necesario realizar su desarrollo para la explotación comercial, éste tendría:

Dificultad técnica:
☐ elevada
☒ normal
☐ baja

Coste económico:
☐ elevado
☐ medio
☒ bajo

8.- PROYECTO DE DESARROLLO TECNOLÓGICO DE LA INVENCIÓN.

Describa, si lo conoce, cómo tendría que ser el proyecto de desarrollo tecnológico (fases y temporización, presupuestos, recursos necesarios, resultados esperables, etc.) necesario para poner la invención en el mercado (escalabilidad, experiencias piloto, prototipos, pruebas de concepto, etc.)

9.- EXPLOTACIÓN Y COMERCIALIZACIÓN DE LA PATENTE

Se considera que sería un producto (procedimiento) con posible éxito comercial:

☒ elevado ☐ medio ☐ bajo

El mercado de la patente es:

☐ exclusivamente nacional

☒ internacional (señalar):

☒ EE.UU. ☒ Europa ☒ Japón ☒ América del Norte
☒ África ☒ Australia ☐ Otros:

¿Se ha contactado con alguna empresa para su posible explotación?

☐ SI ☒ NO

En caso afirmativo, ¿con cuál?

En caso negativo, o si procediese, conteste la siguiente pregunta:

¿Conoce alguna empresa que pudiera estar interesada?

☐ SI ☒ NO

Indique cuál o cuáles:

¿Ha pensado en montar su propia empresa para desarrollar y/o explotar esta tecnología o conocimiento?

☐ SI ☒ NO

10.- BIBLIOGRAFÍA

1 P. Claus. Selective hydrogenation of α,β–unsaturated aldehydes and other C=O and C=C bonds containing compounds, *Topics in Catalysis* **5**(1), 51, 1998.

2 P. Gallezot and D. Richard. Selective Hydrogenation of α, β-Unsaturated Aldehydes, *Catalysis Reviews* **40**(1-2), 81, 1998.

3 V. Ponec. On the role of promoters in hydrogenations on metals; α,β–unsaturated aldehydes and ketones, *Applied Catalysis A: General* **149**(1), 27, 1997.

4 *http://www.bugband.net*2013).

5 *http://www.fulltec.org*2013).

6 M. Eisenacher, S. Beschnitt, and W. Hölderich. Novel route to a fruitful mixture of terpene fragrances in particular phellandrene starting from natural feedstock geraniol using weak acidic boron based catalyst, *Catalysis Communications* **26**(0), 214, 2012.

7 J. Groling, *ullmann's encyclopedia of industrial chemistry*, Seven ed. (Electronic Release, Weinheim, 2003).

8 S.C. Rastogi, J.D. Johansen, and T. Menné. Natural ingredients based cosmetics. Content of selected fragrance sensitizers, *Contact Dermatitis* **34**(6), 423, 1996.

9 S.C. Rastogi, J.D. Johansen, P. Frosch, T. Menne, M. Bruze, J.P. Lepoittevin, B. Dreier, K.E. Andersen, and I.R. White. Deodorants on the European market: quantitative chemical analysis of 21 fragrances, *Contact Dermatitis* **38**(1), 29, 1998.

[10] S.C. Rastogi, S. Heydorn, J.D. Johansen, and D.A. Basketter. Fragrance chemicals in domestic and occupational products, *Contact Dermatitis* **45**(4), 221, 2001.

[11] K. Sato, S. Krist, and G. Buchbauer. Antimicrobial effect of vapours of geraniol, (R)-(–)-linalool, terpineol, γ–terpinene and 1,8-cineole on airborne microbes using an airwasher, *Flavour and Fragrance Journal* **22**(5), 435-437, 2007.

[12] Y. Shoji, H. Ishige, N. Tamura, W. Iwatani, M. Norimatsu, J. Shimada, and Y. Mizushima. Enhancement of anti-herpetic activity of antisense phosphorothioate oligonucleotides 5' end modified with geraniol, *Journal of Drug Targeting* **5**(4), 261, 1998.

[13] H. Surburg and J. Panten, *common fragrance and flavor materials: preparation, properties and uses*, 5th ed. (WILEY-VCH, Weinheim, Germany, 2006).

[14] G. Neri, I. Arrigo, F. Corigliano, L. Luca, and A. Donato. Selective Hydrogenation of Cinnamaldehyde on Pt and Pt-Fe Catalysts Supported on Zeolite P, *Catalysis Letters* **141**(11), 1590, 2011.

[15] F. Delbecq and P. Sautet. A Density Functional Study of Adsorption Structures of Unsaturated Aldehydes on Pt(111): A Key Factor for Hydrogenation Selectivity, *Journal of Catalysis* **211**(2), 398, 2002.

[16] H. Rojas, G. Díaz, J.J. Martínez, C. Castañeda, A. Gómez-Cortés, and J. renas-Alatorre. Hydrogenation of α,β-unsaturated carbonyl compounds over Au and Ir supported on SiO_2, *Journal of Molecular Catalysis A: Chemical* **363–364**(0), 122, 2012.

[17] M.S. Ide, B. Hao, M. Neurock, and R.J. Davis. Mechanistic Insights on the Hydrogenation of α,β-Unsaturated Ketones and Aldehydes to Unsaturated Alcohols over Metal Catalysts, *ACS Catalysis* **2**(4), 671, 2012.

[18] B.F. Machado, S. Morales-Torres, A.F. Pérez-Cadenas, F.J. Maldonado-Hódar, F. Carrasco-Marín, A.M.T. Silva, J.L. Figueiredo, and J.L. Faria. Preparation of carbon aerogel supported platinum catalysts for the selective hydrogenation of cinnamaldehyde, *Applied Catalysis A: General* **425–426**(0), 161, 2012.

[19] A.B. Merlo, B.F. Machado, V. Vetere, J.L. Faria, and M.L. Casella. $PtSn/SiO_2$ catalysts prepared by surface controlled reactions for the selective hydrogenation of cinnamaldehyde, *Applied Catalysis A: General* **383**(1–2), 43, 2010.

[20] E.V. Ramos-Fernández, J.M. Ramos-Fernández, M. Martínez-Escandell, A. Sepúlveda-Escribano, and F. Rodríguez-Reinoso. Selective Hydrogenation of Cinnamaldehyde over (111) Preferentially Oriented Pt Particles Supported on Expanded Graphite, *Catalysis Letters* **133**(3-4), 267, 2009.

[21] A.J. Plomp, H. Vuori, A.O. Krause, K.P. de Jong, and J.H. Bitter. Particle size effects for carbon nanofiber supported platinum and ruthenium catalysts for the selective hydrogenation of cinnamaldehyde, *Applied Catalysis A: General* **351**(1), 9, 2008.

[22] P. Gao, A. Wang, X. Wang, and T. Zhang. Synthesis and Catalytic Performance of Highly Ordered Ru-Containing Mesoporous Carbons for Hydrogenation of Cinnamaldehyde, *Catalysis Letters* **125**(3-4), 289, 2008.

[23] A. Cabiac, T. Cacciaguerra, P. Trens, R. Durand, G. Delahay, A. Medevielle, D. Plée, and B. Coq. Influence of textural properties of activated carbons on Pd/carbon catalysts synthesis for cinnamaldehyde hydrogenation, *Applied Catalysis A: General* **340**(2), 229, 2008.

[24] J.C. Serrano-Ruiz, A. López-Cudero, J. Solla-Gullón, A. Sepúlveda-Escribano, A. Aldaz, and F. Rodríguez-Reinoso. Hydrogenation of α,β–unsaturated aldehydes over polycrystalline, (111) and (100) preferentially oriented Pt nanoparticles supported on carbon, *Journal of Catalysis* **253**(1), 159, 2008.

[25] P.G.N. Mertens, F. Cuypers, P. Vandezande, X. Ye, F. Verpoort, I.F.J. Vankelecom, and D.E. De Vos. Ag^0 and Co^0 nanocolloids as recyclable quasihomogeneous metal catalysts for the hydrogenation of α,β-unsaturated aldehydes to allylic alcohol fragrances, *Applied Catalysis A: General* **325**(1), 130, 2007.

[26] V.I. Pârvulescu, V. Pârvulescu, U. Endruschat, G. Filoti, F.E. Wagner, C. Kübel, and R. Richards. Characterization and Catalytic-Hydrogenation Behavior of SiO2-Embedded Nanoscopic Pd, Au, and Pd–Au Alloy Colloids, *Chemistry- A European Journal* **12**(8), 2343, 2006.

[27] J. Hájek, N. Kumar, T. Salmi, and D.Y. Murzin. Short overview on the application of metal-modified molecular sieves in selective hydrogenation of cinnamaldehyde, *Catalysis Today* **100**(3–4), 349, 2005.

[28] J. Hájek, N. Kumar, D. Francová, I. Paseka, P. Mäki-Arvela, T. Salmi, and D.Y. Murzin. Hydrogenation of Cinnamaldehyde over Pt-Modified Molecular Sieve Catalysts, *Chemical Engineering & Technology* **27**(12), 1290, 2004.

[29] M.L. Toebes, Y. Zhang, J. Hájek, T. exander Nijhuis, J.H. Bitter, A. Jos van Dillen, D.Y. Murzin, D.C. Koningsberger, and K.P. de Jong. Support effects in the hydrogenation of cinnamaldehyde over carbon nanofiber-supported platinum catalysts: characterization and catalysis, *Journal of Catalysis* **226**(1), 215, 2004.

[30] J. Alvarez-Rodríguez, I. Rodríguez-Ramos, A. Guerrero-Ruiz, E. Gallegos-Suarez, and A. Arcoya. Influence of the nature of support on Ru-supported catalysts for selective hydrogenation of citral, *Chemical Engineering Journal* **204-205**, 169, 2012.

[31] U.K. Singh and M.A. Vannice. Liquid-phase citral hydrogenation over SiO_2-supported group VIII metals, *Journal of Catalysis* **199**(1), 73, 2001.

[32] G. Szollosi, I. Kun, B. Torok, and M. Bartok. Chemoselective hydrogenation of the C=O group in unsaturated aldehydes over clay-supported platinum catalysts, *Porous Materials in Environmentally Friendly Processes* **125**, 539, 1999.

[33] J. Zhao, X. Xu, X. Li, and J. Wang. Promotion of Sn on the Pd/AC catalyst for the selective hydrogenation of cinnamaldehyde, *Catalysis Communications* **43**(0), 102, 2014.

[34] Z. Liu, X. Tan, J. Li, and C. Lv. Easy synthesis of bimetal PtFe-containing ordered mesoporous carbons and their use as catalysts for selective cinnamaldehyde hydrogenation, *New Journal of Chemistry* **37**(5), 1350, 2013.

[35] K.Q. Sun, Y.C. Hong, G.R. Zhang, and B.Q. Xu. Synergy between Pt and Au in Pt-on-Au Nanostructures for Chemoselective Hydrogenation Catalysis, *ACS Catalysis* **1**(10), 1336, 2011.

[36] Z. Guo, C. Zhou, D. Shi, Y. Wang, X. Jia, J. Chang, A. Borgna, C. Wang, and Y. Yang. Toward the decoration of Pt nanoparticles supported on carbon nanotubes with Fe oxides and its effect on the catalytic reaction, *Applied Catalysis A: General* **435–436**(0), 131, 2012.

[37] X. Yang, D. Chen, S. Liao, H. Song, Y. Li, Z. Fu, and Y. Su. High-performance Pd–Au bimetallic catalyst with mesoporous silica nanoparticles as support and its catalysis of cinnamaldehyde hydrogenation, *Journal of Catalysis* **291**(0), 36, 2012.

[38] A.B. Merlo, B.F. Machado, V. Vetere, J.L. Faria, and M.L. Casella. $PtSn/SiO_2$ catalysts prepared by surface controlled reactions for the selective hydrogenation of cinnamaldehyde, *Applied Catalysis A: General* **383**(1–2), 43, 2010.

[39] N. Mahata, F. Gonçalves, M.F. Pereira, and J.L. Figueiredo. Selective hydrogenation of cinnamaldehyde to cinnamyl alcohol over mesoporous carbon supported Fe and Zn promoted Pt catalyst, *Applied Catalysis A: General* **339**(2), 159, 2008.

[40] H. Li, H. Yang, and H. Li. Highly active mesoporous Co–B amorphous alloy catalyst for cinnamaldehyde hydrogenation to cinnamyl alcohol, *Journal of Catalysis* **251**(1), 233, 2007.

[41] Y. Li, R.X. Zhou, and G.H. Lai. Effect of transition metals (Cr, Mn, Fe, Co, Ni and Cu) on selective hydrogenation of cinnamaldehyde over Pt/CNTs catalyst, *Reaction Kinetics and Catalysis Letters* **88**(1), 105, 2006.

[42] P.V. Samant, M.F.R. Pereira, and J.L. Figueiredo. Mesoporous carbon supported Pt and Pt–Sn catalysts for hydrogenation of cinnamaldehyde, *Catalysis Today* **102–103**(0), 183, 2005.

[43] M. Zhu, X. Wang, J. Lai, and Y. Yuan. Selective Hydrogenation of trans-Cinnamaldehyde over SiO2-Supported Co–Ir Bimetallic Catalysts, *Catalysis Letters* **98**(4), 247, 2004.

[44] J. Hájek, P. Mäki-Arvela, E. Toukoniitty, N. Kumar, T. Salmi, D.Y. Murzin, L. Cervený, I. Paseka, and E. Laine. The Effect of Chemical Reducing Agents in the Synthesis of Sol-Gel Ru-Sn Catalysts: Selective Hydrogenation of Cinnamaldehyde, *Journal of Sol-Gel Science and Technology* **30**(3), 187, 2004.

[45] J. Hájek, N. Kumar, H. Karhu, L. Cerveny, J. Vayrynen, T. Salmi, and D.Y. Murzin, "Preparation and Properties of Bimetallic Ru-Sn Sol-Gel Catalysts: Influence of Catalyst Reduction",in *Studies in Surface Science and Catalysis Scientific Bases for the Preparation of Heterogeneous Catalysts Proceedings of the 8th International Symposium*, Volume 143 ed. edited by E. Gaigneaux (Elsevier, 2000), pp.757-765.

[46] J.N. Coupe, E. Jordao, M.A. Fraga, and M.J. Mendes. A comparative study of SiO_2 supported Rh-Sn catalysts prepared by different methods in the hydrogenation of citral, *Applied Catalysis A-General* **199**(1), 45, 2000.

[47] T. Ekou, A. Vicente, G. Lafaye, C. Especel, and P. Marecot. Bimetallic Rh-Ge and Pt-Ge catalysts supported on TiO_2 for citral hydrogenation I. Preparation and characterization of the catalysts, *Applied Catalysis A-General* **314**(1), 64, 2006.

[48] T. Ekou, A. Vicente, G. Lafaye, C. Especel, and P. Marecot. Bimetallic Rh-Ge and Pt-Ge catalysts supported on TiO_2 for citral hydrogenation II. Catalytic properties, *Applied Catalysis A-General* **314**(1), 73, 2006.

[49] Z. Guo, C. Zhou, D. Shi, Y. Wang, X. Jia, J. Chang, A. Borgna, C. Wang, and Y. Yang. Toward the decoration of Pt nanoparticles supported on carbon nanotubes with Fe oxides and its effect on the catalytic reaction, *Applied Catalysis A: General* **435–436**(0), 131, 2012.

[50] X. Zhang, Y.C. Guo, Z. Cheng Zhang, J.S. Gao, and C.M. Xu. High performance of carbon nanotubes confining gold nanoparticles for selective hydrogenation of 1,3-butadiene and cinnamaldehyde, *Journal of Catalysis* **292**(0), 213, 2012.

[51] X. Ni, B. Zhang, C. Li, M. Pang, D. Su, C.T. Williams, and C. Liang. Microwave-assisted green synthesis of uniform Ru nanoparticles supported on non-functional carbon nanotubes for cinnamaldehyde hydrogenation, *Catalysis Communications* **24**(0), 65, 2012.

[52] Z. Guo, Y. Chen, L. Li, X. Wang, G.L. Haller, and Y. Yang. Carbon nanotube-supported Pt-based bimetallic catalysts prepared by a microwave-assisted polyol reduction method and their catalytic applications in the selective hydrogenation, *Journal of Catalysis* **276**(2), 314, 2010.

[53] A. Jung, A. Jess, T. Schubert, and W. Schütz. Performance of carbon nanomaterial (nanotubes and nanofibres) supported platinum and palladium catalysts for the hydrogenation of cinnamaldehyde and of 1-octyne, *Applied Catalysis A: General* **362**(1–2), 95, 2009.

[54] A.J. Plomp, H. Vuori, A.O. Krause, K.P. de Jong, and J.H. Bitter. Particle size effects for carbon nanofiber supported platinum and ruthenium catalysts for the selective hydrogenation of cinnamaldehyde, *Applied Catalysis A: General* **351**(1), 9, 2008.

[55] Z.T. Liu, C.X. Wang, Z.W. Liu, and J. Lu. Selective hydrogenation of cinnamaldehyde over Pt-supported multi-walled carbon nanotubes: Insights into the tube-size effects, *Applied Catalysis A: General* **344**(1–2), 114, 2008.

[56] X. Han, R. Zhou, B. Yue, and X. Zheng. Selective Hydrogenation of Cinnamaldehyde over Pt/ZrO_2 Catalyst Modified by Cr, Mn, Fe, Co and Ni, *Catalysis Letters* **109**(3-4), 157, 2006.

[57] J.P. Stassi, P.D. Zgolicz, S.R. de Miguel, and O.A. Scelza. Formation of different promoted metallic phases in PtFe and PtSn catalysts supported on carbonaceous materials used for selective hydrogenation, *Journal of Catalysis* **306**(0), 11, 2013.

[58] P.D. Zgolicz, J.P. Stassi, M.J. Yañez, O.A. Scelza, and S.R. de Miguel. Influence of the support and the preparation methods on the performance in citral hydrogenation of Pt-based catalysts supported on carbon nanotubes, *Journal of Catalysis* **290**(0), 37, 2012.

[59] J. Shi, R. Nie, P. Chen, and Z. Hou. Selective hydrogenation of cinnamaldehyde over reduced graphene oxide supported Pt catalyst, *Catalysis Communications* **41**(0), 101, 2013.

[60] S. Bhogeswararao and D. Srinivas. Intramolecular selective hydrogenation of cinnamaldehyde over CeO_2–ZrO_2-supported Pt catalysts, *Journal of Catalysis* **285**(1), 31, 2012.

[61] E.V. Ramos-Fernández, J. Ruiz-Martínez, J.C. Serrano-Ruiz, J. Silvestre-Albero, A. Sepúlveda-Escribano, and F. Rodríguez-Reinoso. Effect of the support, Al_2O_3 or SiO_2, on the catalytic behaviour of Cr–ZnO promoted Pt catalysts in the selective hydrogenation of cinnamaldehyde, *Applied Catalysis A: General* **402**(1–2), 50, 2011.

62 C.Y. Hsu, T.C. Chiu, M.H. Shih, W.J. Tsai, W.Y. Chen, and C.H. Lin. Effect of Electron Density of Pt Catalysts Supported on Alkali Titanate Nanotubes in Cinnamaldehyde Hydrogenation, *The Journal of Physical Chemistry C* **114**(10), 4502, 2010.

63 R. Liu, H. Cheng, Q. Wang, C. Wu, J. Ming, C. Xi, Y. Yu, S. Cai, F. Zhao, and M. Arai. Selective hydrogenation of unsaturated aldehydes in a poly(ethylene glycol)/compressed carbon dioxide biphasic system, *Green Chemistry* **10**(10), 1082, 2008.

64 C.M. Piqueras, V. Gutierrez, D.A. Vega, and M.A. Volpe. Selective hydrogenation of cinnamaldehyde in supercritical CO_2 over Pt/SiO_2 and Pt/HS-CeO_2: An insight about the role of carbonyl interaction with supercritical CO_2 or with ceria support sites in cinamyl alcohol selectivity, *Applied Catalysis A: General* **467**(0), 253, 2013.

65 C. Xi, H. Wang, R. Liu, S. Cai, and F. Zhao. Hydrogenation of cinnamaldehyde over Pt/RHCs in supercritical carbon dioxide - Influence of support pretreatment and phase behavior, *Catalysis Communications* **9**(1), 140, 2008.

66 F. Zhao, S.i. Fujita, J. Sun, Y. Ikushima, and M. Arai. Carbon dioxide-expanded liquid substrate phase: an effective medium for selective hydrogenation of cinnamaldehyde to cinnamyl alcohol, *Chemical Communications* (20), 2326, 2004.

67 M. Chatterjee, Y. Ikushima, and F.Y. Zhao. Highly Efficient Hydrogenation of Cinnamaldehyde Catalyzed by Pt-MCM-48 in Supercritical Carbon Dioxide, *Catalysis Letters* **82**(1-2), 141, 2002.

68 M. Chatterjee, F.Y. Zhao, and Y. Ikushima. Hydrogenation of citral using monometallic Pt and bimetallic Pt-Ru catalysts on a mesoporous support in supercritical carbon dioxide medium, *Advanced Synthesis & Catalysis* **346**(4), 459, 2004.

69 M. Chatterjee, Y. Ikushima, T. Yokoyama, and M. Sato. Density-dependent formation of the pure trans-isomer of the unsaturated alcohol by selective hydrogenation of citral in supercritical carbon dioxide, *Advanced Synthesis & Catalysis* **350**(4), 624, 2008.

70 J. Hao, C. Xi, H. Cheng, R. Liu, S. Cai, M. Arai, and F. Zhao. Influence of compressed carbon dioxide on hydrogenation reactions in cyclohexane with a Pd/C catalyst, *Industrial and Engineering Chemistry Research* **47**(17), 6796, 2008.

71 R.X. Liu, F.Y. Zhao, S. Fujita, and M. Arai. Selective hydrogenation of citral with transition metal complexes in supercritical carbon dioxide, *Applied Catalysis A-General* **316**(2), 127, 2007.

[72] Y. Li, P.F. Zhu, and R.X. Zhou. Selective hydrogenation of cinnamaldehyde to cinnamyl alcohol with carbon nanotubes supported Pt-Co catalysts, *Applied Surface Science* **254**(9), 2609, 2008.

[73] H. Vu, F. Gonçalves, R. Philippe, E. Lamouroux, M. Corrias, Y. Kihn, D. Plee, P. Kalck, and P. Serp. Bimetallic catalysis on carbon nanotubes for the selective hydrogenation of cinnamaldehyde, *Journal of Catalysis* **240**(1), 18, 2006.

[74] J. Qiu, H. Zhang, X. Wang, H. Han, C. Liang, and C. Li. Selective hydrogenation of cinnamaldehyde over carbon nanotube supported Pd-Ru catalyst, *React Kinet Catalysis Letters* **88**(2), 269, 2006.

[75] D. Manikandan, D. Divakar, and T. Sivakumar. Selective hydrogenation of citral over noble metals intercalated montmorillonite catalysts, *Catalysis Letters* **123**(1-2), 107, 2008.

[76] H. Wang, Y. Shu, M. Zheng, and T. Zhang. Selective Hydrogenation of Cinnamaldehyde to Hydrocinnamaldehyde over SiO_2 Supported Nickel Phosphide Catalysts, *Catalysis Letters* **124**(3-4), 219, 2008.

[77] S. Mukherjee and M.A. Vannice. Solvent effects in liquid-phase reactions - I. Activity and selectivity during citral hydrogenation on Pt/SiO_2 and evaluation of mass transfer effects, *Journal of Catalysis* **243**(1), 108, 2006.

[78] Y.Z. Chen, S.W. Wei, and K.J. Wu. Effect of promoter on selective hydrogenation of α,β-unsaturated aldehydes over cobalt borides, *Applied Catalysis A: General* **99**(2), 85, 1993.

[79] J. Hájek and D.Y. Murzin. Liquid-Phase Hydrogenation of Cinnamaldehyde over a Ru-Sn Sol-Gel Catalyst. 1. Evaluation of Mass Transfer via a Combined Experimental/Theoretical Approach, *Industrial and Engineering Chemistry Research* **43**(9), 2030, 2004.

[80] J. Hájek, J. Wärnå, and D.Y. Murzin. Liquid-Phase Hydrogenation of Cinnamaldehyde over a Ru–Sn Sol–Gel Catalyst. 2. Kinetic Modeling, *Industrial & Engineering Chemistry Research* **43**(9), 2039, 2004.

[81] D. Manikandan, D. Divakar, and T. Sivakumar. Utilization of clay minerals for developing Pt nanoparticles and their catalytic activity in the selective hydrogenation of cinnamaldehyde, *Catalysis Communications* **8**(11), 1781, 2007.

[82] J. Zhu, M.H. Lu, M.S. Li, J.J. Zhu, and Y.H. Shan. Selective Hydrogenation of Citral over a Carbon-titania Composite Supported Palladium Catalyst, *Chinese Journal of Chemistry* **29**(4), 655, 2011.

[83] J. Zhu, M. Lu, M. Li, J. Zhu, and Y. Shan. Synthesis of carbon-titania composite and its application as catalyst support, *Materials Chemistry and Physics* **132**(2-3), 316, 2012.

[84] J. Zhu, M. Li, and M. Lu, Synthesis of Carbon Nanofiber-Titania-Cordierite Monolith Composite and Its Application As Catalyst Support on Citral Hydrogenation, *Advanced Materials Research* **535-537**, pp.178-185.

[85] J. Kijenski and P. Winiarek, "Concept of the Synthesis of Novel Platinum Catalysts for the Selective Hydrogenation of Unsaturated Carbonyl Compounds",in *Studies in Surface Science and Catalysis. Scientific Bases for the Preparation of Heterogeneous Catalysts Proceedings of the 8th International Symposium*, Volume 143 ed. edited by E. Gaigneaux (Elsevier, 2000), pp.787-794.

[86] S. Bhogeswararao and D. Srinivas. Intramolecular selective hydrogenation of cinnamaldehyde over CeO_2–ZrO_2-supported Pt catalysts, *Journal of Catalysis* **285**(1), 31, 2012.

[87] S. Santiago-Pedro, V. Tamayo-Galván, and T. Viveros-García. Effect of the acid–base properties of the support on the performance of Pt catalysts in the partial hydrogenation of citral, *Catalysis Today* **213**(0), 101, 2013.

[88] J.C. Serrano-Ruiz, A. Sepulveda-Escribano, F. Rodriguez-Reinoso, and D. Duprez. Pt-Sn catalysts supported on highly-dispersed ceria on carbon - Application to citral hydrogenation, *Journal of Molecular Catalysis A-Chemical* **268**(1-2), 227, 2007.

[89] T. Ekou, A. Flura, L. Ekou, C. Especel, and S. Royer. Selective hydrogenation of citral to unsaturated alcohols over mesoporous Pt/Ti-Al_2O_3 catalysts. Effect of the reduction temperature and of the Ge addition, *Journal of Molecular Catalysis A-Chemical* **353**, 148, 2012.

[90] T. Ekou, C. Especel, and S. Royer. Catalytic performances of large pore Ti-SBA15 supported Pt nanocomposites for the citral hydrogenation reaction, *Catalysis Today* **173**(1), 44, 2011.

[91] G. Borda, H. Rojas, J. Murcia, J.L.G. Fierro, P. Reyes, and M. Oportus. Hydrogenation of citral on Ir/SiO_2 catalysts. Effect of the addition of Nb_2O_5 on surface and catalytic properties, *Reaction Kinetics and Catalysis Letters* **92**(2), 369, 2007.

[92] M. Bidaoui, C. Especel, N. Bouchenafa-Saib, D. Duprez, O. Mohammedi, and S. Royer. Citral hydrogenation on high surface area mesoporous TiO 2-SiO2 supported Pt nanocomposites: Effect of titanium loading and reduction temperature on the catalytic performances, *Applied Catalysis A: General* **445-446**, 14, 2012.

8.2. MÉTODO DE PREPARACIÓN DE MATERIALES COMPUESTOS ÓXIDO DE ZIRCONIO-CARBÓN Y SUS APLICACIONES COMO FOTO-CATALIZADORES ACTIVOS EN LA DEGRADACIÓN DE COMPUESTOS ORGÁNICOS

D. JUAN ANTONIO MUÑOZ ORELLANA, TÉCNICO DE LA OFICINA DE TRANSFERENCIA DE RESULTADOS DE INVESTIGACION DE LA UNIVERSIDAD DE GRANADA

INFORMA: Que según nuestros archivos, Dña. Ester María José Bailón García figura como inventora en la invención "***Método de preparación de materiales compuestos óxido de zirconio-carbón y sus aplicaciones como fotocatalizadores activos en la degradación de compuestos orgánicos***", para la que se ha solicitado protección mediante patente y a la que esta oficina le ha asignado la referencia interna **IPR- 572**.

Y que en estos momentos se está preparando la correspondiente solicitud de patente ante la Oficina Española de Patentes y Marcas por lo que **toda la información relativa a esta invención debe ser considerada confidencial** para salvaguardar la patentabilidad de la misma.

Granada, a 20 de febrero de 2015.

Fdo.: Juan Antonio Muñoz Orellana

Universidad de Granada

Ref. Interna: IPR-572

MÉTODO DE PREPARACIÓN DE MATERIALES COMPUESTOS ÓXIDO DE ZIRCONIO-CARBÓN Y SUS APLICACIONES COMO FOTO-CATALIZADORES ACTIVOS EN LA DEGRADACIÓN DE COMPUESTOS ORGÁNICOS

INFORMACIÓN PARA LA VALORIZACIÓN DE LA INVENCIÓN

El cuestionario que sigue a continuación pretende proporcionar a la OTRI elementos para evaluar la patentabilidad de la invención y agilizar su posible transferencia, si ésta no está ya comprometida. Trate de responder a los apartados que pueda, pero deje en blanco los que no sepa responder para rellenarlos, junto con el personal técnico de la OTRI, en los contactos que está previsto mantener al efecto.

1.- ORIGEN DE LA INVENCIÓN

La invención es resultado de:

☒ proyecto de investigación *(citar título, entidad financiadora y código de referencia):*

Reduccion de Emisiones de CO_2 y Tecnologías de Almacenamiento de Energías Renovables empleando Materiales Avanzados de Carbón. Ministerio de Economía y Competitividad ref. CTQ2013-44789-R.

☐ un contrato de investigación (*citar nombre de la empresa/entidad*):

☐ un proyecto de Investigación con participación empresarial (*citar código de referencia, entidad financiadora y empresa*):

☐ otros (explicar):

¿La titularidad de la posible patente debe ser compartida con otra entidad?

SI ☐ NO ☒

En caso afirmativo,

¿qué entidad?

¿en qué % debe ser propietario la UGR? %

¿hay documento contractual que así lo acredita ? SI ☐ NO ☐

2.- GRADO DE DIFUSIÓN DE LA INVENCIÓN

¿Se ha difundido previamente el objeto de la invención?

☐ SI ☒ NO

En caso afirmativo, indique medio de difusión, fecha y contenido (depósito y defensa de tesis, publicaciones, congresos, proyectos fin de carrera, medios de comunicación,…)

3.- ESTADO DE LA TÉCNICA

Describa el estado del arte del campo de su invención. Incluya referencias conocidas cercanas a su tecnología (artículos, patentes, páginas webs, proyectos, etc.). Si es necesario, anexe los citados documentos a este impreso.

El óxido de titanio, puro o dopado, es el material más ampliamente usado y estudiado como foto-catalizador. Constantemente se están desarrollando nuevas estrategias para mejorar dichas propiedades foto-catalíticas del óxido de titanio (titania o TiO_2), estando la gran mayoría de ellas enfocadas a mejorar su actividad foto-catalítica mediante la preparación de materiales híbridos o dopados. El objetivo de introducir un segundo componente es la obtención de mayores áreas superficiales, estabilidad mecánica y térmica, así como otras características superficiales mejoradas[1,2]. Varios óxidos metálicos se han empleado para preparar materiales híbridos foto-catalíticos con el óxido de titanio, así como materiales de carbón, entre ellos, ZrO_2 [1,2], Al_2O_3[3], V_2O_5[4], SiO_2[5] y nanotubos de carbón[6,7]. Varios estudios han mostrado un efecto sinérgico en foto-catálisis empleando materiales híbridos carbón-titanio[8].

Por otro lado, en los procesos foto-catalíticos, una radiación de energía mayor que el band-gap del semiconductor excita a un electrón desde la banda de valencia a la banda de conducción generando el par electrón-hueco encargado del efecto foto-catalítico[9]. En el caso del óxido de titanio con fase anatasa, la cual presenta un band gap de 3.26 eV, requiere el empleo de luz UV ($\lambda \leq 387$ nm). El mayor inconveniente de estos semiconductores es el mencionado alto valor de band-gap, y por tanto no funcionan bien como foto-catalizadores con luz solar. Para mejorar la eficiencia de estos semiconductores bajo radiación solar (o visible) es necesario modificar el material

para facilitar la adsorción de la radiación en la región del visible, para lo cual, el método más usado es el dopado del óxido de titanio con elementos, compuestos o materiales que tenga la capacidad de reducir su band-gap, o sean capaces de crear estados electrónicos localizados en el band-gap que mejoren la adsorción de luz visible[10,11]. El dopado con metales reduce el band gap, pero tiene los siguientes inconvenientes: inestabilidad térmica del óxido de titanio así dopado, captura de los electrones por los centros metálicos disminuyendo la actividad foto-catalítica, y finalmente los costes del proceso de dopado [12,13]. Por estas razones, el dopado con elementos no metalicos, como N y S, son las estrategias más empleadas [12,14] ya que podrían reducir el band gap permitiendo el uso de luz visible[15], pero sin embargo no se evita la recombinación electrón-hueco perdiéndose la actividad del foto-catalizador. El dopado con carbono también se está estudiando aunque en menor medida que el dopado con N[16] encontrándose actividad foto-catalítica en la región del visible[17]; algunos investigadores ponen de manifiesto una mejora de la reactividad del "hueco" del TiO_2, mientras que el electrón es absorbido por el carbono, evitando la combinación electrón-hueco y consecuentemente, la pérdida de actividad. Esto da como resultado una mejorada actividad foto-catalítica en todo el rango del espectro[18]. Otra alternativa de dopado de la titania es la utilización de materiales (como los materiales de carbón) que pueden actuar como "sensibilizadores", los cuales son excitados por la luz visible y son capaces de transferir electrones o huecos al TiO_2. El carbón absorbe en un amplio rango de la luz visible por lo que puede actuar como un "sensibilizador eficiente", de modo que el carbón excitado transfiere electrones a la banda de conducción del TiO_2 para iniciar la reacción. Dicha sensibilización del carbón hace posible la obtención de un foto-catalizador activo a la luz visible[10,19]. La utilización de materiales carbonosos mejoraría la actividad foto-catalítica del óxido de titanio a través de los siguientes posibles mecanismos: i) minimización de la recombinación electrón-hueco, ii) modificación del band-gap o extensión de la longitud de onda de excitación por fotosensibilización o/y iii) proporcionando mayor área superficial para la adsorción de los compuestos o contaminantes[20]. De este modo la adecuada combinación de materiales de carbón y óxidos metálicos fotosensibles como TiO_2 pueden dar lugar a

materiales de altas prestaciones en foto-catálisis, y especialmente sustituyendo la luz ultravioleta por luz visible haciendo más viable el proceso.

Por el contrario, el óxido de zirconio ha sido mucho menos estudiado y utilizado como foto-catalizador. El band-gap del óxido de zirconio es 5 eV, pero dependiendo del método de síntesis pueden alcanzarse valores desde 2.3 ev[21], alcanzando valores similares al óxido de titanio en algunas síntesis[1] siendo así adecuado para su empleo como foto-catalizador. Algunos estudios ponen en evidencia la actividad del óxido de zirconio puro y dopado como foto-catalizador en la degradación de contaminantes y otras aplicaciones [22-24].

Finalmente cabe destacar la importancia de las propiedades texturales de los materiales desarrollados como foto-catalizadores, pues la eliminación del contaminante también se produce por adsorción de éste en la porosidad de los mismos, por lo tanto, en procesos en fase líquida, la presencia de un volumen adecuado de mesoporosidad donde el contaminante pueda ser adsorbido es determinante.

4- OBJETO DE LA INVENCIÓN

Por favor, defina su resultado (elija una o varias opciones):

- ☒ un nuevo producto (considerar 'producto' en sentido general)
- ☐ un nuevo procedimiento de invención
- ☐ mejora de un producto existente
- ☒ mejora de un proceso existente
- ☐ una idea
- ☐ un servicio nuevo o mejorado

Por favor, enumere los productos alternativos a su invención que ya existen en el mercado actualmente

Indique qué ventajas técnicas y beneficios económicos tiene la invención respecto a los citados productos:

- ✓ La invención se centra en desarrollar un método de síntesis sencillo, de los denominados “one pot”, que permita la obtención del foto-catalizador sin tratamientos de funcionalización adicionales.
- ✓ Se observa que el orange G no se degrada bajo luz visible en ausencia de catalizador. Con el uso del óxido de titanio pre-tratado en H_2 como foto-catalizador se obtiene a 170 min una degradación del orange G de alrededor de un 35 % mientras que para el material compuesto xerogel de carbón-óxido de zirconio es de 77 %. Hay pues un claro efecto sinérgico entre el C y el óxido metálico.
- ✓ Para el uso de óxidos semiconductores, como el óxido de titanio, en la foto-degradación con luz visible se necesita una reducción del band-gap o el uso de un sensibilizador eficiente. Estos resultados ponen de manifiesto que el gel de carbón actúa como fotosensibilizador eficiente. Además se facilita la adsorción del contaminante debido a la mayor superficie del material compuesto xerogel de carbón-óxido de zirconio frente al P25, facilitándose así la interacción del contaminante con los centros activos y por tanto, su degradación.
- ✓ Por otro lado, el empleo de estos materiales compuestos facilita la dispersión del óxido de zirconio de modo que reduce la posibilidad de la recombinación hueco-electrón, la cual, es mayor a mayores tamaños de partícula, ya que si el tamaño de partícula es pequeño la distancia que el electrón o el hueco foto-generado debe recorrer hasta la superficie para la reacción redox es menor y por tanto menor es la posibilidad de recombinación [20], aumentando la actividad foto-catalítica del material compuesto, en nuestro caso: los tamaños de cristal del óxido de zirconio son menores a 5 nm frente a los tamaños de cristal de 30 nm que contiene el P25 o 40 nm del óxido de zirconio.
- ✓ La mejor dispersión del óxido de zirconio (observado por difracción de rayos X) debido a la alta superficie del material carbonoso permite una mayor generación de vacantes de oxigeno o óxidos parcialmente reducibles que reducen el band-

gap permitiendo la degradación mediante el uso de luz visible. Además, la fase del óxido de zirconio observada mediante difracción de rayos es la cúbica, la cual puede ser responsable de la reducción del band-gap y por tanto, de sus excelentes prestaciones bajo luz visible.

- ✓ Además con el uso de óxido de zirconio se ha abierto una nueva posibilidad de materiales tan eficientes, e incluso con mejores prestaciones, como los de óxido de titanio en aplicaciones foto-catalíticas.
- ✓ La posibilidad de emplear luz visible en lugar de otras radiaciones más energéticas no solo reduce el consumo energético de los procesos de descontaminación sino que proporcionará, por ejemplo, de un método sencillo de descontaminación y potabilización de aguas en países en vías de desarrollo.
- ✓ Es necesario también señalar que el mayor volumen de poros que conlleva a una mayor capacidad de adsorción de los foto-catalizadores soportados sobre los materiales compuestos, favorece pues la concentración del contaminante en las cercanías de la fase fotoactiva, lo que obviamente también favorece la velocidad de degradación del mismo. Además, el volumen de mesoporos se incrementa con el aumento del % de óxido de zirconio presente en la fase carbonosa incrementándose su capacidad de adsorción.
- ✓ El procedimiento de síntesis permite obtener materiales compuestos con un alto contenido en la fase fotoactiva sin perder dispersión de la misma ni porosidad del material lo cual mejora su actividad fotocatalítica.
- ✓ Con el presente proceso de síntesis la fase cúbica del óxido de zirconio es estabilizada debido a la presencia del xerogel de carbón la cual puede ser la responsable de la redución del band gap haciendo posible el uso de radicación visible y por tanto, haciendo más sencillo y económicamente más viable estos procesos de descontaminación avanzados.

La invención se considera nueva porque:

☒ no se ha encontrado nada igual en bancos de datos de patentes
☒ no se ha encontrado nada igual en la bibliografía científica consultada
☒ no se ha encontrado nada igual en un informe de búsqueda completo

Universidad de Granada

Ref. Interna: IPR-572

5.- APLICACIONES DE LA INVENCIÓN

Describa las aplicaciones industriales de la invención

Los nuevos materiales compuestos obtenidos están basados de geles de carbón altamente dopados con óxido de zirconio empleando nuevas rutas de síntesis. La utilización de estos materiales compuestos está basada en sus altas prestaciones como foto-catalizadores en la degradación de moléculas orgánicas empleando luz ultravioleta (UV) y luz visible. La foto-actividad que presentan estos materiales utilizando luz visible permite una implementación mucho menos costosa.

SECTOR INDUSTRIAL

Indique los sectores a los que va dirigida (señale el sector que la produciría y el que la utilizaría):

SECTOR		Producción	Utilización
A.	ACUICULTURA Y PESCA	☐	☐
B.	ADMINISTRACIÓN PÚBLICA	☐	☐
C.	AERONÁUTICO	☐	☐
D.	ALIMENTACIÓN	☐	☐
E.	AUTOMOCIÓN, TRANSPORTE Y LOGÍSTICA	☐	☐
F.	BIOTECNOLOGÍA	☐	☐
G.	CERÁMICA Y MATERIALES	☐	☒
H.	CONSTRUCCIÓN	☐	☐
I.	CONSULTORÍA, GESTIÓN Y SERVICIOS EMPRESARIALES	☐	☐
J.	EDUCACIÓN Y FORMACIÓN	☐	☐
K.	ELECTRÓNICA, INFORMÁTICA Y TELECOMUNICACIONES (TIC)	☐	☐
L.	ENERGÍA	☐	☐
M.	FARMACIA Y COSMÉTICA	☒	☐
N.	MADERA Y MUEBLES	☐	☐
O.	MAQUINARÍA, AUTOMATIZACIÓN Y EQUIPAMIENTO INDUSTRIAL	☐	☐
P.	MEDIO AMBIENTE	☐	☐
Q.	MINERÍA	☐	☐
R.	QUÍMICA Y PLÁSTICOS	☒	☐
S.	SALUD	☐	☐
T.	AGRICULTURA Y GANADERÍA	☐	☐
U.	SEGURIDAD Y DEFENSA	☐	☐
V.	TEXTILES Y CALZADO	☐	☐
W.	TURISMO	☐	☐
X.	OTROS:	☐	☐

6.- DESCRIPCIÓN GENERAL DE LA INVENCIÓN

Describa con detalle el objeto de la invención, en qué consiste, qué problema técnico resuelve y qué ventajas aporta respecto al estado de la técnica actual. Si es necesario, incluya dibujos, figuras o esquemas.

El sistema propuesto pretende obtener materiales compuestos carbón-óxido de zirconio foto-activos bajo luz visible en la degradación de contaminantes en aguas o aire. La invención se centra en obtener xerogeles de carbón altamente dopados con óxido de zirconio exaltando su actividad foto-catalítica, lográndose un efecto sinérgico entre el carbón y el óxido de zirconio que permite el empleo de luz visible en los procesos de foto-eliminación de contaminantes, y mejorando también sus propiedades foto-catalíticas bajo radiaciones de mayor longitudes de onda.

En un aspecto la invención se relaciona con un método para la preparación de materiales compuestos carbón-óxido de zirconio, dónde la fase carbón será un xerogel de carbón obtenido a partir de la polimerización de resorcinol y formaldehido, y la fase no carbonosa corresponderá al óxido de zirconio. Este método optimizado para la obtención de los materiales compuestos carbón con óxido de zirconio altamente disperso que se caracteriza tanto por la secuencia metodológica utilizada como por la particularidad de algunos de sus pasos, como son: la utilización de heptano como medio de reacción; la adicción lenta gota a gota de una solución que contiene la mezcla polimérica resorcinol-formaldehído sobre una disolución en heptano que contiene al compuesto precursor de la fase no carbonosa; la temperatura de reacción (70ºC), tiempo de reacción (24 horas), y velocidad de agitación (470 rpm); el empleo de microondas para la etapa de secado; una rampa de velocidad de carbonización muy lenta (1ºC/min) en atmósfera de argón hasta 900ºC y mantenida dicha temperatura durante 2 horas.

Dicho método en adelante método de la invención comprende las siguientes etapas:

1.- Preparación materiales compuestos xerogel de carbón-óxido de zirconio

(i) Obtención de un hidrogel compuesto, gel orgánico dopado con óxido de zirconio a partir de un compuesto fenólico (R), un aldehído, (F) y un alcóxido metálico (A)

(ii) Curado del hidrogel compuesto resultante de la etapa (i)

(iii) Secado del hidrogel compuesto resultante de la etapa (ii) mediante microondas en atmósfera de argon dando lugar a un gel seco.

(iv) Carbonización del gel seco resultante de la etapa (iii).

La obtención del hidrogel compuesto de la etapa (i) se lleva acabo a su vez a través de las siguientes etapas:

(i)-Obtención del hidrogel compuesto gel orgánico - óxido de zirconio

a) Preparar una solución del alcóxido metálico en un disolvente orgánico.

b) Calentar la solución (a) por debajo del punto de ebullición del disolvente orgánico, bajo agitación.

c) Preparar una solución acuosa que contenga un compuesto fenólico y un aldehído.

d) Adicionar gota a gota la solución acuosa del apartado (c) sobre la solución de alcóxido obtenido en el apartado (b).

e) Gelificación de la solución obtenida en el apartado (d) a temperatura constante hasta la obtención del hidrogel.

PALABRAS CLAVE

Indique las palabras clave para efectuar búsquedas en bases de datos (en español y en inglés):

7.- GRADO DE DESARROLLO DE LA INVENCIÓN.

Elija las opciones que más se aproximen al grado de desarrollo de la invención:

- ☒ se ha realizado en laboratorio, exclusivamente.
- ☐ se ha realizado ensayo en planta piloto.
- ☐ existe prototipo preparado para su desarrollo y comercialización.
- ☐ habría que realizar desarrollos para su comercialización o implantación industrial

Si fuera necesario realizar su desarrollo para la explotación comercial, éste tendría:

Universidad de Granada

Ref. Interna: IPR-572

Dificultad técnica:

☐ elevada
☒ normal
☐ baja

Coste económico:

☐ elevado
☐ medio
☒ bajo

8.- PROYECTO DE DESARROLLO TECNOLÓGICO DE LA INVENCIÓN.

Describa, si lo conoce, cómo tendría que ser el proyecto de desarrollo tecnológico (fases y temporización, presupuestos, recursos necesarios, resultados esperables, etc.) necesario para poner la invención en el mercado (escalabilidad, experiencias piloto, prototipos, pruebas de concepto, etc.)

9.- EXPLOTACIÓN Y COMERCIALIZACIÓN DE LA PATENTE

Se considera que sería un producto (procedimiento) con posible éxito comercial:

☒ elevado ☐ medio ☐ bajo

El mercado de la patente es:

☐ exclusivamente nacional

☒ internacional (señalar):

☒ EE.UU. ☒ Europa ☒Japón ☒ América del Norte
☒ África ☒ Australia ☐ Otros:

¿Se ha contactado con alguna empresa para su posible explotación?

☐ SI ☒ NO

En caso afirmativo, ¿con cuál?

En caso negativo, o si procediese, conteste la siguiente pregunta:

¿Conoce alguna empresa que pudiera estar interesada?

☐ SI ☒ NO

Indique cuál o cuáles:

¿Ha pensado en montar su propia empresa para desarrollar y/o explotar esta tecnología o conocimiento?

☐ SI ☒ NO

10.- BIBLIOGRAFÍA

1 S. Polisetti, P.A. Deshpande, and G. Madras. Photocatalytic Activity of Combustion Synthesized ZrO_2 and ZrO_2–TiO_2 Mixed Oxides, *Industrial & Engineering Chemistry Research* **50**(23), 12915, 2011.

2 B.M. Reddy and A. Khan. Recent Advances on TiO_2–ZrO_2 Mixed Oxides as Catalysts and Catalyst Supports, *Catalysis Reviews* **47**(2), 257, 2005.

3 M.A. Ahmed and M.F. bdel-Messih. Structural and nano-composite features of TiO_2–Al_2O_3 powders prepared by sol–gel method, *Journal of Alloys and Compounds* **509**(5), 2154, 2011.

4 J. Liu, R. Yang, and S. Li. Preparation and characterization of the TiO_2-V_2O_5 photocatalyst with visible-light activity, *Rare Metals* **25**(6), 636, 2006.

5 U. Sirimahachai, N. Ndiege, R. Chandrasekharan, S. Wongnawa, and M. Shannon. Nanosized TiO_2 particles decorated on SiO_2 spheres (TiO_2/SiO_2): synthesis and photocatalytic activities, *Journal of Sol-Gel Science and Technology* **56**(1), 53, 2010.

6 M.Y. Guo, F. Liu, Y.H. Leung, A.M.C. Ng, A.B. Djurišic, and W.K. Chan. TiO_2–carbon nanotube composites for visible photocatalysts-Influence of TiO2 crystal structure, *Current Applied Physics* **13**(7), 1280, 2013.

7 S.w. Lee and W.M. Sigmund. Formation of anatase TiO_2 nanoparticles on carbon nanotubes, *Chemical Communications* (6), 780, 2003.

8 H. Langhuan, W. Houjin, L. Yingliang, J. Zibin, and S. Zibei. TiO_2/Carbon Nanotube Composites and Their Synergistic Effects on Enhancing the Photocatalysis Efficiency, *Progress in Chemistry* **22**(5), 867, 2010.

9 M. Pelaez, N.T. Nolan, S.C. Pillai, M.K. Seery, P. Falaras, A.G. Kontos, P.S.M. Dunlop, J.W.J. Hamilton, J.A. Byrne, K. O'Shea, M.H. Entezari, and D.D. Dionysiou. A review on the visible light active titanium dioxide photocatalysts for environmental applications, *Applied Catalysis B: Environmental* **125**(0), 331, 2012.

10 S. Lee, Y. Lee, D.H. Kim, and J.H. Moon. Carbon-Deposited TiO_2 3D Inverse Opal Photocatalysts: Visible-Light Photocatalytic Activity and Enhanced Activity in a Viscous Solution, *ACS Applied Materials & Interfaces* **5**(23), 12526, 2013.

11 J. Zhang, Y. Wu, M. Xing, S.A.K. Leghari, and S. Sajjad. Development of modified N doped TiO_2 photocatalyst with metals, nonmetals and metal oxides, *Energy & Environmental Science* **3**(6), 715, 2010.

[12] Y. Izumi, T. Itoi, S. Peng, K. Oka, and Y. Shibata. Site Structure and Photocatalytic Role of Sulfur or Nitrogen-Doped Titanium Oxide with Uniform Mesopores under Visible Light, *The Journal of Physical Chemistry C* **113**(16), 6706, 2009.

[13] Y. Wang, H. Cheng, Y. Hao, J. Ma, W. Li, and S. Cai. Photoelectrochemical properties of metal-ion-doped TiO_2 nanocrystalline electrodes, *Thin Solid Films* **349**(1–2), 120, 1999.

[14] C. Di Valentin, E. Finazzi, G. Pacchioni, A. Selloni, S. Livraghi, M.C. Paganini, and E. Giamello. N-doped TiO_2: Theory and experiment, *Chemical Physics* **339**(1–3), 44, 2007.

[15] A.I. Kontos, A.G. Kontos, Y.S. Raptis, and P. Falaras. Nitrogen modified nanostructured titania: electronic, structural and visible-light photocatalytic properties, *Physica Status Solidi (RRL): Rapid Research Letters* **2**(2), 83, 2008.

[16] F. Dong, H. Wang, and Z. Wu. One-Step "Green" Synthetic Approach for Mesoporous C-Doped Titanium Dioxide with Efficient Visible Light Photocatalytic Activity, *The Journal of Physical Chemistry C* **113**(38), 16717, 2009.

[17] Y.T. Lin, C.H. Weng, Y.H. Lin, C.C. Shiesh, and F.Y. Chen. Effect of C content and calcination temperature on the photocatalytic activity of C-doped TiO_2 catalyst, *Separation and Purification Technology* **116**(0), 114, 2013.

[18] L. Zhao, X. Chen, X. Wang, Y. Zhang, W. Wei, Y. Sun, M. Antonietti, and M.M. Titirici. One-Step Solvothermal Synthesis of a Carbon@TiO_2 Dyade Structure Effectively Promoting Visible-Light Photocatalysis, *Advanced Materials* **22**(30), 3317, 2010.

[19] J. Zhong, F. Chen, and J. Zhang. Carbon-Deposited TiO_2: Synthesis, Characterization, and Visible Photocatalytic Performance, *The Journal of Physical Chemistry C* **114**(2), 933, 2009.

[20] R. Leary and A. Westwood. Carbonaceous nanomaterials for the enhancement of TiO_2 photocatalysis, *Carbon* **49**(3), 741, 2011.

[21] B. Králik, E.K. Chang, and S.G. Louie. Structural properties and quasiparticle band structure of zirconia, *Physical Review B* **57**(12), 7027, 1998.

[22] S.G. Botta, J.A. Navío, M.C. Hidalgo, G.M. Restrepo, and M.I. Litter. Photocatalytic properties of ZrO_2 and Fe/ZrO_2 semiconductors prepared by a sol–gel technique, *Journal of Photochemistry and Photobiology A: Chemistry* **129**(1–2), 89, 1999.

[23] M. Alvarez, T. López, J.A. Odriozola, M.A. Centeno, M.I. Domínguez, M. Montes, P. Quintana, D.H. Aguilar, and R.D. González. 2,4-Dichlorophenoxyacetic acid (2,4-D) photodegradation using an Mn^{+}/ZrO_2 photocatalyst: XPS, UV–vis, XRD characterization, *Applied Catalysis B: Environmental* **73**(1–2), 34, 2007.

[24] C. Karunakaran and S. Senthilvelan. Photocatalysis with ZrO_2: oxidation of aniline, *Journal of Molecular Catalysis A: Chemical* **233**(1–2), 1, 2005.

8.3. FOTO-CATALIZADORES ESTRUCTURADOS CON ALTO RENDIMIENTO BAJO RADIACIÓN VISIBLE BASADOS EN RECUBRIMIENTOS DE MICROESFERAS DE XEROGEL DE CARBÓN CON ÓXIDO DE TITANIO

D. JUAN ANTONIO MUÑOZ ORELLANA, TÉCNICO DE LA OFICINA DE TRANSFERENCIA DE RESULTADOS DE INVESTIGACION DE LA UNIVERSIDAD DE GRANADA

INFORMA: Que según nuestros archivos, Dña. Ester María José Bailón García figura como inventora en la invención "***Fotocatalizadores estructurados con alto rendimiento bajo radiacion visible basados en recubrimientos de microesferas de xerogel de carbono con oxido de titanio***", para la que se ha solicitado protección mediante patente y a la que esta oficina le ha asignado la referencia interna **IPR-571**.

Y que en estos momentos se está preparando la correspondiente solicitud de patente ante la Oficina Española de Patentes y Marcas por lo que **toda la información relativa a esta invención debe ser considerada confidencial** para salvaguardar la patentabilidad de la misma.

Granada, a 20 de febrero de 2015.

Fdo.: Juan Antonio Muñoz Orellana

Universidad de Granada

Ref. Interna: IPR-571

FOTO-CATALIZADORES ESTRUCTURADOS CON ALTO RENDIMIENTO BAJO RADIACIÓN VISIBLE BASADOS EN RECUBRIMIENTOS DE MICROESFERAS DE XEROGEL DE CARBÓN CON ÓXIDO DE TITANIO

INFORMACIÓN PARA LA VALORIZACIÓN DE LA INVENCIÓN

El cuestionario que sigue a continuación pretende proporcionar a la OTRI elementos para evaluar la patentabilidad de la invención y agilizar su posible transferencia, si ésta no está ya comprometida. Trate de responder a los apartados que pueda, pero deje en blanco los que no sepa responder para rellenarlos, junto con el personal técnico de la OTRI, en los contactos que está previsto mantener al efecto.

1.- ORIGEN DE LA INVENCIÓN

La invención es resultado de:

☒ proyecto de investigación *(citar título, entidad financiadora y código de referencia):*

Transformado de desechos del olivar en materiales avanzados para la conversión electro-catalítica de CO_2 en hidrocarburos. Consejería de Innovación, Ciencia y Empresa de la Junta de Andalucía, ref. P12-RNM-2892

☐ un contrato de investigación (*citar nombre de la empresa/entidad*):

☐ un proyecto de Investigación con participación empresarial (*citar código de referencia, entidad financiadora y empresa*):

☐ otros (explicar):

¿La titularidad de la posible patente debe ser compartida con otra entidad?

SI ☐ NO ☒

En caso afirmativo,

¿qué entidad?

¿en qué % debe ser propietario la UGR? %

¿hay documento contractual que así lo acredita ? SI ☐ NO ☐

2.- GRADO DE DIFUSIÓN DE LA INVENCIÓN

¿Se ha difundido previamente el objeto de la invención?

☐ SI ☒ NO

En caso afirmativo, indique medio de difusión, fecha y contenido (depósito y defensa de tesis, publicaciones, congresos, proyectos fin de carrera, medios de comunicación,…)

3.- ESTADO DE LA TÉCNICA

Describa el estado del arte del campo de su invención. Incluya referencias conocidas cercanas a su tecnología (artículos, patentes, páginas webs, proyectos, etc.). Si es necesario, anexe los citados documentos a este impreso.

El óxido de titanio (TiO_2) es ampliamente usado como material foto-catalítico. Constantemente se están desarrollando nuevas estrategias para mejorar sus propiedades foto-catalíticas, estando la gran mayoría de ellas enfocadas a la preparación de materiales híbridos mediante la introducción de un segundo componente. Se han empleado varios óxidos metálicos ZrO_2[1,2], Al_2O_3[3], V_2O_5[4], SiO_2[5] así como materiales de carbón, fundamentalmente nanotubos de carbón[6]. Estos estudios han mostrado un efecto sinérgico entre las fases [7] al tiempo que se consiguen mayores áreas superficiales o mejor estabilidad mecánica y térmica.

En los procesos foto-catalíticos cualquier radiación de mayor energía que el band-gap del semiconductor excita electrones desde la banda de valencia a la banda de conducción, generando pares electrón-hueco responsables de la actividad foto-catalítica del material[8]. El TiO_2 presenta dos fases cristalinas, la anatasa y el rutilo. En general los estudios muestran que la fase anatasa exhibe mayor actividad foto-catalítica comparada con la fase rutilo, lo cual es atribuido al mayor potencial redox y a la mayor densidad de grupos hidroxilos en su superficie[9]. Pero a su vez, determinadas combinaciones de fases rutilo y anatasa exhiben mayor actividad foto-catalítica que las fases puras[9-13]. A título de ejemplo, este hecho explica la elevada actividad catalítica del foto-catalizador comercial P25 (Degussa) en comparación con el óxido de titanio en fase anatasa puro. El P25 es una mezcla anatasa-rutilo (75-25%) en la que la mayor actividad se atribuye a una relajación de la banda en la interfase anatasa rutilo que

favorece la transferencia de carga interfacial, y al incremento de defectos superficiales e intersticiales[9,10].

En su fase anatasa (la más activa) el TiO_2 presenta un band gap de 3.2 eV y requiere por tanto el empleo de luz UV ($\lambda \leq 387$ nm) para ser excitado, en consecuencia, presenta bajo rendimiento con luz solar. Para mejorar su eficiencia es necesario modificar el material para facilitar la adsorción de la radiación en la región del visible, para lo cual, el método más usado es el dopado con distintos elementos (Ag, Sn, etc)[14,15]. El dopado con estos metales reduce el band gap, pero tiene también inconvenientes: aumenta la inestabilidad térmica y favorece la captura de los electrones por los centros metálicos disminuyendo la actividad foto-catalítica, y finalmente los altos costes del propio proceso de dopado[16,17].

Alternativamente se usa el dopado con no metales, como N y S[18,19], los cuales podrían también reducir el band gap permitiendo el uso de luz visible[20]. Sin embargo, no se evita la recombinación electrón-hueco, perdiéndose actividad. También se está estudiando el dopado con carbono, aunque en menor medida[21], encontrándose también una mejora en la actividad foto-catalítica en la región del visible[22]. Algunos investigadores ponen de manifiesto una mejora de la reactividad del "hueco" del TiO_2 pues el electrón es absorbido por el carbono, evitando la combinación electrón-hueco. Esto da como resultado una mejor actividad foto-catalítica en todo el rango del espectro[23].

Otra alternativa en el dopado del TiO_2 es la utilización de materiales que puedan actuar como "sensibilizadores", los cuales al ser excitados por la luz visible son capaces de transferir electrones o huecos al TiO_2. Los materiales de carbón absorben gran parte de la luz visible, por lo que puede actuar como un "sensibilizador eficiente"[15,24]. La utilización de materiales carbonosos mejora la actividad foto-catalítica del óxido de titanio a través de los siguientes mecanismos posibles: i) minimización de la recombinación electrón-hueco, ii) modificación del band-gap o extensión de la longitud de onda de excitación por foto-sensibilización o/y iii)

proporcionando mayor área superficial para la adsorción de los compuestos o contaminantes [25]. De este modo la adecuada combinación de materiales de carbón y óxidos metálicos fotosensibles, como el TiO_2, pueden dar lugar a materiales foto-catalíticos de altas prestaciones usando luz solar que hagan más viable el proceso.

En los últimos años, se han planteado foto-catalizadores activos en el visible usando diferentes formas de materiales de carbón como nanotubos[26-30], y más recientemente grafeno[31,32] y óxido de grafeno reducido[33,34]. Todos ellos son materiales de carbón con alta conductividad, con el objetivo de que el material de carbón capte los electrones evitando la recombinación electrón-hueco para mejorar el papel foto-catalítico del óxido de titanio. A pesar del fuerte interés por el grafeno y de su indiscutible mayor conductividad, la influencia de la morfología del soporte carbonoso parece ser muy importante, encontrándose que los nanotubos de carbón son fotosensibilizadores más efectivos que el propio grafeno[31].

Sin embargo, la preparación de foto-catalizadores basados en CNT-TiO_2 presenta diversos problemas, en principio hay que considerar el elevado coste de los nanotubos de carbón (CNT)[35], pero además, la deposición de TiO_2 sobre la superficie CNT necesita procesos técnicamente muy complejos que aseguren un verdadero contacto químico entre las dos fases. La introducción de grupos funcionales como –COOH y –OH en la superficie de los CNT mejora la interacción de éstos con el TiO_2[36,37], sin embargo, la densidad de nano-partículas de TiO_2 depositadas no es muy alta debido a la baja densidad de grupos funcionales que se generan y/o a las débiles interacciones entre ambas fases [38]. Alternativamente los CNT se modifican con moléculas de surfactante como docecilsulfato sódico o polietilenimina[39,40]. El uso de estos surfactantes permite fuertes interacciones entre CNT y TiO_2. Sin embargo, puesto que estas moléculas reducen o incluso eliminan la actividad fotocatalítica[35], son necesarios tratamientos adicionales para retirarlos del material, lo cual, además del coste añadido, produce adicionalmente daños en la superficie de los CNT.

Otro factor que influencia el rendimiento del TiO_2 es el tamaño de partícula. El rendimiento fotónico aumenta al disminuir éste, de forma que el uso de nano-partículas de TiO_2 puede favorecer su aplicación como fotocatalizador[41-43]. No obstante, y a pesar del desarrollo tecnológico que trae asociado el desarrollo de la nanotecnología, el uso de nano-partículas (en este caso TiO_2) está siendo también considerado como una nueva fuente de contaminación[44-51]. Por ello, se requieren tratamientos de precipitación/coagulación adicionales antes de proceder al vertido del agua tras los procesos de oxidación de los compuestos orgánicos. Es conveniente por tanto anclar dichas nano-partículas sobre los soportes adecuados, de forma que se mantenga la actividad de las mismas, o incluso se mejore por el efecto sinérgico anteriormente descrito, evitando la contaminación por nano-partículas del foto-catalizador al favorecer su separación del medio.

Por tanto, se requiere estudiar otras posibles combinaciones material de carbón – TiO_2 con morfología y propiedades fisicoquímicas adecuadas para ser foto-catalíticamente activos en el visible. Los geles de carbón son también una nueva forma de materiales de carbón[52,53] que presentan unas excelentes propiedades en catálisis[53]. Los procesos sol-gel mediante los que son sintetizados permiten obtener materiales en distinto formato[53], y por tanto, la optimización de la morfología del soporte de carbón. Por otro lado, facilitan también los procesos de dopado del carbón obteniendo fases activas en diversas reacciones, como ya hemos puesto de manifiesto con distintos compuestos metálicos[54,55]. Adicionalmente, permiten un control de la porosidad y consecuentemente, de la superficie específica del material. La eliminación del contaminante se produce por adsorción de éste en la porosidad del foto-catalizador previamente a ser degradado, por lo tanto, en procesos en fase líquida, la presencia de un volumen adecuado de mesoporos donde el contaminante pueda ser adsorbido (concentrado) es pues determinante.

Se describe a continuación la síntesis de foto-catalizadores basados en un soporte estructurado de xerogel de carbón en microesferas, altamente recubierto con una capa estable y delgada de nano-partículas de TiO_2, que presenta además un

desarrollado volumen de poros (superficie específica) y como consecuencia, una actividad foto-catalítica, tanto en visible como en UV, muy superior a materiales comerciales como el P25, usado como referencia

4- OBJETO DE LA INVENCIÓN

Por favor, defina su resultado (elija una o varias opciones):

- ☒ un nuevo producto (considerar 'producto' en sentido general)
- ☐ un nuevo procedimiento de invención
- ☐ mejora de un producto existente
- ☒ mejora de un proceso existente
- ☐ una idea
- ☐ un servicio nuevo o mejorado

Por favor, enumere los productos alternativos a su invención que ya existen en el mercado actualmente:

Indique qué ventajas técnicas y beneficios económicos tiene la invención respecto a los citados productos:

- ✓ La invención se centra en desarrollar un método de síntesis sencillo, de los denominados "one pot", que permita la obtención del foto-catalizador sin tratamientos de funcionalización adicionales.
- ✓ Se observa que el orange G no se degrada bajo luz visible en ausencia de catalizador. Usando el P25 pre-tratado en H_2 como foto-catalizador se obtiene a 170 min una degradación del orange G de alrededor de un 35 % mientras que para los foto-catalizadores propuestos xerogel de carbón-óxido de titanio es de 66 %. Este mayor rendimiento se debe a un efecto sinérgico entre el C y el óxido metálico.
- ✓ Para uso de óxidos semiconductores, como el óxido de titanio, en la foto-degradación con luz visible se necesita una reducción del band-gap o el uso de un sensibilizador eficiente. Estos resultados ponen de manifiesto que el gel de

carbón preparado en microesferas actúa como fotosensibilizador eficiente. Además se facilita la adsorción del contaminante debido a la mayor superficie de las microesferas recubiertas frente al P25, facilitándose así la interacción del contaminante con los centros activos y por tanto, su degradación.

- ✓ Por otro lado, el empleo de estas microesferas de carbón y la disposición del TiO_2 como un recubrimiento delgado reduce la posibilidad de la recombinación hueco-electrón, la cual, es mayor a mayores tamaños de partícula de TiO_2, ya que si el tamaño de partícula es pequeño la distancia que el electrón o el hueco foto-generado debe recorrer hasta la superficie para la reacción redox es menor, y por tanto menor es la posibilidad de recombinación [25], aumentando consecuentemente la actividad foto-catalítica del material.
- ✓ Por otro lado, el método de síntesis garantiza una buena interacción del óxido de titanio con el gel de carbón. El anclaje del material fotoactivo es efectivo y resistente, no se han observado pérdida de actividad (desprendimiento y pérdida de fase activa) tras tratamientos del foto-catalizador mediante ultrasonidos. La naturaleza reductora del soporte de carbón (microesferas) permite cierta transferencia de electrones hacia la fase activa, y favorece la generación de vacantes de oxígeno en el TiO_2 o la formación de óxidos de titanio con estado de oxidación intermedios durante el pretratamiento, efectos que contribuyen a la reducción del band-gap y permiten la degradación mediante el uso de luz visible.
- ✓ La posibilidad de emplear luz visible en lugar de otras radiaciones más energéticas no solo reduce el consumo energético de los procesos de descontaminación sino que proporcionará, por ejemplo, de un método sencillo de descontaminación y potabilización de aguas en países en vías de desarrollo.
- ✓ Es necesario también señalar que el mayor volumen de poros que conlleva a una mayor capacidad de adsorción de los foto-catalizadores soportados sobre las microesferas de carbón, favorece pues la concentración del contaminante en las cercanías de la fase TiO_2, lo que obviamente también favorece la velocidad de degradación del mismo.
- ✓ Finalmente cabe resaltar, que tras los procesos de oxidación de contaminantes orgánicos en agua, los catalizadores, fundamentalmente los sólidos inorgánicos

nano-particulados deben ser retirados del agua previo a su vertido, pues son en sí mismos un nuevo tipo de contaminantes. La mayoría de estos sólidos inorgánicos de pequeño tamaño de partícula (poco peso) son también fuertemente hidrofílicos, por lo que tienden a mantenerse en suspensión dificultando su separación. En nuestro caso, el soporte de carbón es hidrofóbico, y las esferas presentan por sí mismas un tamaño suficientemente grande para que la combinación de ambos efectos favorezca la precipitación del catalizador sin procesos adicionales de centrifugación que son necesarios para los fotocatalizadores convencionales. Tras el ensayo de oxidación del total del contaminante (desaparece completamente el color) se produce la precipitación espontánea del fotocatalizador CTi40S2h al cesar la agitación de la suspensión, mientras que el P25 permanece en suspensión, y necesita un proceso adicional de centrifugación para ser depositado y separado del agua antes del vertido.

La invención se considera nueva porque:

☒ no se ha encontrado nada igual en bancos de datos de patentes
☒ no se ha encontrado nada igual en la bibliografía científica consultada
☒ no se ha encontrado nada igual en un informe de búsqueda completo

5.- APLICACIONES DE LA INVENCIÓN

Describa las aplicaciones industriales de la invención

Los nuevos materiales sintetizados se han desarrollado con el fin de poder oxidar completamente las moléculas orgánicas que contaminan comúnmente el agua o el aire. Las propiedades foto-catalíticas del material permitirán un proceso de oxidación más simple y menos costoso que los actualmente disponibles o implantados, lo cual radica en la posibilidad de empleo de radiación visible (luz solar) en lugar de otras radiaciones más energéticas como es la luz ultravioleta. El empleo de la radiación solar no solo reduce el consumo energético de los procesos de descontaminación sino que proporcionará, por ejemplo, de un método sencillo de descontaminación y potabilización de aguas en países en vías de desarrollo.

Por tanto se requieren foto-catalizadores que sean activos en el rango del espectro visible de la radiación electromagnética. Estos materiales encuentran aplicaciones en una gran variedad de procesos medioambientales y/o energéticos, que abarcan desde celdas solares sensibilizadas por colorantes (DSC) hasta eliminación de contaminantes en fase acuosa o gaseosa. La optimización de los materiales para que presenten un mayor rendimiento en el visible, o que mejoren actividad de los foto-catalizadores actuales que usan radiación ultravioleta, se basa en el desarrollo de nuevos métodos de síntesis.

SECTOR INDUSTRIAL

Indique los sectores a los que va dirigida (señale el sector que la produciría y el que la utilizaría):

SECTOR		Producción	Utilización
A.	ACUICULTURA Y PESCA	☐	☐
B.	ADMINISTRACIÓN PÚBLICA	☐	☐
C.	AERONÁUTICO	☐	☐
D.	ALIMENTACIÓN	☐	☐
E.	AUTOMOCIÓN, TRANSPORTE Y LOGÍSTICA	☐	☐
F.	BIOTECNOLOGÍA	☐	☐
G.	CERÁMICA Y MATERIALES	☐	☒
H.	CONSTRUCCIÓN	☐	☐
I.	CONSULTORÍA, GESTIÓN Y SERVICIOS EMPRESARIALES	☐	☐
J.	EDUCACIÓN Y FORMACIÓN	☐	☐
K.	ELECTRÓNICA, INFORMÁTICA Y TELECOMUNICACIONES (TIC)	☐	☐
L.	ENERGÍA	☐	☐
M.	FARMACIA Y COSMÉTICA	☒	☐
N.	MADERA Y MUEBLES	☐	☐
O.	MAQUINARÍA, AUTOMATIZACIÓN Y EQUIPAMIENTO INDUSTRIAL	☐	☐
P.	MEDIO AMBIENTE	☐	☐
Q.	MINERÍA	☐	☐
R.	QUÍMICA Y PLÁSTICOS	☒	☐
S.	SALUD	☐	☐
T.	AGRICULTURA Y GANADERÍA	☐	☐
U.	SEGURIDAD Y DEFENSA	☐	☐
V.	TEXTILES Y CALZADO	☐	☐
W.	TURISMO	☐	☐
X.	OTROS:	☐	☐

Universidad de Granada

Ref. Interna: IPR-571

6.- DESCRIPCIÓN GENERAL DE LA INVENCIÓN

Describa con detalle el objeto de la invención, en qué consiste, qué problema técnico resuelve y qué ventajas aporta respecto al estado de la técnica actual. Si es necesario, incluya dibujos, figuras o esquemas.

El sistema propuesto pretende obtener foto-catalizadores activos bajo luz visible en la degradación de contaminantes orgánicos del agua o del aire. Para ello el óxido de titanio se dispone formando un recubrimiento estable sobre microesferas de xerogel de carbón (Figura 1).

La invención se centra en desarrollar un método de síntesis sencillo, de los denominados “one pot”, que permita la obtención del foto-catalizador sin tratamientos de funcionalización adicionales.

En un aspecto la invención se relaciona con un método para la preparación de materiales de carbón recubiertos con óxido de titanio buscando el sinergismo entre fases, donde la fase carbón será un xerogel de carbón estructurado en forma de microesferas obtenido a partir de la polimerización de resorcinol y formaldehído, y la fase no carbonosa corresponderá al óxido de titanio, obtenido por hidrólisis de un precursor de titanio (alcóxido de titanio). Este método se ha optimizado para la obtención de los materiales recubiertos en forma de microesferas y se caracteriza tanto por la eficacia de la secuencia metodológica utilizada como por la particularidad de algunos de sus pasos, como son, la utilización de heptano como medio de reacción; el uso de un surfactante en el medio de reacción; el control de la temperatura de reacción (70 ºC) en dicho medio; la adicción lenta y gota a gota de una solución que contiene la mezcla resorcinol-formaldehído como precursor orgánico; la adición gota a gota de un precursor inorgánico de titanio (alcóxido); el control del tiempo de reacción (24 horas) y la velocidad de agitación (470 rpm); el empleo de microondas para la etapa de secado del polímero; una rampa de velocidad de carbonización muy lenta (1 ºC/min) en atmósfera de argón hasta 900ºC y mantenida dicha temperatura durante 2 horas.

Dicho método en adelante método de la invención comprende las siguientes etapas:

1. Preparación del catalizador
2. Caracterización textural, cristalográfica y química
3. Determinación de su actividad foto-catalítica

1. La preparación del catalizador se llevó a cabo mediante:

(i) Obtención de un hidrogel polimérico y estructurado en microesferas preparado en suspensión de heptano en presencia de un surfactante (S) por polimerización de un compuesto fenólico (R), un aldehído (F)
(ii) Recubrimiento de las microesferas poliméricas formadas en suspensión en la etapa (i) con TiO_2 obtenido en el mismo medio de reacción usando un alcóxido de titanio (A)
(iii) Envejecimiento y curado del hidrogel estructurado y recubierto de TiO_2 resultante de la etapa (ii)
(iv) Filtración y secado del hidrogel resultante de la etapa (iii) mediante microondas en atmósfera de argon dando lugar a un xerogel.
(v) Carbonización del xerogel resultante de la etapa (iv) dando lugar a microesferas de xerogel de carbón homogéneamente cubiertas de una capa delgada de TiO_2.

Las etapas i a iii se llevan a cabo de forma consecutiva en el mismo reactor para evitar etapas adicionales y/o contaminación de la muestra, manteniendo asimismo los parámetros de reacción como naturaleza del disolvente y concentración de reactivos, velocidad de agitación y temperatura del medio, para ello es necesario:

a) Preparar una solución de surfactante en un disolvente orgánico.
b) Calentar la solución (a) por debajo del punto de ebullición del disolvente orgánico, bajo agitación.
c) Preparar una solución acuosa que contenga un compuesto fenólico y un aldehído.
d) Pre-gelificar por calentamiento la disolución preparada en c) durante la mitad del tiempo necesario para alcanzar el punto de gel

e) Adicionar gota a gota la solución acuosa del apartado (d) pre-gelificada sobre la solución de surfactante (b).

f) Mantener la suspensión formada bajo agitación y a la T de reacción, para la formación y homogenización de las microesferas de hidrogel polimérico R-F.

g) Adicionar a la suspensión obtenida durante la etapa (f) la cantidad adecuada de un alcóxido metálico (A).

g) Curado y envejecimiento de la suspensión obtenida en el apartado (g) bajo agitación y a temperatura constante.

A continuación se realizan las etapas iv y v previamente descritas.

PALABRAS CLAVE

Indique las palabras clave para efectuar búsquedas en bases de datos (en español y en inglés):

7.- GRADO DE DESARROLLO DE LA INVENCIÓN.

Elija las opciones que más se aproximen al grado de desarrollo de la invención:

- ☒ se ha realizado en laboratorio, exclusivamente.
- ☐ se ha realizado ensayo en planta piloto.
- ☐ existe prototipo preparado para su desarrollo y comercialización.
- ☐ habría que realizar desarrollos para su comercialización o implantación industrial

Si fuera necesario realizar su desarrollo para la explotación comercial, éste tendría:

Dificultad técnica:

- ☐ elevada
- ☒ normal
- ☐ baja

Coste económico:

- ☐ elevado
- ☐ medio
- ☒ bajo

8.- PROYECTO DE DESARROLLO TECNOLÓGICO DE LA INVENCIÓN.

Describa, si lo conoce, cómo tendría que ser el proyecto de desarrollo tecnológico (fases y temporización, presupuestos, recursos necesarios, resultados esperables, etc.) necesario para poner la invención en el mercado (escalabilidad, experiencias piloto, prototipos, pruebas de concepto, etc.)

Universidad de Granada

Ref. Interna: IPR-571

9.- EXPLOTACIÓN Y COMERCIALIZACIÓN DE LA PATENTE

Se considera que sería un producto (procedimiento) con posible éxito comercial:

☒ elevado ☐ medio ☐ bajo

El mercado de la patente es:

☐ exclusivamente nacional

☒ internacional (señalar):

☒ EE.UU. ☒ Europa ☒ Japón ☒ América del Norte

☒ África ☒ Australia ☐ Otros:

¿Se ha contactado con alguna empresa para su posible explotación?

☐ SI ☒ NO

En caso afirmativo, ¿con cuál?

En caso negativo, o si procediese, conteste la siguiente pregunta:

¿Conoce alguna empresa que pudiera estar interesada?

☐ SI ☒ NO

Indique cuál o cuáles:

¿Ha pensado en montar su propia empresa para desarrollar y/o explotar esta tecnología o conocimiento?

☐ SI ☒ NO

10.- BIBLIOGRAFÍA

[1] S. Polisetti, P.A. Deshpande, and G. Madras. Photocatalytic Activity of Combustion Synthesized ZrO_2 and ZrO_2–TiO_2 Mixed Oxides, *Industrial & Engineering Chemistry Research* **50**(23), 12915, 2011.

[2] B.M. Reddy and A. Khan. Recent Advances on TiO_2–ZrO_2 Mixed Oxides as Catalysts and Catalyst Supports, *Catalysis Reviews* **47**(2), 257, 2005.

[3] M.A. Ahmed and M.F. bdel-Messih. Structural and nano-composite features of TiO_2–Al_2O_3 powders prepared by sol–gel method, *Journal of Alloys and Compounds* **509**(5), 2154, 2011.

[4] J. Liu, R. Yang, and S. LI. Preparation and characterization of the TiO_2-V_2O_5 photocatalyst with visible-light activity, *Rare Metals* **25**(6), 636, 2006.

[5] U. Sirimahachai, N. Ndiege, R. Chandrasekharan, S. Wongnawa, and M. Shannon. Nanosized TiO_2 particles decorated on SiO_2 spheres (TiO_2/SiO_2): synthesis and photocatalytic activities, *Journal of Sol-Gel Science and Technology* **56**(1), 53, 2010.

[6] H. Wang, X. Quan, H. Yu, and S. Chen. Fabrication of a TiO_2/carbon nanowall heterojunction and its photocatalytic ability, *Carbon* **46**(8), 1126, 2008.

[7] H. Langhuan, W. Houjin, L. Yingliang, J. Zibin, and S. Zibei. TiO_2/Carbon Nanotube Composites and Their Synergistic Effects on Enhancing the Photocatalysis Efficiency, *Progress in Chemistry* **22**(5), 867, 2010.

[8] M. Pelaez, N.T. Nolan, S.C. Pillai, M.K. Seery, P. Falaras, A.G. Kontos, P.S.M. Dunlop, J.W.J. Hamilton, J.A. Byrne, K. O'Shea, M.H. Entezari, and D.D. Dionysiou. A review on the visible light active titanium dioxide photocatalysts for environmental applications, *Applied Catalysis B: Environmental* **125**(0), 331, 2012.

[9] K. Woan, G. Pyrgiotakis, and W. Sigmund. Photocatalytic carbon-nanotube-TiO_2 composites, *Advanced Materials* **21**(21), 2233, 2009.

[10] D.C. Hurum, A.G. Agrios, S.E. Crist, K.A. Gray, T. Rajh, and M.C. Thurnauer. Probing reaction mechanisms in mixed phase TiO_2 by EPR, *Journal of Electron Spectroscopy and Related Phenomena* **150**(2-3), 155, 2006.

[11] D.C. Hurum, A.G. Agrios, K.A. Gray, T. Rajh, and M.C. Thurnauer. Explaining the Enhanced Photocatalytic Activity of Degussa P25 Mixed-Phase TiO_2 Using EPR, *The Journal of Physical Chemistry B* **107**(19), 4545, 2003.

[12] T. Ohno, K. Tokieda, S. Higashida, and M. Matsumura. Synergism between rutile and anatase TiO_2 particles in photocatalytic oxidation of naphthalene, *Applied Catalysis A: General* **244**(2), 383, 2003.

[13] K.L. Schulte, P.A. DeSario, and K.A. Gray. Effect of crystal phase composition on the reductive and oxidative abilities of TiO_2 nanotubes under UV and visible light, *Applied Catalysis B: Environmental* **97**(3-4), 354, 2010.

[14] J. Zhang, Y. Wu, M. Xing, S.A.K. Leghari, and S. Sajjad. Development of modified N doped TiO_2 photocatalyst with metals, nonmetals and metal oxides, *Energy & Environmental Science* **3**(6), 715, 2010.

[15] S. Lee, Y. Lee, D.H. Kim, and J.H. Moon. Carbon-Deposited TiO_2 3D Inverse Opal Photocatalysts: Visible-Light Photocatalytic Activity and Enhanced Activity in a Viscous Solution, *ACS Applied Materials & Interfaces* **5**(23), 12526, 2013.

16 Y. Wang, H. Cheng, Y. Hao, J. Ma, W. Li, and S. Cai. Photoelectrochemical properties of metal-ion-doped TiO_2 nanocrystalline electrodes, *Thin Solid Films* **349**(1–2), 120, 1999.

17 H. Yamashita, M. Honda, M. Harada, Y. Ichihashi, M. Anpo, T. Hirao, N. Itoh, and N. Iwamoto. Preparation of Titanium Oxide Photocatalysts Anchored on Porous Silica Glass by a Metal Ion-Implantation Method and Their Photocatalytic Reactivities for the Degradation of 2-Propanol Diluted in Water, *The Journal of Physical Chemistry B* **102**(52), 10707, 1998.

18 Y. Izumi, T. Itoi, S. Peng, K. Oka, and Y. Shibata. Site Structure and Photocatalytic Role of Sulfur or Nitrogen-Doped Titanium Oxide with Uniform Mesopores under Visible Light, *The Journal of Physical Chemistry C* **113**(16), 6706, 2009.

19 C. Di Valentin, E. Finazzi, G. Pacchioni, A. Selloni, S. Livraghi, M.C. Paganini, and E. Giamello. N-doped TiO_2: Theory and experiment, *Chemical Physics* **339**(1–3), 44, 2007.

20 A.I. Kontos, A.G. Kontos, Y.S. Raptis, and P. Falaras. Nitrogen modified nanostructured titania: electronic, structural and visible-light photocatalytic properties, *Physica Status Solidi (RRL): Rapid Research Letters* **2**(2), 83, 2008.

21 F. Dong, H. Wang, and Z. Wu. One-Step "Green" Synthetic Approach for Mesoporous C-Doped Titanium Dioxide with Efficient Visible Light Photocatalytic Activity, *The Journal of Physical Chemistry C* **113**(38), 16717, 2009.

22 Y.T. Lin, C.H. Weng, Y.H. Lin, C.C. Shiesh, and F.Y. Chen. Effect of C content and calcination temperature on the photocatalytic activity of C-doped TiO_2 catalyst, *Separation and Purification Technology* **116**(0), 114, 2013.

23 L. Zhao, X. Chen, X. Wang, Y. Zhang, W. Wei, Y. Sun, M. Antonietti, and M.M. Titirici. One-Step Solvothermal Synthesis of a Carbon@TiO_2 Dyade Structure Effectively Promoting Visible-Light Photocatalysis, *Advanced. Materials* **22**(30), 3317, 2010.

24 J. Zhong, F. Chen, and J. Zhang. Carbon-Deposited TiO_2: Synthesis, Characterization, and Visible Photocatalytic Performance, *The Journal of Physical Chemistry C* **114**(2), 933, 2009.

25 R. Leary and A. Westwood. Carbonaceous nanomaterials for the enhancement of TiO_2 photocatalysis, *Carbon* **49**(3), 741, 2011.

26 M.Y. Guo, F. Liu, Y.H. Leung, A.M.C. Ng, A.B. Djurišic, and W.K. Chan. TiO2–carbon nanotube composites for visible photocatalysts-Influence of TiO_2 crystal structure, *Current Applied Physics* **13**(7), 1280, 2013.

[27] Y.T. Liang, B.K. Vijayan, O. Lyandres, K.A. Gray, and M.C. Hersam. Effect of dimensionality on the photocatalytic behavior of carbon-titania nanosheet composites: Charge transfer at nanomaterial interfaces, *The Journal of Physical Chemistry Letters* **3**(13), 1760, 2012.

[28] B.K. Vijayan, N.M. Dimitrijevic, D. Finkelstein-Shapiro, J. Wu, and K.A. Gray. Coupling titania nanotubes and carbon nanotubes to create photocatalytic nanocomposites, *ACS Catalysis* **2**(2), 223, 2012.

[29] Z. Li, B. Gao, G.Z. Chen, R. Mokaya, S. Sotiropoulos, and G. Li Puma. Carbon nanotube/titanium dioxide (CNT/TiO_2) core-shell nanocomposites with tailored shell thickness, CNT content and photocatalytic/photoelectrocatalytic properties, *Applied Catalysis B: Environmental* **110**, 50, 2011.

[30] S. Wang and S. Zhou. Photodegradation of methyl orange by photocatalyst of $CNTs/P\text{-}TiO_2$ under UV and visible-light irradiation, *Journal of Hazardous Materials* **185**(1), 77, 2011.

[31] Y.T. Liang, B.K. Vijayan, O. Lyandres, K.A. Gray, and M.C. Hersam. Effect of dimensionality on the photocatalytic behavior of carbon-titania nanosheet composites: Charge transfer at nanomaterial interfaces, *The Journal of Physical Chemistry Letters* **3**(13), 1760, 2012.

[32] H. Mahmood, A. Habib, M. Mujahid, M. Tanveer, S. Javed, and A. Jamil. Band gap reduction of titania thin films using graphene nanosheets, *Materials Science in Semiconductor Processing* **24**(1), 193, 2014.

[33] C.P. Athanasekou, S. Morales-Torres, V. Likodimos, G.E. Romanos, L.M. Pastrana-Martinez, P. Falaras, J.L. Faria, J.L. Figueiredo, and A.M.T. Silva. Prototype composite membranes of partially reduced graphene oxide/TiO_2 for photocatalytic ultrafiltration water treatment under visible light, *Applied Catalysis B: Environmental* **158-159**, 361, 2014.

[34] S. Morales-Torres, L.M. Pastrana-Martínez, J.L. Figueiredo, J.L. Faria, and A.M.T. Silva. Graphene oxide-P25 photocatalysts for degradation of diphenhydramine pharmaceutical and methyl orange dye, *Applied Surface Science* **275**(0), 361, 2013.

[35] S. Takenaka, T. Arike, H. Matsune, and M. Kishida. Coverage of carbon nanotubes with titania nanoparticles for the preparation of active titania-based photocatalysts, *Applied Catalysis B: Environmental* **125**(0), 358, 2012.

[36] F.F. Cao, Y.G. Guo, S.F. Zheng, X.L. Wu, L.Y. Jiang, R.R. Bi, L.J. Wan, and J. Maier. Symbiotic Coaxial Nanocables: Facile Synthesis and an Efficient and Elegant Morphological Solution to the Lithium Storage Problem, *Chemistry of Materials* **22**(5), 1908, 2010.

[37] X.b. Yan, B.K. Tay, and Y. Yang. Dispersing and Functionalizing Multiwalled Carbon Nanotubes in TiO2 Sol, *The Journal of Physical Chemistry B* **110**(51), 25844, 2006.

[38] J. Sun, M. Iwasa, L. Gao, and Q. Zhang. Single-walled carbon nanotubes coated with titania nanoparticles, *Carbon* **42**(4), 895, 2004.

[39] S.w. Lee and W.M. Sigmund. Formation of anatase TiO_2 nanoparticles on carbon nanotubes, *Chemical Communications* (6), 780, 2003.

[40] W. Fan, L. Gao, and J. Sun. Anatase TiO_2-Coated Multi-Wall Carbon Nanotubes with the Vapor Phase Method, *Journal of the American Ceramic Society* **89**(2), 731, 2006.

[41] X. Liang and R.L. Patel. Porous titania microspheres with uniform wall thickness and high photoactivity, *Ceramics International* **40**(2), 3097, 2014.

[42] W. Li, C. Ni, H. Lin, C.P. Huang, and S.I. Shah. Size dependence of thermal stability of TiO_2 nanoparticles, *Journal of Applied Physics* **96**, 6663, 2004.

[43] A.A. Gribb and J.F. Banfield. Particle size effects on transformation kinetics and phase stability in nanocrystalline TiO_2, **82**(7-8), 717, 1997.

[44] R. Handy, M. Whitt, M. Rodriguez, and M.J. Jackson, "Chapter 9 - Environmental and Occupational Health Issues With Nanoparticles",in *Emerging Nanotechnologies for Manufacturing (Second Edition). Micro and Nano Technologies*, edited by W. Ahmed and M.J. Jackson (William Andrew Publishing, Boston, 2015), pp.255-269.

[45] R. Zhang, Y. Bai, B. Zhang, L. Chen, and B. Yan. The potential health risk of titania nanoparticles, *Journal of Hazardous Materials* **211–212**(0), 404, 2012.

[46] P. Boffetta, V. Gaborieau, L. Nadon, M.E. Parent, E. Weiderpass, and J. Siemiatycki. Exposure to titanium dioxide and risk of lung cancer in a population-based study from Montreal, *Scandinavian Journal of Work, Environment & Health* **27**(4), 227, 2001.

[47] P.M. Hext, J.A. Tomenson, and P. Thompson. Titanium dioxide: Inhalation toxicology and epidemiology, *Annals of Occupational Hygiene* **49**(6), 461, 2005.

[48] J. Njuguna and S. Sachse, "5 - Measurement and Sampling Techniques for Characterization of Airborne Nanoparticles Released From Nano-Enhanced Products",in *Health and Environmental Safety of Nanomaterials*, edited by J. Njuguna, K. Pielichowski, and H. Zhu (Woodhead Publishing, 2014), pp.78-111.

[49] L. Mbundi, H. Gallar-Ayala, M.R. Khan, J.L. Barber, S. Losada, and R. Busquets, "Chapter Two - Advances in the Analysis of Challenging Food Contaminants:

Nanoparticles, Bisphenols, Mycotoxins, and Brominated Flame Retardants",in *Advances in Molecular Toxicology*, Volume 8 ed. edited by C.F.a.J. James (Elsevier, 2014), pp.35-105.

50 S. Dalai, V. Iswarya, M. Bhuvaneshwari, S. Pakrashi, N. Chandrasekaran, and A. Mukherjee. Different modes of TiO_2 uptake by Ceriodaphnia dubia: Relevance to toxicity and bioaccumulation, *Aquatic Toxicology* **152**(0), 139, 2014.

51 A. Bour, F. Mouchet, L. Verneuil, L. Evariste, J. Silvestre, E. Pinelli, and L. Gauthier. Toxicity of CeO_2 nanoparticles at different trophic levels- Effects on diatoms, chironomids and amphibians, *Chemosphere* **120**(0), 230, 2015.

52 F.J. Maldonado-Hódar. Advances in the development of nanostructured catalysts based on carbon gels, *Catalysis Today* **218–219**(0), 43, 2013.

53 C. Moreno-Castilla and F.J. Maldonado-Hódar. Carbon aerogels for catalysis applications: An overview, *Carbon* **43**(3), 455, 2005.

54 F.J. Maldonado-Hódar, M.A. Ferro-García, J. Rivera-Utrilla, and C. Moreno-Castilla. Synthesis and textural characteristics of organic aerogels, transition-metal-containing organic aerogels and their carbonized derivatives, *Carbon* **37**(8), 1199, 1999.

55 F.J. Maldonado-Hódar, C. Moreno-Castilla, J. Rivera-Utrilla, Y. Hanzawa, and Y. Yamada. Catalytic graphitization of carbon aerogels by transition metals, *Langmuir* **16**(9), 4367, 2000.

Capítulo IX

APLICACIONES BIOMÉDICAS

A PRELIMINARY STUDY ABOUT THE USE OF FUNCTIONALIZED CARBON XEROGEL IN OSTEOCYTES GROWTH

Article in progress

Highlights

- Carbon xerogel structurated in microsphere was prepared.
- Carbon nanofibers were grown on the surface of carbon spheres at different percentages by chemical vapor deposition.
- Carbon xerogel-based materials were functionalized using Prato and Tour reaction.
- Non toxicity was detected on osteocytes and the viability of cells increases.
- Carbon xerogels are presented as excellent candidates for their use in biomedical applications.

Abstract

In the present study, carbon nanofibers were grown on the surface of carbon xerogels microsperes at different percentages by chemical vapor deposition (A8NF). The impact of functionalized A8NF on bone cells (osteocytes) was addressed. These materials were functionalized following the 1,3-dipolar cycloaddition of azomethine ylides (Prato reaction) or the addition of aryl diazonium salts (Tour reaction). Higher functionalization degrees were obtained by both types of reaction, being however greater using Tour reaction. Cells viability has been evaluated for a fibroblast cell line. Data show that samples are non-toxic for this kind of cells. After 24 hours the viability of cells seeded in presence of all the types of tested materials is comparable to the control whereas and after 72 hours the viability of cells seems to be increased. On the other hand, from these preliminary tests it seems that the presence of fibers on the surface of the spheres increases the cells proliferation in comparison with the unmodified ones.

9.1. INTRODUCTION

Carbon materials such as carbon nanotube, fullerenes and graphenes has attracted the attention of many researchers worldwide for their use in biological application because these materials have many interesting and unique properties potentially useful in a variety of biological and biomedical systems and devices. Significant progress has been made in the effort to overcome some of barriers toward bio applications such as the aqueous solubility and biocompatibility of carbon materials which make difficult their manipulation and limits their use in biological application. So that, functionalization is one of the requirements to increase the hydrophilicity (e.g. –OH, –COOH, $–NH_2$) and to prepare new compounds presenting biological and pharmacological activity[1].

Various types of functionalization have been used to improve the application of carbon materials in biomedical application, mainly on carbon nanotube. Using carbon nanotubes tree main strategies are followed: i) covalent functionalization such as oxidation reactions[2,3], esterification-amidation reaction[4,5], complexation reaction[6], halogenation[7], cycloadittion reactions[8,9], radical, nucleophilic and electrophilic additions[10-12]; ii) non-covalent functionalization by adsorption of molecules on their sidewall mainly adsorption of molecules containing aromatic groups with the conjugated surface of the nanotubes through π–π interactions[13]; and iii) endohedral filling such as encapsulation of fullerenes in the inner empty cavity or other organic and inorganic molecules[14,15] for drug delivery, targeting, and imaging.

On the other hand, osteoporosis is the most common type of bone disease whereby the bones become less dense than is normal for a person and so that is the cause of the most of bone fractures in elderly people. Therefore tissue bioengineering to create artificial scaffold materials that have the capacity to sustain bone cell growth and proliferation and increment or replace bone tissue has become an important study field. Bone structure and function depend intimately on the arrangement of cellular and noncellular components at the micro- and nanoscale level. These include cell types such as osteoblasts, osteoclasts, and osteocytes embedded in a mineralized extracellular matrix consisting of collagen and a number of noncollagenous proteins. Hench and Wilson [16] defined two needed condition to the success of a biomaterial: (i) it must be

able to form a stable interface with the surrounding natural tissue and (2) it must functionally provide the mechanical behaviour of the replaced tissue. In this sense, CNT has extensively used for this application due to CNTs are a stronger material and their implantation in bone may improve the mechanical properties of damaged bone tissue. But the purity of CNTs is a lack of this material and a purification process are needed in order to reduce their toxicity. Unrefined CNTs include accelerated oxidative stress, decreased cell viability, and altered cell morphology as well as induce apoptosis and decrease of cellular adhesion. Intratracheal inhalation of CNT particles in mice and rats can cause pulmonary toxicity. These adverse effects may be due to lack of purity and functionalization.

In this sense, carbon aerogels could be interesting materials in biological application. Carbon aerogels are obtained by sol-gel policondensation of certain organic monomers, such as resorcinol and formaldehyde which provides them unique properties such as very high purity, controlled-form as well as a well-developed and controlled micro- and mesoporosity, a large surface area and easily-functionalized surface. These properties make them excellent for bio application as drug delivering or bone regeneration system, between others. Carbon nanomaterials with improved unique structure properties such as, high specific surface areas, large pore volume, ease of surface functionalization and generally none or low cytotoxicity could facilitate larger amount of drug loadings[17-21]. Besides, it is observed that carbon nanomaterials are capable of transporting covalently bonded drugs or molecular probes across cell membranes and releasing anticancer drugs effectively in cancer cells. Currently, carbon nanosphere carriers for drug delivery are mainly obtained by carbonization of different chemical hydrocarbons (i.e., pentane, cyclohexane, xylene, mesitylene, anthracene, etc.)[22,23]. But the carbon spheres prepared by these complex procedures present inconveniences for their use as drug delivering vectors such as sizes generally larger than the required diameters for transmembrane delivery carrier (below 100 nm)[24] and impurities because of residual chemical precursors. Therefore, recently carbon spheres has been produced using a diverse of biomass precursors (i.e., glucose, xylose, sucrose, maltose, amylopectin, plant cellulose and others) and biomass derivatives (i.e., hydroxylmethyl-furfural (HMF) and furfural) but the most of the prepared carbon spheres are a size larger than 100 nm[25].

For everything commented above, carbon aerogels could be an interesting materials in biological applications and in our knowledge have not been previously used in this field. The main objective of this study was to provide a first insight into the likely toxicity associated with functionalised carbon xerogel structured in spheres by evaluating their potential acute effects on bone cells such as osteocytes.

9.2. EXPERIMENTAL

9.2.1. Preparation of carbon xerogel spheres

The carbon xerogel (A8) was prepared by polycondensation of resorcinol with formaldehyde in aqueous media, using Cs_2CO_3 as polymerization catalyst by modifying a previous synthesis procedure[26]. The synthesis procedure was published elsewhere [27,28]. In brief, the proper amount of resorcinol and cesium carbonate were added to deionised water in a three-necks glass reactor provided of reflux, controlled temperature (85 ºC) and stirring. Then, formaldehyde solution (Sigma, 37 wt.%) was added drop wise in the flask under agitation (250 rpm) and the gel formed was aged at 85°C for 24 hours. Finally, the suspension was filtered and placed in acetone (3 days, changing acetone twice daily) to exchange water within the pores by acetone, in order to reduce the porosity collapse during the subsequent drying process[29]. The gel was dried by microwave using a Saivod MS-287W microwave oven under nitrogen atmosphere in periods of 1 minute at 384 W until constant weight and carbonized to obtain the corresponding carbon xerogel in N_2 flow at 150 cm^3/min, heating to 900 ºC at a heating rate of 1 ºC/min, in order to allow a soft removing of pyrolysis gases, and soaking time of 2 h.

9.2.2. Preparation of composites carbon xerogel spheres-carbon nanofibers

Carbon nanofibers were grown on the surface of carbon xerogel spheres (A8) by chemical vapour deposition (CVD). For that, the previously synthesized carbon sphere were impregnated at 3 wt. % Ni-loading with an aqueous solution of nickel (II) acetate tetrahydrate, so the appropriate amount of Ni $(CH_3CO_2)_2(H_2O)_4$ was dissolved in the minimum amount of water (according to the salt solubility) and then slowly dropped on the support under constant homogenization by shaking. Impregnated

supports were dried at room temperature for 1 day and at 110 °C in an oven for additional 24 h and stored in a desiccator in the lab. 300 mg of Ni-carbon spheres were placed in a tubular oven under 60 cm^3/min H_2 flow, then temperature was increased at 360 ºC (heating rate of 5 °C/min) for 12 h in order to produce an *in situ* reduction of the Ni precursor. CNF were grown on the carbon spheres under ethylene (10% in He):H_2 (5:1) atmosphere for 3, 4 or 6h at 550 °C. The CNF percentages was calculated with the increase of the weight on the samples after the treatment and was 23.5, 30.0, 62.3 wt. % (30.7, 42.8 and 165.3 wt. %, CNF growth percentages) respectively. Samples were named as A8NF20, A8NF30 and A8NF60. After the growing treatment, Ni was removed of the samples using the following acidic treatment: i) HF (6 ml HF/g carbon) for 1 h at 55-60 ºC and after filtering ii) HCl (4 ml HCl/ g carbon) for 1 h at 55-60 ºC. Finally, samples after filtering were washed with distilled water until constant pH and until chlorides had been removed and dried in an oven at 110 ºC for 24 h before storage.

9.2.3. Functionalization of carbon samples

The functionalization of A8NFX composites was done using two different type of reaction: i) with aryl diazonium salts generated in situ (Tour reaction)[30]; and ii) 1,3-dipolar cycloadittion of azomethine ylides (Prato reaction)[31,32].

9.2.3.1. Tour reaction

Generally, the reaction is performed by adding first an aniline derivative and then alkyl nitrite to an aqueous solution of carbon spheres-based material. Both reagents are responsible for the diazonium salt formation, which then reacts with double bonds presents on carbon-based material. In this way, using a battery of aniline derivatives, a numerous type of functionalized materials could be obtained (Figure 9.1).

In this work, the reaction was performed using isopentyl nitrate from Sigma-Aldrich and 4-[(N-Boc)aminomethyl]aniline from SAFC. 60 mg of sample was dispersed in 50 ml of distilled water and sonicated in a water bath for 20 min. The reaction was performed under stirring (500 rpm) and reflux at 80 ºC. At this point, 1 g of 4-[(N-Boc)aminomethyl]aniline and 1 ml of isopentyl nitrate were added. The

reaction was stirred under the same conditions overnight. After that, the reaction mixture was cooled at room temperature filtered and washed with water until transparent permeate, and then, extensively washed with methanol and finally with diethyl ether to help them dry which was performed under vacuum. As prepared samples were referred to as A8NFXT (being X 20, 30 or 60).

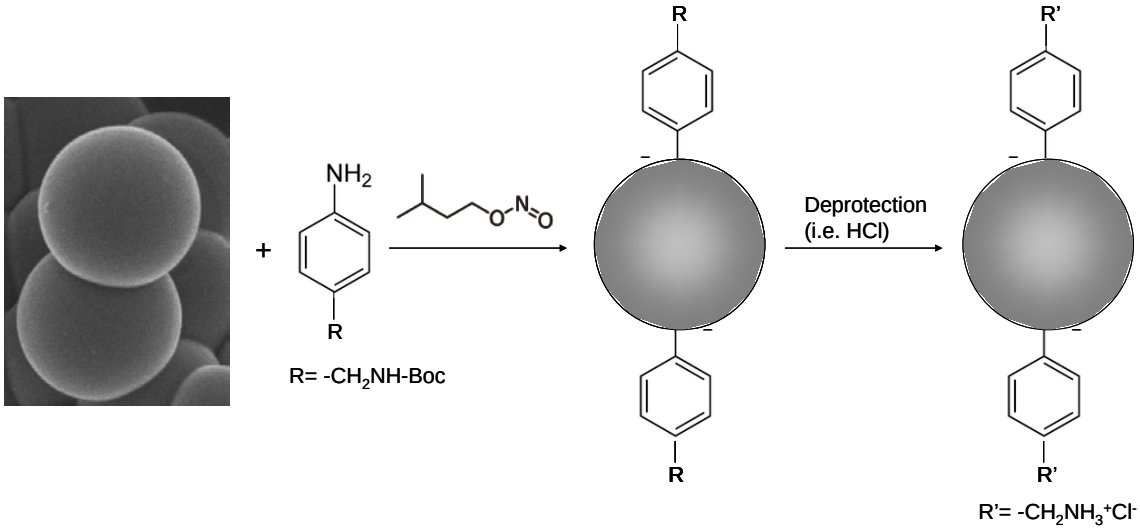

Figure 9.1. Functionalization of carbon spheres by Tour reaction with in situ generated diazonium compounds, using an aniline derivate and an alkyl nitrite.

The Boc group was cleaved using an HCl solution. So, 50 mg of A8NFXT were dispersed in 50 ml of dioxane and sonicated for 30 min. Then, 20 ml of HCl 37% was added under stirring and room temperature. After overnight, the solution was filtered and the solid was washed with 1,4-dioxane until neutral pH and then with methanol repeatedly, and finally with diethyl ether. The solid was placed under vacuum overnight to dry it. The deprotected samples were referred to as A8NFXTd (being X 20, 30 or 60).

9.2.3.2. Prato reaction

The method is based on 1,3-dipolar cycloadittion of an ylide generated by the condensation of N-methylglycine (sarcosine) with an aldehyde to C60 (Figure 2). This approach is widely used for the functionalization of fullerenes and in particular, in the syntheses of porphyrinfullerenes. The reaction proceeds via the intermediate

azomethine ylide which further reacts with double bonds of carbon materials in a 1,3-dipolar cycloadittion (Figure 9.2).

The use of other N-substituted glycines instead of sarcosine makes it possible to introduce two different substituents into the pyrrolidine ring. The Prato reaction has a diverse range of applications in the field of organic materials.

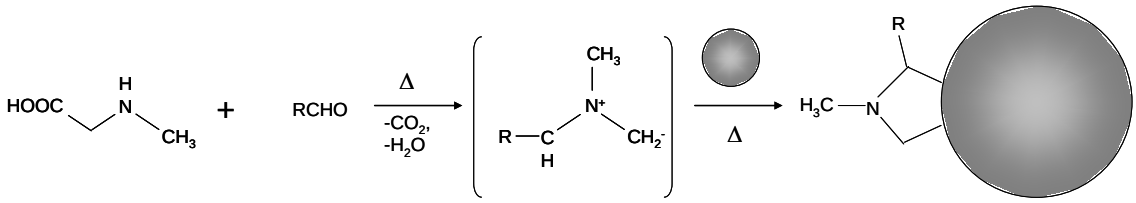

Figure 9.2. Prato reaction mechanism.

In this work, the Prato reaction was performed using paraformaldehyde from Sigma-Aldrich and a previously synthetized amino acid in our lab (N-pht-amino-diethoxy-ethilamino-acetic acid)[33,34]. 20 mg of sample was dispersed in 20 ml of 1,2-diclorobenzene and sonicated in a water bath for 30 min. The reaction was performed under stirring (300 rpm) and reflux at 180 ºC. At this point, 56 mg of amino acid and 30 mg paraformaldehyde were added. After 2 h, another addition of 56 mg of amino acid and 30 mg paraformaldehyde were done. A total of five additions were done (Total amounts were 280 mg of amino acid and 150 mg of paraformaldehyde in 8 h) The reaction was stirred under the same conditions overnight. After that, the reaction mixture was cooled at room temperature, filtered and washed with 1,2-diclorobenzene, DMF, Methanol and finally with diethyl ether to help them dry which was performed under vacuum. As prepared samples were referred to as A8NFXP (being X 20, 30 or 60).

The protected group was cleaved using hydrazine hydrate. So, 50 mg of A8NFXP were dispersed in 50 ml of ethanol and sonicated for 30 min. Then, 312 μl of $NH_2NH_2 \cdot H_2O$ was added under stirring and room temperature. After overnight, the solution was filtered and the solid was washed Methanol, DMF, Methanol and finally with diethyl ether. The solid was placed under vacuum overnight to dry it. The deprotected samples were referred to as A8NFXPd (being X 20, 30 or 60).

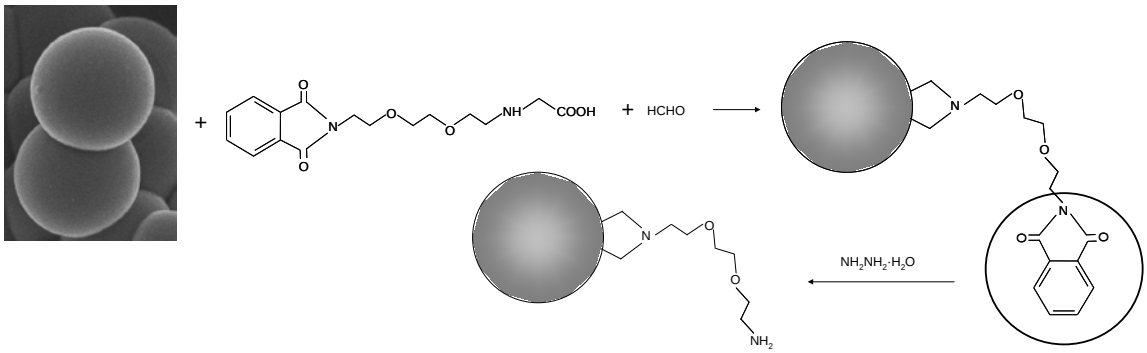

Figure 9.3. Prato Reaction over carbon xerogel spheres.

9.2.4. Characterization of the samples

9.2.4.1. Morphology of A8NF samples

The morphology of A8NF samples was studied by scanning electron microscopy (SEM) using a LEO (Carl Zeiss) GEMINI-1530 microscope and transmission electron microscopy using a high-resolution transmission electron microscopy (HRTEM). HRTEM experiments were carried out using a Phillips CM-20 microscope equipped with EDAX microanalysis system.

9.2.4.2. Textural characterization

Textural characterization was carried out by N_2 and CO_2 adsorption at −196 °C and 0 °C, respectively, using a Quantachrome Autosorb-1 equipment. The BET equation was applied to the N_2-adsorption isotherms to determine the apparent surface area (S_{BET}) and the Dubinin–Radushkevich and Stoeckli equations applied to both N_2 and CO_2-adsorption isotherms to determine the micropore volume (V_{mic}), the mean micropore width (L_0) and the microporous surface (S_{mic}), respectively[35-38]. Furthermore, the BJH method was used to calculate the mesopore volume of the samples (V_{meso}) and the mean mesopore width (L_{meso}). Pore size distributions (PSD) were also obtained by applying the BJH method[39]. The total pore volume (V_{Total}) was considered as the volume of N_2 adsorbed at $P/P_0 = 0.95$[40].

9.2.4.3. Chemical characterization

The chemical characterization of the catalysts was further analyzed by X-ray photoelectron spectroscopy (XPS). The spectra were obtained on a Kratos Axis Ultra-DLD X-ray photoelectron spectrometer equipped with a hemispherical electron analyzer connected to a detector DLD (delay-line detector). The Ni_{2p}, C_{1s} and O_{1s} spectral regions were registered. The Ni_{2p} spectral region was scanned several times to obtain good signal-to-noise ratios.

9.2.4.4. Functionalization degree

Functionalization degree was followed by the Kaiser test[41]. This test is a color test for qualitative and quantitative detection of free terminal amino groups (as is the case of the both functionalization performed in this work).

The test is based on the reaction of primary amines with nihydin which turn the colour of the reaction solution in dark blue if the reaction is positive (qualitative measurement). The reaction mechanism is shown in Figure 9.4.

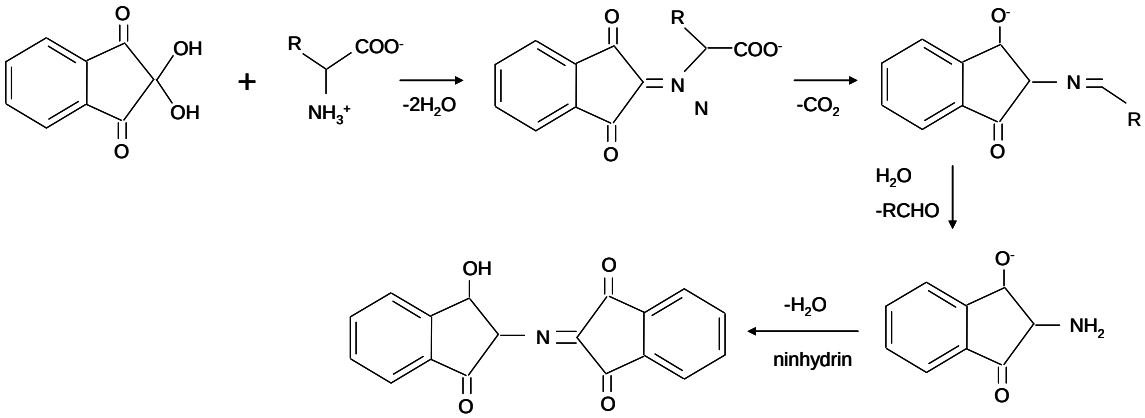

Figure 9.4. Kaiser test mechanism. The formed complex is responsible for the dark blue colour.

The test was performed using a Fluka Kaiser trdt kit. For that, 0.5 mg of sampled were placed in a glass test tube. Also a blank solution was prepared as well. Then, 75 μl of the kit solution of phenol (80% in ethanol) and 100 μl of the kit solution of KCN (in pyridine) were added to the test tube containing the sample and the

resulting dispersion was sonicated in a water bath for 5 min. After that, 75 μl of the kit solution of ninhydrin (6% in ethanol) were added to the test tube and they were closed. Finally, the tubes were heated at 120 ºC for 10 min. Afterwards, the mixture was cooled in order to stop the reaction and diluted with 2750 μl ethanol (60% in water) to obtain a final volume of 3 ml.

The quantification of the functionalization degree was measured UV-Vis spectroscopy. For that, the samples were centrifuged at 3000 rpm for 10 min and the supernatant was collected and the absorbance was measured at 570 nm (characteristic of the formed complex). The zero was previously set using the blank solution which was prepared at the same time those samples. The quantification of the present of free amino group was done applying a slightly modified Lamber-Beer law:

$$\frac{\mu mol}{g} = \frac{Abs \cdot dil}{\varepsilon \cdot W} 10^6$$

where, Abs is the measured absorbance of the sample registered at 570 nm, dil is the dilution factor and it corresponds to the final volume of sample (3 ml), ε is the extinction coefficient (15000 $M^{-1}cm^{-1}$) and W is the weight of functionalized carbon materials (mg). The results for each sample are the mean of at least two independent measurements.

9.2.4.5. Thermogravimetric analysis

The functionalization degree is also determined by TGA. In inert atmosphere carbon materials are stable at temperature up to 800 ºC, so that, weight loss produced at temperatures lower than 800 ºC could be related with the organic material present in the sample, which usually begin to burn at 350 ºC (weight loss up to 600 ºC are consider to obtain the results). In this way, the organic functional moieties attached to the carbon surface could be estimate. The obtained by TGA are usually compared to the results of Kaiser Test. Both are considered as two complementary techniques which are able to provide a good estimation of the functionalization degree of the samples.

The TGA procedure was: first, an equilibration step at 100 ºC for 20 min was done in order to remove residue solvent. Then, a linear ramp of temperature was applied (10ºC/min) up to 850 ºC under N_2 flow.

2.4.6. Toxicity tests on osteocytes

Cells viability has been evaluated for a fibroblast cell line (NIH/3T3 ATCC® CRL1658™) cells line through a modified LDH assay. Absorbance measurements have been performed on Tecan Nano Quant Infinite M200 Pro plate reader. NIH/3T3 monolayers have been cultured in DMEM medium supplemented with 10% fetal bovine serum FBS (v/v), 100 U penicillin, 0,1 mg/ml streptomycin, L-glutamine 2 mM and maintained at 37 °C and 5% (v/v) CO_2. Once reached the 80-90% of confluence, Cells have been passaged twice a week using trypsin/EDTA 0.25%.

Modified LDH assay: cells have been seeded into 24-well plates (40000 NIH/3T3 cells per well) and left 24 hours before incubation in presence of the material to promote the adhesion. The modified LDH assay has been employed to evaluate the degree of cell proliferation in presence of suspended carbon spheres. Cells have been incubated for 24 and 72 hours in presence of functionalized A8NFX at different concentrations (10, 50 and 100 µg/mL). The LDH assay, previously described, has been modified to avoid the interference on the UV-Vis absorbance due to the presence of suspended materials. According to the LDH assay, the amount of released LDH is calculated on the culture medium after the induced-cell death. In the modified LDH assay proposed by Ali-Baucetta *et al.* the LDH content is assessed in intact cells that survived the treatment[42]. Briefly, the medium culture is removed after the incubation period and cells are lysed in presence of 10 µL of lysis buffer (SIGMA TOX-7 kit) mixed with 100 µL of serum free medium for 45 min at 37°C. The cell lysate is diluted with 800 µl of serum free medium and centrifuged at 16100×g for 5 minutes in order to pellet down the suspended carbon material. 45 µL of the supernatant is mixed with 90 µL of LDH reagent substrate mix in a 96-well plate and incubated for 20 minutes at room temperature in shelter from the light. The absorbance is measured at 490 nm and 690 nm (phenol red). The amount of detected LDH represents the number of cells that survived the treatment. The percentage of cell survival is calculated using the following equation:

$$\%\text{Cell Survival} = \frac{\left(\text{Abs}_{490} - \text{Abs}_{690}\text{treated and untreated cells}\right) - \left(\text{Abs}_{490} - \text{Abs}_{690}\text{blank}\right)}{\left(\text{Abs}_{490} - \text{Abs}_{690}\text{untreated cells}\right) - \left(\text{Abs}_{490} - \text{Abs}_{690}\text{blank}\right)} \cdot 100$$

The viability values at 24 and 72 hours have been normalized for the day 0.

9.3. RESULTS AND DISCUSSION

9.3.1. Characterization of A8NF samples

The textural characteristics of A8 and their derivative A8-NF composites are summarized in Table 9.1. A8 is an exclusively microporous material with a moderate surface area. The grown of nanofibers on the surface of A8 decrease enormously the surface area of carbon sphere due to a blockage or filling of microporosity with carbon deposits on the surface spheres but increase the mesopores volume. It is well known that carbon nanofibers are mainly macroporous and mesoporous materials as a result of the nanofibers criss-cross during their growth. On the other hand, increasing the number of nanofibers on the carbon spheres an increase in the surface area and micro and mesoporous volume can be observed. This manifests the contribution of the carbon nanofibers to the surface area and pore volume of samples.

Table 9.1. Textural characteristics of carbon materials.

	N_2-adsorption					**CO_2-adsorption**		
Sample	**S_{BET}** $m^2 \cdot g^{-1}$	**W_0** $cm^3 \cdot g^{-1}$	**L_0** nm	**V_{meso}** $cm^3 \cdot g^{-1}$	**$V_{0.95}$** $cm^3 \cdot g^{-1}$	**W_0** $cm^3 \cdot g^{-1}$	**S_{mic}** $m^2 \cdot g^{-1}$	**L_0** nm
A8	614	0.25	0.78	0.00	0.31	0.285	952	0.60
A8NF20	124	0.05	1.86	0.33	0.35	0.221	748	0.59
A8NF30	185	0.07	1.80	0.47	0.43	0.217	647	0.67
A8NF60	274	0.11	1.69	0.49	0.49	0.139	453	0.61

* S_{BET}= BET surface area, W_0 = micropore volume, L_0 = micropore wide, V_{meso}= BJH mesopore volume, $V_{0.95}$ = total pore volume, S_{mic} = microporous surface.

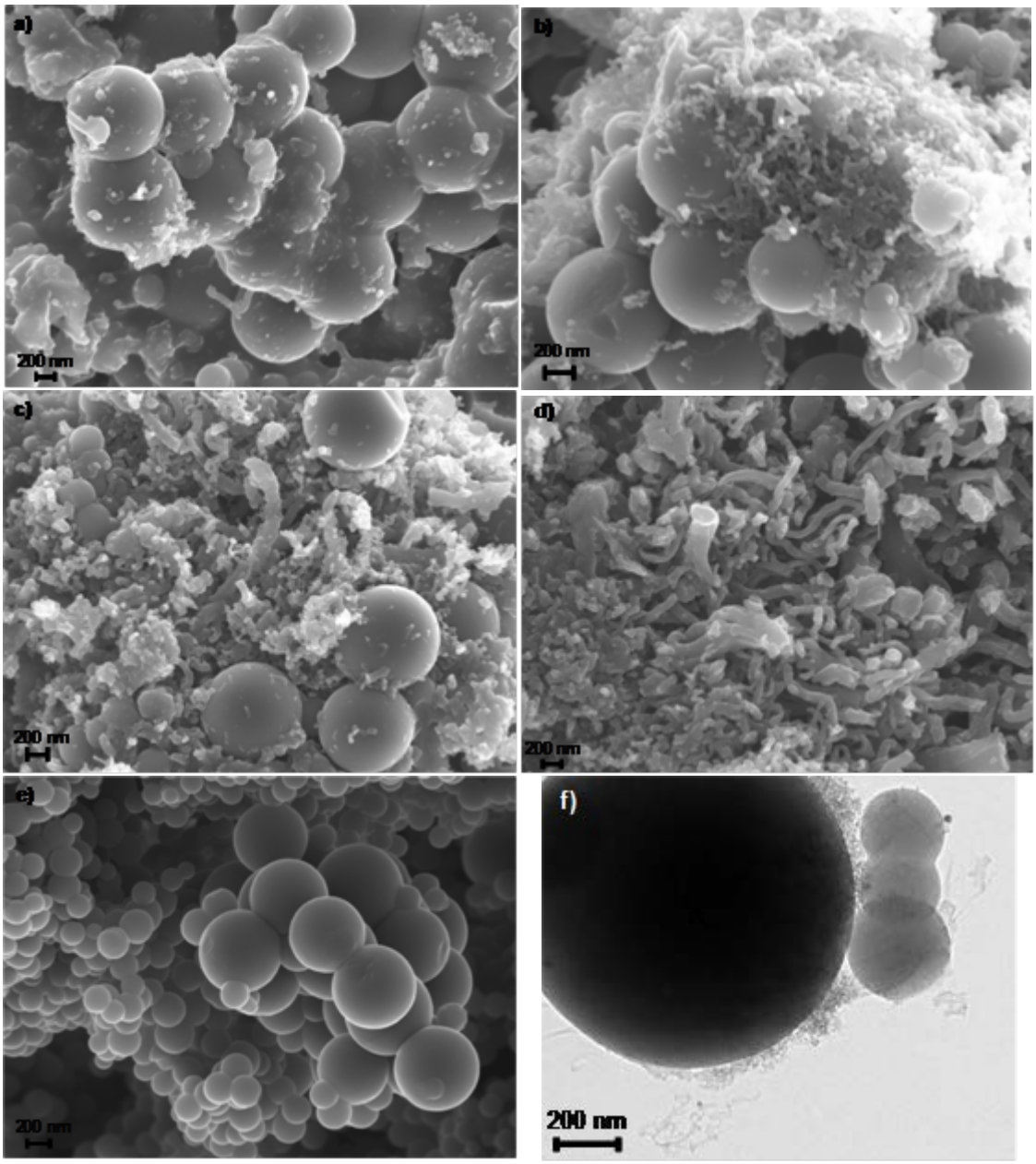

Figure 9.5. SEM microphotographs of a) A8NF20, b) A8NF30, c) and d) A8NF60, e) A8 and f) TEM microphotograph of A8NF30.

The morphology was studied by SEM and representative microphotographs are shown in Figure 9.5. Carbon xerogels have a network structure of interconnected primary particles where micropores are related to the intraparticle structure, whereas mesopores and micropores are produced by inter-particle structure[43]. A8 are formed by non-connected microspheres with a mean particle size of around 200 nm so that, the sample have a null mesopores volume (related with the spaces between primary particles) and micropores are related to the porosity inside the spheres particles. With respect to A8NF, increasing the time of CVD treatment, longer and better defined

carbon nanofibers are obtained, increasing the amount of carbon nanofibers from 23.5 % to 62.3 % increasing the treatment time from 3 to 6 h. Short carbon nanofibers or amorphous carbon can be seen after 2 h of treatment (Figure 9.5a). Increasing the time from 2 to 3 h better defined carbon nanofibers are obtained (Figure 9.5b), which manifests the necessity of time higher than 2 h for an effective carbon nanofibers growth. A treatment time of 6 h produces a high amount of carbon nanofibers (higher than 60 %) which produces a high connection between carbon spheres (Figure 9.5c and d).

The diameter of carbon nanofibers range from 10 nm to more than 100 nm as it shown in Figure 9.5 and it is related with the metal particle size, as well as the growth temperature.

XPS survey spectra of A8NF samples are shown in Figure 9.6. Ni are not detected on the samples which indicates that purification process of A8NF is effective to remove all Ni present on the sample surface and consequently, non-toxicity is expected in toxicity tests on osteocytes due to Ni contents.

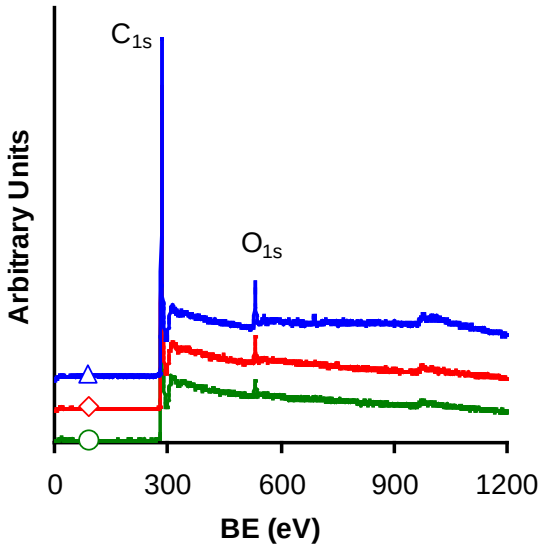

Figure 9.6. XPS survey spectra of A8NF samples. A8NF20(△), A8NF30 (◇), A8NF60 (○).

9.3.2. Functionalization degree of A8NF samples

Data from Kaiser test and thermogravimetric analysis are shown in Table 9.2. In general, a good agreement is obtained from both technics. Using Tour reaction higher functionalization degrees than with Prato reaction are achieved instead the hydrophobicity of samples and consequently the worse dispersion in the reaction medium. As exception, using A8 carbon xerogel higher functionalization degree are achieved using Prato reaction versus Tour reaction, that could be explained on the base of the high hydrofobicity of this sample that limits a good dispersion in water reaction medium of Tour reaction and consequently a worse contact with the reagents.

On the other hand, the presence of nanofibers favour the functionalization degree regardless the type of reaction instead the lower surface area and microporous volume of this samples compared with A8. This could indicate that functionalization occurs mainly on the external surface due to transfers limitation of reagents into the narrow microporosity. Increasing the amount of nanofibers increase mainly the mesopore and macropore volumes as well as the external surface and so, a higher functionalization degree are obtained using A8-CNF composites.

Table 9.2. Functionalization degree obtained by Kaiser test and TGA.

Sample	Reaction	μmol/g Kaiser	μmol/g TGA
A8Td	Tour	58.7	52.2
A8NF30Td	Tour	371.6	342.5
A8NF60Td	Tour	393.7	362.8
A8Pd	Prato	152.4	153.2
A8NF30Pd	Prato	205.5	200.2
A8NF60Pd	Prato	268.6	250.5

A high degree of functionalization might be required for other potential uses of CNTs (for example), such as drug delivery. High functionalization degrees are achieved using carbon xerogels spheres-carbon nanofibers composites which could make them as promising materials in this application field. Usual values range up to 100 μmol/g using Prato reaction and up to 200 μmol/g using Tour Reaction[44].

9.3.3. Cells viability test

The modified LDH assay proposed by Ali-Boucetta *et al*. turns out to be a reliable method to evaluate the viability of the cells in presence of f-CNTs. We evaluated the viability of cells seeded in presence of with different concentrations of modified carbon spheres in order to avoid the interference noticed in the previous described essays. A 500 μg/ml solution of A8, A8NF60, A8NF30td and A8NF60td in sterilized mQ water has been sonicated for 30' and added to the medium culture in order to obtain 3 different final concentrations (100, 50 and 10 μg/ml).

Data show that tested samples are non-toxic for this kind of cells at the used concentration range (10-100 μg/ml). After 24 hours the viability of cells seeded in presence of all the types of tested materials is comparable to the control. In spite that further experiments are necessary to confirm the data obtained, it is obtained that after 72 hours the viability of cells clearly increased. Moreover, Figure 9.7 shows that even increasing the concentration of non-functionalized carbon xerogels in the culture medium the cell viability also increases, indicating that the presence of carbon xerogels not only are not toxic for the tested cell but, moreover, they are beneficial to cell improving their growth. On the other hand, from these preliminary tests it seems that the presence of fibers on the surface of the spheres increases the cells proliferation in comparison with the unmodified ones.

Looking data for functionalized samples, Figure 9.7 c and d, the same conclusions are achieved. The viability of cells is higher than the control one, this fact manifests non-toxicity of samples and an improvement of cell growth. However, cell growth rates are higher using unfunctionalized carbon xerogels (Figures 9.7 a, b) which could be related with a blockage of porosity of samples after the functionalization process, and consequently, lower surface area. Thus, lower interactions of cells with the carbon surface could be achieved. Moreover, the cells growth increases increasing the sample concentration from 10 to 50 μg/ml but is more or less constant increasing from 50 to 100 μg/ml. The higher is the amount of sample the higher is the cell viability up to 50 μg/ml and then the cell growth rate is constant instead of the amount of sample. Consequently, the functionalization of samples is acting in a way that does not

increases the cell growth rate increasing the amount of material in the culture medium above a certain material concentration.

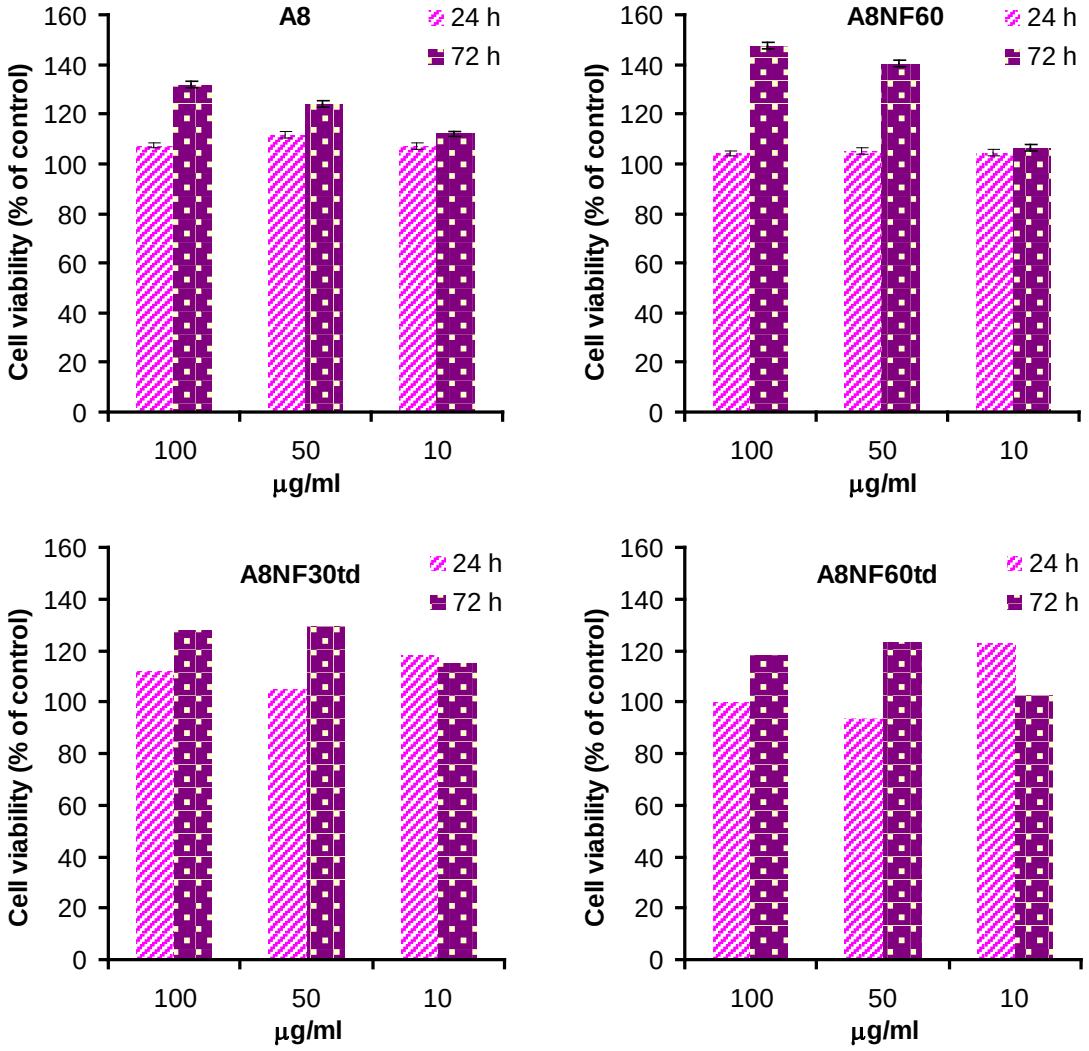

Figure 9.7. LDH assay after incubation with carbon materials in fibroblast cell line at different carbon concentration for indicated times.

Nevertheless, non-toxicity and beneficial effect over the cell viability are achieved using both non-functionalized and functionalized carbon xerogels microspheres, which open a new field of application of this type of materials with interesting results.

9.4. CONCLUSIONS

In the present work, carbon nanofibers were grown on the surface of carbon xerogels microspheres (A8) at different percentages by chemical vapour deposition (A8NF). We have here reported the first thorough study on the impact of functionalized carbon xerogles on osteocytes belonging to the bone system. Interestingly, we show that high functionalization degrees are achieved using Prato and Tour reactions, (3-dipolar cycloadittion of azomethine ylides and the addition of aryl diazonium salts generated in situ, respectively) which could be so interesting in field such us drug delivering, among others.

Cells viability of functionalized and non-functionalized carbon xerogels has been evaluated for a fibroblast cell line (NIH/3T3 ATCC® CRL1658™) through a modified LDH assay. Data show that tested samples are non-toxic for this kind of cells. After 24 hours the viability of cells seeded in presence of all the types of tested materials is comparable to the control whereas and after 72 hours the viability of cells seems to be increased. Indeed, using non-functionalized materials, a higher viability of cells has been observed increasing the concentration of carbon material in the culture medium indicating a beneficial effect of carbon materials on the cells growth.

However, in spite of the non-toxicity and the increase of the cell viability observed using functionalized materials, lower cell growth rates are obtained in comparison with non-functionalized ones. This fact could be related with a blockage of porosity of samples after the functionalization process and consequently, lower surface area and so, lower interactions of cells with the carbon surface.

In brief, this study evidences that carbon aerogels could be interesting materials in biological applications, being not toxic and achieving high functionalization degrees, and in our knowledge have not been previously used in this field.

9.5. REFERENCES

[1] A. Battigelli, C. Ménard-Moyon, T. Da Ros, M. Prato, and A. Bianco. Endowing carbon nanotubes with biological and biomedical properties by chemical modifications, *Advanced Drug Delivery Reviews* **65**(15), 1899, 2013.

[2] F. Avilés, J.V. Cauich-Rodríguez, L. Moo-Tah, A. May-Pat, and R. Vargas-Coronado. Evaluation of mild acid oxidation treatments for MWCNT functionalization, *Carbon* **47**(13), 2970, 2009.

[3] Y. Xing, L. Li, C.C. Chusuei, and R.V. Hull. Sonochemical Oxidation of Multiwalled Carbon Nanotubes, *Langmuir* **21**(9), 4185, 2005.

[4] C. Aprile, R. Martín, M. Alvaro, H. Garcia, and J.C. Scaiano. Covalent Functionalization of Short, Single-Wall Carbon Nanotubes: Photophysics of 2,4,6-Triphenylpyrylium Attached to the Nanotube Walls, *Chemistry of Materials* **21**(5), 884-890, 10-3-2009.

[5] Y. Wang, Z. Iqbal, and S.V. Malhotra. Functionalization of carbon nanotubes with amines and enzymes, *Chemical Physics Letters* **402**(1–3), 96, 2005.

[6] A.S. Lobach, R.G. Gasanov, E.D. Obraztsova, A.N. Shchegolikhin, and V.I. Sokolov. Sidewall Functionalization of Single–Walled Carbon Nanotubes by Organometallic Chromium–Centered Free Radicals, *Fullerenes, Nanotubes and Carbon Nanostructures* **13**(4), 287, 2005.

[7] M. Liu, Y. Yang, T. Zhu, and Z. Liu. Chemical modification of single-walled carbon nanotubes with peroxytrifluoroacetic acid, *Carbon* **43**(7), 1470, 2005.

[8] S.J. Pastine, D. Okawa, B. Kessler, M. Rolandi, M. Llorente, A. Zettl, and J.M.J. Fréchet. A Facile and Patternable Method for the Surface Modification of Carbon Nanotube Forests Using Perfluoroarylazides, *Journal of the American Chemical Society* **130**(13), 4238-4239, 1-4-2008.

[9] Z. Yinghuai, A.T. Peng, K. Carpenter, J.A. Maguire, N.S. Hosmane, and M. Takagaki. Substituted Carborane-Appended Water-Soluble Single-Wall Carbon Nanotubes: New Approach to Boron Neutron Capture Therapy Drug Delivery, *Journal of the American Chemical Society* **127**(27), 9875-9880, 1-7-2005.

[10] Y. Xu, X. Wang, R. Tian, S. Li, L. Wan, M. Li, H. You, Q. Li, and S. Wang. Microwave-induced electrophilic addition of single-walled carbon nanotubes with alkylhalides, *Applied Surface Science* **254**(8), 2431, 2008.

[11] R. Graupner, J. Abraham, D. Wunderlich, A. Vencelová, P. Lauffer, J. Röhrl, M. Hundhausen, L. Ley, and A. Hirsch. Nucleophilic–Alkylation–Reoxidation: A Functionalization Sequence for Single-Wall Carbon Nanotubes, *Journal of the American Chemical Society* **128**(20), 6683-6689, 1-5-2006.

[12] J.L. Hudson, H. Jian, A.D. Leonard, J.J. Stephenson, and J.M. Tour. Triazenes as a Stable Diazonium Source for Use in Functionalizing Carbon Nanotubes in Aqueous Suspensions, *Chemistry of Materials* **18**(11), 2766-2770, 1-5-2006.

[13] Y.L. Zhao and J.F. Stoddart. Noncovalent Functionalization of Single-Walled Carbon Nanotubes, *Accounts of Chemical Research* **42**(8), 1161-1171, 18-8-2009.

[14] K. Yanagi, K. Iakoubovskii, S. Kazaoui, N. Minami, Y. Maniwa, Y. Miyata, and H. Kataura. Light-harvesting function of β-carotene inside carbon nanotubes, *Physical Review B* **74**(15), 155420, 18-10-2006.

[15] M. Monthioux, E. Flahaut, and J.P. Cleuziou. Hybrid carbon nanotubes: Strategy, progress, and perspectives, *Journal of Materials Research* **21**(11), 2774, 2006.

[16] L.L. Hench and J. Wilson, *"introduction," an introduction to bioceramics* (World Scientific, Singapore, 1993).

[17] T.W. Kim, P.W. Chung, I.I. Slowing, M. Tsunoda, E.S. Yeung, and V.S.Y. Lin. Structurally Ordered Mesoporous Carbon Nanoparticles as Transmembrane Delivery Vehicle in Human Cancer Cells, *Nano Letters* **8**(11), 3724-3727, 12-11-2008.

[18] Z. Liu, X. Sun, N. Nakayama-Ratchford, and H. Dai. Supramolecular Chemistry on Water-Soluble Carbon Nanotubes for Drug Loading and Delivery, *ACS Nano* **1**(1), 50, 2007.

[19] X. Ma, H. Tao, K. Yang, L. Feng, L. Cheng, X. Shi, Y. Li, L. Guo, and Z. Liu. A functionalized graphene oxide-iron oxide nanocomposite for magnetically targeted drug delivery, photothermal therapy, and magnetic resonance imaging, *Nano Research* **5**(3), 199-212, 2012.

[20] L. Zhang, J. Xia, Q. Zhao, L. Liu, and Z. Zhang. Functional Graphene Oxide as a Nanocarrier for Controlled Loading and Targeted Delivery of Mixed Anticancer Drugs, *Small* **6**(4), 537, 2010.

[21] S. Wen, H. Liu, H. Cai, M. Shen, and X. Shi. Targeted and pH-Responsive Delivery of Doxorubicin to Cancer Cells Using Multifunctional Dendrimer-Modified Multi-Walled Carbon Nanotubes, *Advanced Healthcare Materials* **2**(9), 1267, 2013.

[22] X.B. Zhang, H.W. Tong, S.M. Liu, G.P. Yong, and Y.F. Guan. An improved Stober method towards uniform and monodisperse Fe_3O_4@C nanospheres, *Journal of Materials Chemistry A* **1**(25), 7488-7493, 2013.

[23] V.G. Pol, M. Motiei, A. Gedanken, J. Calderon-Moreno, and M. Yoshimura. Carbon spherules: synthesis, properties and mechanistic elucidation, *Carbon* **42**(1), 111, 2004.

[24] S. Nie, Y. Xing, G.J. Kim, and J.W. Simons. Nanotechnology Applications in Cancer, *Annual Review of Biomedical Engineering* **9**(1), 257-288, 25-7-2007.

[25] B. Hu, K. Wang, L. Wu, S.H. Yu, M. Antonietti, and M.M. Titirici. Engineering Carbon Materials from the Hydrothermal Carbonization Process of Biomass, *Advanced Materials* **22**(7), 813-828, 16-2-2010.

[26] S. Morales-Torres, F.J. Maldonado-Hódar, A.F. Pérez-Cadenas, and F. Carrasco-Marín. Textural and mechanical characteristics of carbon aerogels synthesized by polymerization of resorcinol and formaldehyde using alkali carbonates as basification agents, *Physical Chemistry Chemical Physics* **12**(35), 10365, 2010.

[27] E. Bailón-García, F. Carrasco-Marín, A.F. Pérez-Cadenas, and F.J. Maldonado-Hódar. Microspheres of carbon xerogel: an alternative Pt-support for the selective hydrogenation of citral, *Applied Catalysis A: General* **482**, 318, 2014.

[28] E. Bailón-García, F. Carrasco-Marín, A.F. Pérez-Cadenas, and F.J. Maldonado-Hódar. Development of carbon xerogels as alternative Pt-supports for the selective hydrogenation of citral, *Catalysis Communications* **58**, 64, 2014.

[29] E. Gallegos-Suárez, A.F. Pérez-Cadenas, F.J. Maldonado-Hódar, and F. Carrasco-Marín. On the micro- and mesoporosity of carbon aerogels and xerogels. The role of the drying conditions during the synthesis processes, *Chemical Engineering Journal* **181–182**(0), 851, 2012.

[30] J.L. Bahr and J.M. Tour. Highly Functionalized Carbon Nanotubes Using in Situ Generated Diazonium Compounds, *Chemistry of Materials* **13**(11), 3823-3824, 1-11-2001.

[31] M. Maggini, G. Scorrano, and M. Prato. Addition of azomethine ylides to C60: synthesis, characterization, and functionalization of fullerene pyrrolidines, *Journal of the American Chemical Society* **115**(21), 9798-9799, 1-10-1993.

[32] O. Tsuge and S. Kanemasa, "Recent Advances in Azomethine Ylide Chemistry",in *Advances in Heterocyclic Chemistry. Advances in Heterocyclic Chemistry*, Volume 45 ed. edited by R.K. Alan (Academic Press, 1989), pp.231-349.

[33] V. Georgakilas, N. Tagmatarchis, D. Pantarotto, A. Bianco, J.P. Briand, and M. Prato. Amino acid functionalisation of water soluble carbon nanotubes, *Chemical Communications* (24), 3050-3051, 2002.

[34] K. Kordatos, T. Da Ros, S. Bosi, E. Vázquez, M. Bergamin, C. Cusan, F. Pellarini, V. Tomberli, B. Baiti, D. Pantarotto, V. Georgakilas, G. Spalluto, and M. Prato. Novel Versatile Fullerene Synthons, *The Journal of Organic Chemistry* **66**(14), 4915-4920, 1-7-2001.

[35] S. Brunauer, P.H. Emmett, and E. Teller. Adsorption of Gases in Multimolecular Layers, *Journal of the American Chemical Society* **60**(2), 309-319, 1-2-1938.

[36] M.M. Dubinin. Generalization of the theory of volume filling of micropores to nonhomogeneous microporous structures, *Carbon* **23**(4), 373, 1985.

[37] MM. Dubinin. Contemporary state of the theory of volume filling of micropores of adsorbents in the adsorption of gases and vapors on carbon adsorbents, *Russian Journal of Physical Chemestry* **39**, 1305, 1965.

[38] F. Stoeckli, *porosity in carbons - characterization and applications* (Arnold, London, 1995).

[39] E.P. Barrett, L.G. Joyner, and P.P. Halenda. The Determination of Pore Volume and Area Distributions in Porous Substances. I. Computations from Nitrogen Isotherms, *Journal of the American Chemical Society* **73**(1), 373-380, 1-1-1951.

[40] R. Ubago-Pérez, F. Carrasco-Marín, D. Fairén-Jiménez, and C. Moreno-Castilla. Granular and monolithic activated carbons from KOH-activation of olive stones, *Microporous and Mesoporous Materials* **92**(1–3), 64, 2006.

[41] E. Kaiser, R.L. Colescott, C.D. Bossinger, and P.I. Cook. Color test for detection of free terminal amino groups in the solid-phase synthesis of peptides, *Analytical Biochemistry* **34**(2), 595, 1970.

[42] H. Ali-Boucetta, K.T. Al-Jamal, K.H. Müller, S. Li, A.E. Porter, A. Eddaoudi, M. Prato, A. Bianco, and K. Kostarelos. Cellular Uptake and Cytotoxic Impact of Chemically Functionalized and Polymer-Coated Carbon Nanotubes, *Small* **7**(22), 3230, 2011.

[43] C. Moreno-Castilla and F.J. Maldonado-Hódar. Carbon aerogels for catalysis applications: An overview, *Carbon* **43**(3), 455, 2005.

[44] J.M. González-Domínguez, M. González, A. Ansón-Casaos, A.M. Díez-Pascual, M.A. Gómez, and M.T. Martínez. Effect of Various Aminated Single-Walled Carbon Nanotubes on the Epoxy Cross-Linking Reactions, *The Journal of Physical Chemistry C* **115**(15), 7238-7248, 21-4-2011.

Publicaciones

Catalysts **2013**, *3*, 853-877; doi:10.3390/catal3040853

OPEN ACCESS

catalysts

ISSN 2073-4344

www.mdpi.com/journal/catalysts

Review

Catalysts Supported on Carbon Materials for the Selective Hydrogenation of Citral

Esther Bailón-García *, Francisco J. Maldonado-Hódar, Agustín F. Pérez-Cadenas and Francisco Carrasco-Marín

Carbon Materials Research Group, Department of Inorganic Chemistry, Faculty of Sciences, University of Granada, Campus Fuentenueva s/n, 18071 Granada, Spain;
E-Mails: fjmaldon@ugr.es (F.J.M.-H.); afperez@ugr.es (A.F.P.-C.); fmarin@ugr.es (F.C.-M.)

* Author to whom correspondence should be addressed; E-Mail: estherbg@ugr.es; Tel.: +34-958-243-235; Fax: +34-958-248-526.

Received: 14 August 2013; in revised form: 22 September 2013 / Accepted: 11 October 2013 / Published: 22 October 2013

Abstract: The heterogeneously catalyzed selective-hydrogenation of citral is one of the more feasible ways for obtaining its appreciated unsaturated-alcohols, nerol and geraniol, which are present in over 250 essential oils. Thus, citral has very recently come to be produced petro-chemically in very large quantities, and so partial hydrogenation of citral has become a very economical route for the production of these compounds. However, the selective hydrogenation of citral is not easy, because citral is an α,β-unsaturated aldehyde which possesses three double bonds that can be hydrogenated: an isolated C=C bond and the conjugated C=O and C=C bonds. For this reason, in catalyst selection there are several important issues which affect the product selectivity, for example, the active metal and metal particle size which are factors related to the catalyst preparation method, catalyst precursor, or support surface area, as well as other factors such as porosity, the addition of a second catalytic metal, and, of course, the type of catalyst support. About this last one, carbon materials are very interesting supports for this type of hydrogenation reaction due to their unique chemical and textural properties. This review collects and analyzes the results obtained in the selective hydrogenation of citral catalyzed by carbon material supported metals.

Keywords: citral; hydrogenation; activated carbon; graphite; carbon nanotubes

---

Applied Catalysis A: General 482 (2014) 318–326

Contents lists available at ScienceDirect

Applied Catalysis A: General

journal homepage: www.elsevier.com/locate/apcata

Microspheres of carbon xerogel: An alternative Pt-support for the selective hydrogenation of citral

E. Bailón-García, F. Carrasco-Marín, A.F. Pérez-Cadenas, F.J. Maldonado-Hódar*

Grupo de Investigación en Materiales de Carbón, Departamento de Química Inorgánica, Facultad de Ciencias, Universidad de Granada, Granada 18071, Spain

ARTICLE INFO

Article history:
Received 17 February 2014
Received in revised form 9 June 2014
Accepted 10 June 2014
Available online 17 June 2014

Keywords:
Citral hydrogenation
Pt-catalysts
Inorganic supports
Carbon xerogels
Acidity
Pre-treatments

ABSTRACT

A new carbon xerogel (A8) was obtained in powder by polymerization of resorcinol-formaldehyde using a stirred batch reactor, microwave drying and carbonization in inert atmosphere. The ability of this material as Pt-support regarding SiO_2, TiO_2 and Al_2O_3 to develop selective catalysts for the citral hydrogenation was analyzed on the basis of their morphologic, textural and acid characteristics. Inorganic supports are crystalline and mesoporous materials while the carbon xerogel is exclusively microporous and is formed by spherical nanoparticles of around 250 nm in diameter of amorphous carbon. The supports acidity (pH_{pzc}) vary in the sense $Al_2O_3 > TiO_2 > SiO_2 > A8$. The Pt-dispersion depends on the support nature and pretreatment conditions used; in general, an increase of Pt-particle size favors the selectivity to unsaturated alcohols but the catalytic activity decrease. The conversion also strongly depends on the acidity of supports, but selectivity is more specifically influenced by the strength of the acid sites and pore size distribution. Cracking reactions are favored by Brönsted acid sites present in Al_2O_3 and the high mesopore volume of SiO_2 induces mainly secondary cyclization and hydrogenation reactions. Pt-supported on carbon xerogel (Pt/A8) provided selectivity values to unsaturated alcohols of around 80%, a very high value for monometallic Pt-catalyst and only comparable with those obtained with Pt/TiO_2 pretreated in H_2-flow.

1. Introduction

The selective hydrogenation of carbonyl groups of α,β-unsaturated aldehydes is a challenging process, either from a scientific and economic point of view [1–3]. Citral (3,7-dimethyl-2,6-octadienal) is a multi-unsaturated compound, which contains both an isolated double bond (C=C) and another C=C conjugated to a carbonyl (–C=O) group. Citral is one of the main components of the lemongrass oil and therefore a cheap raw material to produce highly valuable products by hydrogenation, being specially interesting their derivatives unsaturated alcohols (UA, nerol and geraniol) used in organic synthesis, fine chemistry, perfumery or pharmaceutical industry [4–10]. However, the citral hydrogenation presents a complex reaction scheme [11] leading to a variety of products. The main problem is that the hydrogenation of C=C bonds is thermodynamically favored over the C=O bond's one, but also, there is a series of side reactions like acetalization, cyclization or cracking [11–13] that reduces the UA yield. Thus, the use of monometallic catalysts leads mainly to the formation of saturated aldehyde (citronellal) [14,15].

The catalytic performance is influenced by both the active phase and support nature, and their interactions. The activity and selectivity of Group VIII metals was previously pointed out [16] being Os and Ru highly selective to produce UA. The support characteristics strongly influence the catalytic performance. Pt is more active when supported on basic hydrotalcites but the selectivity to UA (S_{UA}) is favored on acid supports [17]. The metal-support interactions (SMSI effect) was suggested as one additional key factor to increase the selectivity of catalysts [18,19], but different mechanisms were proposed. Thus studying the influence of supports (graphite, KL zeolite and ZrO_2) on Ru-catalysts performance [20] it was pointed out that using graphite as Ru-support, the selectivity to UA is favored by electronic transfers from graphite to the Ru-particles with formation of electron-rich metal species. In the case of Ru-supported on ZrO_2, this effect is associated to the formation of Ru^0-Zr^{n+} species and when supported on zeolite KL the hydrogenation of the carbonyl group and poisoning resistance are favored by geometrical factors (pore characteristics and localization of the Ru-particles). Ru/KL is the more selective catalyst to UA (around 50%), but it is poorly active.

* Corresponding author. Tel.: +34 958240444.
E-mail address: fjmaldon@ugr.es (F.J. Maldonado-Hódar).

http://dx.doi.org/10.1016/j.apcata.2014.06.011
0926-860X/

Catalysis Communications 58 (2015) 64–69

Contents lists available at ScienceDirect

Catalysis Communications

journal homepage: www.elsevier.com/locate/catcom

Short Communication

Development of carbon xerogels as alternative Pt-supports for the selective hydrogenation of citral

Esther Bailón-García, Francisco Carrasco-Marín, Agustín F. Pérez-Cadenas, Francisco J. Maldonado-Hódar *

Group of Research in Carbon Materials, Dpt. of Inorganic Chemistry, Faculty of Sciences, University of Granada, Avda. Fuentenueva s/n. 18071, Granada, Spain

ARTICLE INFO

Article history:
Received 5 May 2014
Received in revised form 28 August 2014
Accepted 1 September 2014
Available online 15 September 2014

Keywords:
Citral hydrogenation
Selective catalysts
Pt-catalysts
Activated carbons
Carbon xerogels

ABSTRACT

The role of activated carbons and carbon xerogels as Pt-supports for the selective citral hydrogenation is compared. The influence of porosity and inorganic matter impurities in activated carbons determines the performance of their derivative catalysts. The presence of Pt-particles inside mesopores and acid mineral matter favors secondary reactions decreasing the unsaturated alcohols (UA) yield. Highly active and selective monometallic Pt-catalysts were obtained using pure carbon xerogels structured in microspheres as support.

1. Introduction

The selective hydrogenation of carbonyl groups of α,β-unsaturated aldehydes is a challenging process, either from a scientific and economic point of view [1]. Among them, citral is a cheap raw material obtained from different natural sources being their derivative unsaturated-alcohols (UA), nerol and geraniol, highly demanded by pharmaceutical and chemical industries. The design and development of catalysts for the selective citral hydrogenation are influenced by several factors determining the catalysts performance: the active metal phase and support nature [2], metal particle size [3], bimetallic catalysts [1,4] and factors related with the preparation method and metal–support interactions [5,6]. All these factors and the evolution of the designed catalysts were recently reviewed [7].

Carbon materials are very interesting catalyst supports due to their ability to fit their chemical and textural properties. Doing a bibliography review [8], it can be seen that three types of carbon materials have been used in the selective hydrogenation of citral: activated carbons [9,10], graphite [10,11], carbon nanotubes (CNT) or nanofibers (CNF) [11–13], being the best selectivity achieved around 65% at 30% conversion obtained with monometallic Pt- supported on electron-donor graphite [14].

It is noteworthy that no reference has been found in which carbon aerogels or xerogels were used as support, in spite of the benefits that these kinds of materials show in very different catalyzed reactions [15]. In this manuscript we have prepared two nanostructured carbon xerogels and their performance as Pt-support was compared to activated carbons on the basis of the different textural properties and purity.

2. Experimental

Two carbon xerogels (A1, A8) were prepared by polycondensation of resorcinol (R) with formaldehyde (F) in aqueous (W) media, using Cs_2CO_3 as polymerization catalyst (C). Briefly, the appropriate amounts of resorcinol (24.7 g) and Cs_2CO_3 (0.72 or 0.09 g) were dissolved in deionized water (670 mL) using a three-neck glass reactor (2 L) provided of reflux, controlled temperature and stirring. The temperature of this solution was fitted to 85 °C under stirring (250 rpm) and then, 36.3 g of formaldehyde solution (Sigma, 37 wt.%) was added dropwise. Thus, the composition of the mixture (molar ratio) was R/F = 1/2, R/W = 3/500 for both samples and R/C was 100 and 800, for A1 and A8 respectively. The gel formed was aged at 85 °C for 24 h, filtered and placed in acetone for 3 days, in order to reduce the porosity collapse during the subsequent drying process by microwave [16]. The gel was dried by microwave heating using a Saivod MS-287 W microwave oven under nitrogen atmosphere in periods of 1 min at 384 W until constant weight. Pyrolysis of organic xerogels was carried out at 900 °C for 2 h in N_2 flow (300 cm^3 min^{-1}). An activated carbon (EG) was also prepared in our laboratories by chemical activation of olive stones with KOH following the experimental procedure previously published [17]. Olive stones were milled and sieved to 1.0–2.0 mm, treated with sulphuric acid (1 N) to remove the rest of pulp and washed until all sulfates had been removed. An initial carbonization was carried out by heating at 10 °C min^{-1} to 400 °C and a soak time of 2 h under a

* Corresponding author. Tel.: +34 958240444.
E-mail address: fjmaldon@ugr.es (F.J. Maldonado-Hódar).

http://dx.doi.org/10.1016/j.catcom.2014.09.001
1566-7367/